# PROCESS INTENSIFICATION: A STUDY OF CALCIUM CARBONATE PRECIPITATION METHODS ON A SPINNING DISC REACTOR

by

**Paul Hetherington MEng (Hons)**

**Thesis submitted for the degree of Doctor of Philosophy in the Faculty of Science Agriculture and Engineering of the University of Newcastle upon Tyne**

Process Intensification and Innovation Centre

School of Chemical Engineering and Advanced Materials

University of Newcastle upon Tyne

NE1 7RU

UK

**July 2006**

## Abstract

Over recent years, the spinning disc reactor (SDR) has been developed as a chemical processing device whereby rapid mass and heat transfer rates can be obtained from the thin film of liquid produced by the act of rotation. In exploiting these characteristics, the SDR is considered a tool of process intensification; compact, flexible, intrinsically safe, continuous and capable of delivering better product quality. An SDR and spinning cone reactor were previously investigated in the precipitation of barium sulphate crystals. It was seen that incredibly rapid mixing coupled with high levels of supersaturation lead to very small crystals with a tighter size distribution being produced. This was seen to produce better quality than conventional process techniques.

The present study investigates the potential of the spinning disc as a reactor for the precipitation of calcium carbonate. Three different process routes were identified for the study. The first route is the carbonation of calcium hydroxide solution; the second is the carbonation of calcium hydroxide slurry. The third was the precipitation from mixing sodium carbonate and calcium chloride solutions.

For each study, the process parameters and crystal size distributions of the product are evaluated for the spinning disc and complimentary batch reactions. As calcium carbonate is capable of forming three polymorphs, the size, size distribution and shape of the crystals are studied using particle size analysis and electron microscopy.

The gas-liquid reaction study showed the SDR to have a higher mass transfer rate than a 1-litre batch with a smaller crystal size distribution. The calcium hydroxide slurry carbonation showed that the SDR could process the slurry faster than the batch with comparable size distribution. Mixing two solutions together yielded different sizes and shapes at different supersaturations but by adding glutamic acid to the process, some degree of shape control was achieved.

# Contents

# Index of Figures

# Index of tables

# Nomenclature and Glossary of Terminology

## Nomenclature

| | |
|---|---|
| $\alpha(t)$ | function of the surface age in penetration theory (eq.3.29) |
| $\beta$ | geometric shape factor |
| $\delta$ | film thickness (m) |
| $\gamma^s$ | surface energy ($J/m^2$) |
| $\varepsilon$ | specific dispersed power ($W.kg^{-1}$) |
| $\varepsilon_T$ | local energy dissipation rate/unit mass ($W.kg^{-1}$) |
| $\xi$ | zeta potential (mV) |
| $\theta$ | angle of inclination (degrees) |
| $\Theta$ | wetting angle |
| $\lambda_B$ | Batchelor concentration microscale (m) |
| $\lambda_k$ | Kolmogoroff microscale (m) |
| $\lambda_T$ | turbulent eddy size (m) |
| $\mu$ | liquid 'absolute' viscosity ($N.s.m^{-2}$) |
| $\nu$ | dynamic viscosity ($m^2.s^{-1}$) |
| $\rho$ | fluid density ($kg.m^{-3}$) |
| $\sigma$ | relative supersaturation, surface tension ($J/m^2$) |
| $\tau$ | shear stress ($N.m^{-2}$) |
| $\upsilon$ | molecular volume $m^3$ |
| $\phi$ | rate of absorption over whole disc ($mol.s^{-1}$) or affinity |
| $\omega$ | disc angular velocity $rad.s^{-1}$ |
| $\Delta c$ | concentration driving force ($mol.l^{-1}$ or $g.l^{-1}$) |
| $\Delta c_{met}$ | metastable concentration ($mol.l^{-1}$ or $g.l^{-1}$) |
| $\Delta[CO_2]_w$ | concentration driving force for the absorption process ($mol.l^{-1}$ or $g.l^{-1}$) |
| $\Delta G_{hom}$ | change in Gibbs energy associated to the homogeneous nucleation |
| $\Delta G_{het}$ | change in Gibbs energy associated to the heterogeneous nucleation |
| $[CO_2]_w$ | weight concentration of carbon dioxide in water ($mol.l^{-1}$ or $g.l^{-1}$) |
| $[CO_2]_w^*$ | concentration at the gas-liquid interface ($mol.l^{-1}$ or $g.l^{-1}$) |
| [OH-] | hydroxyl ion concentration in solution ($mol.l^{-1}$) |

| | |
|---|---|
| a | acceleration ($m.s^{-2}$) |
| A | area of film exposed to atmosphere ($m^2$) |
| $A_C$ | surface area of crystal ($m^2$) |
| $A_N$ | Surface area of nucleus ($m^2$) |
| B | overall nucleation rate or parameter in equation 3.27 defined in 3.28 |
| c | solution concentration ($mol.l^{-1}$) |
| c* | equilibrium saturation concentration ($mol.l^{-1}$) |
| $c_c$ | suspension density of the crystalline phase ($g.l^{-1}$) |
| $c_T$ | total concentration in the liquid phase |
| C | coefficient used in equation 9.10 |
| $C_i$ | solubility of gas in liquid ($mol.l^{-1}$) |
| D | diffusivity of $CO_2$ in the liquid ($m^2.s^{-1}$) |
| D[3,2] | Sauter mean diameter (μm) |
| $D_{10}$ | size of which 10% of particles are below {also expressed as D[v,0.1]} (μm) |
| $D_{50}$ | size of which 50% of particles are below {also expressed as D[v,0.5]} (μm) |
| $D_{90}$ | size of which 90% of particles are below {also expressed as D[v,0.9]} (μm) |
| $D_h$ | hydraulic diameter (m) |
| $D_i$ | impeller diameter (m) |
| $D_M$ | diffusion coefficient ($m^2.s^{-1}$) |
| $D_v$ | vessel diameter (m) |
| G | mass flow rate ($kg.s^{-1}$) |
| g | gravitational constant ($m.s^{-2}$) |
| $h_s$ | height of shell (m) |
| $H^*_{CO_2,w}$ | Henry's coefficient of CO2 in water ($atm.m^3/mol$) |
| J | homogeneous nucleation rate ($munber.s^{-1}$) |
| K | kinetic constant for the reaction $CO_{2(liq)} + OH^- \leftrightarrow HCO_3^-$ |
| K | parameter in eq 3.31 defined in 3.32 |
| $k_a$ | area shape factor |
| $k_v$ | volume shape factor |
| $K_G$ | overall growth coefficient |
| $k_L$ | liquid side mass transfer coefficient ($m.s^{-1}$) |
| $k_n$' | kinetic nucleation constant (eq. 3.36) |

| | |
|---|---|
| $K_{SP}$ | solubility product ($mol^2.m^{-6}$) |
| M | film conversion parameter |
| m | mass (kg) |
| $m_0$ | maximum particle concentration (used in figure 3.21) |
| N | rotational speed (rpm), number of molecules in an embryo/cluster |
| N* | critical nucleus size |
| $N_c$ | number of crystals formed |
| $N_w$ | overall mass transfer rate of $CO_2$ into water ($g.s^{-1}$) |
| P | total pressure (atm) |
| $P_f$ | power dissipated by fluid on the disc (W) |
| Q | liquid volumetric flowrate ($m^3.s^{-1}$) |
| r | radial position on disc (m) |
| $r_{crit}$ | critical particle radius (m) |
| Re | Reynolds Number |
| r | radius |
| $r_i$ | disc inner radius (m) |
| $r_o$ | disc outer radius (m) |
| S | supersaturation ratio |
| $S_0$ | initial supersaturation ratio |
| $S_{max}$ | maximum supersaturation from available solution concentrations |
| t | time (s) |
| $t_C$ | circulation time (s) |
| $t_{ind}$ | induction time (s) |
| $t_M$ | characteristic mixing time (m) |
| $t_R$ | characteristic reaction or nucleation time (s) |
| $t_{res\ shell}$ | residence time of film draining down shell wall (s) |
| $t_{res}$ | mean fluid residence time on disc surface (s) |
| u | radial velocity ($m.s^{-1}$) |
| $u_m$ | mean radial velocity ($m.s^{-1}$) |
| $V_{SDR}$ | volume of liquid on the SDR ($m^3$) |
| w | plane surface width (m) |
| $X_{OH^-}$ | conversion of hydroxyl ion |
| y | distance from gas liquid interface (m) |
| z | vertical position above surface (m) |

**subscripts**

| | |
|---|---|
| drop | droplet |
| f | fluid |
| G or g | gas |
| i | inner, initial |
| L or l | liquid |
| m | mean |
| o | outer |
| s | solid |
| w | water |
| y | distance from gas liquid interface |

**superscripts**

| | |
|---|---|
| n | kinetic order coefficient |

## Glossary of terminology

| | |
|---|---|
| ACC | amorphous calcium carbonate |
| API | active pharmaceutical ingredient |
| CHE | compact heat exchanger |
| CPI | chemical and process industries |
| CSD | crystal size distribution |
| GCC | ground calcium carbonate |
| HEC | hydroxyethyl cellulose |
| JIT | just-in-time |
| MSMPR | mixed suspension mixed product reactor |
| NTP | normal temperature and pressure |
| PCC | precipitated calcium carbonate |
| PEEK | poly ether ether ketone |
| PEG | poly(ethylene glycol) |
| PFCHE | polymer film compact heat exchanger |
| PI | process intensification |
| PS | potato starch |
| RPB | rotating packed bed |
| SCR | spinning cone reactor |
| SDR | spinning disc reactor |
| SEM | scanning electron microscope |
| TEM | transmission electron microscope |
| XRD | x-ray diffraction |

## Acknowledgements

The contributions of the following cannot be put into words; my eternal gratitude goes out to:

Dr Roshan Jachuck for his time and input, endless energy and burning enthusiasm whilst supervising me.

Dr Kamelia Boodhoo for her faith in me, stepping in as my supervisor and for giving me the support I needed to finally finished writing.

Prof. Colin Ramshaw whose teachings first sparked the curiosity in me to look beyond the borders of undergraduate engineering convention.

The EPSRC for funding the project and maintaining my student lifestyle for three years. For funding the Engineering Instrument Pool. For without the Mastersizer I would be a bit stuffed for data!

All the technical and clerical staff in the department and university for their time and effort especially Brian for all the times he came to fix something or advised.

To all my colleagues in the research group where ideas and discussion bounce around. Special thanks to Matt Scalley, Sarah Porritt and Giuliana Trippa for their significant collaborative input in generating ideas and participation in furthering the lab research in the topic area.

To all my friends, wherever they may be. For being there, putting up with me and letting us share a big belly laugh together, for without them I would have surely gone insane. You still don't really know what this was all about, do you!? Spinning disc DJ, here we go!

And finally, to my parents who have always let me go with my dreams and supported me to the last. I now have to pay it all back.

# 1 Introduction

The field of process intensification (PI) has been growing since its embryonic industrial beginnings in the 1970s. The underlying philosophy of PI is to get more out of the process however that may be achieved. By better knowledge of the physical characteristics of a process, new plant may be designed which is more compact, reducing capital cost; which is more efficient, leading to energy and raw material saving; which produces less waste, lessening environmental impact; which is more flexible, increasing the range of products made; which allows each molecule to experience the same physical effects, leading to better quality of the products. PI can contribute to each of these factors. In doing so, a number of PI related technologies are in research and development in research centres across the world. The next few years are key to the development and implementation of PI and to that effect academia and industry are collaborating in order to assess and deliver these technologies to world markets.

A key PI technology is the spinning disc reactor (SDR). A thin liquid film is propagated across the disc surface under the act of rotation. This highly sheared film is subjected to high rates of heat and mass transfer and exhibits very short residence times. It is from these characteristics that the SDR is seen to be beneficial to rapid chemical reactions whereby controlling reaction rate, residence time and mixing are crucial to making quality product. Processes such as crystallisation, and more specifically in the present study, precipitation may benefit from rapid mixing, fast depletion of reactants (rapid development and depletion of supersaturation) and short residence time in order to have better control of the size distribution and the shape of the crystals.

Calcium carbonate is a common material used in a plethora of products for a multitude of uses. The alkali paper industry uses a very large quantity in papermaking as a binder and as an optical brightener. Satellite precipitated calcium carbonate (PCC) plants produce material nearby in order to serve the industry. It is also a by-product of the water softening

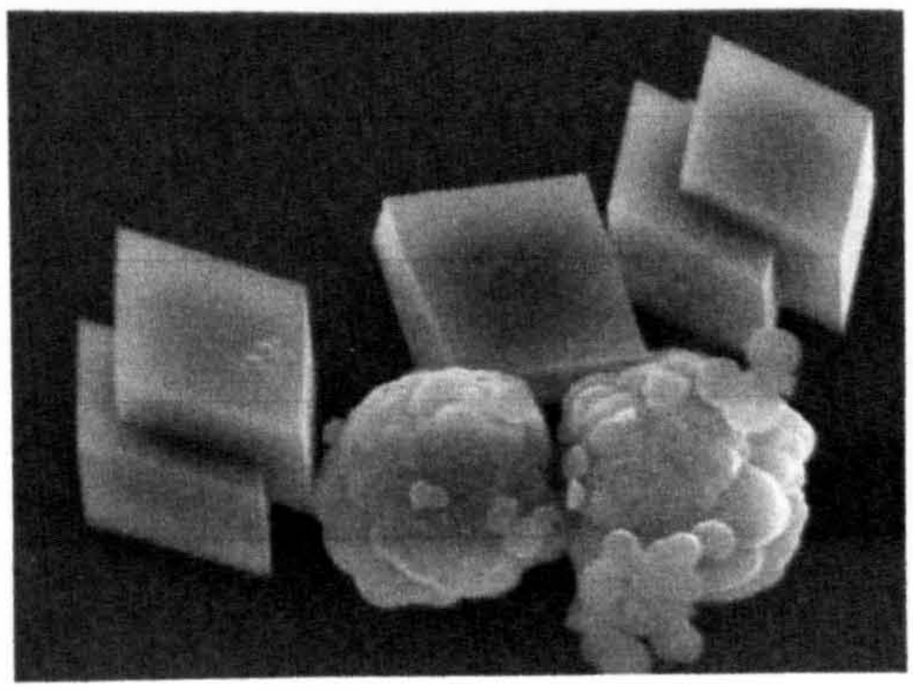

**Figure 1.1 Calcium carbonate of different morphologies formed during a reaction**

process and used in toothpastes, cosmetics, antacid remedies to name a few. The quantity of PCC produced per year is in the 'millions of tonnes' category yet specialty shapes and sizes are required for various products and are made in smaller quantities.

Herein lies the challenge for the SDR. It's compact size and mass transfer capabilities lend itself to the possibility of it becoming the heart of precipitation processes for small to medium scale whereby control of size and shape is important. In order to do so, it must effectively demonstrate its ability to control the size, size distribution and shape of the crystals being produced. Further to promoting better product quality, the SDR must be shown to reduce capital and operating costs in order for the broader range of PI philosophies to be met.

In the present study, the precipitation of calcium carbonate from three different process routes is investigated through literature and through experimentation in order to understand the underlying physical characteristics of the process and compare traditional batch precipitation methods with the continuous method the SDR presents. The three precipitation methods chosen are as follows:

- The carbonation of limewater (calcium hydroxide solution) using $CO_2$ gas.
- The carbonation of milk-of-lime (calcium hydroxide slurry) using $CO_2$ gas.
- The liquid-liquid precipitation from mixing calcium chloride and sodium carbonate solutions.

The key elements in each of these processes are rapid mixing and depletion of supersaturation and the morphology and nature of the precipitate formed.

The present study discusses the potential impact PI might have on modern industry. The fundamentals of the operation of the SDR and the mechanisms involved in precipitation are described. In carrying out a review of the present literature on the precipitation of calcium carbonate, knowledge of the process mechanisms and product are discussed. In studying the process routes through experimentation, comparisons can be made between the processing methods carried out in the literature and the experimental methods carried out in the laboratory. With the data from the present study to hand, the use of the SDR as a calcium carbonate precipitation device is discussed with view to it's future potential on the industrial scale.

# 2 Aims and objectives

The aims and objectives of the present study are set out below.

- To gain an in-depth knowledge of process intensification philosophy; its technologies, applications, strategy, benefits and future possibilities.
- To understand the operation of a spinning disc reactor; its applications, design andthe underlying physics of its fluid dynamics.
- To understand the phenomena and industrial application of precipitation of the solid phase from chemical reaction. To understand the kinetics of nucleation and growth of crystals as well as secondary processes, such as agglomeration and aging and to look at how process intensification techniques, especially spinning disc reactors might compliment these processes.
- To develop background knowledge of calcium carbonate; its structure, manufacture, applications and economics. To examine the research into its crystallisation kinetics; its polymorphology and synthesis routes. To examine the use of chemical additives by which might transform and control its shape and size.
- To set out an experimental study, comparing the spinning disc reactor operation to that of a conventional batch process. To develop experimental techniques to enable comparisons to be made. To examine a number of synthesis routes; gas-liquid, gas-liquid-solid and liquid-liquid. To determine the mass transfer rates of the different reactors employed. To determine the characteristics of the product formed; shape, size and size distribution. To examine these results by comparing them with relevant references where possible and reporting the findings herein.
- To discuss the outcomes of the work, making recommendations for future study of the topic. To discuss the suitability of a spinning disc reactor as a device for future crystallisation/precipitation processes.

# 3 Literature review

The aim of this chapter is to introduce the reader to the philosophies and technologies that process intensification represents. The operation of a spinning disc reactor (SDR) is described in detail. The basic principles of crystallisation and precipitation are presented along with the physical and chemical factors that influence its kinetics. Aspects of calcium carbonate chemistry and synthesis are reviewed. In completing the picture, previous precipitation work using SDR as a processing device is reviewed. It is with this information that the work that leads into the experimental section.

## *3.1 Introduction to the philosophy of process intensification*

### 3.1.1 The drivers for process intensification

The philosophies of Process Intensification (PI) in the chemical and process industries (CPI) were first explored in the 1970s. These came out of the need to reduce the rising capital cost of building chemical facilities. It was seen that the cost of the main plant items accounted for only 30 to 40% of the overall costs incurred. A large percentage of the rest involved the cost of the foundations, supporting structures and pipework required for each item. It was envisaged that by reducing the size of the main plant items, a significant reduction in the cost of supporting structures could be attained. (Ramshaw, 1983 and 1985) suggested that "telescoping" of equipment such that it would reduce main plant item size by up to a 1000-fold but still perform the same process function could have significant impact. This would not only reduce the size of the plant but also have a significant effect on safety and environmental factors. A smaller piece of equipment performing the same function would have a smaller fluid inventory, e.g. in the case of a distillation column, a large quantity of (say) flammable liquid is contained within the reboiler, which in the event of a leak poses a significant safety and environmental risk. A more compact reboiler unit and distillation vessel would have less risk associated with them. If we take the idea of reducing the size of a reboiler by 10 times, what was potentially tonnes of liquid escaping is now kilograms of liquid. Reduce the size by 100 times, and the risk involving the fluid is now reduced such that anybody involved with containing a leak is dealing with a few grams to a few kilograms.

### 3.1.2 The advantages of PI

Whenever feasible in the process design stage, it is desirable to eliminate or minimise process hazards (Hendershot, 2000). However, no engineering or management system can ever be perfect. PI has the opportunity to lead designers to more inherently safe processes by the action of reducing or eliminating chemical inventory and operating at more extreme process conditions.

Another environmental benefit of a PI plant is that it would be much smaller in height such that it could be contained within a 1 to 2 storey building, easily disguised behind a line of trees or bank of earth it therefore has a less imposing visual impact and therefore improves the perception of the chemical industry.

A consequence of the inflated oil prices of the early 1970s was there was a drive towards energy efficiency. In general terms, processing large volumes of fluids, mixing, heating, reacting, separating, recycling and storing requires a large amount of energy input. This problem is compounded by the heat losses through pipework and main plant item external surfaces. A smaller plant performing the same job would have higher rates of heat and mass transfer and have less pipework. Being more energy efficient would not only be an exercise in saving operating costs but would have lower environmental burden.

In Ramshaw's early vision of PI, the obstacles to overcome this progress are more to do with our own prejudices (i.e. mindset/attitude/cultural barriers) rather than fundamental technical difficulties. By decreasing the size of the modern process facility by such a large factor was somewhat radical in the eyes of many, however, others still advocate PI in ways that are more conservative. (Stankiewicz *et al*, 2000) suggests that even a two times reduction in plant size would have a significant impact on capital cost savings and such equipment would be more readily accepted as process intensification. Process intensification is not limited to the shrinking of process equipment but can be defined as the employment of novel apparatus and techniques to processes. In short, Stankiewicz defines, "any chemical engineering development that leads to a substantially smaller, cleaner and more energy efficient technology is process intensification".

### 3.1.3 How does PI fit in with other elements of process design?

During the 1970s, the offshore oil industry in the North Sea was experiencing a massive expansion in facilities and infrastructure. The cost of putting equipment on the deck of an oilrig was, and continues to be incredibly, expensive. Compact processing plant would maximise production per unit area of deck space. In a similar mould to process intensification are the ideas encompassed in process integration. This philosophy suggests that by incorporating two or more unit operations together (e.g., a distillation column integrates with its reboiler and condenser) there would be a saving in space and weight and would lead to greater energy efficiency. This was born out of the integration of heat exchanger networks for heat recovery, reducing the number of heat exchanger units required on a process plant. Further to this, multifunctional unit operations in one unit are being investigated. Reactive distillation is one example where reaction and separation are all carried out within a single column thus making the need for a separate reactor vessel redundant. (Stankiewicz *et al*, 2000) highlights a task-integrated methyl acetate column incorporating elements of reaction and distillation, which replaced the conventional system made up of eleven separate distillation columns, reactors and stream mixers. The catalyst supported on packing within the column is continually converting reactants and being separated by the fractionation process thus overcoming equilibrium limitations. The application of reactive distillation is now commonplace in the CPI.

### 3.1.4 PI in today's CPI

Bringing PI into the present day climate, there are additional drivers for the processing sectors to embrace compact technologies. It seems somewhat odd that in the electronics industry, the push towards smaller and smaller components has continued unhindered for over 50 years. In contrast, in the chemical industry, little change has been seen in the size of equipment during this period. In fact, facilities and individual unit operations have only appeared to get larger to accommodate higher production throughputs, which are an advantage of economies of scale. The new drivers for chemical and process engineers have been centred on producing better and more consistent quality product. This has been sought mainly through automation and process control methods. Small incremental changes have been made in the process technology, as new techniques become known. Powerful computing allows for the

monitoring of many process variables, which can be statistically analysed allowing the root cause of a problem or defect to be found from a sea of data. Advanced process control modelling has allowed for predictive methods of operating the plant, which has facilitated better control of process variables during day-to-day operations. This has allowed for better productivity of both continuous and batch processes but also has reduced the number of staff required to operate the plant at any given time. At present, control technologies have matured and such automation is commonplace throughout industry.

Any technology that can increase reaction conversion and selectivity, reduces the downstream burden of separating, recycling and treatment of materials would benefit the operator. This would have a significant benefit to the environment, as it would reduce energy usage. A technology utilising aspects of 'green chemistry' such that the process does not require a potentially harmful chemical in its manufacture would again benefit health, safety and the environment. Today there is a drive towards using greener chemicals in all aspects of manufacturing and in industrial, commercial and domestic usage. It has been shown that PI technologies can compliment aspects of green chemistry in such process areas as catalysts and solvent-less reactions.

In recent times, technologies that are radically different to current methods have been demonstrated by the Process Intensification and Innovation Centre at Newcastle University. Other workers around the world are also demonstrating fresh approaches to process technologies, which fall under the banner of process intensification.

Future process technologies will wholly incorporate the philosophies of process intensification, process integration, advanced process control and green chemistry to allow the design and operation of future facilities such that they are cleaner, greener and meaner than today's counterparts.

## 3.2 *Overview of some PI technologies*

The achievement of PI relies on the enhancement by orders of magnitude of process equipment performance by active (e.g. agitation, vibration and rotation) or passive methods (e.g. roughening of surfaces, addition of fins, machining of grooves). In order for it to be successful, it must be capable of being applied to all types of process equipment i.e. reactors, mixers, separators and heat transfer equipment such that an entire plant and all of it's unit operations would be intensified. Almost all unit operations employ some form of heat/mass/momentum transfer - so enhancing these transport properties is the key to process intensification. Below are some examples of process intensification.

### 3.2.1 Compact heat exchangers

Intensification of heat exchange operations has been commonplace for many years in the CPI. The enhancement of heat transfer processes has been undertaken without applying the term process intensification to this activity, yet it employs the philosophy of getting more out of the space or unit operation in question (hence 'compact heat exchanger' (CHE)). A typical example might be the enhancement of heat transfer in pool boiling apparatus by the application of a sintered metal coating to the heat transfer surface. Enhancement can be made to shell and tube heat exchangers by the use of fins on the external walls of tubes, by the insertion of baffles in the shell or by inserting mesh or angled surfaces within the tubes to create more turbulence to enhance heat transfer. These enhancements will have some bearing upon operating cost due to the increase in pressure drop exerted by these surfaces. However, increased pressure drop may be offset by reduced capital cost and higher thermal efficiency. The use of compact heat exchangers has been employed in industry for decades. Plate-frame, plate-fin in cross-flow and counter-current flow arrangements or spiral configurations have a much larger heat transfer surface per unit area than the conventional shell and tube type. Cross-corrugated heat exchangers are very compact and have the advantage of high mechanical strength. Flow passages associated with compact heat exchangers are typically small ($D_h \leq 5mm$) and the flow is usually laminar.

These cross-corrugated types have conventionally been manufactured from metal, however it has been demonstrated that they can been made of thin corrugated sheets of polymer such as PEEK (Poly Ether Ether Ketone) and yet still perform exceptionally well (Burns and Jachuck, 2001). The thin sheets (approximately 100μm thick) facilitate a low conductive resistance. PEEK offers mechanical strength and robustness capable of withstanding 10bar pressure at room temperature and operates up to 220°C along with exhibiting excellent corrosion resistance.

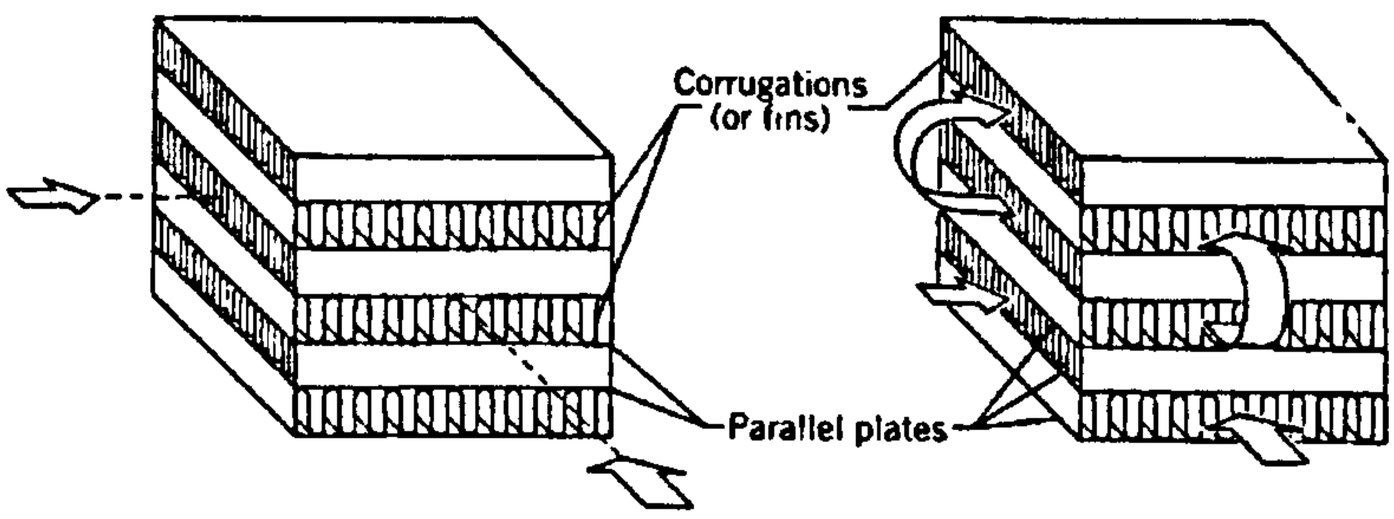


**Figure 3.1 Cross-corrugated plate fin heat exchanger (Incropera & Dewitt, 1990 pg. 600)**

A polymer exchanger is also lighter than a metal one that performs the same duty. This would be an advantage in aviation, transport or offshore applications, whereby a weight saving would be of benefit. Moreover, the fouling characteristics should be superior to those of metal due to the smooth hydrophobic surfaces of the polymer. The polymer sheets may be made porous to act as a membrane that would open up possibilities of separation and reaction within the heat exchange matrix allowing for multifunctionality. Catalytic properties could be added to the exchangers surfaces to allow the device to perform as reactor. Other polymers or plastic composites could be employed to improve upon performance. These Polymer Film Compact Heat Exchangers (PFCHE) with their high heat transfer surface per unit area, robustness and performance could be employed in many and varied applications.

### 3.2.2 Microreactors

Narrow channelled microreactors offer opportunities as processing equipment for rapid reactions in heterogeneous liquid-liquid reactions. Narrow channels can be manufactured by a variety of methods to give a channel width in the region of 10 to 1000μm. The channels may be etched (mechanically or chemically) into metal, glass or plastic sheets. A sheet is placed on top to enclose the channel. In addition, a

capillary tube may be employed in the same fashion. In this region of channel width, liquid flow is generally laminar with diffusion being the main controlling factor in heat and mass transfer. The benefit of using narrow channels is the high mass and heat transfer rates due to the short diffusion path lengths. Flow in the channel is very low; in the region of 0.1μl/s. Scaling up of the equipment requires the use of many channels in parallel such that each channel is an individual reactor, which has identical conditions as all the other channels. (Burns & Ramshaw, 1999) showed that highly exothermic nitration reactions can be performed in these single channel devices and hypothesise that scale-up to a multi-channelled device would require heat transfer equipment to control the temperature in the channels. Conceivably, it is possible that compact heat exchanger units could be integrated with microreactor plates to perform such a task. Rapid heat removal and control of temperature is key to the operation of exothermic reactions to prevent potential explosion hazards and by-product formation. With such tiny reactant volume inventory in a microreactor, the inherent safety of such a device greatly reduces any potential hazard.

(Burns & Ramshaw, 2001) demonstrated different flow regimes are obtainable within the channel. Not only can two immiscible liquids operate in parallel flow to each other but they can also be induced into a slug flow regime such that the length of the slugs can be controlled. It was seen that each slug of liquid creates an internal circulation as it moves along the channel and enhances the convective mass transfer between phases.

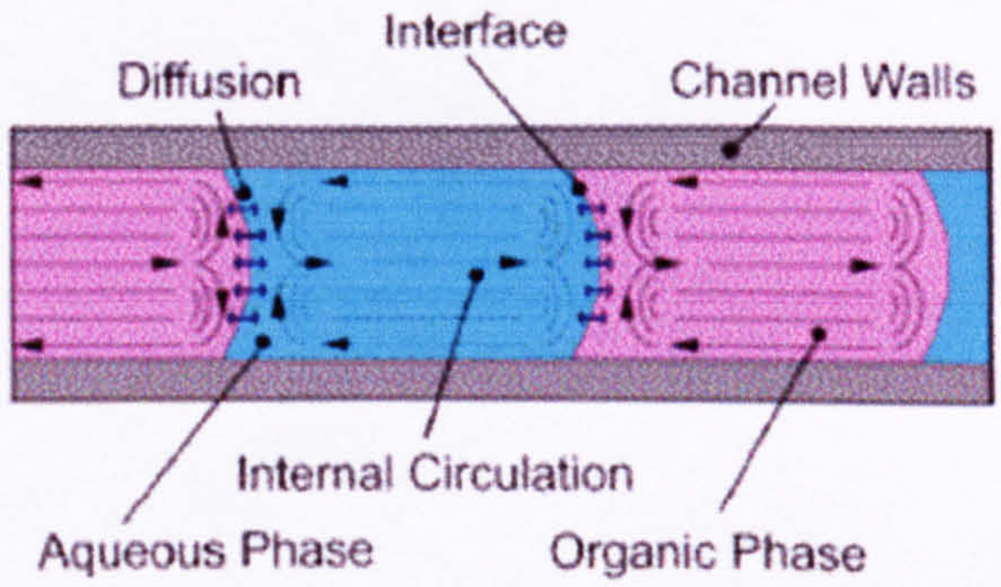


**Figure 3.2 Slug flow in a microchannel (Burns & Ramshaw, 2001)**

The potential of these microreactors as compact portable devices in the CPI is for high value, low volume products, with such a role in pharmaceutical development and manufacture or in the inherently safe processing of exothermic products. It is possible that micro-electronic components (e.g. miniature pumps, valves and sensors) could be incorporated within the channels creating a truly miniature process/laboratory facility

on (say) a credit card sized unit, commonly known as 'lab-on-a-chip'. In the mode of a chemical production device, a multi-channelled microreactor has mechanical design hurdles to overcome in manifolding many channels together in one unit such that the flow regime in each is the same. 'Lab-on-a-chip' devices may find themselves in portable analysis instruments (Saxl, 2000). Strands of DNA could be incorporated into the channels whereby they become diagnostic sensors to therapeutic applications. Miniaturising the analytical process has the benefit of both reducing costs of analysis, as well as dramatically speeding it up, making it possible to identify disease or pollutants within minutes. These techniques will quickly displace conventional analytical methods where samples are sent to a laboratory and put though labour intensive processes that may take several hours to achieve a result.

### 3.2.3 Rotating packed beds or 'hi-gee'

Conventional, classically designed packed towers are used for different mass transfer operations such as distillation and absorption. The tower consists of a vertically positioned cylindrical shell filled with packing. This packing may be randomly filled or of a structured nature. Liquid enters at the top of packed column and flows downward under the influence of gravity. The gas enters at the bottom and flows upward through the packing. Thus, a counter-current mass transfer takes place and the packing provides for a high area for mass transfer contact. The gravitational acceleration is constant throughout the packing and the pressure drop is due to drag forces exerted by the fluids on each other and by the packing on the fluids. The efficiency of the packed tower for mass transfer depends upon specific area of packing and liquid irrigation rates.

A rotating packed bed (RPB) or 'hi-gee' mass transfer machine has different shape and operation mode (Ramshaw, 1983). The Higee machine consists of a torus (or 'doughnut-shaped') rotor, which is mounted on a shaft, and filled with high specific area packing. Gas enters under pressure from the packing periphery, flows radially inwards, and passes through the rotating material before exiting through the centre eye. Liquid is sprayed through a nozzle into the centre of the packing and propagates radially outwards through the packing under the influence of centrifugal force. The liquid, moving counter-currently to the vapour exits at the periphery. Rotational speed gives an extra degree of freedom, e.g. by selecting a specific rotational speed; both the residence time and thickness of mass transfer film can be controlled.

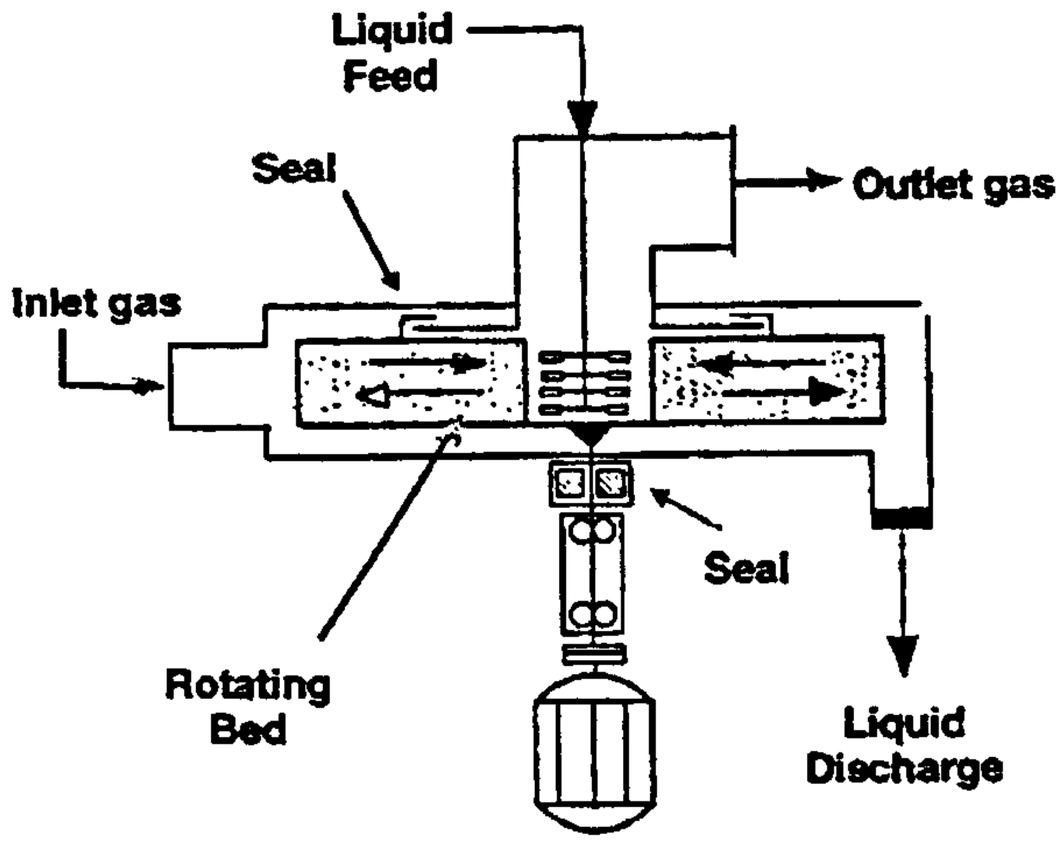


**Figure 3.3 Rotating packed bed schematic**

By imposing high acceleration fields upon the fluids, thinner films for mass transfer result in higher rates of mass transfer when coupled with packings of high voidage and high specific surface area. Mass transfer operations e.g. distillation, absorption, stripping and liquid-liquid extraction found in conventional packed towers can be carried out in a RPB.

(Kelleher & Fair, 1996) tested a pilot scale RPB distillation of a cyclohexane/n-butane mixture operating at rotational speeds in the range 400 to 1200rpm. They observed that the mass transfer efficiency increased with rotational speed and the amount of packing required for a given separation is lower in a RPB than for conventional columns.

(Balasundaram *et al*, 1990) and (Peel, 1998) developed the RPB as a seawater de-aerator to be used in offshore operations. Seawater is pumped into the wells to maintain pressure. Removal of oxygen from seawater reduces the fouling of pipelines from biological material found in wells. The compact nature of a RPB makes it suitable for offshore applications due to its low weight and compact nature, which would reduce the premium capital cost of offshore equipment.

A successful commercial application of the device has been described by (Trent *et al*, 2001). Here a RPB was used in the production of low-chloride hypochlorous acid (HOCl). The rapid mass transfer rates involved with the RPB allowed for the device to operate as a reactive stripping unit. This lead to high product yields in excess of 90%. Conventional equipment was only capable of a yield below 80% in a tower in the

region of 50m in height. The RPB in comparison was very much smaller demonstrating the PI philosophy that "small is beautiful" (and probably cheaper to construct!). With regards to its reliability, little maintenance has been required and the machine has proved easy to start up and shut down during a year of "full-scale production".

(Chen *et al*, 2000) studied the precipitation of particles in multiphase reaction systems operating within a RPB. In the case of the precipitation of $CaCO_3$, they reported particle sizes in the order of 20 to 50nm in size. Not only were these particles much smaller in size and of tighter size distribution than those made from conventional batch techniques but also the processing times were considerably reduced using their RPB method. This paper is of double interest for the present study. Not only is it of interest of using a PI method for precipitation but also the particle sizes of $CaCO_3$ they are claiming are far smaller than every other author has reported on the subject. Accordingly, this paper will be discussed further once other concepts have been introduced in this section.

### 3.2.4 Spinning disc reactors

Spinning disc reactors (SDR) operate on a similar principle as RPB. The disc can be horizontally or vertically mounted on an axle. Liquid fed near or at the centre flows across the surface of a spinning disc under the influence of centrifugal force. This force stretches and contorts the film. The thin liquid film allows for high rates of mass transfer such that it favours absorption, stripping, mixing and reaction processes. Residence times on the disc are low, typically in the range of 3 seconds down to tenths of a second. Both film thickness and residence time are dependent on fluid physical properties, rotational speed and radial location of the fluid. On exiting the periphery of the disc, the liquid is thrown onto an enclosing wall whereupon it drains away. Heating or cooling can be applied to the disc surface and the enclosing wall in order to control reaction temperature.

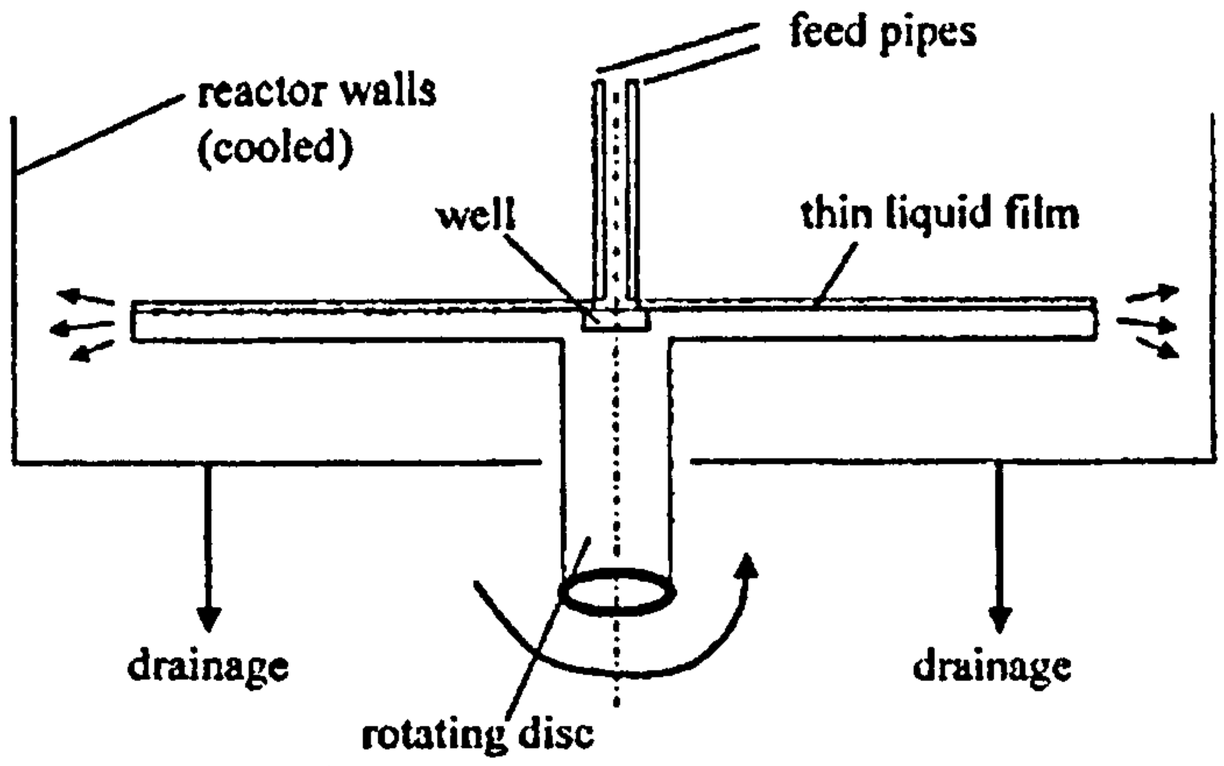


**Figure 3.4 Spinning disc reactor schematic**

The operation of SDRs will be covered in more detail later on in this chapter.

### 3.2.5 Miscellaneous equipment examples

Static mixers have come to the fore in the chemical industry over the past two decades (Stankiewicz *et al*, 2000). They offer more size and energy efficient methods of contacting fluids over mechanically agitated devices. Sulzer manufacture a static mixer, which incorporates mixing elements made from heat transfer tubes allowing the device to become multifunctional. Furthermore, it is possible to support catalyst on the structured packing elements however the disadvantage in catalytic reactor-mixer mode is the device's relatively low specific geometric area.

Monolithic substrates made from metallic and non-metallic structures provide a multiple narrow channel body of defined uniform cross sectional shape whereupon catalyst may be supported. Important features of the monolith are low pressure drop in single and two-phase flow compared to conventional packed bed systems, high geometric area per reactor, high catalytic efficiency due to short diffusional path lengths and good performance in processes in which selectivity is hampered by mass transfer resistances. Monolithic catalysts may be installed in-line, like static mixing elements, having the advantage of lower investment costs; more compact plant design; easier replacement (it is designed as a length of pipe); the possibility of installing multiple feed points along its length; easy attainment of near-to-plug-flow regime. (Stankiewicz *et al*, 2000) reports an example of a monolithic unit replacing a conventional device with an approximately 100-fold decrease in reactor size.

### 3.2.6 Energy field effects

As examples of passive mechanical enhancement of mass and heat transfer such as extending a surface by roughening or adding structured elements such as fins and grooves, active mechanical enhancement has been demonstrated by the use of rotation and agitation. However, alongside these mechanical methods of process improvement as means to realising PI other effects may also be considered.

Power ultrasound has been employed in reactors to help initiate crystallisation and some chemical reactions by the cavitation of very small bubbles (Stankiewicz *et al*, 2000). These cavities can be thought of as high-energy microreactors. A collapsing bubble releases very high local energy release reported to be as high as 5000°K and negative pressures of up to 10,000atm. Usually this involves the immersion of an ultrasonic horn in a body of liquid i.e. the reactor vessel. By (say) attaching the horn to a liquid feed pipe onto an SDR, the ultrasonic waves could be used in thin film processes.

The electromagnetic spectrum can also be employed along with mechanical methods in a reactor. In the case of an SDR, the large surface are presented on the top of the continuous film flowing across the disc enables direct exposure of a radiant field produced in the infrared, ultraviolet, microwave or even X-ray wavelengths. This radiation may be used to initiate and sustain polymerisation reactions or to denature biological or chemical contaminants due to the thin film mixing and exposure. The SDR is seen as perhaps a key reactor-type in this field as it is capable of exposing all its reaction volume to the radiation as the radiation tends to have a maximum penetration depth of 1-2mm in a bulk fluid.

By finding the most suitable energy form in the correct range of wavelength and intensity the process can be further optimised.

## 3.3 The impact of PI on 21st century technology?

Process intensification equipment and methods have been highlighted above. In summary, many forms of implementing PI exist and are in development. (Stankiewicz *et al*, 2000) has collated these in tabular form, reproduced below.

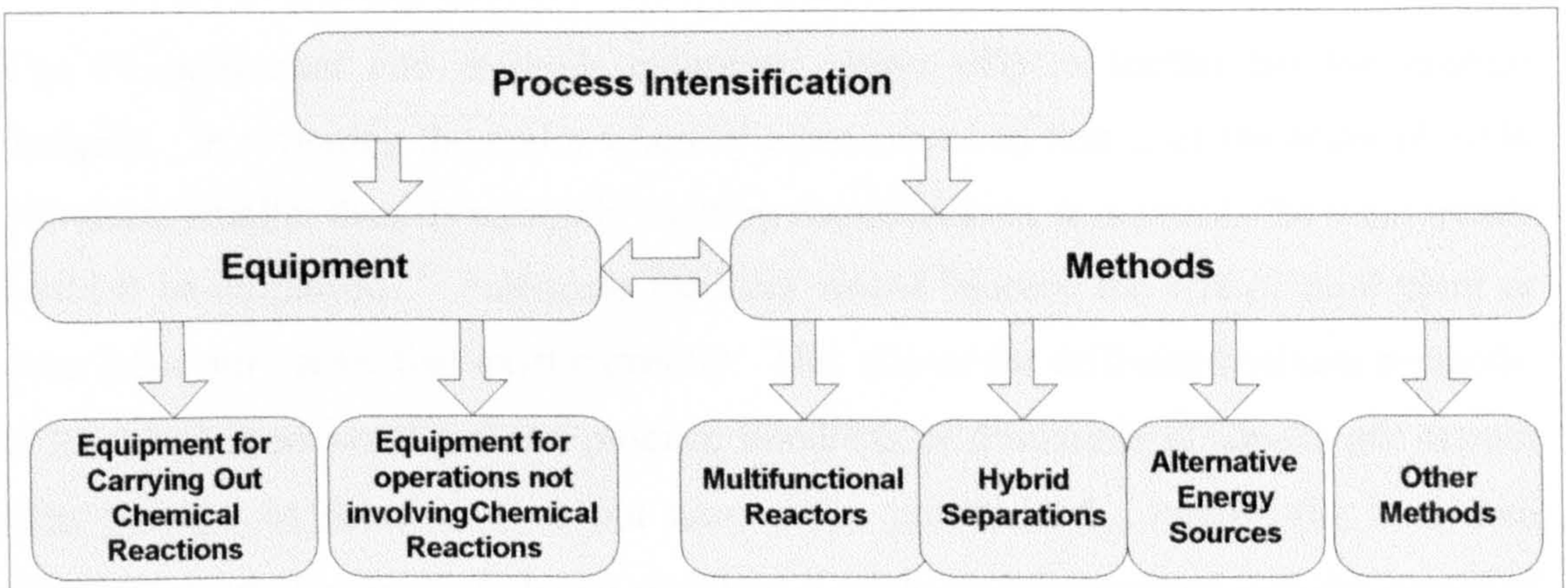


Examples

| | | | | | |
|---|---|---|---|---|---|
| spinning disc reactor (SDR) | static mixers | reverse flow reactors | membrane absorption | centrifugal fields | supercritical fluids |
| static mixer reactor (SMR) | compact heat exchangers | reactive distillation | | ultrasound | dynamic/periodic reactor operation |
| static mixing catalysts | microchannel heat exchangers | reactive extraction | membrane distillation | solar energy | |
| KATAPAKs | rotor/stator mixers | reactive crystallisation | | microwaves | |
| monolythic reactors | rotating packed beds | chromographic reactors | adsorptive distillation | electric fields | |
| microreactors | centrifugal adsorber | periodic separating reactors | | plasma technology | |
| heat exchange reactors (HEX) | | membrane reactors | | | |
| supersonic gas-liquid reactor | | reactive extrusion | | | |
| jet-impingement reactor | | reactive commintion | | | |
| rotating packed bed reactor | | fuel cells | | | |

reproduced from Stankiewicz et al, 2000

**Figure 3.5 Process Intensification Equipment and Methods (Stankiewicz *et al*, 2000)**

In considering the development of PI processes, immediate advantages of their implementation over current technologies must be sought. (Keller, 2000) highlights the seven themes for process design improvements in the future in order for cost-effective production to continue. They are:

- Raw material cost reduction
- Capital investment reduction
- Energy use reduction
- Increased process flexibility and inventory reduction

- Ever greater emphasis on process safety
- Increased attention to quality
- Better environmental performance

Further exploring, it may be seen that PI involves itself in each of these themes.

The PI equipment and methods examined above offer a toolkit for the process designer. In revisiting the realm whereby a process plant that is of the order of 10 to 100 times smaller than its currently existing counterpart is, it is asked, "by what means could it be employed?" Full-scale facilities would become the size of pilot plant or even laboratory scale that exist currently. This allows for different business methods. If the plant is so small yet can produce hundreds or thousands of tonnes per annum then perhaps its location does not have to be constrained. Firstly, the land area footprint would be greatly reduced such that it could be incorporated into the corner of an existing site rather than to look for a new one – reducing transport costs and handling hazards. Lower chemical inventories may allow for planning consent in areas where it would not normally be given. It is possible for intensified plant to be moved around the globe to a location where it is most needed or is closest to its customer or raw material base. This raises the possibility of 'distributed manufacturing' allowing the processes to go where the current demand is rather than restricting location, shipping in raw materials and exporting products. Transport costs would be reduced if a product were made locally. Secondly, the capital cost should be greatly reduced due to the lower costs of structural and civil engineering work and the smaller amount of process pipework required. Complimentary to this, such a plant could be made of materials that are more 'exotic', its small size allowing these to be used cost effectively, allowing for a longer plant lifetime. Thirdly, operating costs would be lower; the exotic materials employed could facilitate lower corrosion rates and better catalysts. Lower recycling rates and therefore lower energy cost due to higher reaction conversion and selectivity reduces the size of pipework, pumping and separation equipment (that would be intensified as well). A higher percentage of on-specification products can be synthesised. These would allow for lower environmental burden, less waste and less energy used.

As a consequence of developing compact plant, it is possible that full-scale facilities today could be accommodated into lab sized facilities tomorrow. This would allow for

development chemists and technologists to work on the process scale from the inception of the project. A process of 'scale out' rather than 'scale up' could be engaged e.g. banks of modular spinning disc reactors or micro reactors could be employed all of which were the same size of the lab test rig and running under identical chemical and physical kinetic conditions. The kinetics of reactions examined in the lab would match that of the production plant. 'Plug and play' additions in capacity could be carried out when new process modules are required. Process modules could be chopped and changed to cater for a change of product grade as a response to market demand. As a result, shorter times to market of a product could be attained due to the reduced development time i.e. lab scale development could lead directly to production rather than the traditional lab to pilot plant to production plant route that is traditionally followed.

Opportunities would exist for niche applications, on-site manufacturing of small (or very small) amounts of product e.g. intermediates, catalysts, electronics chemicals, polymer fillers, essences and fragrances rather than buying in expensive product. Operators can add their own value to the raw materials. Better control and reliance of their own product allows for in-house product development faster than relying on outside sourcing of intermediate materials.

Under traditional design methodologies, a choice has to be made between batch and continuous processes. PI technologies could offer better flexibility and operability of both methods with shorter turnaround time for multiple product plant. This can facilitate Just-In-Time (JIT) manufacturing. Currently, large centralized production plants store large quantities of a few grades ("you can have any colour as long as its black") of product in warehouses. This is inefficient as some is lost, some goes off etc. It also means that a part of the money is tied up in stock – a big problem for some businesses. Instead, as a result of flexible PI modules, products could be made to order and reduce warehousing and intermediate storage. Grade changes can be made quickly, and new grades can be made to better suit the customer. New operating regimes offered by PI modules can act as a powerful driver for making new products that just cannot be accomplished with traditional bits of chemical kit.

A seed has been sown to revolutionise process technologies that may find applications outside the chemical and process industries, such as the built environment, healthcare,

air conditioning and power for homes and business, aerospace, transport and environmental protection. A paradigm shift in these technologies may present endless possibilities and advantages to mankind and the global environment.

## 3.4 The spinning disc reactor: fundamentals, design and operation

### 3.4.1 Fundamentals of SDR operation

Historical reference can be made to spinning discs used for mass transfer operations in the NASA space program (Rahman & Faghri, 1993). In space, conventional mass transfer contacting devices are unsuitable because the driving force of a liquid flowing under gravitational force cannot be performed in 'low g' or 'zero g' conditions. Research was undertaken into the use of such a device to generate centrifugal forces upon a liquid such that it generated a thin film for a mass transfer operation to occur.

Terrestrial applications of elevated 'g' are becoming known and have potential in the CPI. As previously discussed, spinning disc reactors (SDR) operate on a similar principle as rotating packed beds. Liquid is fed near or at the centre and flows as a continuous film across the surface of a horizontally or vertically mounted spinning disc under the influence of centrifugal force. This force stretches and contorts the film. The thin liquid film allows for high rates of mass transfer. Residence times on the disc are low, typically in the range of a few seconds down to tenths of a second. Both film thickness and residence times are dependent on fluid physical properties, rotational speed and the radial location of the fluid. On exiting the periphery of the disc, the liquid is thrown onto an enclosing shell wall whereupon it drains away. Heating or cooling can be applied to both the disc surface and the enclosing shell wall in order to control reaction temperature.

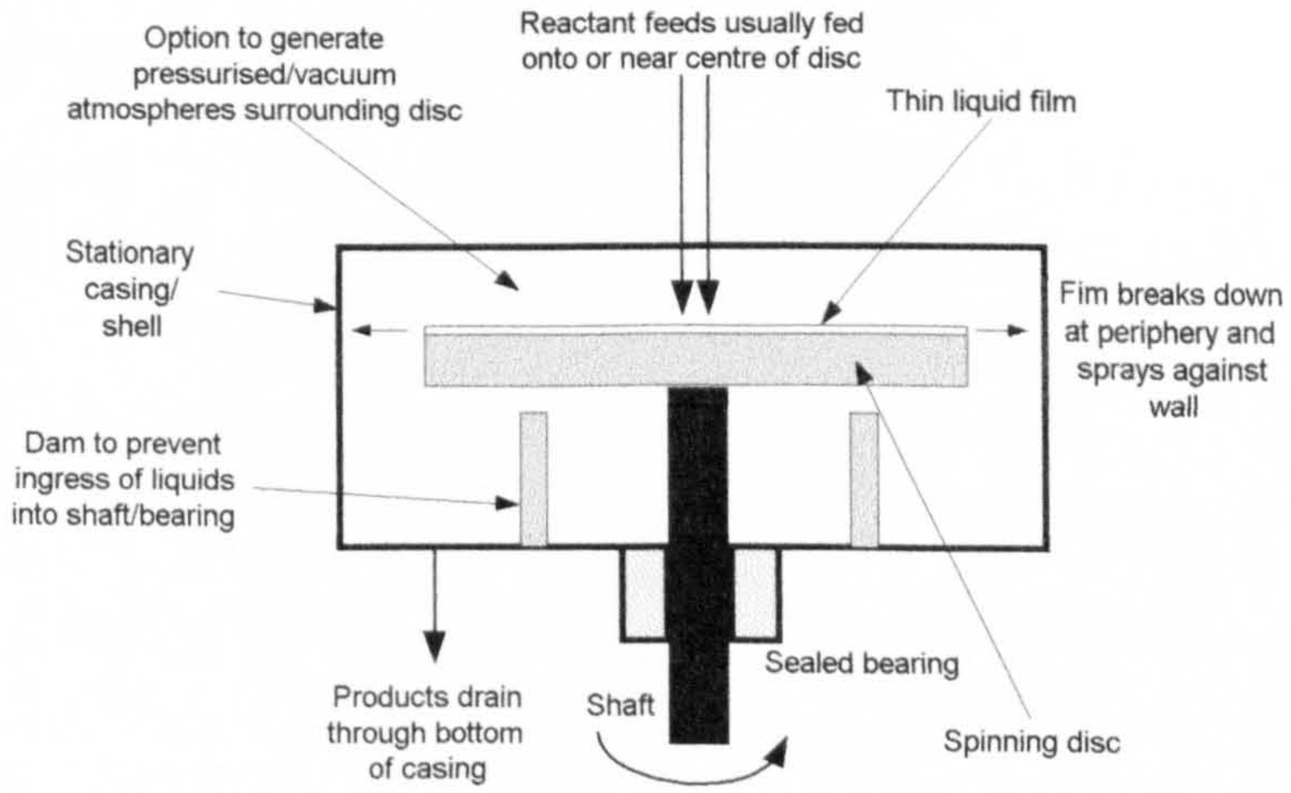


**Figure 3.6 General layout of spinning disc reactor**

### 3.4.2 Hydrodynamic characteristics of thin film flow on a spinning disc

Terrestrial gravity affects most chemical engineering systems. An example would be a thin film falling down the wall of a column. The film thickness is inversely proportional to the applied force in the direction of the flow (i.e. in this case downwards due to gravity). A thinner film of fluid can be obtained by increasing the force applied. This will give rise to increased mass transfer in the film due to the smaller distance through which diffusion has to occur. On earth, the force on a system in the vertical axis is limited to that of terrestrial gravity. The spinning disc concept is an attempt to take advantage of the effects of elevated gravitational force to achieve the aims of the PI philosophy.

A fluid on a horizontal rotating disc will experience a force radially outwards proportional to the rotational speed of the disc and the radial distance of the fluid from the axis of the disc. Thus, the force on the fluid can be controlled by the rotational speed of the disc and hence a centrifugal force greater than that of gravity can be applied to the fluid in the horizontal direction. Therefore, a thin film of fluid will result, which will have high mass and heat transfer characteristics as the diffusional path lengths are significantly reduced.

The thin film flow on the disc surface as it moves from the centre to the periphery is intrinsically unstable. This instability results in minor disturbances being amplified to generate a chaotic system of ripples and wavelets. (Brauner and Maron, 1982) explained that the creation of surface waves of a fluid flowing down an inclined plane results in higher rates of heat and mass transfer than predicted by diffusion alone. Surface waves form with accompanied sub-surface turbulent eddies. These swirling eddies enhance the transport rates due to their convective mixing properties. This effect will have significant effect upon heat and mass transfer performance on an SDR although the influence of the ripples upon mass transfer enhancement is not currently described sufficiently by the hydrodynamic model equations. This is due to the appearance of the waves apparently at random, which depend upon rotational speed, flowrate, radial position, the fluid properties and the nature of the disc surface. As the fluid propagates outward from the centre, the area for flow is increased and the film thickness changes along with the average velocity of the fluid. The changing radius affects the Reynolds Number of the fluid. The Reynolds Number of the fluid on the disc surface is described as:

$$\mathrm{Re} = \frac{2\rho Q}{\pi\mu r} = \frac{2.Q}{\pi.\upsilon.r} \qquad (3.1)$$

Under certain conditions, the flow regime may change from laminar to turbulent as the fluid propagates across the disc. The criteria governing the type of flow (smooth laminar, wavy laminar and turbulent) obtained on a plane vertical surface have been measured experimentally by several researchers in terms of the Reynolds number defined by (Brauer, 1958) as:

$\mathrm{Re} < 4$: smooth laminar flow (no surface waves)

$4 \leq \mathrm{Re} < 10$: Undulations across the film (small amplitude waves)

$10 \leq \mathrm{Re} < 20$: Sinusoidal waves gradually replaces by regular waves

$20 \leq \mathrm{Re}$: Random surface waves

Several workers have observed surface waves on an SDR. During the present study, the author performed experiments on water flowing across the SDR (the same disc equipment employed by (Woods, 1995) using high-speed video capture of the motion of the waves as they propagated across the disc surface under different flow and rotational speed conditions. Still pictures obtained from the video are used to illustrate the nature of the waves.

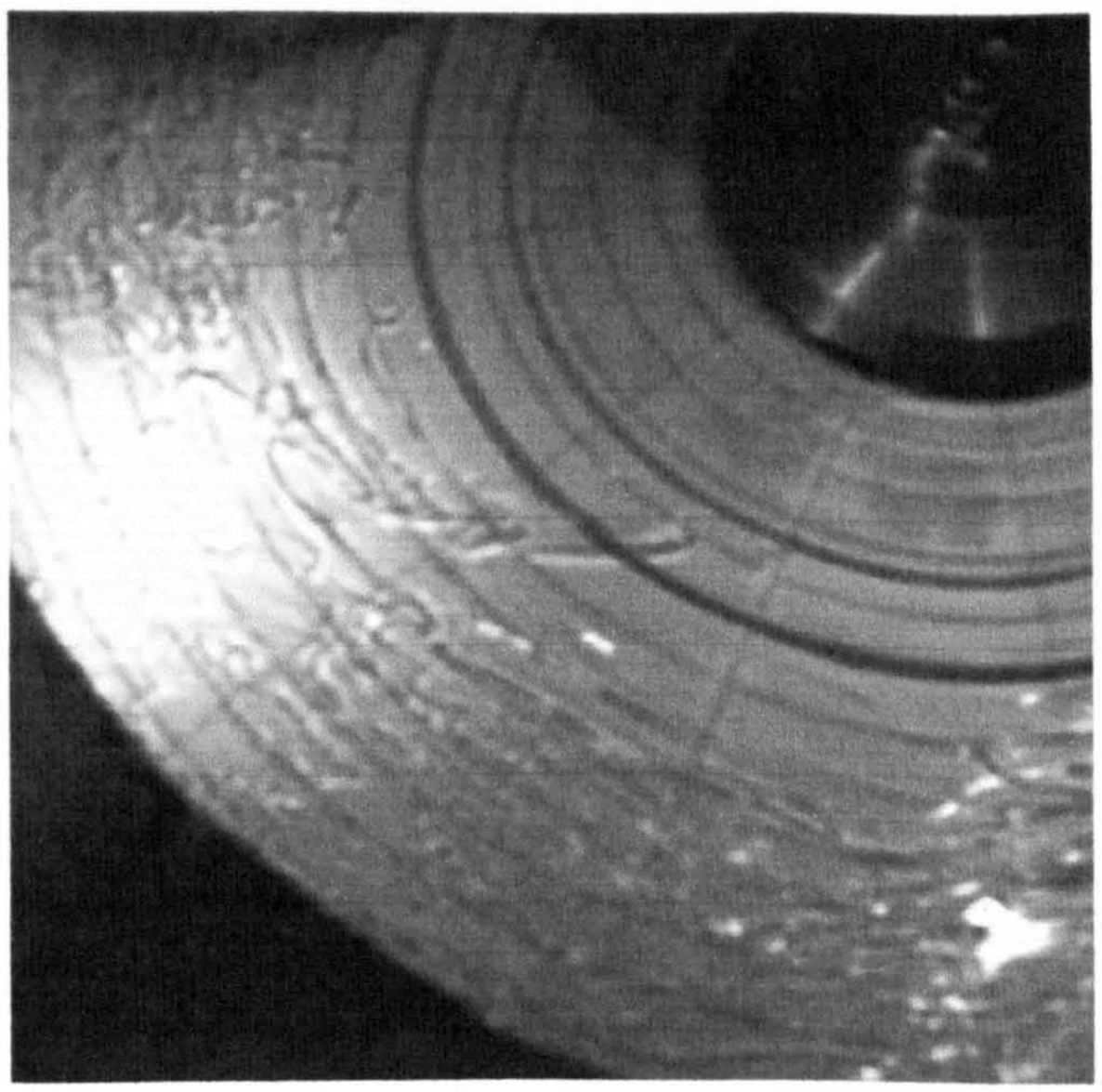

**Figure 3.7 Random wave propagation of water on a spinning disc**

Here we can see in figure 3.7 the random nature of the surface waves of water flowing from a central distributor on a spinning disc. Toward the centre, there are no waves however as the flow moves radially outward, the waves become more abundant and randomised. The number of waves observed on the disc surface increased with both increasing flow rate and rotational speed.

### 3.4.3 The spinning disc hydrodynamic model

The simplest model to describe the flow of liquid on the surface of a spinning disc is derived from the 'Nusselt' approach whereby the film is assumed to be laminar and circumferentially uniform. This is also termed the centrifugal model since it takes into account radial acceleration. It is not the author's intention to present the full mathematical derivation of the hydrodynamic model here. A full mathematical derivation may be found in (Woods, 1995). Presented here will be an explanation of the equations and terms required to describe the flow parameters on the disc from known variables. Other workers have presented the equations (Wood & Watts, 1973) (Moore, 1986) (Aoune and Ramshaw, 1998) (Khan, 1986) when describing their work. An example will be used to illustrate how the flow parameters change as the film propagates across the disc surface.

#### 3.4.3.1 Film thickness and film velocity

The Nusselt model (as described by Wood and Watts, 1973) assumes that the flow on a spinning disc is analogous to the fully developed laminar flow of a liquid film flowing down a vertical wall, thus the equation for such film flow are used with the gravitational constant g replaced by $r\omega^2$. Using this model, the film thickness, δ at radial position, $r$, is given by:

$$\delta = \left( \frac{3.\mu.Q}{2.\pi.r^{2}.\varpi^{2}.\rho} \right)^{\frac{1}{3}} \qquad (3.2)$$

where the angular velocity, ω, is defined in terms of the rotational speed of the disc, $N$:

$$\varpi = \frac{2.\pi.N}{60} \qquad (3.3)$$

and the local radial velocity at distance $z$ above the surface by:

$$u = 3.\mathcal{U}_m.\left[\frac{z}{\delta} - \frac{1}{2}.\left(\frac{z}{\delta}\right)^2\right] \qquad (3.4)$$

where the mean radial velocity:

$$\mathcal{U}_m = \frac{Q}{2.\pi.r.\delta} = \left(\frac{\rho.\varpi^2.Q^2}{12.\pi.r.\mu}\right)^{\frac{1}{3}} \qquad (3.5)$$

As to illustrate, typical plots depicting film thickness and mean radial velocity at different radial positions according to Nusselt model predictions are seen in figures 3.8 and 3.9.

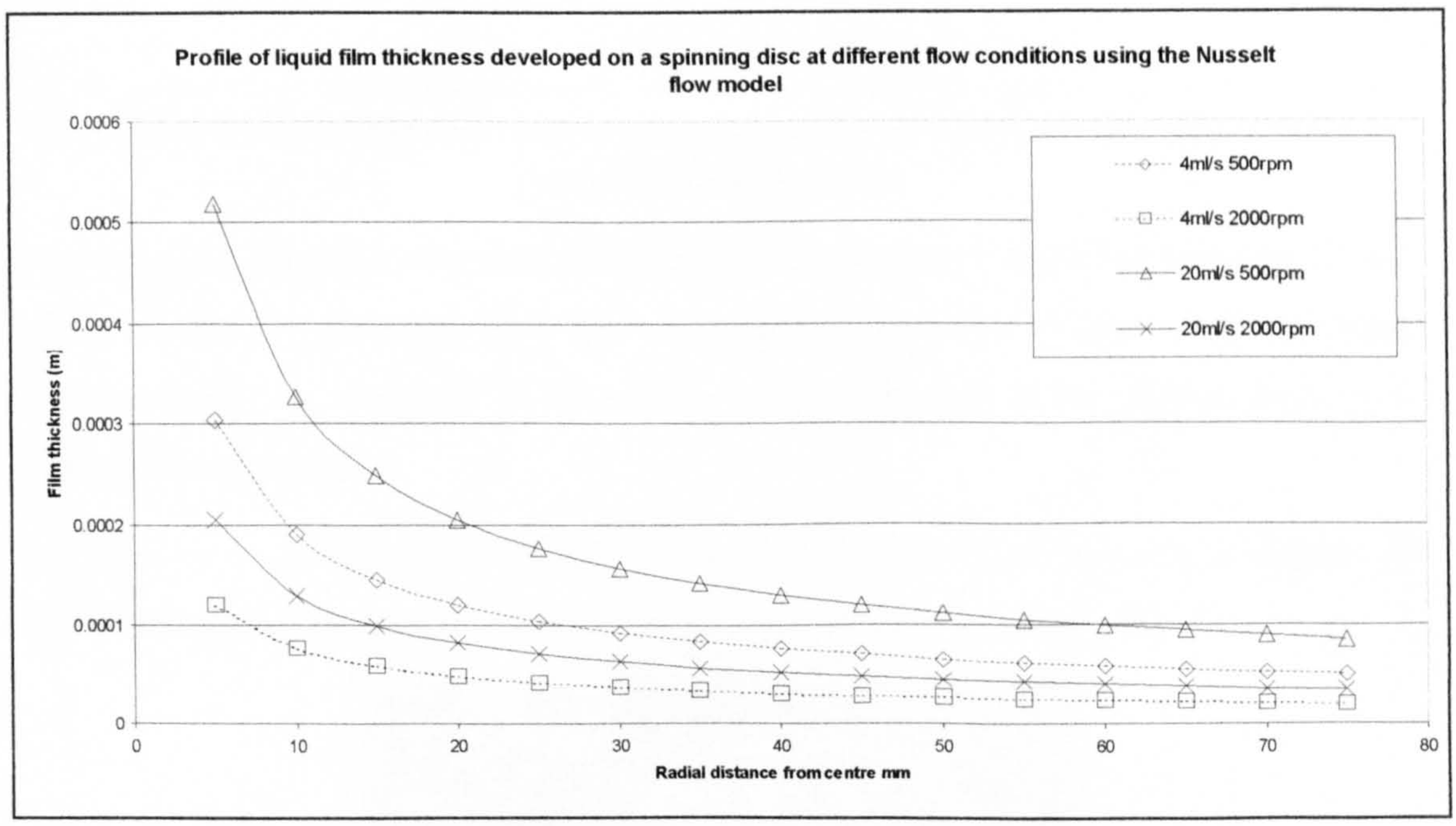


**Figure 3.8 Profile of liquid film thickness developed on a spinning disc at different flow conditions using the Nusselt flow model**

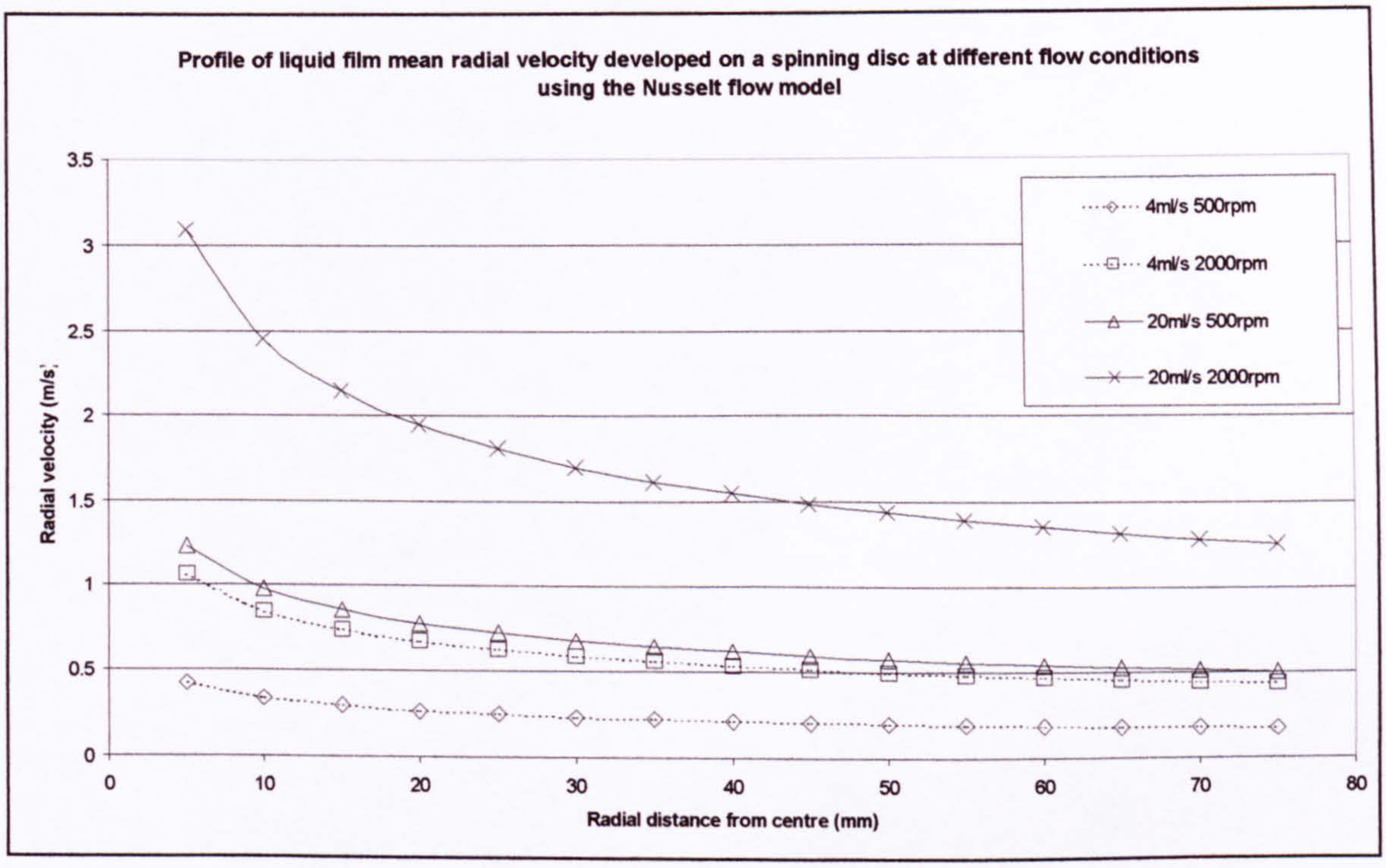


**Figure 3.9 Profile of liquid film mean radial velocity developed on a spinning disc at different flow conditions using the Nusselt flow model**

The two plots depict profile data for water at a flowrate of 4 and 20ml/s and rotational speed of 500 and 2000rpm on a disc of 75mm in diameter. These conditions were chosen as they are boundary to the experimental range used in the present study on a SDR of the same radius.

As there is a distribution in fluid velocity within the film, there is a degree of separation and contortion of the fluid which contributes to fluid mixing.

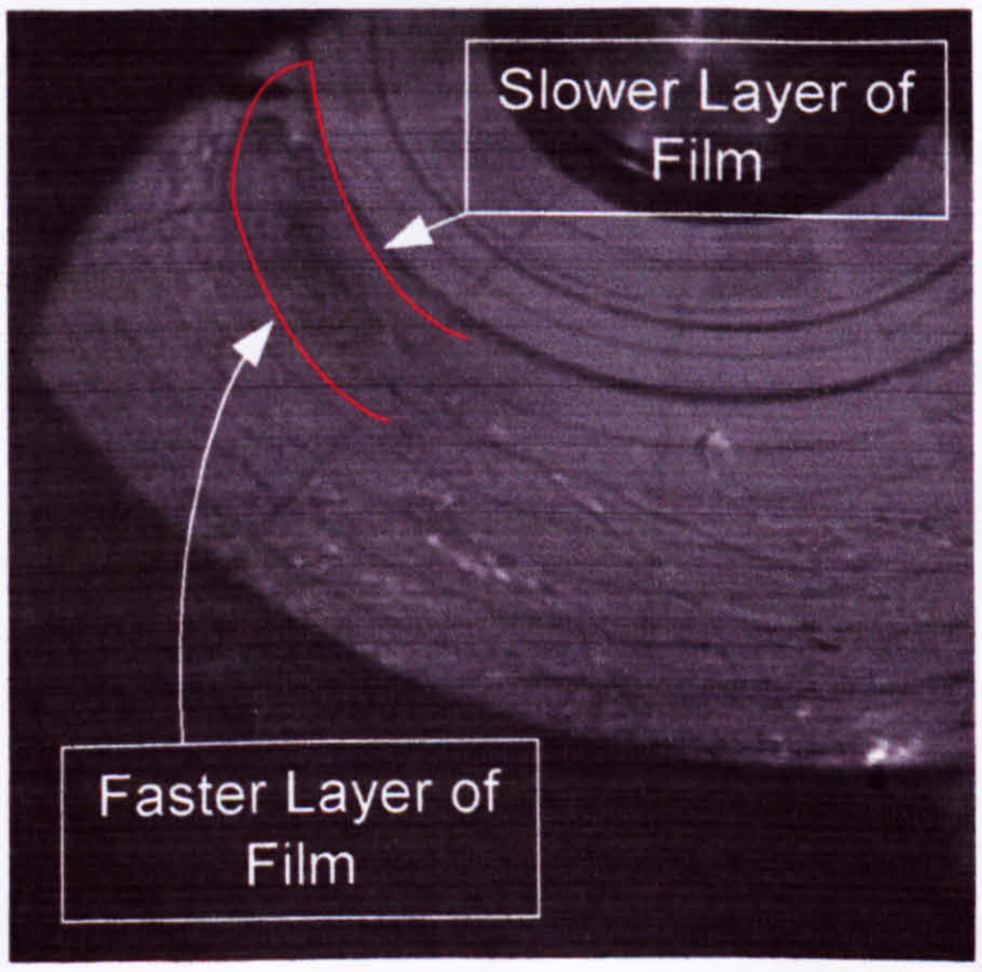


**Figure 3.10 Dispersion of an ink drop in film of liquid flowing on a spinning disc**

Figure 3.10 shows an image captured from high-speed video (1000 frames per second) of the motion of the flow of water on the surface of a spinning disc. The radial lines represent 1cm increments in the change in radius whereas the axial lines are spaced 30° apart. A drop of ink is dripped onto the surface of the flow. The ink drop then spreads out under the forces induced by the centrifugal flow. The line show the profile of the ink drop as it accelerates. The line closer to the inner radius depicts the slower bottom layer of the film, whereas the bottom line shows the faster top layer of the fluid. In a short period, the ink has dispersed, both axially and radially on the disc surface within the bulk of the fluid. A similar pattern can be seen when ink is fed as a continuous flow on the disc surface.

Unlike the analogous situation of a film flow down a wall, there is no steady state situation due to the film thickness and the radial velocity is continuously changing as the fluid flows across the disc. This fully developed laminar flow model is only approximate and relies on the assumptions of:

1. The absence of Coriolis forces.

2. That the fluid tangential velocity at any radius is equal to that of the disc.

### 3.4.3.2 Coriolis criterion

Amongst the other models that have been developed to improve the accuracy in representing the hydrodynamic conditions generated on the spinning disc, the Coriolis model; in its derivation also the action of the Coriolis force is also considered; the Coriolis force acts in a circumferential direction, opposite to the direction of rotation so that the liquid film moves at a lower speed than the disc itself. It has been shown that the Coriolis model is equivalent to the centrifugal model if:

$$\frac{Q^2}{\upsilon.\varpi.r^4} << 1 \quad (3.6)$$

From the criterion we can see that it can be particularly sensitive at small radii or excessive flowrates.

### 3.4.3.3 Residence time

The residence time of the fluid on the disc is another important parameter when considering reactions on the SDR. As described by (Moore, 1986), this can be expressed as:

$$t_{res} = \frac{3}{4}.\left(12.\pi^2\right)^{\frac{1}{3}}.\left[\frac{\mu.\left(r_o^4 - r_i^4\right)}{\rho.\varpi^2.Q^2}\right]^{\frac{1}{3}} \qquad (3.7)$$

where $t_{res}$ denotes the mean residence time of the liquid on the disc.

### 3.4.3.4 Power dissipation

It is useful to know the amount of energy transferred into the fluid by the action of rotation. The energy transferred to the fluid is an indication of the rate of mixing achieved in the system.

(Khan, 1986) proposed that the kinetic energy given to the liquid by the disc was equal to the frictional power dissipated by the fluid given by:

$$P_f = \frac{1}{2}Q\rho\varpi^2\left(r_o^2 - r_i^2\right)$$
$$or \approx \frac{1}{2}Q\rho\varpi^2 r_o^2 \qquad (3.8 \& 3.9)$$

Therefore, the total power dissipation is proportional to the flowrate and the square of the disc speed.

Furthermore, as described by (Moore, 1986) we can determine the specific dispersed power on the fluid exerted by the disc due to rotation:

$$\varepsilon = \frac{1}{2.t_{res}}.\left\{\left(r^2.\varpi^2 + u_m{}^2\right)_o - \left(r^2.\varpi^2 + u_m{}^2\right)_i\right\} \qquad (3.10)$$

where the subscripts 'i' and 'o' indicate conditions at the inner and outer radius of the disc respectively.

### 3.4.4 Mixing

#### 3.4.4.1 Introduction to fluid mixing

In developing an understanding of the mass transfer on the SDR, we have to examine the role of mixing on the mass transfer process. The SDR has been seen to improve mass transfer rates by increasing the rate of mixing through a rapid transfer of kinetic energy by rotation from the disc surface to the fluid. Firstly, the general principles of mixing are discussed before mixing on an SDR is developed.

#### 3.4.4.2 Mixing in single phase chemical reactors

For a well-designed reactor with turbulent flow, the time needed for mixing is often in the order of 0.1 to 1.0 seconds (Bourne in Harnby *et al*, 1992). If the chemical reaction is slower (e.g. needing more than 100s), mixing is practically complete before the reaction has proceeded to a significant extent. Therefore mixing does not limit the reaction. However, if the half-life of these two processes is of a similar magnitude or when the mixing is slower than the reaction, mixing and reaction occur simultaneously, not consecutively. The reaction becomes localised into zones, whose width shrinks to a plane as the inherent reaction rate rises. In practice this happens when the chemical half-life falls to a time in the order of a millisecond or less. In such cases, only a minute fraction of the total volume available is usefully employed in achieving reaction. Therefore, the reaction is throttled by insufficient mixing and does not proceed at its inherent rate. Concentration gradients are present in the reactor and when multiple reactions occur, their relative rates can be influenced by inhomogeneity i.e. the product distribution obtained can depend upon the mixing intensity. Often this leads to reagents being wasted on manufacturing unwanted products, and further, energy is wasted separating the desired product which has been manufactured at low selectivity from unwanted materials. In such cases of fast reaction, attention should be given to mixing even if it is only a single fluid system.

#### 3.4.4.3 General principles of fluid mixing

Mixing is usually carried out to enhance a rate process such as chemical reaction. (Harnby *et al*, 1992) and (Oldshue, 1983) provide a comprehensive overview on the role of mixing and provide examples of application in the process industries.

In the mixing of two miscible liquids, it is necessary to reduce the non-uniformity of the fluids i.e. reduce the variation in concentration throughout the bulk material to some acceptable level. In the case of chemical reaction, it is required to mix the reagents to the degree where uniformity of the mixture occurs on a molecular level.

Solid-liquid mixing processes (including crystallisation, dissolution or dispersion) have the necessary requirement to suspend particles in a relatively low viscosity fluid to provide conditions suitable for good liquid-solid mass transfer and/or chemical reaction. In the case of gas-liquid mixing, often the objective of such processes is to agitate the gas-liquid mixture to generate a dispersion of bubbles in the continuous liquid phase to facilitate mass transfer at the gas-liquid interface.

For the mixing of two miscible liquids, two elements are important for any mixing device;

1. There must be an overall bulk or convective flow such that no stagnant regions exist within the device.
2. The must be an intensive or high shear mixing region which is capable of providing the reduction in inhomogeneity or rate process enhancement required by the duty.

Laminar mixing is normally associated with high viscosity fluids. Under laminar conditions, inertial forces die out quickly under the action of high viscosity. Close to the rotating surfaces of impellers (e.g. used in stirred tank reactors), large velocity gradients and high laminar regions of shear stress exist. Each fluid element is stretched and deformed. Therefore, the element continually thins and elongates as it passes through the high shear region. If there are solid agglomerates present, high shearing can lead to their break up and homogenisation.

Molecular diffusion is occurring all the time, however until the fluid elements are sufficiently small, their specific surface area is not great enough for the rate of diffusion to be significant. Conversely, molecular diffusion is required for the ultimate homogeneity of miscible liquids to occur necessary for chemical reaction. Diffusivity is inherently slow in such cases i.e. from the Stokes-Einstein relationship,

$$D \propto \frac{1}{\mu} \qquad (3.11)$$

where $\mu$ is the viscosity.

The bulk flow of a fluid < 10mPa.s in a stirred tank is generally turbulent. The inertia imparted to the fluid by the rotating impeller is sufficient to cause circulation readily throughout the vessel and back to the impeller again. During the fluid's passage, turbulent eddy diffusion takes place at a maximum in the impeller region. This eddy diffusion occurs at an elevated rate to that under laminar flow conditions. Again, for homogenisation to occur at the molecular scale, molecular diffusion must occur. The overall mixing process from the bulk to the molecular level in the turbulent regime is much more rapid than under the laminar regime.

Turbulent mixing rates are highest close to the impeller when using stirred tanks. Here there are high shear rates due to the trailing vortices. In addition, there are large Reynolds stresses in the radial discharge stream. A large proportion of the energy induced by the impeller is dissipated here. Homogenisation rates of miscible liquids are greatest in this region and gas dispersion occurs predominantly here.

The Kolmogoroff theory of local isotropic turbulence can be used to gain insight into the complex structure of a flow field. Turbulent motion can be considered as a superposition of a spectrum of velocity fluctuations and eddy sizes on an overall mean flow. Large primary eddies have large velocity fluctuations of low frequency and are of size comparable with a physical dimension of (say) the impeller diameter, $D_i$. They are anisotropic (have different physical properties in different directions) and contain the bulk of the kinetic energy.

Interactions between large eddies and slow moving streams produce smaller eddies of high frequency which further disintegrate until they are dissipated into heat by viscous forces. A transfer of energy propagates down the scale from large eddies to small eddies with the directional elements of the main flow being progressively lost in the process.

This transfer of energy on different scales may be described as a set of stages when two liquids are mixed:

1. One liquid is dispersed in another so to achieve a uniform average composition. On the microscale, however, the mixture consists of entirely segregated parts of the two liquids and therefore the local concentration differences correspond to the difference of concentrations of non-mixed liquids.

2. The size of the segregated regions of uniform composition increases and the contact area between the regions of different composition grows.

3. Mixing by molecular diffusion occurs to such an extent that the segregated areas of uniform but mutually different composition disappear; the mixture attains complete homogeneity on the molecular level.

The first of these three stages represents 'macromixing' while the further two stages are termed 'micromixing'. Hence, micromixing is the process by which liquid contact and mixing occurs at the molecular level.

Mixing at the macro level reduces the scale of the concentration in-homogeneities from sizes of the order of the vessel diameter, $D_v$ to that of the Kolmogoroff velocity microscale, $\lambda_k$. Kolmogoroff argued that for large Reynolds numbers, the small eddies are first a function of the local energy dissipation rate/unit mass, $\varepsilon_T$, below the eddy size $\lambda_k$ at which viscous dissipation occurs, their properties depending on the viscosity. An equilibrium is established containing a wide range of eddy sizes. With the larger of these eddies ($D_v >> \lambda_T >> \lambda_k$) energy passes from bigger to smaller without dissipation. This is called the inertial subrange. Sizes below $\lambda_k$ over which viscous dissipation occurs are in what is called the viscous subrange.

An eddy Reynolds number is defined on the Kolmogoroff length scale as

$$Re_k = \lambda_k v_k/\nu \qquad (3.12)$$

Where $\nu$ is the dynamic viscosity ($\eta/\rho$), and $v_k$ is the velocity of the eddy

Conceptually, the Reynolds number represents the balance of inertial and viscous forces, it is seen that:

$$\lambda_k = \left(\frac{(\mu/\rho_f)^3}{\varepsilon_T}\right)^{1/4} = \left(\frac{\nu^3}{\varepsilon_T}\right)^{1/4} \qquad (3.13)$$

and the velocity scale $v_k$ associated with it is;

$$v_k = (\nu\varepsilon_T)^{1/4} \qquad (3.14)$$

For an energy dissipation rate of 1 W/kg in water, $\lambda_k \approx 30\mu m$.

Processes which are particularly dependent on turbulent eddies and their associated forces are likely to be well correlated by energy dissipation rate. Bubble formation and micromixing fall into this category.

According to (Sohnel and Garside, 1992), in the micromixing region, the final mixing process is by laminar convection and molecular diffusion over length scales smaller than $\lambda_k$ and these processes are rapid at scales of the order of the Batchelor concentration microscale, $\lambda_B$, where;

$$\lambda_B = \left[(\mu/\rho_f)D^2/\varepsilon_T\right]^{1/4} = \lambda_k Sc^{-1/2}, \quad Sc >> 1 \qquad (3.15)$$

(Schmidt number, $Sc = \mu/(D.\rho_f)$)

For an energy dissipation rate of 1 W/kg in water, $\lambda_B \approx 1\mu m$.

In the case of two reactant solutions mixed together, the reaction cannot take place in the segregated regions of the liquid but only at the boundaries between or within the regions mixed at the molecular level. The kinetics of the reaction will depend on the homogenisation rate at the molecular level if the half-life of the chemical reaction within the homogeneous solution is comparable with, or shorter than, the half-life of micromixing (Bourne, 1983 via Sohnel and Garside, 1992). In such a case, mixing can influence not only the kinetics of the reaction but also the yield and the percentage of different products.

### 3.4.4.4 Mixing time

In considering precipitation processes utilising concentrated ionic solutions, the characteristic reaction and nucleation times are very short, in the order of milliseconds or less. The time scales for various mixing processes depend upon the size and conditions of the mixing vessel.

The average lifetime of a vortex, $t_M$, which can be taken as a characteristic time for the micromixing process, is (Baldyga and Bourne, 1984 via Sohnel and Garside, 1992)

$$t_M = 12\left[(\mu/\rho)/\varepsilon\right]^{1/2} \qquad (3.16)$$

Standard laboratory and plant vessels used for reaction operations can have remarkably dissimilar values for circulation time and mixing time. Average circulation time in a laboratory vessel may be in the order of 1s whereas it can be an order of magnitude

larger on the plant scale. These values compare with micromixing times in the region of 0.01s. In reality, comparing laboratory and plant operation is more difficult because the local energy dissipation rate varies greatly within the vessel, being up to 20 times the average energy dissipation rate in the impeller region and perhaps as low as 0.2 times the average energy dissipation rate near the liquid surface and vessel corners. Consequently, the relative importance of micromixing and reaction rates can vary significantly within the vessel due to this hundred-fold difference.

Three regimes may be identified by comparing the characteristic reaction (or nucleation) time, $t_R$ with the mixing time, $t_M$:

1. $t_M << t_R$: slow regime, the reaction or nucleation kinetics control the process, the vessel is essentially homogeneous and the reaction takes place throughout the reactor.

2. $t_M \approx t_R$: fast regime, the rate is influenced by both physical and chemical factors and the reaction takes place in the narrow zone on either side of the diffusion plane.

3. $t_M >> t_R$: instantaneous regime, the rate is limited by the rate of mixing by diffusion and the reaction takes place in the diffusion plane.

### 3.4.4.5 Mixing on the SDR

From the equations developed in the hydrodynamic model and from the equations that apply to mixing, we can combine them to gain an appreciation of the level of mixing achievable on the SDR. Since equations for specific dispersed power on the disc have been developed, then the Kolmogoroff and Batchelor microscale can be determined as in addition to the mixing time.

In considering the micromixing profiles produced from Nusselt model data, a plot of the Kolmogoroff and Batchelor microscale values can be determined for a set of flow conditions for an SDR. In figure 3.11 below, the microscale profiles for water are presented with flow conditions of 4ml/s and 500rpm at radial distances in the range 10 to 75mm on a spinning disc.

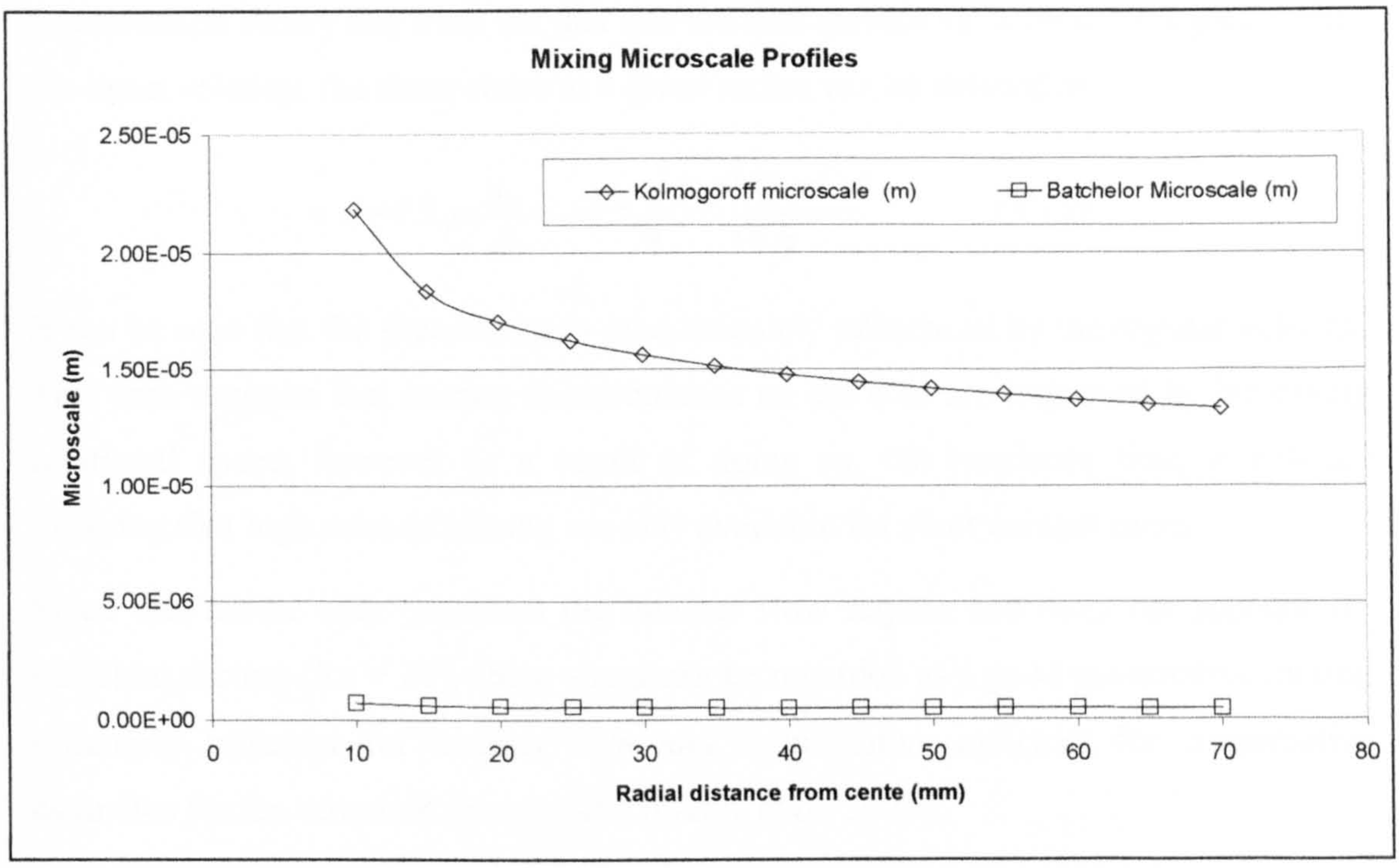


**Figure 3.11 Micromixing profiles on an SDR for water at 4ml/s and 500rpm**

The SDR flow conditions chosen represent the lowest mixing intensity experienced in the experimental range in the present study. For any set of flow conditions on the SDR, the lowest mixing intensity is close to the centre (the smaller the value on the microscale, the higher the mixing intensity). In this example, the Kolmogoroff microscale at 10mm from the centre is 21.9μm, however if the rotational speed was increased to 2000rpm for a flow of 4ml/s then the Kolmogoroff microscale is reduced to 8.1μm at 10mm radius. The mixing intensity is of importance when two reactants are fed at, or near to the disc centre, since it will govern mixing time and therefore the reaction rate etc. It is therefore important to determine local values for specific power dissipation rather than using estimates for the whole disc especially when reaction time is of the same order as mixing time.

(Moore, 1986) determined the mixing time of the fluid on a spinning disc on the basis of the hydrodynamic properties and the specific dispersed power:

$$t_M = 2.\left(\frac{\nu_L}{\varepsilon}\right).\arcsin(0.05.Sc) \quad (3.17)$$

Mixing intensity may also be expressed in terms of shear stress. From the correlations described in (Boodhoo, 1999), which involve a modification of the Nusselt's

condensation theory and from the fact that the film surface velocity is 50% greater than the mean velocity, the shear stress at a given radius can be defined as:

$$\tau = -1.5.\mu.\frac{u_m}{\delta} = -1.5.\sqrt[3]{\frac{\mu.\rho^2.Q.\varpi^4.r}{18.\pi}} \qquad (3.18)$$

It can be seen that the shear stress is predominately influenced by the angular velocity. This case suggests that mixing characteristics on the disc are improved by increasing rotational speed, however as a result of doing so, the residence time is reduced implying that high rates of mixing are only available for short contact times.

Since this model only considers the laminar flow regime and does not account for turbulent mixing (Re > 20), shear stress can be regarded as a good quantitative mixing efficiency indicator for laminar flow and a qualitative indicator for conservative estimates for the turbulent flow regime (Oxley *et al*, 2000).

Complimentary to all of these describing equations, it is useful to estimate the volume of liquid on the disc and the surface area of the film exposed to the space above. Determination of the volume of liquid on the disc can be derived from a number of approaches. The simplest approach to determine the film (reactor) volume is:

$$V_{SDR} = t_{res}.Q \qquad (3.19)$$

This is analogous to the usual expressions of space-time for conventional reactor types. Assuming a ripple-free film and $\delta_i << r_o$, then the exposed surface area may be approximated as the area of an annulus:

$$A = \pi\left(r_o^2 - r_i^2\right) \qquad (3.20)$$

This area can be used in evaluating absorption mass transfer performance.

### 3.4.5 Gas absorption on the SDR

#### 3.4.5.1 The absorption mass transfer of $CO_2$ in water on a smooth spinning disc.

(Moore, 1986) studied the absorption of $CO_2$ in water on a smooth rotating surface at different values of liquid flowrate and disc speed and measured the weight concentration of carbon dioxide in the water at the outlet of the disc, $[CO_2]_w$. He then used this value to calculate the overall mass transfer rate, $N_w$ (g/s):

$$N_w = Q[CO_2]_w \qquad (3.21)$$

This expression assumes that the concentration of carbon dioxide in water at the disc inlet is negligible, Moore measured the concentration of $CO_2$ in the feed water and concluded that this assumption was acceptable. The knowledge of $N_w$ allows the calculation of the liquid side mass transfer coefficient from the basic definition of a mass transfer rate:

$$k_L = \frac{N_w}{A\,\Delta[CO_2]_w} \qquad (3.22)$$

$A$ ($m^2$) is the mass transfer area and it is assumed to be equal to the surface area of the film flowing on the disc (eq. 3.19):

The equipment used by Moore had the following values: $r_o$=0.15m, $r_i$=$1.75\cdot10^{-2}$ m.

$\Delta[CO_2]_w$ is the concentration driving force for the absorption process. Moore employed a log-mean driving force in order to represent the change in the concentration gradient from the interface to the bulk of the liquid between the inlet and the outlet positions, $\Delta[CO_2]_w$ has the following expression:

$$\Delta[CO_2]_w = \frac{\left([CO_2]_w^* - 0\right) - \left([CO_2]_w^* - [CO_2]_w\right)}{\ln\left[\frac{\left([CO_2]_w^* - 0\right)}{\left([CO_2]_w^* - [CO_2]_w\right)}\right]} \qquad (3.23)$$

Moore observed that the concentration at the gas-liquid interface, $[CO_2]_w^*$, does not remain constant during the absorption process since the partial pressure of carbon dioxide, if a gas mixture is used, decreases. In order to avoid having to take into consideration a change of this quantity, he used a high gas flowrate so that the decrease of the gas pressure could be considered negligible. The $k_L$ values calculated using

equation(3.22) referred to the temperature at which the experimental runs were performed, which ranged from 14°C to 22°C. In order to be able to compare his data with other data reported in the literature or predicted by correlations, Moore decided to modify all the determined values so that they referred to the same temperature of 20°C. As Higbie's penetration theory, on which all the mass transfer models for films on rotating surfaces are based (as described later), considers a 0.5 order dependence between the mass transfer coefficient $k_L$ and the diffusivity of the gas in the liquid phase, Moore adopted the following relationship for the conversion:

$$k_{L\,20} = k_L(T)\sqrt{\frac{1.7\cdot10^{-5}}{D_{GL}(T)}} \qquad (3.24)$$

where $k_{L\,20}$ (cm/s) is the mass transfer coefficient at 20°C and $1.7\cdot10^{-5}$ ($cm^2/s$) is the diffusivity of carbon dioxide in water at a temperature of 20°C

Table 3.1 shows the results obtained from equations (3.22) and (3.24) for the absorption of carbon dioxide in water on a smooth spinning disc (vertically rotating about a horizontal axis) with 1 atm of $CO_2$ pressure

| N (rpm) Q ($cm^3/s$) | 500 | 750 | 1000 | 1250 | 1500 |
|---|---|---|---|---|---|
| **50.0** | 0.0218 | 0.0238 | 0.0227 | 0.0214 | 0.0195 |
| **66.7** | 0.0275 | 0.0312 | 0.0312 | 0.0293 | 0.0277 |
| **83.3** | 0.0307 | 0.0374 | 0.0392 | 0.0370 | 0.0362 |
| **100.0** | 0.0326 | 0.0426 | 0.0466 | 0.0455 | 0.0463 |

**Table 3.1 $k_{L20}$ values (cm/s) for different flowrates and rotational speeds, for the absorption of $CO_2$ in water on a smooth vertical spinning disc ($p(CO_2)$= 1 atm) (Moore, 1986).**

It was observed for each flowrate in the study that the mass transfer coefficient first increases and then decreases with rotational speed. Moore attributes this behaviour to a film breakdown phenomenon due to the presence of entrained solid particles in the liquid that had a tendency to stick to the disc surface. Moore reported a stability analysis does not predict film breakdown for the values of flowrate and rotational speed considered. The series of experiments conducted with a flowrate of $83.3cm^3/s$ was repeated for a $CO_2$ partial pressure of 0.5atm and for the disc in the horizontal position to confirm that the gas side mass transfer coefficient and the effect of gravity

had no influence on the amount of carbon dioxide absorbed in water; in fact approximately the same values as the ones shown in Table 3.1 above were obtained.

### 3.4.5.2 Mass transfer: penetration theory

Several models based on Higbie's penetration theory have been developed to describe mass transfer phenomena for films flowing on rotating surfaces. As far as the present study of the literature, no other approach to mass transfer of gases to liquid films is reported herein. The models all change in the way they define the "exposure time" of a fluid element. Moore summarises these models in his work. Here, the two models developed by Venkataraman, both considering a laminar regime on the disc, one of which showed good agreement with Moore's results will be reported. The first, the so-called "crude model", considers that a surface element of liquid exposed to the gas is neither stretched nor contracted as it grows older. The rate of absorption can therefore be described by the following expression:

$$dN = (c^* - c)\sqrt{\frac{D}{\pi\theta}}\,dA(t) \qquad (3.25)$$

The exposure time is considered as being equal to the mean residence time on the disc as given by the centrifugal model (eq. 3.7) and the mass transfer area is considered equal to the area limiting the thin film:

$$dA(t) = 2\pi r < v_r > dt \quad (3.26)$$

Substituting equation (3.7) in equation (3.25) in the relationship defining dN gives:

$$dN = 4(c^* - c)\sqrt{\frac{\pi DB}{3}}\frac{r}{(r^{4/3} - r_i^{4/3})^{1/2}}dr \qquad (3.27)$$

to obtain which $t(r) = t_{res}(r)$ has to be considered; B is defined as follows:

$$B = 0.306\frac{\omega^{2/3}Q^{2/3}}{\nu^{2/3}} \quad (3.28)$$

Equation (3.27) can be integrated to give an expression for the mass transfer rate, however it was found out that this model predicted values some 23% lower than the values determined from experimental measurements. A further refining of the model, which brought to the definition of the so called "approximate model" took into consideration the variation of the velocity component normal to the disc surface as the

surface element grows older. As reported by Lim, limiting the analysis to a small depth of penetration from the gas-liquid interface, the normal velocity is taken to be proportional to the distance from the gas-liquid interface *y*:

$$v_y = -\alpha(t)y \quad (3.29)$$

where $\alpha(t)$ is a function of the surface age. This model finally gives the following relationship for the mass transfer rate:

$$N = 4(c^* - c)\sqrt{\pi DB}\left(\frac{3}{8}(r^{8/3} - r_i^{8/3})\right)^{1/2} \quad (3.30)$$

where *B* is the same as previously defined in equation 3.28. Venkataraman observed that this model produced values, which were approximately 7 % greater than his experimental results obtained for films flowing on rotating surfaces in a laminar regime. Moore found that the values predicted by this model were in good agreement with the ones he determined from his experimental measurements.

Furthermore, (Moore, 1986) performed a study of mass transfer to a thin liquid film on rotating surfaces with and without chemical reaction. In the work, he studied the performance of smooth, perforated and mesh discs in their mass transfer ability to absorb $CO_2$ into water and aqueous diethanolamine solutions. He compared the work with (Lim, 1980) and (Watts, 1971) experimental data of mass transfer coefficient. Moore found his results to bear similar resemblance with Watts' data but found discrepancies between Lim's results and other workers. He states that due to the unavailability of Lim's raw data he could not draw conclusions upon its validity.

In the present study of the absorption of carbon dioxide into calcium hydroxide solution on the SDR, the low solubility and approximately the same physical properties of the solution to water would suggest this model could be used to predict the mass transfer coefficient values for the ranges of operating variables that will be employed in the experimental part of the present study.

In (Wood and Watts, 1973) investigation of $CO_2$ absorption by water on a spinning disc, they represented Venkataraman's equations as follows:

$$\phi = KC_i \left( \frac{D\,\varpi^{\frac{2}{3}} Q^{\frac{2}{3}}}{\nu^{\frac{1}{3}}} \right)^{\frac{1}{2}} \quad (3.31)$$

where $K$ is the following function of the disc inner and outer radii:

$$K = 3\left\{ \frac{3}{4\pi} \left( \frac{2\pi}{3} \right)^{\frac{4}{3}} \left( r_o^{\frac{8}{3}} - r_i^{\frac{8}{3}} \right) \right\}^{\frac{1}{2}} \quad (3.32)$$

Vankataraman's model does not include any term to account for the nature (composition, flowrate, counter-current or co-current contact) of the gas above the disc. The model is based purely on liquid and disc parameters. Considering the liquids flowrates and the 15cm diameter disc in the present study, the overall rate of absorption, determined by the model is seen in figure 3.12 below.

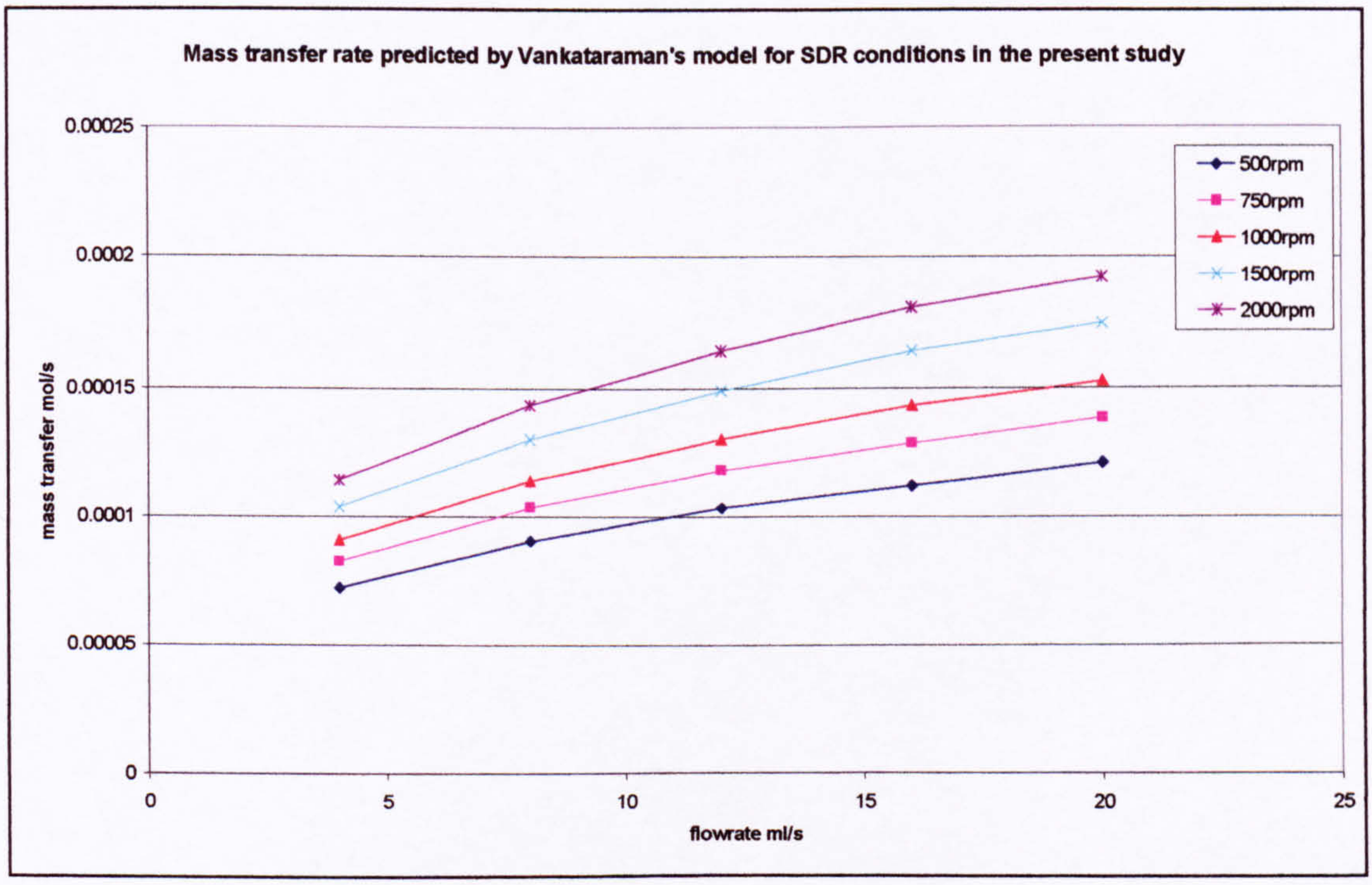


**Figure 3.12 Mass transfer rate predicted by Vankataraman's model for SDR conditions in the present study**

(Wood and Watts, 1973) measured the absorption of $CO_2$ in water on a spinning disc and compared their results with Vankataraman's model. It was seen that over the range of the experiments, fairly good agreement between the model and the experimental results was seen. However, the experimental results did not follow a mass transfer rate proportional to $Q^{1/3}$ relationship as the model predicted. They concluded that due to the water not behaving according to the Nusselt flow model

(from which Vankataraman's model is derived) then this was the reason why the model does not fully describe the mass transfer characteristics of the disc. In examining their range of flowrates used, it is believed that at quite high flow conditions such that the Coriolis criterion may not hold (at least on part if not all of the disc) and therefore the Nusselt model becomes invalid. Their data at lower flowrates appears to be in closer agreement with the model than at higher flowrates. In the present study, total liquid flowrates between 4 and 24ml/s whereas in their work the lowest flowrate investigated is 37ml/s [300 lb/hr]. This would indicate in the present study, the Nusselt model might more closely describe the flow/absorption data derived from experiment.

### 3.4.6 Applying the nusselt model to experimental systems

It is possible that the Nusselt model will not hold under real conditions due to the inertia of the fluid relative to the disc as it leaves a feed pipe or distributor and flows upon the disc. The area whereby the fluid tangential velocity is unequal to the disc tangential velocity is called the 'spin-up zone'. In the present study, for the experimental set-up described later, a small central well on the disc is employed. It is assumed that outside the well the model holds. The estimates are based between the radii at the edge of the well to the edge of the disc. Since there is no way of determining the real flow conditions at any given point on the disc used in the experimental set-up then the Nusselt model is used to provide estimates of experimental parameters.

In using the model equations to predict local conditions near the centre, parameters such as film thickness, mean radial velocity and Reynolds number approach infinity as radius approaches zero. Furthermore, the Coriolis criterion (eq 3.6) is likely to be violated close to the centre of the disc.

### 3.4.7 Experimental work on spinning disc processes

(Wood and Watts 1973) investigated the flow, heat and mass transfer characteristics of a liquid film on a spinning disc. In their flow studies they presented the Nusselt laminar flow model and attempted to profile the radial velocity by seeding the flow with tracer particles and photographing their trajectories on a disc 24" in diameter. They examined water, water/glycerol mixtures and castor oil in order to determine flow velocity profiles for a range of viscosities. They used oil droplets as tracer

particles, which broke up in the film and were photographed by a cine-camera. They found that their experimental results did not agree with the Nusselt model for water, the radial velocity increasing rather than decreasing as it moved radially outward. The flow path of water appeared to have a circumferential path with considerable angular slip whereas the more viscous fluids followed a radial path more closely and were in much closer agreement to the Nusselt model i.e. the radial velocity decreased as the flow moved radially outward. From personal experience, their flowrates chosen for water (500 to 1500 lbs/hr) [63 to 189ml/s] appear to be rather high, it is conceivable that the Nusselt model would not hold for the conditions on the disc surface as the Coriolis criterion (eq 3.6) would be broken.

In examining the heat transfer characteristics of water flowing over a 30cm diameter spinning disc, (Wood and Watts, 1973) reported film velocities in the range of 3.3 to 10m/s with a film thickness in the region of 25μm. Such a small film thickness leads to excellent heat transfer properties; they report overall heat transfer coefficients in the range 1000 to 2000 Btu/h $ft^2$ °F (5.7 to 11.4 $kW/m^2K$).

(Wood and Watts, 1973) obtained mass transfer data of the absorption of $CO_2$ in water on a 30cm diameter spinning disc in the experimental ranges of rotational speeds of 320 to 1100 rpm and flowrates of 31.6 to 252ml/s. They created a sealed $CO_2$ atmosphere saturated with water vapour around the disc with the gas operating under a slight pressure (4in w.g.) but there was no measurement of gas flowrate. Titrimetric analysis in standard caustic was carried out to establish the amount of $CO_2$ absorbed. They reported experimental results of total absorbed $CO_2$ in the range (2.1 to 8.6 lbmol/hr (0.953 to 3.9 kmol/hr, 0.27 to 1.08 mol/s). The results were compared to the mass transfer model proposed by (Vankataraman, 1966). It was seen that over the range of the experiments, fairly good agreement between the model and the experimental results was seen. However, the experimental results did not follow a mass transfer rate proportional to a $Q^{1/3}$ relationship as the model predicted. They concluded that the water was not behaving according to the Nusselt flow model (from which Vankataraman's model is derived) and for this reason, the model does not fully describe the mass transfer characteristics of the disc.

(Rahman & Faghri, 1993) produced analytical and numerical solutions for mass transfer to a thin liquid film on a spinning disc. They observed that all transport phenomena were dominated by inertial and viscous resistance at smaller radii and by

rotation at larger radii. It was seen that the spinning disc offered large enhancement of mass transfer coefficient over the entire disc radius by increasing rotational speed. However, enhancement of mass transfer coefficient with increasing flowrate was limited to the inertia-dominated region.

(Woods, 1995) performed a visual study of the waves produced by a fluid upon a spinning disc. It was observed that an initially uniform film was broken down into well-defined spiral ripples, which further break down into more confused wavelets as the film progresses radially outward. The study revealed that the nature, frequency and location of the wavefronts were determined by rotational speed and flowrate.

(Jachuck and Ramshaw 1994), proposed the use of a spinning disc as an intensified heat transfer device. In studying the heat transfer to water on the surface of a spinning disc operating in a rotational speed range of 250 to 890rpm, they reported average heat transfer coefficients as high as 16 $kWm^{-2}K^{-1}$. In reviewing the work on the effect of ripples in a liquid film flowing down an inclined surface (Brauner and Maron, 1982) it was reported that the ripples had significant effect upon heat transfer performance. In extending this idea, the use of roughened surfaces and mechanically machined grooves were employed on the disc surface; this was seen to improve heat transfer performance over a smooth disc. By employing a spinning disc in a heat transfer operation, varying rotational speed gives an extra degree of freedom in design and operation. The disc induces a self-cleaning action whereby it can handle viscous liquids and liquids containing solids. Short residence times on the disc may help in processing heat sensitive fluids. (Jachuck, Lee *et al* 1997) suggest that the high disc/liquid and gas/liquid heat and mass transfer coefficients reported for thin liquid films on a spinning disc would ideally suit gas-liquid reactions, which conventionally are mass transfer limited.

In the field of heat transfer, (Yanniotis and Kolokotsa, 1996 [2papers]) studied boiling and condensation characteristics on the surface of a spinning disc. Reporting values for water at rotational speeds in the range 0-1000rpm, they report experimental values of heat transfer coefficient in the range 2 to 9 $kW/m^2K$ (based on a heat flux to the disc in the range 10-30 $kW/m^2$). They also noted that the feed flowrate (in this case, 1 to 5 l/min) does not affect the heat flux or heat transfer coefficient significantly. In the same rotational speed range for vapour condensation on the spinning disc, they report values of heat transfer coefficient of 10 to 30 $kW/m^2K$. In this paper the authors state

(for zero rotational speed). As the temperature difference increases and nucleate boiling becomes more intense (as observed by direct visualization) the effect of flowrate becomes less important. They did not state as to whether any bubbles are formed during rotating experiments (because they did not or were unable to observe them) and assumed only surface evaporation occurs in their heat transfer estimates.

(Aoune and Ramshaw, 1999) performed heat and mass transfer experiments on a 50cm diameter brass spinning disc. Again, it is reported that very high heat transfer rates are achieved on the disc for water. In the mass transfer study of the absorption of oxygen in de-aerated water, they showed that mass transfer rates were dominated by disc speed and only a weak function of liquid flowrate and disc radius. At a liquid flowrate of $80cm^3/s$ local mass transfer coefficients were reported in the range of 2 to 10 x $10^4$ m/s. In comparing their experimental results with the Higbie penetration model of mass transfer, they discovered that the experimental values were over 5 times higher than those predicted by the model. Although it is not abundantly clear, the text of the paper suggests that the transit time of a surface element used in the Higbie model prediction of mass transfer coefficient is determined by the derived residence time of the velocity of the film on the surface. In other words, the authors assume for their predictions that the exposure time of a fluid element is that of the residence time of the fluid on the surface predicted in the Nusselt model describing the flow. This would be consistent with the work described by Moore and the model developed by (Vankataraman, 1966). They suggest that the film instabilities and the propagation of the ripples generate exposure times far less than the liquid surface residence time on the disc.

(Boodhoo & Jachuck, 1999) performed polymerisation experiments on a grooved SDR 360mm in diameter. The grooves in the surface of the disc acted to induce a large number of surface waves in the film thus promoting heat and mass transfer. They observed that there was a substantial increase in the rate of free radical polymerisation of styrene over the batch process when performed on the SDR. It was observed that the SDR could operate with viscous polymer masses in excess of 3-4 $N/m^2s$. By manipulating rotational speed, optimal polymer conversion could be attained. They also concluded that a significant time saving could be made using SDR technology when processing higher viscosity polymer feeds due to the superior heat and mass transfer characteristics of the SDR. As well as reducing processing time, the SDR

improved the product quality by producing a product with a tighter molecular weight distribution than that of a batch process.

## 3.5 *Precipitation*

### 3.5.1 Introduction to precipitation

Precipitation may be difficult to define when opposed to the more general term "crystallisation" since there is no clear dividing line between the two phenomena. (Sohnel and Garside, 1992), who have compiled a definitive work on the topic suggest it is perhaps best to define precipitation as the embodiment of fast crystallisation. The rapid development of high supersaturation is the driving force of a precipitation process.

A number of consequences flow from this definition, most of which give rise to other characteristics of precipitation. Firstly, it is usually relatively insoluble materials that lead to precipitation since the low solubility leads to the development of high supersaturation ratios. Secondly, high supersaturation leads to very high rates of primary nucleation, thus nucleation plays an important role in precipitation processes. As a consequence of these two factors, a large number of crystals are produced. This limits the size to which the crystals can grow, resulting in a very high particle concentration in suspension (typically between $10^{11}$ and $10^{16}$ particles $cm^{-3}$). Crystal size is relatively small, generally between 0.1 and 10μm. If the precipitated crystals are sufficiently small, then secondary processes such as ripening, aging, agglomeration and coagulation may occur. These may have a major effect upon the crystal size distribution.

Precipitation is sometimes referred to as reactive crystallisation, as most frequently the supersaturation is generated by chemical reaction. The reaction may involve two liquids, a liquid and a solid or a gas and a liquid. It may be possible that 3 or more phases are involved in the overall process, making the understanding of the reaction kinetics and mass transfer mechanisms involved complex.

Many such reactions possess fast kinetics and so the role of mixing is important. Usually the precipitation process is carried out at constant temperature and does not rely upon cooling to generate the supersaturation driving force.

### 3.5.2 Precipitation in the chemical and process industries

Many industrial processes employ the use of precipitation somewhere in the process route to the final product. These may be the final product themselves or a by-product as result of a separation/purification step. Many of these processes are long established. The Solvay process, invented in 1863 to produce sodium carbonate is still in commercial use today. Many simple inorganic materials are produced from wet processes this way. Catalysts manufacture frequently involves precipitation of key components and many ceramic precursors are precipitated products. Increasingly, there are more consumer products from precipitation products. Silver halides for photographic use and ferric or chromic oxides for magnetic data storage are mass-produced from precipitation.

There is increasing emphasis on high added value speciality organic chemical products from precipitation processes. Many of these are organic products used as dyes, pigment, paints, printing inks, pharmaceuticals and agrochemicals.

Precipitation processes are useful in environmental applications. The use of powdered limestone in flue gas desulphurisation reduces the sulphur dioxide content of the gas and forms gypsum, which is employed as a raw material in the building trade. Wastewater treatment employs the precipitation of calcium salts. Many other elements may be removed this way such as iron from mine drainage or mercury from contaminated brown field sites.

Some precipitation processes result in the formation of nano-scale particles. These very small crystals may have special chemical and or physical properties due to their size, such as to be used in catalysis or for the storage of electrical charge.

Whatever the size of the crystals being produced, control of the particle size is of key importance. The crucial properties of size distribution and corresponding surface area and of the crystal habit or morphology have significant impact on the particles' application and it's processing. The particle characteristics affect its physical processing e.g. the ease of liquid solid separation by filtration or centrifugation, drying rates, its bulk density and particle flow properties, its packing characteristics and propensity to cake. In slurry form, the viscosity and other rheological characteristics are critically dependent upon these particle properties.

The other aspect of the particle characteristics is chemical in nature. Chemical composition, in terms of the degree of purity and impurity is obviously a concern. Many precipitated products can form a range of polymorphs or amorphous phases. It is also possible to form different hydrate or solvate phases. In most applications it is desirable to form only one specific form, hence precipitation conditions need to be controlled to ensure the formation of the desired product. Accordingly, these conditions must be produced from batch to batch or continuously over long production periods to produce products of consistent quality. This is critically important in the pharmaceutical industry in order to meet compliance of stringent regulatory requirements.

### 3.5.3 The kinetic processes of precipitation

Precipitation involves many individual steps and kinetic processes. This is illustrated in figure (3.13)

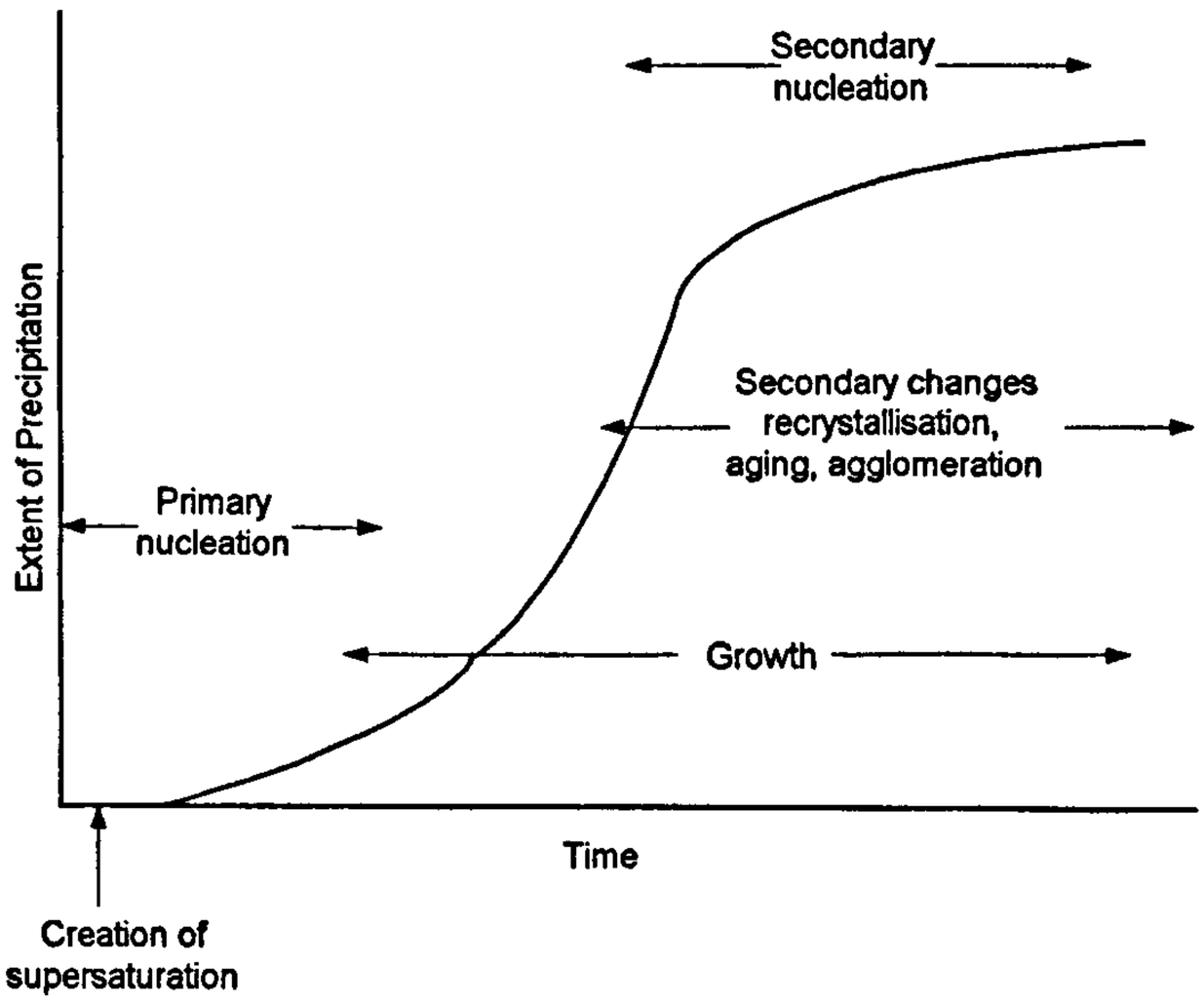


**Figure 3.13 The kinetic processes involved in precipitation (reproduced from Sohnel & Garside 1992)**

The time scale for these processes can vary between fractions of a second to many days but the relative importance of the different rate processes always changes during the course of a given precipitation. The key variable for any precipitation process is the level of supersaturation. This governs the rates of the different processes. Supersaturation is central to the whole outcome of precipitation and is shown schematically in figure (3.14)

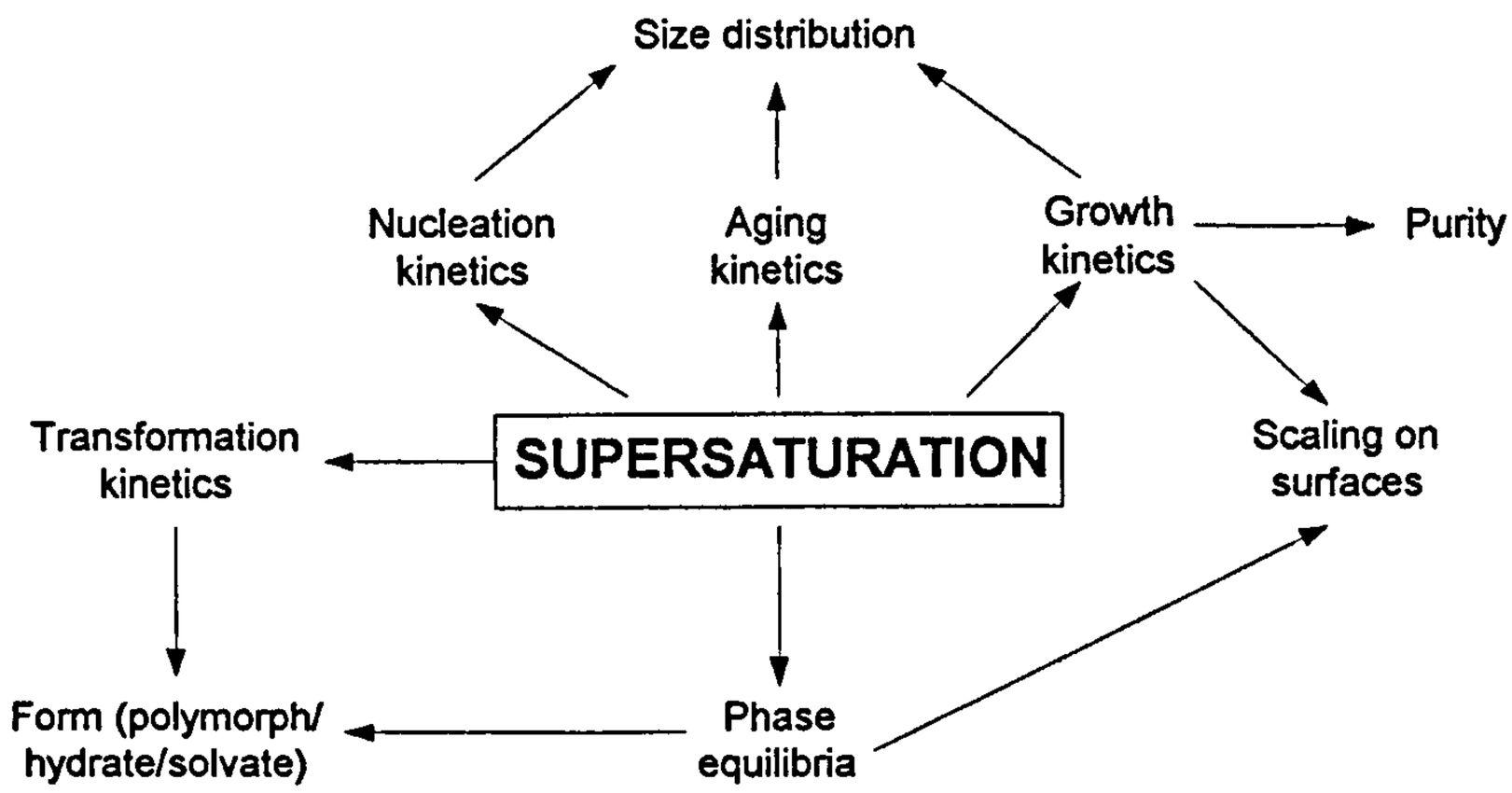


**Figure 3.14 The role of supersaturation in precipitation processes (reproduced from Sohnel & Garside, 1992)**

Thus the nucleation, growth and aging kinetics influence the particle size distribution; growth rate has an important effect on purity and on the extent to which the crystals will grow on surfaces and produce scaling. Transformation kinetics control the polymorphs, hydrate and solvate habit whilst the position of the system in the appropriate phase diagram also depends upon the level of supersaturation.

During the course of the precipitation process, supersaturation usually changes. In the case of batch precipitation, the level decreases unless the process is run in such a way as to match the rate at which supersaturation depletes with the addition of fresh material. Continuous processes may operate at steady state conditions, and with steady state, the supersaturation and other parameters will remain constant with time apart from the start up and shut down deviation from it. Supersaturation may also exhibit spatial variations in a reaction vessel, the extent of these variations being determined by the mixing processes taking place within the vessel, this has been discussed within the section on mixing. These physical and chemical mechanisms are underpinned by the importance of mixing. Getting the right hydrodynamic effects allows for homogenised reactants to come together for the control of local supersaturation and resulting in the correct conditions to be achieved in producing a desired crystal size distribution.

### 3.5.3.1 Supersaturation

Supersaturation in precipitation reactions tends to be high with respect to other crystallisation techniques. High supersaturation leads to a rapid onset of precipitation

whereas other crystallisation processes with low supersaturation can take a long time before the onset of crystallisation begins.

The supersaturation of a system may be expressed in a number of ways and considerable confusion may arise if the basic units of concentration are not clearly defined (Mullin, 1972). Among the most common expressions of supersaturation are the concentration driving force, $\Delta c$, the supersaturation ratio, $S$ and a quantity sometimes referred to as the absolute or relative supersaturation, $\sigma$, or percentage supersaturation, $100\sigma$. These quantities are defined by;

$$\Delta c = c - c^* \qquad (3.33)$$

$$S = \frac{c}{c^*} \qquad (3.34)$$

$$\sigma = \frac{\Delta c}{c^*} = S - 1 \qquad (3.35)$$

where $c$ is the solution concentration and $c^*$ is the equilibrium saturation at a given temperature. In precipitation, the supersaturation may also be expressed in terms of the solubility product and chemical potential. (Sohnel and Garside, 1992) present details of the thermodynamics of crystallisation and develop an approach to solubility and supersaturation based on activity and osmotic coefficients.

If the concentration of a solution can be measured at a given temperature and the corresponding equilibrium saturation concentration is known, then it is a simple matter to calculate the supersaturation. Just as there are many methods to measure concentration, so there are also many ways of measuring supersaturation but not all of these are readily applicable to industrial crystallisation practice. For purposes of the present study, the solubility of reactants and the products is found in the literature and hence the supersaturation ratio may be inferred by calculation using these values.

From the viewpoint of thermodynamics, supersaturated solutions are always unstable. Up to a certain concentration, however, they appear to be stable in that their properties do not change for a comparatively long length of time. This metastable state is found for supersaturated solutions of both readily and sparingly soluble substances.

The characteristics of the metastable region can be best illustrated using a binary phase diagram for the case when the solubility of the solid phase increases with temperature seen in figure 3.15 below.

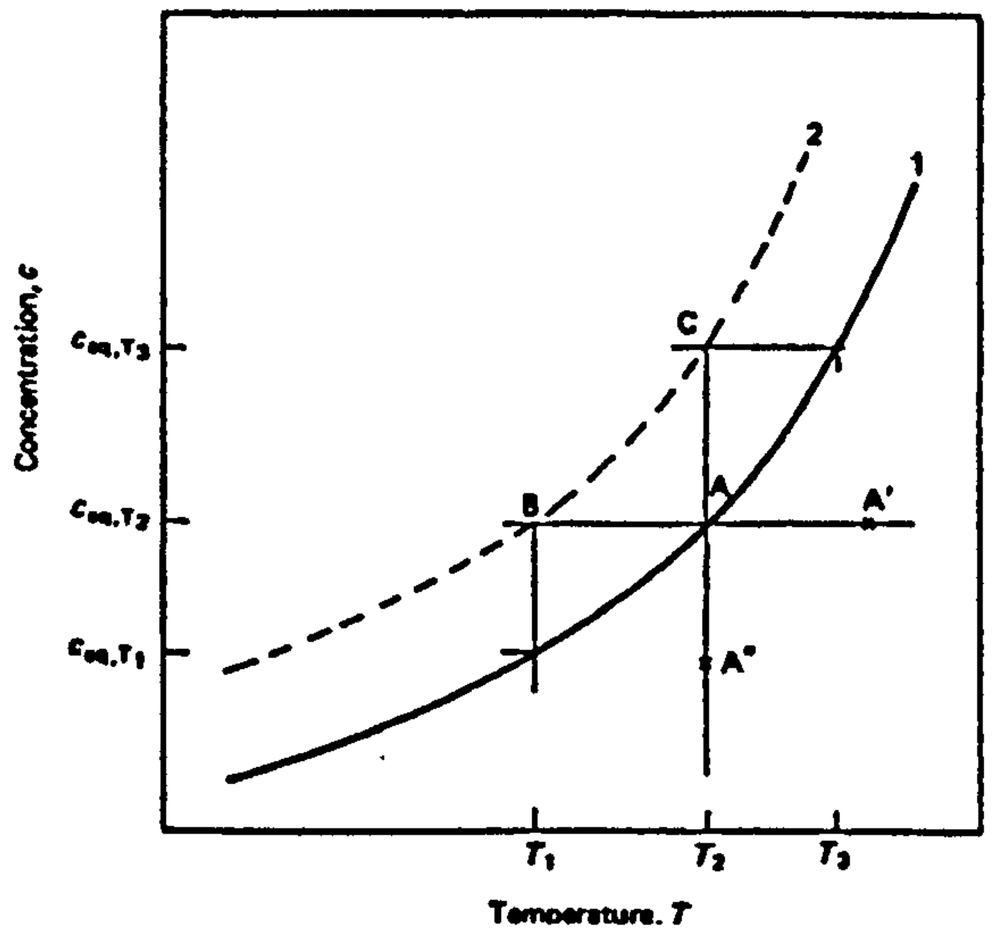


**Figure 3.15 Phase diagram of a binary solid-liquid system. 1-saturation curve; 2- boundary of the metastable zone (Sohnel and Garside, 1992)**

Cooling an under-saturated solution from initial point *A'* results in the solution reaching saturation at *A* where the solution may be at equilibrium with any solid phase that may be present. On further cooling, a state is reached where the solution contains more solute than that corresponding to the equilibrium solubility at the given temperature; the solution thus becomes supersaturated. However, spontaneous formation of the solid phase does not occur until a point such as *B* is reached, corresponding to the boundary of the metastable zone. The metastable zone width can be expressed as either the maximum attainable undercooling or by the supersaturation $(\Delta c_{max} = c_{eq,T2} - c_{eq,T1})$.

The path *A'-A-B* represents a polythermal method of preparing a metastable solution. In an isothermal process, the starting point would be *A''* and by evaporating the solvent at constant temperature, point *C* would be reached, again saturation being attained at point *A*. When the metastable limit is exceeded, the solution becomes labile and spontaneous formation of the solid phase immediately occurs.

### 3.5.3.2 Nucleation

The condition of supersaturation alone is not sufficient cause for a system to begin to crystallise. Before crystals can grow there must exist in solution a number of solid

bodies known as seeds, embryos or most commonly, nuclei. Nucleation may occur spontaneously or it may be induced artificially; these two cases are referred to as homogeneous and heterogeneous nucleation respectively. However, it is not always possible to determine whether a system has nucleated of its own accord or whether it has done so under the influence of external stimuli.

'Primary' nucleation is the term given to all cases of nucleation, homogeneous or heterogeneous, in systems that do not contain crystalline matter. On the other hand, nuclei are often generated in the vicinity of crystals present in a supersaturated solution; this phenomenon is termed 'secondary' nucleation. Thus we have;

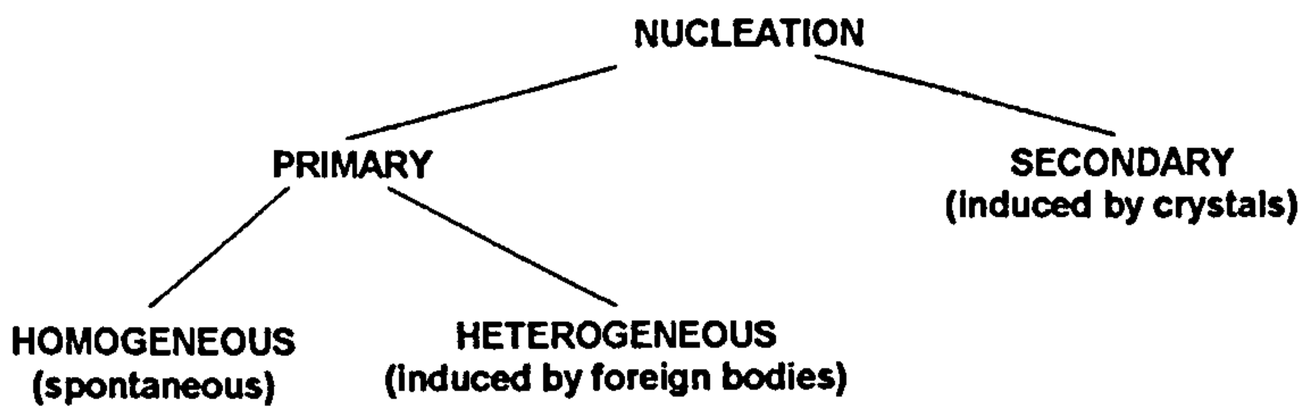


**Figure 3.16 Nucleation mechanisms**

The formation of crystal nuclei is a difficult process. Not only do the constituent molecules have to coagulate, resisting the tendency to redissolve, but they also have to become orientated into a fixed lattice. The number of molecules in a stable crystal nucleus can vary from ten to several thousand. The actual formation of a nucleus can hardly result from the simultaneous collision of the required number of molecules, as such an event is considered extremely unlikely. The most probable mechanism is by bimolecular addition of molecules according to the scheme (Mullin, 1972);

$$A + A \Leftrightarrow A_2$$
$$A_2 + A \Leftrightarrow A_3$$
$$A_{n-1} + A \Leftrightarrow A_n (critical cluster)$$

Further molecular additions to the critical cluster would result in nucleation and subsequent growth. Ions or molecules in solution can interact with one another to form short-lived clusters. Short chains may be formed initially, or flat monolayers, and eventually a lattice structure builds up. This construction process will occur very rapidly and continue in local regions of high supersaturation. Many of the 'sub-nuclei' will fail to reach maturity and redissolve because they are unstable. If however, a nucleus grows beyond a certain critical size, it becomes stable under average conditions of supersaturation obtained in the bulk of the fluid.

Primary nucleation is an activated process which means that local or temporary peaks of supersaturation are quickly reduced to the metastable supersaturation ($\Delta c \rightarrow \Delta c_{met}$). The primary nucleation rate is a function of the actual local supersaturation. After this nucleation step, particles will grow at the moderate supersaturation ratio with the growth rate being a function of $\Delta c$.

The homogeneous nucleation rate is highly dependant on the supersaturation and has rapid changes over a very narrow supersaturation interval. This indicates that there is a critical interval for supersaturation, below this the nucleation is negligible and above this the rate is very rapid. The critical region is usually the saturation at which 1,10 or 100 nuclei $s^{-1}cm^{-3}$ is equal to the nucleation rate. If the supersaturation or the temperature increases the nucleation rate increases. Also at a particular supersaturation the nucleation rate increases with increasing equilibrium solubility.

The general dependence of the homogeneous nucleation rate, $J$, on supersaturation can be represented by the relation;

$$J = k_n' S^n \qquad (3.36)$$

where $n$ is the kinetic order of nucleation and although $k'_n$ has no physical significance, it is very useful in practice (Sohnel and Garside, 1992). Experimental studies of homogeneous nucleation have confirmed that a small change in supersaturation can lead to a steep increase in the number of crystals being formed and to a simultaneous decrease in their size (Nielsen, 1964).

Sohnel and Garside, (1992) describe the extension of classical nucleation theory from gaseous and liquid phases to that of the nucleation of the solid phase from a supersaturated solution. The model of both is the same - gradual attachment of separate molecules to a cluster. The change in Gibbs energy accompanying the formation of an embryo comprising of N molecules and having surface area $A_N$ is given by

$$\Delta G_{\text{hom}} = -N\phi + A_N \gamma^s \qquad (3.37)$$

Both terms in this expression for $\Delta G_{hom}$ depend upon the embryo size, N, since $A_N \sim N^{2/3}$. The first term on the right hand side of equation 3.37 is always negative whereas the second is always positive. For small values of N the magnitude of the latter term exceeds the former, the resulting $\Delta G_{hom}$ at first increases. Eventually, the first term

outweighs the second and $\Delta G_{hom}$ starts to decrease. Thus $\Delta G_{hom}$ goes through a maximum. This maximum is the critical nucleus size, $N^*$ and at this size the probabilities of growth and decay are equal.

The critical nucleus size can be determined by differentiation with respect to N to give

$$\frac{d\Delta G_{\text{hom}}}{dN} = -\phi + \gamma^s \frac{dA_N}{dN} = -\phi + \frac{2k_a \upsilon \gamma^s}{3k_v r} \qquad (3.38)$$

where the following relationships have been used

$$A_N = k_a r^2$$

$$V_N = k_v r^3$$

The constants $k_a$ and $k_v$ are often size dependent and may vary throughout the development of the crystal.

Equation 3.37 is set is equal to zero to find the critical nucleus size giving

$$r^* = \frac{2k_a \upsilon \gamma^s}{3k_v \phi} \qquad (3.39)$$

The energy barrier to nucleation corresponds to the change of Gibbs energy accompanying formation of the critical nucleus. This is evaluated by introducing the quantities corresponding to the critical nucleus into eq 3.37

$$\Delta G^*_{\text{hom}} = -N^* \phi + A_{N^*} \gamma^s = -\frac{k_v r^{*3}}{\upsilon} \phi + k_a r^{*2} \gamma^s = \frac{\beta \upsilon^2 \gamma^{s2}}{\phi^2} \qquad \text{(eq 3.40)}$$

where the geometric shape factor β is defined by

$$\beta = \frac{4k_a^3}{27k_v^2} \qquad (3.41)$$

### 3.5.4 Heterogeneous Nucleation

Much more frequently, the formation of a new solid phase is governed by the presence of another solid phase within the system; the new phase therefore appears as a result of heterogeneous nucleation. Particles of a foreign solid phase that can act as a 'catalyst' of nucleation are present in any liquid or gaseous system that has not been thoroughly cleaned. The catalytic effect of a foreign solid phase on nucleation is explained by the resulting decrease in the energy barrier to nucleation if the nucleus forms on the

surface of the foreign phase. According to (Mersmann, 1999), experiments carried out with foreign particles added to the reactants, the nucleation work is reduced to approximately 10% of the value for homogeneous primary nucleation. Furthermore, the rate of heterogeneous nucleation is proportional to the specific surface area of the foreign particles.

The Volmer nucleation model (Walton, 1969 in Sohnel and Garside, 1992) describes the heterogeneous nucleation of a solid in a liquid.

$$\Delta G^{*}_{het} = \frac{\beta \gamma^{s3} v^2 f(\Theta)}{\phi^2} = \Delta G^{*}_{\text{hom}} f(\Theta) \qquad (3.42)$$

where the function $f(\Theta)$, which depends on the wetting angle of the solid phase by the liquid is given by

$$f(\Theta)=(2-3\cos\Theta+\cos^3\Theta)/4 \qquad (3.43)$$

If the solid phase is not wetted by the liquid, that is if $\Theta = 180^{\circ}$, then $f(\Theta) = 1$ and according to equation 3.42, $\Delta G^{*}_{het} = \Delta G^{*}_{hom}$. In this case, nucleation is not influenced by the foreign solid phase. For liquids wetting the surface of the solid phase $\Theta < 180^{\circ}$, $f(\Theta) < 1$ and therefore $\Delta G^{*}_{het} < \Delta G^{*}_{hom}$. The foreign solid phase then makes nucleation easier and serves as a nucleation catalyst so that nucleation occurs at a lower supersaturation than without the foreign surface being present.

For nucleation of one solid phase onto a foreign solid phase, the wetting angle has no real physical meaning. The form of equation 3.42 is still advantageous for further application and so $f(\Theta)$ can be best considered as a measure of the nucleation enhancement by the foreign surface without ascribing to it any precise physical interpretation.

The catalytic effect of foreign solid phase particles on the nucleation is a function of particle size, furthermore, surfaces within the reactor geometry (walls, blades, shafts etc,) may also have some contributing effect.

The formation of crystals by heterogeneous nucleation is independent of the supersaturation, but dependent on the foreign particles in the solution. If the supersaturation is kept constant the nucleation rate will vary with time. This will result in a variation of the nuclei sizes until steady state has been achieved. Once steady state has been reached the nucleation rate will also stabilise.

Formation of new crystals by homogeneous nucleation is feasible only under specific conditions. Only the temperature and the presence of admixtures of an ionic nature essentially influence homogeneous nucleation. Nucleation rate increases as a function of temperature, most likely due to higher molecular mobility at higher temperature. Admixtures in the lattice of the crystallising solid or built into the nucleus bring about an increase or decrease of the surface energy of the solid phase. The kinetics of heterogeneous nucleation, unlike those of homogeneous nucleation are influenced by a number of external parameters. The principal difficulty encountered in any experimental study lies in deciding whether a parameter influences nucleation itself, the subsequent growth of the nuclei, or both processes simultaneously. As a rule, experiments have to be performed to study the influence of a given parameter on the crystallisation induction period and the width of the metastable zone on the nucleation rate.

Determination of the nucleation rate is based on the relation:

$$J \sim N_c / t_{ind} \qquad (3.44)$$

Exact determination of the nucleation rate is problematic as the measured values of the number of crystals formed, $N_c$ and the induction time, $t_{ind}$, are dependent on the experimental techniques employed (Sohnel, 1981). Moreover, values for nucleation rate can be modified by secondary processes such as agglomeration or re-crystallisation. Any results achieved for nucleation rate should therefore be treated with caution.

Secondary nucleation is experienced if the formation of new particles in a supersaturated solution result from the prior presence of the solid phase being formed. The mechanism can be divided into three main categories (Garside and Davey, 1980):

1. Apparent secondary nucleation when the nuclei are brought into the system along with inoculating crystals.
2. True secondary nucleation where new nuclei are formed due to crystal-solution interactions.
3. Contact nucleation where nuclei are formed by collisions between crystals or between crystals and crystalliser.

During precipitation involving the crystallisation of sparingly soluble substances, true secondary nucleation may occur with the nuclei formed in several ways:

1. Formation of nuclei on the surface of the solid phase to give structures such as dendrites which grow on the surface of the mother crystal and subsequently break off from the mother crystal.
2. Formation of nuclei in the liquid phase due to structural changes of the liquid adjacent to a crystal or as a result of the presence of dissolved admixtures inhibiting the crystallisation process.
3. Formation of nuclei in the absorption layer on the surface of the growing crystal in the form of molecular aggregates having a crystalline structure, from where they are washed into the solution.

In sparingly soluble substances, secondary nucleation is unlikely to take place at all or only to some small extent. The numbers of crystals resulting from secondary nucleation are significantly lower than the primary nucleation and hence secondary nucleation is overshadowed by primary mechanisms.

### 3.5.4.1 Induction period

The time elapsed between the establishment of supersaturation and the first changes in the system physical properties due to the formation of solid phase is called the crystallisation induction period (also know as 'induction time', 'waiting time' or 'incubation period'). The induction period is determined by; the appearance of the first visible crystals, an increase in turbidity, a concentration decrease or a change in solution conductivity. The corresponding induction period is designated as the induction period determined visually, turbidimetrically, by concentration or by conduction respectively.

If determined visually, it represents the sum of the times taken for a critical nucleus to form and for the time it takes for the nucleus to grow to a visible size. If determined by concentration measurement, it represents the sum of the times taken for a critical nucleus to form and for the time such that the concentration to decrease by a given value.

The level of supersaturation has a strong influence on the induction period. If the relationship between $log\ t_{ind}$ and $(log\ S_0)^{-2}$ is determined over a sufficient range of

supersaturation, two straight lines having markedly different slopes are usually obtained. An example is shown in figure 3.17 for the precipitation of calcium carbonate.

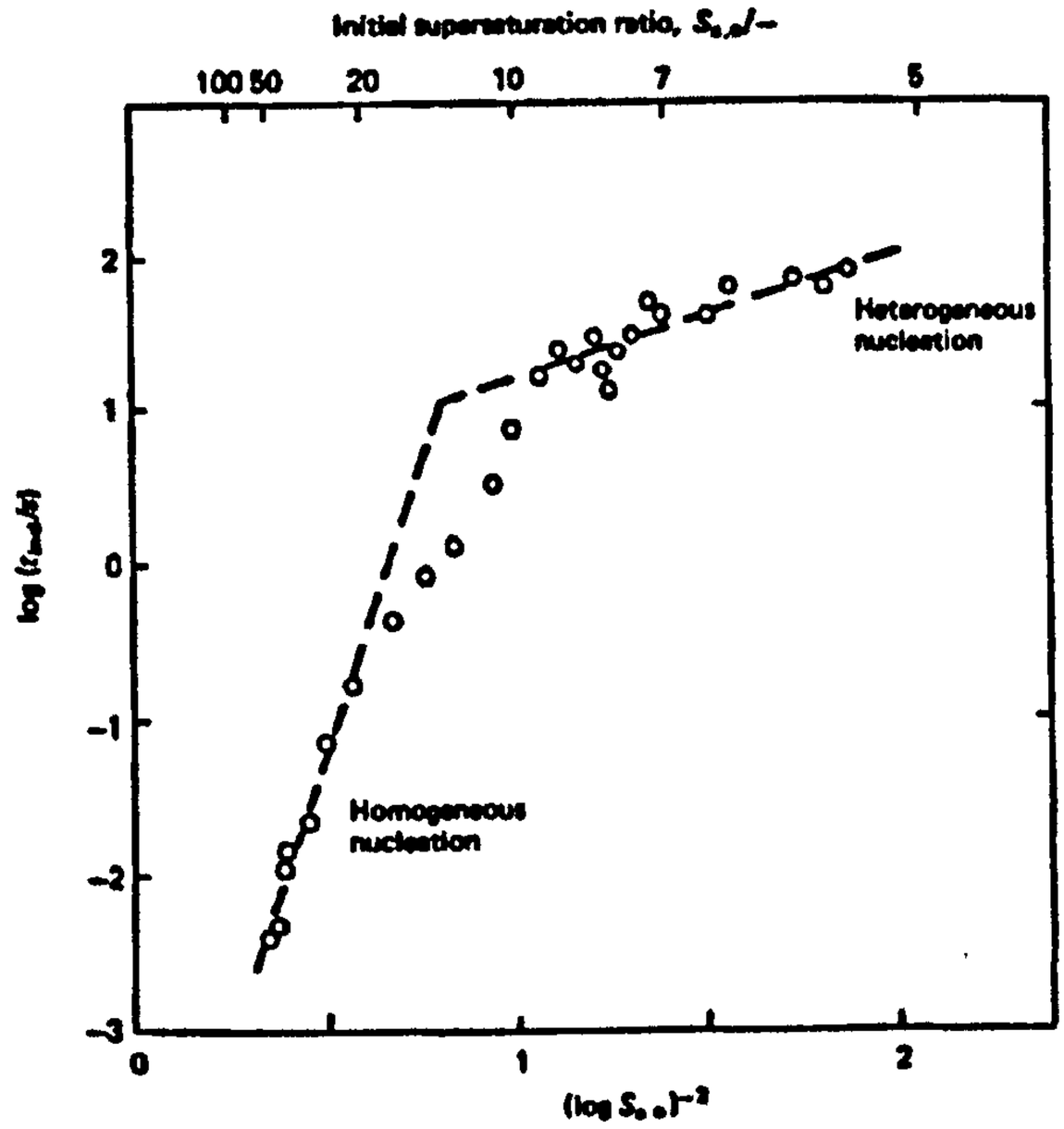


**Figure 3.17 Induction period of $CaCO_3$ precipitated at 25°C as a function of initial supersaturation ratio evaluated in terms of activities (reproduced from Sohnel and Garside, 1992)**

At lower supersaturation, heterogeneous nucleation is the effective mechanism, while at high supersaturation, homogeneous nucleation dominates. The change in the nucleation mechanism necessarily results in a change in slope.

### 3.5.4.2 Crystal growth

Once a stable crystal nucleus has formed in supersaturated solution, molecules will be constantly added to the surfaces of the crystal lattice as the solution desupersaturates. The rate of crystal growth is generally expressed as the rate of displacement of a given crystal face in the direction perpendicular to the face. The growth rate can only be determined in this way if the crystals are sufficiently large. In the case of very small crystals, such as those produced during precipitation, the linear face growth rate cannot usually be determined with any accuracy and it is necessary to determine the overall growth rate. The overall growth rate is expressed as the time derivative of the radius of the sphere having a volume equal to the average volume of one crystal.

Two processes influence the growth of crystals, the mass transport from the solution to the crystal surface by volume diffusion or convection (or both) and the incorporation of material into the crystal lattice through a surface integration process. These processes take place consecutively therefore at steady state the solution concentration adjusts itself so the rates of the two steps are equal. The controlling mechanism is determined by the respective rate constants i.e. if that of the mass transport is the higher rate constant then the overall growth rate is controlled by the surface integration.

If there is movement due to sedimentation or stirring, then the diffusion field which is established around the crystal in a stationary solution is disturbed by the supply of solution with a higher concentration, therefore increasing crystal growth.

The mechanisms of crystal growth are covered in depth by (Mullin, 1972) and (Sohnel and Garside, 1992). A general expression for the overall driving force can be written as;

$$\frac{dm}{dt} = K_G A_C (c - c^*)^n \qquad (3.45)$$

where $K_G$ is an overall growth coefficient, $A_C$ is the surface area of the crystal and *dm/dt* is the mass deposited in time *t*. The exponent, *n*, is usually referred to as the 'order' of the overall crystal growth rate process, but the use of this term should not be confused with its more conventional use in chemical kinetics. Obviously the parameters in equation 3.45 are dynamic as the precipitation progresses since the concentration driving for decreases and the surface area of the crystals increase.

#### *3.5.4.2.1 Growth controlled by transport processes*

Steady state diffusion is established around every growing crystal which is stationary in solution. If the distance between the crystals is greater than about 20 particle diameters, the diffusion fields around separate crystals do not influence each other and may be taken to be infinite in extent. (Sohnel & Garside, 1992) provide equations relating the steady state diffusive mass flow towards a crystal according to Fick's law for determining growth rate and introduce a crowding factor which is a function of the distance between crystals in diffusion fields. When the distance between crystals is less than about 20 particle diameters, the diffusion fields around each crystal begin to influence each other. This results in the concentration gradients around each crystal

being greater than when the crystals are further apart. The crowding factor increases rapidly with decreasing mean particle size and therefore crystal growth rate also increases. When overlapping diffusion fields have been established around individual crystals, both the values of crowding factor and the growth rate are independent of the diffusion layer thickness.

In the case where crystals are in relative motion with the surrounding solution i.e. under agitation or sedimentation, the diffusion field will be disturbed by the supply of solution with higher concentration, resulting in a higher growth rate. The critical crystal size at which such convective processes begin to influence diffusion to crystals growing under sedimentation or gentle stirring conditions were estimated by (Nielsen, 1980):

$$r_{crit} = \left( \frac{9.D.\mu}{2.a.|\Delta\rho|} \right)^{\frac{1}{3}} \qquad (3.46)$$

where $D$ is the diffusion coefficient of the solution, $\mu$ is the solution viscosity, $a$ is the acceleration and $\Delta\rho = \rho_s - \rho_f$. If the crystal is greater than the critical crystal size, the influence of convection for diffusion controlled growth becomes significant. This can normally be ignored for crystals smaller than 5 to 10μm. However, in the present study where the solution and crystals are under high accelerations due to the rotation of the disc, the critical size may become much smaller; the high rates of mixing leading to a reduction in the diffusion layer thickness. Hence it is feasible that the spinning disc may contribute to higher crystal growth rates than that experienced in conventional precipitation equipment.

### 3.5.4.3 Agglomeration

The phenomenon of agglomeration takes place when some particles join together within a supersaturated solution to form crystals of higher dimensions than the original ones. This occurs through three consecutive steps (Klein and David in Mersmann, 1995):

1. the collision between particles
2. the existence of a sufficiently long period of time in which the two particles stay united

3. the adherence of the particles with the contribution of supersaturation.

Many factors influence these steps and this partly explains why it is difficult to analyse. In each situation, the most important factor in the development of the agglomeration process can be contributed to the following fundamental parameters:

- the hydrodynamics
- the solvent properties (density, viscosity etc.)
- the dimensions of the crystals, which greatly influence how the second step occurs in such a way that the time for the development of the third step is sufficient; the experimental results acquired show that for every case of precipitation that leads to the formation of small primary particles, agglomeration will play a significant role in determining the final crystal dimension
- the population density of the crystals which directly influences the collision frequency of the particles
- the supersaturation level and consequent growth rate which determine the development of the third step
- the existing forces between solvent, impurities and the particles, which are very important for the second step

The study of the agglomeration process is compounded by the difficulty of differentiating it from the growth process in relation to the crystal structure and the measurement of the mono-crystal size and number within the agglomerated particle.

In determining the collision step, the process can be divided into two phenomena, the motion of very small particles (with dimensions below 1μm) in a solution at rest, know as perikinetic agglomeration, and the motion of particles in agitated solution, know as orthokinetic agglomeration. Smoluchowski's model described in (Mersmann, 1995) implies that for a solution at rest, the degree of agglomeration varies proportionally with time, whereas for an agitated solution, the degree of agglomeration has an exponential dependence with time and this will be influenced by the local velocity gradients in the agitated solution.

### 3.5.5 Aging

Aging is the term given when precipitate in contact with the mother liquor leads to changes in the physical and/or chemical properties of the solid phase. One such process involves the re-crystallisation of non-equilibrium shapes of primary particles (needles, dendrites, plates etc) into more compact forms such as cubes. This may also involve the transformation of metastable to stable crystal forms. (Sohnel and Mullin, 1982) observed the aging of an amorphous calcium carbonate gel into crystalline calcite. During this process, water was liberated from the recrystallisation.

### 3.5.6 Ostwald's law

(Ostwald 1897) formulated the original statement to describe the observed appearance of thermodynamically metastable phases.

*"If the supersaturated state has been spontaneously removed then, instead of a solid phase which under given conditions is thermodynamically stable, a less stable phase will be formed."*

In other words, the formation of a thermodynamically stable phase will be preceded by that of a number of metastable phases possessing greater energy than the stable phase provided that the formation of solid proceeds sufficiently quickly. During precipitation from highly supersaturated solutions, the solid phase that first precipitates is frequently metastable. In the case of calcium carbonate, it can appear in the crystalline modifications of calcite, aragonite and vaterite, and as amorphous carbonate. During precipitation from strongly supersaturated aqueous solutions at 25°C, amorphous carbonate is first formed, with further contact with the mother liquor, this converts to the metastable vaterite, which in turn changes to calcite (Sohnel and Mullin, 1982). In general, metastable nuclei may first form followed by rapid dissolution and the nucleation of stable nuclei, however this process may occur in parallel with the formation of stable nuclei from the onset of precipitation. Growth (and dissolution) may occur on both metastable and stable nuclei within the precipitating system as well as secondary processes such as aggregation and agglomeration. Ostwald's law as well as its application is much more complicated than was originally proposed and reliable conclusions can only be arrived at by considering the crystallisation kinetics and possible modification of the solid phase being formed (Sohnel and Garside 1992).

### 3.5.7 General kinetic concepts of precipitation on controlling crystal size

Mersmann (1999) echoes the work of many other workers in stating that median crystal size and crystal size distribution mainly depend upon the crystallisation kinetics. The rates of nucleation and crystal growth are controlled by supersaturation. In reaction crystallisation (precipitation), two or more components react chemically, with a result that a new product is formed. If the initial reactant concentration is high, there will be a correspondingly high supersaturation (assuming the solubility of the product is low), leading to high rates of primary nucleation. Since foreign particles in the nanometre range are always present in reaction solutions, heterogeneous nucleation will take place. Homogeneous nucleation can be dominant at very high supersaturation.

The rate of primary nucleation is a function of the actual local supersaturation. After this nucleation step particles grow at the moderate supersaturation. If the residence time in the precipitator is small, the size increase is small too. Nano-sized particles can be obtained by applying very high nucleation rates, which require very strong supersaturations achieved by the following;

- high concentration of reactants
- products with high concentration but low solubility
- rapid micromixing at the feed point of the reactants for a fast chemical reaction.

Furthermore, controlling the size distribution requires;

- rapid quenching or diluting in order to stop growth
- fast local micromixing of the reactants but poor macromixing
- avoidance of agglomeration (addition of surfactants and/or a change in pH)

### 3.5.8 Crystal size and morphology

According to (Walton in Sohnel and Garside, 1992) the supersaturation ranges whereby each primary nucleation mechanism and resulting precipitate structure might be seen are summarised in table (3.2) below. However, the supersaturation will also have an influence on crystal growth.

| Initial supersaturation ratio, $S_o$ | Nucleation mechanism | Mechanism of Growth | Product morphology |
|---|---|---|---|
| <2 | Heterogeneous | Surface reaction | Compact crystal shape, well developed |
| 2-10 | Heterogeneous | Surface reaction | Compact crystal shape, well developed |
| 10-50 | Heterogeneous | Compound | poorly developed crystals, dendrites |
| >100 | Homogeneous | Compound or diffusion | Small isometric crystalline particles, often agglomerated |
| >1000 | Homogeneous | Diffusion | Very small particles or colloids, often amorphous agglomerates |

**Table 3.2 Effect of supersaturation ratio on nucleation and product morphology (Sohnel and Garside, 1992)**

The physical aspects of size and morphology principally determine the characteristics of a crystalline product. These properties are determined by the mechanisms and relative rates of the individual processes that take place during precipitation and influence the reactivity of the solid and it's mechanical and optical properties.

With heterogeneous nucleation predominating at low supersaturation, the number of crystals is determined by the number of active heteronuclei within the solution. Nucleation is followed by crystal growth, the mechanism of which largely governs the crystal shape. If surface reaction controlled growth takes place at low supersaturation, compact crystal shapes are formed such as spheres or octahedra. The equilibrium state of the crystal corresponds to the most compact shape and governed by the minimum overall surface energy of the crystal surface, and is usually reached only during very slow growth conditions ('quasi-stationary conditions'). Precipitation is always a dynamic process yet the crystals very often approach the equilibrium shape. If the growth rate is pronouncedly anisotropic (having different properties in different directions), elongated shapes such as needles, rods and plates may be formed (Sohnel and Garside, 1992).

In the heterogeneous nucleation region, the specific crystal shape that is formed is dependent upon the initial supersaturation. At high supersaturation, the rate of crystal growth can reach such high values that the heat of crystallisation released cannot be transferred sufficiently quickly from the crystal into the neighbouring solution or conducted into the bulk of the crystal. The crystal faces become surrounded by depleted solution, as molecular diffusion cannot supply solute to the crystal at a fast enough rate. In this scenario, the crystal edges, reaching into regions of less depleted

solution tend to continue growing causing elongation and at the same time, extension of the crystal surface aiding the transfer of the heat of crystallisation. However, it is imagined that the size of the crystal involved would be in the region of 10μm and above when this effect becomes a factor if the reactor is well mixed.

Further increasing the supersaturation contributes a greater mass available to precipitate so that the system can attain equilibrium is also increased. If it is supposed that the activity of the heteronuclei does not depend too much on the supersaturation, the number of particles that form in the system is essentially constant and independent of the initial supersaturation. A larger amount of mass is being deposited on these given nuclei and therefore results in a larger final mean particle size (figure 3.19 curve a).

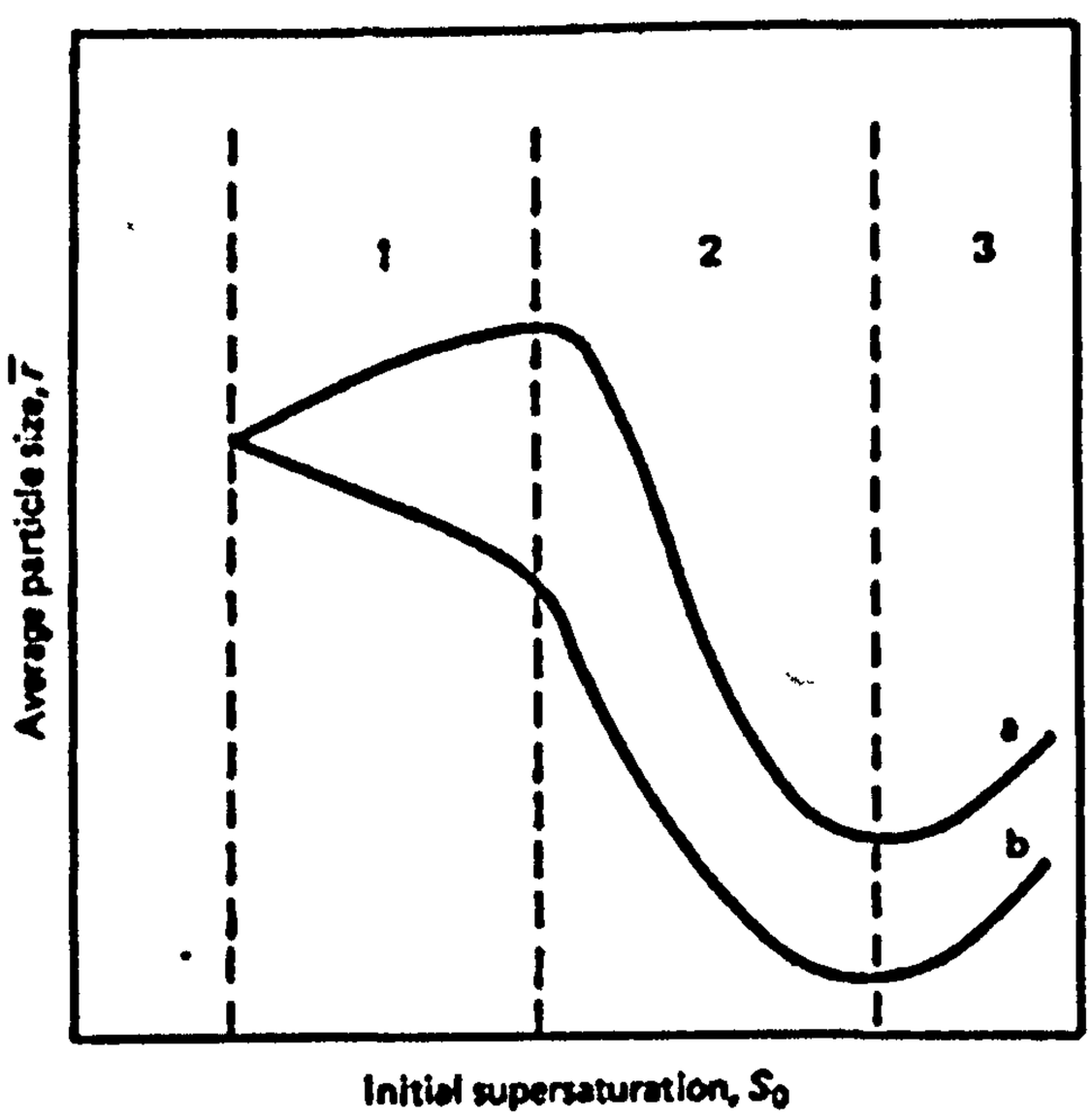


**Figure 3.18 Schematic relation between average particle size and initial supersaturation, region 1 - heterogeneous nuclei; 2 - homogeneous nucleation; 3 - agglomeration. Efficiency of heteronuclei independent of supersaturation (curve a) and increasing with increasing supersaturation (curve b) Reproduced from Sohnel & Garside, 1992.**

If the initial supersaturation is continually increased, the critical supersaturation at which homogeneous nucleation becomes important will eventually be attained and this results in a sudden rise in the number of particles formed. As a result, their final size begins to decrease and the crystals become more isometric, having insufficient time to develop well-defined crystal faces. Precipitates formed under these conditions often appear amorphous and will attain crystalline character only after a period of time.

The decrease in particle size in the region of homogeneous nucleation is pronounced since the amount of mass which must be deposited before equilibrium is attained increases far more slowly than the number of crystals being formed. For this reason, the maximum crystal size is usually reached in the region of the critical supersaturation before the effect of homogeneous nucleation is significant. This relation between supersaturation, size and crystal shape is only schematic. The crystals are not always largest in the region of the critical supersaturation for homogeneous nucleation, represented by a narrow region around the boundary between region 1 and 2 in figure 3.19.

If heteronuclei become increasingly effective as the supersaturation increases so that the number of particles rises with increasing supersaturation, the final crystal size will decrease with increasing supersaturation (figure 3.19 curve b). After exceeding the critical supersaturation, however, the particle size decreases more rapidly. In both cases an apparent increase in crystal size at high supersaturation may be observed as a result of agglomeration of very small particles.

A number of other parameters influence the shape and size of crystals; specific admixtures, excess of one constituent ion, temperature, system pH, intensity of stirring, ionic strength and the order and rate at which the reactants are mixed together.

### 3.5.9 Choice of crystalliser

In crystallisation from solution the degree of supersaturation determines the properties of the crystalline product. This supersaturation can be achieved by cooling, evaporation, drowning out, or in the present study, reaction (reactive crystallisation). The properties which can be altered by the degree of supersaturation are:

- Crystal size distribution
- Median crystal size
- Purity
- Crystal shape.

These are also strongly influenced by

- Geometry and size of crystalliser
- Operating conditions

- Properties of liquid and solid phases.

Therefore the choice of crystalliser is determined by the product requirements. If the product has a specific outline then the local and mean supersaturation as well as the residence time of the solid must be controlled. The degree of supersaturation is determined by the flows of materials and energies and by crystallisation kinetics, i.e. nucleation and growth. As a certain size distribution is usually required the population balance is also very important.

In determining the choice of crystalliser, the following aspects may be considered in its design and operation:

- Agglomeration for small crystals and attrition for large crystals
- As crystals usually have a higher density then the solution settling will occur. An up flow current usually compensates for this in a stirred vessel operation. Therefore crystallisers are usually fitted with rotors, stirrers or pump impellers but these can all cause attrition.
- Fluid properties of the slurry also affect the quantity of the product.
- Macromixing is used to aid the distribution of solid material and supersaturation in the solution. This is important for coarse crystalline products.
- In drowning out and precipitation, the local supersaturation is determined by micromixing,
- Continuous crystallisers usually have high production rates, as operation is more economical with respect to investments, energy and labour costs. For several products in the same crystalliser a batch crystalliser is normally used.
- The fluid dynamics of the system varies in each type of apparatus. That is the degree of mixing and attrition varies.
- The supersaturation is the difference between the actual concentration and the equilibrium concentrations and may be dispersed unevenly throughout the crystalliser.
- The rate of nucleation and crystal growth determine the crystal size distribution.

### 3.5.10 Nanoparticles from precipitation

The field of nanoscale science and technology is emerging as the next industrial revolution. Kai (in Saxl, 2000) outlines the future of nanotechnology:

*"Imagine a technology so powerful that it will allow such feats as desktop manufacturing, cellular repair, artificial intelligence, inexpensive space travel, clean and abundant energy, and environmental restoration; a technology so fundamental that it will radically change our economic and political systems; a technology so imminent that most of us will see it's impact within our lifetimes. Such is the promise of Nanotechnology."*

Potential applications cover a multitude of disciplines ranging from pharmaceutical and therapeutic drugs, electronics and computing, ceramics and plastic composites, green chemistry, catalysts and photovoltaics. (Klabunde, 2001) provides a comprehensive guide to the applications of the nano-world.

What all of these applications have in common is the unique chemical and physical properties that exist on the nanoscale (regarded as any size less than a micron). These properties really emerge as 1nm is approached. The nanoscale lies between the realm of chemistry (atoms and molecules) and physics (solid state) and properties of magnetism, optical, melting points, conductivity and specific heat may be changed in this region. In this region, neither quantum chemistry nor the classic laws of physics may not hold true for certain materials, so perhaps a new science will emerge from the two. Nanoscale materials are not a new phenomenon. Colloids and catalysts have been in development in industry for decades and have contributed to significant improvement in processes.

From all these fields, whether it is simply making simple inorganic nanoparticles or complex structured materials built atom by atom, the potential benefits from these materials are vast. New industries will emerge which may prove to be a new epoch in human society comparable to the first industrial revolution.

In the context of the present literature study, the field of nanoparticles and nanocrystals will be considered with emphasis on their manufacture and application. We shall consider the manufacture of these as precursors to more advanced materials and use classic chemical industry products as examples. Inorganic materials lend a significant part to these applications. Most importantly with the manufacture of these materials is

the control of particle size and size distribution. Without uniform product size, application potential cannot be maximised. For example, in catalytic processes, the activity of a heterogeneous catalyst is dependent upon the surface available to incoming reactants. With decreasing particle size, the specific surface area per unit volume increases hence smaller particles of catalyst leads to higher reaction rates. Particle shape is important too. Crystal faces, edges, corners and defects all lead to enhanced surface activity.

Nanoparticles can be prepared by physical vapour deposition, chemical vapour deposition, reactive precipitation, sol-gel and micro-emulsion techniques. Preparation techniques by precipitation methods are convenient due to low cost and mass productivity. However, the conventional methods of precipitation have many disadvantages in that it is difficult to control the product quality and the morphology and size distribution are also variable from batch to batch. Therefore a method is required that will produce repeatable results to give some consistency in the properties of the product.

Paints contain a significant amount of $TiO_2$ particles held in emulsion to provide covering for many surfaces. $TiO_2$ is already produced on the nanoscale but it tends to agglomerate once formed. By changing the individual particle size and shape, it is possible to change the optical properties of the paint. Product size is in the region of 270nm, approximately half the wavelength of green light, which allows the maximum diffracting properties of the paint. Furthermore, pigment properties may be changed with blending particles of different types and sizes to create different colours and finishes. The particles may be subjected to a surface coating of organic or inorganic nature, which in turn change its solubility and transport properties.

Nanoparticles, when structured in bulk materials, may possess enhanced physical properties. Combining needle-like or platelet shaped nanoparticles in polymer matrices may lead to composites, which are stronger, lighter, wear-resistant, tougher and flame retarding with the potential of becoming a replacement for metals in some applications. Current filler materials in plastics such as calcium carbonate, barium sulphate and many other inorganic precipitates may be produced in nanoscale forms to provide for these composite materials.

Regardless of the application, what is really important is the requirement of controlling particle size and shape in manufacturing. Another important requirement is the ability to manufacture nanoparticles by cost effect methods without which nanoscale applications will remain in exclusive niches. It is from these two considerations that PI technologies might compliment the new science significantly.

### 3.5.11 Effect of mixing on precipitation processes

(Nielsen, 1964) considered the mixing effects in precipitation reactions. The basis for his model was for straightforward molecular diffusion at the junction of two solution masses. (Pohorecki and Baldyga, 1983) and (Fitchett and Tarbell, 1990) considered fluid mechanical effects and turbulent mixing. Both discussed the intensity of mixing (i.e. the rate of energy dissipation per unit mass) influence on nucleation and growth rates. The former authors introduced some basic notions of turbulence and micromixing theory, the latter considered both micromixing, in which basic turbulence notions were involved and more macroscopic consequences of turbulence effects, e.g. mass transfer coefficients. Both carried out experiments involving the precipitation of $BaSO_4$ in stirred vessels to which reactant solutions were added. (Fitchett and Tarbell, 1990) were unable to model the nucleation results of (Pohorecki and Baldyga, 1983), although growth rate results were in qualitative agreement. The former researchers were able to model their runs for high reactant feed solutions (0.15 M). This was not so for lower concentration runs. Both residence times and power inputs were varied. The results showed that growth rates increased and nucleation rates decreased with increasing power input and sensitively so. They concluded that high concentrations were successfully modelled because homogeneous nucleation occurred only under those conditions. Micromixing effects did not influence particle growth; there was a limited effect upon nucleation rate. The net effect was that growth rate increased with mixing intensity and brought about a significant decrease in supersaturation and consequently in nucleation. The point made in these studies is that the power input in an MSMPR (mixed suspension mixed product reactor) operation may significantly influence the quality of precipitate. There is justification for further studies in this area; e.g., mixing in this context includes the means by which the reactant feeds are introduced to the reactor.

(Marcant and David, 1991) presented a simplification of earlier models to allow qualitative evaluation of the micromixing versus primary nucleation competition.

They found that an experimental parameter, the ratio of volumes of initial reactants containing stoichiometric amounts of reactants, is useful. They discussed results derived from the batch precipitation of calcium oxalate monohydrate. They found that fluid mechanical mixing affects the extent of primary nucleation when the above-noted ratio is different from unity (e.g., 250 and 1.5), agitator speed is inadequate and feed location of one reactant into the other is at a less turbulent location.

We have seen from the section on mixing that there are 3 characteristic regimes for comparing the characteristic reaction (or nucleation) time, $t_R$ with the mixing time, $t_M$:

1. $t_M << t_R$: slow regime, the reaction or nucleation kinetics control the process, the vessel is essentially homogeneous and the reaction takes place through the reactor.

2. $t_M \approx t_R$: fast regime the rate is influenced by both physical and chemical factors and the reaction takes place in the narrow zone on either side of the diffusion plane.

3. $t_M >> t_R$: instantaneous regime, the rate is limited by the rate of mixing by diffusion and the reaction takes place in the diffusion plane.

$t_M$ varies in water from 0.1 to 0.0004s when the specific energy dissipation rate varies from approximately 0.01 to 1000W/kg. Regarding induction time measurements, the formation of detectable crystals can occur within fractions of a millisecond. Hence it is quite possible that nuclei are formed in the smallest primary vortices at the feed point whereby the two reactants first come into contact with each other. These vortices can be of importance for the mean size of the product. In semibatch precipitation, the early moments of the process can be very important with respect to the final crystal size (Marcant and David, 1991).

Precipitation processes may operate in any of the three characteristic reaction regimes identified above. In the fast and instantaneous regimes, the physical characteristics of the precipitated product can be influenced to a considerable extent by the nature of the micromixing process. (Pohorecki and Baldyga, 1983) applied a micromixing model to a batch process and predicted that by increasing stirrer intensity, the average crystal size decreases. An analogous model applied to a precipitation in a MSMPR led to the conclusion that increased stirring intensity at the same mean residence time increased

the mean crystal size. The initial concentration had almost no effect upon particle size (Pohorecki and Baldyga, 1985, 1988).

These conclusions were applied to double-jet mixing. If however, an MSMPR reactor is fed by a single-jet of premixed reactants, an increase in stirring intensity and a decrease in initial concentration of the reactant solutions result in an increase in particle size; the mean residence time has negligible effect on the mean size (Pohorecki and Baldyga, 1988).

(Tavare and Garside, 1984) studied the influence of nucleation and chemical reaction parameters upon the crystal size distribution and the average crystal size formed in an MSMPR by precipitation in the two extreme limits of micromixing. Computer simulations suggested that the average size would increase with increasing mixing intensity, in agreement with (Pohorecki and Baldyga, 1985).

## 3.6 Calcium carbonate processes, products and precipitation

### 3.6.1 Calcium carbonate in the environment

Calcium carbonate occurs naturally in the environment, a principle constituent of limestone, marble and chalk. These geological formations are abundant on Earth in geological deposits laid down over eons from marine biology from the physiology of molluscs, arthropod exoskeletons and corals. Biomineralisation of calcium carbonate can also be seen in the pathology of kidney stones, gallstones and intravasal deposits.

The crystallisation phenomena of this sparingly soluble salt is complicated because it occurs naturally in three crystal structures; calcite, aragonite and vaterite. Calcite is the thermodynamically stable form, aragonite is metastable, transforming to calcite when heated in dry air at 400°C. Calcite, which gets its name from '*chalix*' the Greek word for lime is one of the world's most common minerals making up about 4%wt of the Earth's crust.

Vaterite is metastable to calcite and aragonite under geological conditions but is found during high temperature precipitation (Kirk-Othmer, 1992). The crystal form of calcite is hexagonal-rhombic, varying in habit with over 300 crystal forms identified. Aragonite is orthorhombic with three common crystal habits, acicular pyramidal, tabular and pseudo hexagonal. Vaterite has a hexagonal lattice and has been seen to form spheres or platelets.

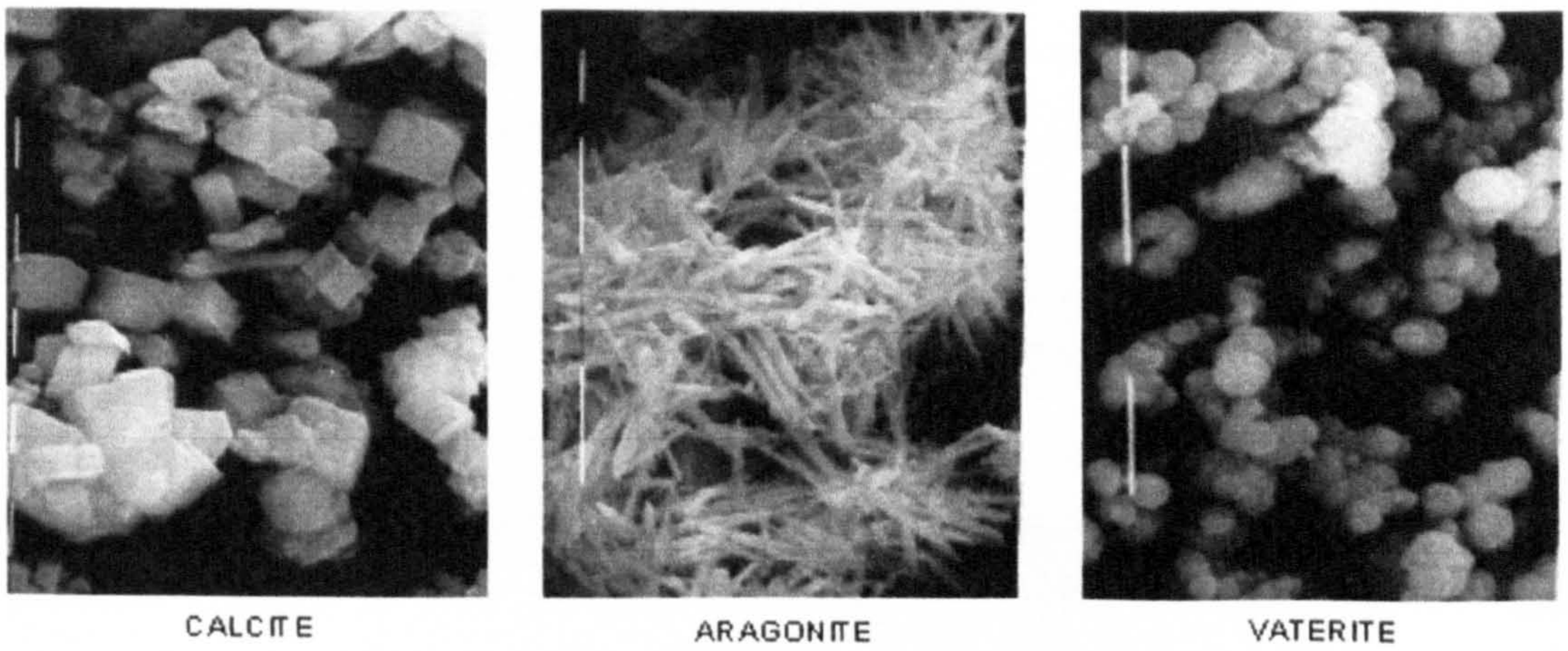


**Figure 3.19 Morphological forms of calcium carbonate**

Calcium carbonate has been seen to form amorphous solids during rapid precipitation as well as monohydrate and hexahydrate forms, which readily decompose and transform to the more stable crystalline phases (Elfil & Roques, 2001).

### 3.6.2 Calcium carbonate in industry

Calcium carbonate is produced by two methods on the industrial scale. It is quarried and ground from naturally occurring deposits. The second method is by precipitation, usually from dissolved calcium hydroxide and carbon dioxide. Naturally ground calcium carbonate (GCC) has been used for many years and is a primary constituent of putty. Processing GCC utilises flotation techniques whereby impurities are removed and grinding equipment to produce finer material. Precipitated calcium carbonate (PCC) was first introduced in England in 1850. Both GCC and PCC compete commercially based primarily on crystal size and the characteristics imparted by the product. Production can be found worldwide and from a variety of processes. Calcium carbonate is a versatile mineral filler, consumed in a wide range of products including paper, paint, plastics, rubber, textiles, caulks, sealants and printing inks. High purity grades find application in food, dentifrices, cosmetics and pharmaceuticals.

Commercial grades of calcium carbonate from natural sources are either calcite, aragonite, or sedimentary chalk. Precipitated grades are predominantly aragonite.

The production of GCC starts with the quarrying of chalk, marble or limestone deposits. These deposits generally have a $CaCO_3$ purity of >90% and high brightness. It is its high opacity that makes it such a useful material in paints etc. Ore is crushed for primary processing and transportation. The process plant is dependent on the final product. Ore is reduced in size further by use of cone or jaw-type crushers, final grinding is by the use of ball or roller mill operations. This reduces the median size to around 5μm. For grades requiring high purity or finer material, a flotation process is employed whereby the impurities are floated out of suspension. The flotation process produces higher brightness material that is typically >98% calcium carbonate. This refined product can have a median size less than 2μm resulting from a wet grind process in a sand mill with the final product being in slurry form. Product may be shipped as dry material or as slurry (typically 50 wt%).

Some grades of calcium carbonate are surface coated to improve handling properties and dispersability in plastics. Treatments used are fatty acids, resins and wetting agents. Coatings reduce the surface energy thereby facilitating dispersion in organic binders.

### 3.6.2.1 Product applications, properties and economics

The use of calcium carbonate in paint, paper and plastics make up the principle part of the market. In the papermaking industry, calcium carbonate has two uses; as a filler and as part of the coating. The demand for calcium carbonate in papermaking has been driven by a change from acid to alkaline papermaking processes.

From the 1980s onward, small satellite PCC processing plants have been built on or near large paper mills to facilitate high demand for calcium carbonate as a filler material in modern paper manufacture. In fact most acid-free paper contains up to 40% calcium carbonate. This is not only because it is a cheaper material than the wood pulp but also because of the properties of calcium carbonate which lead to higher brightness paper and improved mechanical strength and longevity. The market for calcium carbonate is estimate to be in excess of 6.7 million tonnes p.a. and rising at a rate of 4.5 to 7% for the paper and plastics industries respectively (Roskill, 2000).

As a pigment in paper coatings, ultrafine calcium carbonate improves brightness, opacity, printability, smoothness and ink receptivity. In coatings, calcium carbonate may be the sole pigment in the formulation or be mixed with other fillers such as kaolin. (Ishley and Osterhuber, 1998) present the synthesis and performance characteristics of PCC for paper coating and compare with ground calcium carbonate (GCC).

The plastics industry is a primary consumer of calcium carbonate products. Flexible and rigid PVC, polyolefins, thermosets and elastomers, including rubber, utilise a wide variety of coated and uncoated grades. Each category of plastics benefit from calcium carbonate due to its lower cost in relation to the polymer. In addition to cost savings, calcium carbonate facilitates higher mechanical strength, impact resistance, stability, heat resistance, hardness, shrinkage reduction and colour-fastness. In thermosetting materials, the use of calcium carbonate is replacing other materials especially in automotive applications. Increased loadings of calcium carbonate in thermosets reduce cost and provide better surface characteristics.

Calcium carbonate is one of the most common filler/extenders used in the paint/coatings industry. Commercial paint formulas can include products in the sub-micron range to courser material. The calcium carbonate acts as an extender and also improves the brightness, application properties, stability and exposure resistance. Course products create a textured finish or determine the degree of gloss sheen. Calcium carbonate will also extend and enhance the use of titanium dioxide pigment in paints/coatings, reducing the unit cost.

Calcium carbonate is still used in putty and a multitude of caulks, sealants, adhesives and printing inks. Large quantities are used in carpet backing and in joint cements. It is used to improve body reinforcement and other properties.

Flue gas desulphurisation utilises calcium carbonate. This application by a variety of engineering processes traps sulphur-oxygen compounds produced during the combustion of coal.

Calcium carbonate is used in food and pharmaceutical applications for both its chemical and physical properties. It may be used as an antacid, as a calcium supplement in food and as a mild abrasive in toothpaste and chewing gum. There are extensive other uses for this versatile material.

### 3.6.3 Calcium carbonate precipitation

PCC can be produced from several methods, the principle route being the carbonation of lime. Limestone is calcined in a kiln to obtain carbon dioxide and quicklime – CaO. The quicklime can be hydrated to form slaked lime - $Ca(OH)_2$. The quicklime is mixed with water to produce milk-of-lime. Both may be used as a feedstock. Carbon dioxide is contacted with the milk-of-lime in a reactor, predictably called a carbonator. The $CO_2$ may come from combustion flue gases and hence is a method of sequestration whereby a useful product is produced from waste. Carbonation continues until the calcium hydroxide has been converted to the carbonate. The end point can be monitored chemically or by pH measurements. Reaction conditions determine the type of crystal, size of the particles and the size distribution.

The process reaction steps in this method are as follows;

*calcination:* $CaCO_3 \rightarrow CaO + CO_2$

*hydration or slaking:* $CaO + H_2O \rightarrow Ca(OH)_2$

*carbonation:* $Ca(OH)_2 + CO_2 \rightarrow CaCO_3$

Following carbonation, the product may be further purified by screening to control the maximum size of the product. The slurry of PCC is dewatered using rotary vacuum filters, pressure filters or centrifugation. Final drying is achieved in a rotary, spray or flash dryer. Particle size from PCC techniques are in the range of 0.3μm to 10μm.

There are a number of processes by which calcium carbonate can be precipitated. The soda ash-lime process contacts a solution of sodium carbonate (soda ash) with a slurry of calcium hydroxide to produce calcium carbonate and sodium hydroxide. The soda ash-lime process has the advantage of producing caustic as a co-product and it is therefore suited to integrated pulp and paper mills, which utilise both calcium carbonate and caustic soda in the manufacturing process. Although the soda ash-lime process has been used in the past to produce commercial PCC, it has not demonstrated the same particle structure as the carbonation method. However, it has been reported that by controlling key variables such as reaction temperature, rate and method of reactant addition, agitation speed and the type of mixing impeller can yield high opacity PCC (Merris, 1997). The advantages of this process are the production of co-product caustic soda, better control of the reaction temperature over the carbonation process and control over the sodium carbonate concentration where the carbonation process is variable due to the flue gas concentration fluctuation.

Another method of producing calcium carbonate is from reacting the products of the Solvay process. This is a multistage process in which carbon dioxide is generated from limestone and passed through brine saturated with ammonia. Sodium hydrogen carbonate is isolated and heated to yield sodium carbonate. All intermediate by-products are recycled so that the only ultimate by-product is calcium chloride. Mixing calcium chloride and sodium carbonate solutions yields calcium carbonate as precipitate.

Water is not the only solvent to mediate the carbonation process. (Vucak et al, 2002) investigated $CO_2$ absorption into aqueous monoethanolamine solution at 30°C

containing calcium nitrate. This process produced tiny vaterite spheres, which had coagulated suggesting an aggregation mechanism of particle growth. Although there is development in this process area, from an environmental aspect the use of water as solvent would be the most benign to use and follows the principles of green chemistry and hence the focus of this study is centred on water-based processes for calcium carbonate precipitation.

### 3.6.3.1 Gas-liquid precipitation of calcium carbonate

The carbonation of calcium hydroxide solution (limewater) is the basis to this precipitation route. The crystallisation phenomena is a complicated one with the product having the potential to precipitate in 3 different forms and the operating variables such as pH, composition, temperature and ionic strength are inter-related in the crystallisation process. Limewater is only sparingly soluble and is inversely soluble with solution temperature. Because this only yields a small amount of crystals from the solvent volume, a slurry of calcium hydroxide (milk of lime) is carbonated to attain a larger yield from the working solvent.

#### *3.6.3.1.1 Chemical kinetics of the process*

In considering gas liquid mass transfer, the relationship between the rate of absorption into reacting solutions and the homogeneous reaction kinetics is in general not a simple one because of the depletion of reactant near the surface and other factors, in this case, change in pH and presence of particles. Fundamentals and operations in gas-liquid mass transfer with chemical reaction are covered by (Sherwood and Pigford, 1952), (Danckwerts, 1970), (Doraiswarmy and Sharma, 1984) and (Kastenek et al, 1993).

(Hostomsky & Jones 1995) present the characteristics of the carbonation reaction of limewater leading to the formation and subsequent precipitation of calcium carbonate which can be represented by the following reaction steps:

$$(A_1) \quad Ca(OH)_{2\,(aq)} \Leftrightarrow Ca^{2+}_{(aq)} + 2OH^-_{(aq)}$$

$$(A_2) \quad CO_{2\,(g)} \Leftrightarrow CO_{2\,(aq)}$$

$$(B) \quad CO_{2\,(aq)} + OH^-_{(aq)} \Leftrightarrow HCO_3^-{}_{(aq)}$$

$$(C) \quad HCO_3^-{}_{(aq)} + OH^-_{(aq)} \Leftrightarrow CO_3^{2-}{}_{(aq)}$$

$$(D) \quad Ca^{2+}_{(aq)} + CO_3^{2-}_{(aq)} \Leftrightarrow CaCO_{3(s)}\downarrow$$

where the presence of other ionic species not leading to the formation of calcium carbonate is neglected. Reaction ($A_1$) is considered to have a very high equilibrium constant, thus the calcium hydroxide exists only as a completely dissociated species in solution. The influence of the step ($A_2$) on the process will be considered in the following sections.

The kinetics of reaction (B) and (C) can be described by the relationships:

$$\begin{aligned}(-r_B) &= k_B([CO_2][OH^-] - (K_W / K_1)[HCO_3^-]) \\ (-r_C) &= k_C([HCO_3^-][OH^-] - (K_W / K_2)[CO_3^{2-}])\end{aligned} \qquad (3.47 \ \& \ 3.48)$$

where the kinetic constants at 25°C are according to (Hostomsky and Jones, 1995):

$$K_1 = 4.45 \cdot 10^{-4} \text{ mol/m}^3$$

$$K_2 = 4.69 \text{ mol/m}^3$$

$$K_W = 1 \cdot 10^{-8} \text{ mol}^2/\text{m}^6$$

$$k_B = 12.4 \text{ m}^3/(\text{s} \cdot \text{mol})$$

$$k_C = 1000 \text{ m}^3/(\text{s} \cdot \text{mol})$$

the value assumed for $k_C$ is arbitrary and indicates that the reaction is very fast, thus it can be considered to be at equilibrium. This implies that the kinetic step controlling the chemical reaction rate is (B). It can be noted for the bicarbonate ion, that if its concentration is close to the stoichiometric one, it reacts very rapidly with the $OH^-$ ion to give $CO_3^{2-}$. Reaction (B) can be considered to proceed irreversibly. The reaction (D) is the one that leads to the formation of the precipitated phase.

When the $OH^-$ concentration decreases, the following reaction competes with reaction (B) (Danckwerts, 1970 pp239-240)

$$(B^*) \quad CO_2(sol) + H_2O \Leftrightarrow HCO_3^- + H^+$$

In the presence of carbonate ions this reaction is followed immediately by the reaction:

$$(E) \quad H^+ + CO_3^{2-} \Leftrightarrow HCO_3^-$$

It must be noted that in any solution in which pH>10 the rate of reaction of carbon dioxide by reaction (B) will be more than 30 times greater than its rate of reaction by

reaction ($B^*$); conditions that favour reaction ($B^*$) must be avoided because they lead to a decrease in the calcium carbonate yield.

The overall reaction that occurs between carbon dioxide and the $OH^-$ ion to give the carbonate ion can be represented as:

$$(BC) \quad CO_2 + 2OH^- \Leftrightarrow CO_3^{2-} + H_2O$$

therefore it can be observed that the stoichiometric ratio between calcium hydroxide and carbon dioxide for the carbonation reaction is 1.

Introducing the conversion of the reaction (BC) in respect to the concentration of $OH^-$ ion:

$$X_{OH^-} = \frac{[OH^-]^\circ - [OH^-]}{[OH^-]^\circ} \qquad (3.49)$$

where $[OH^-]$ indicates the $OH^-$ concentration at the generic time, t (considering the final concentration the total conversion is obtained) and $[OH^-]^\circ$ is the initial concentration of hydroxyl ion. The concentration of carbonate ion (if the process is conducted in such conditions that no secondary reactions occur) can be calculated:

$$[CO_3^{2-}] = 0.5[OH^-]^\circ X_{OH^-} \qquad (3.50)$$

this relationship can be used to express the potential initial supersaturation ratio in function of the depletion of pH, which can be determined experimentally. In fact the initial supersaturation ratio $S_o$, is defined as follows:

$$S_\circ = \left( \frac{[Ca^{2+}][CO_3^{2-}]}{K_{SP}} \right)^{1/2} \qquad (3.51)$$

where $K_{SP}$ is the solubility product of calcium carbonate in water. Substituting equation (3.50) in equation (3.51) and considering that the calcium ion concentration is equal to the calcium hydroxide initial concentration the following relationship is obtained:

$$S_\circ = \left( 0.5\, X_{OH^-} \frac{[Ca(OH)_2]^\circ [OH^-]^\circ}{K_{SP}} \right)^{1/2} \qquad (3.52)$$

where $[Ca(OH)_2]^\circ$ is the initial concentration of calcium hydroxide; for the solubility product of calcium carbonate in water the following values have been reported by

Hostomsky and Jones: $3.47 \cdot 10^{-3}$ $mol^2/m^6$ (Plummer and Busenberg, 1982) and $4.01 \cdot 10^{-3}$ $mol^2/m^6$(Langmuir, 1969).

### *3.6.3.1.2 Crystallisation kinetics of the process*

In measuring the change in pH with time in the semibatch carbonation of limewater, (Wachi and Jones, 1991) plotted the change of pH with time. It was shown that the carbonation rate increased with increased stirrer speed and the pH affected the degree of agglomeration (figure3.20).

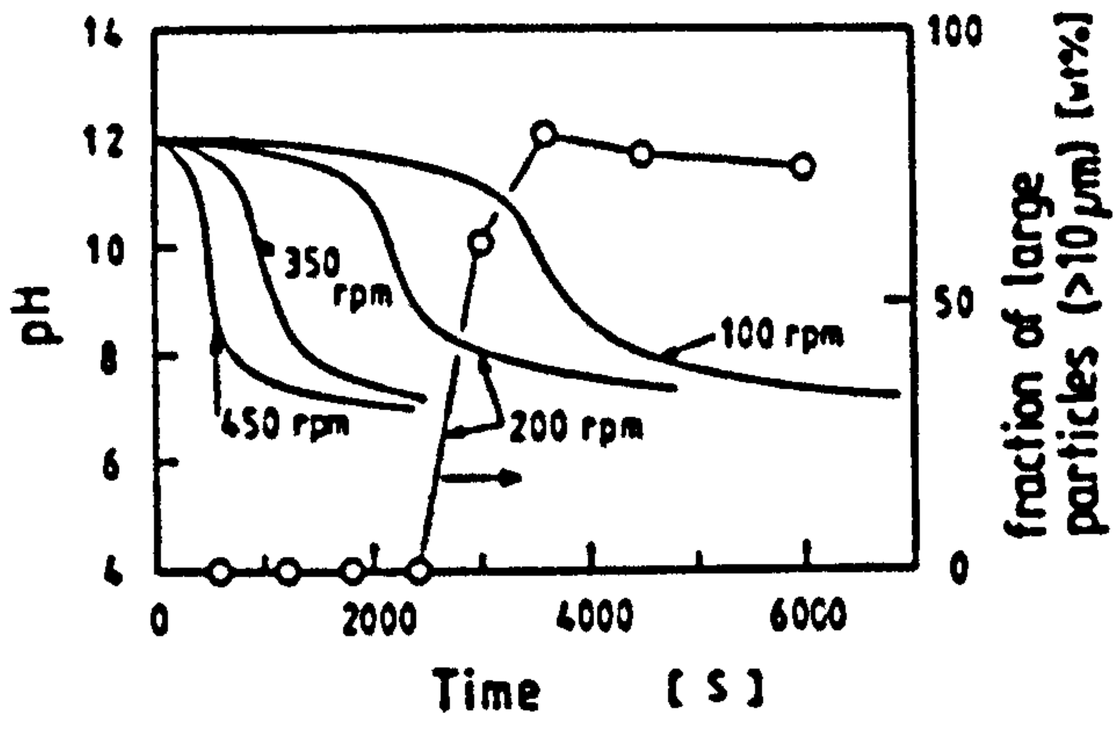


**Figure 3.20 Time course of pH and large particle formation (Wachi and Jones, 1991)**

As is the case of sparingly soluble products from chemical reaction, agglomeration competes with molecular crystal growth as the dominant particle growth mechanism (Wachi and Jones, 1992). The primary crystal size and degree of agglomeration often determine important properties of the particles e.g. settling rate and specific surface area. Agglomeration can contribute to bimodal distribution. Secondary nucleation can be induced by turbulence in industrial crystallisers. In the carbonation of limewater, for example, small crystalline fragments detach from agglomerates due to the vortices created in bubble wakes, hence attrition in agglomerates can produce small crystals. In the present study on the SDR, bubbles may not be present in the liquid film, however the high turbulence generated in the film may contribute to agglomeration and therefore secondary nucleation.

In predicting the CSD kinetics of the multi-step phenomena of nucleation, crystal growth and agglomeration all have to be incorporated in a population balance model, distinguishing between single crystals and agglomerated particles. In modelling the liquid phase concentrations of individual component species near the gas-liquid interface of a solution surface in a semibatch precipitator, (Hostomsky and Jones,

1995) determined the concentration of both reacting species and near the interface developed from the Higbie penetration model. This postulation was considered as an element of solution rising from the bulk to the flat interface, remains there for a period of time (the contact time) and then is swept back into the bulk. It is during this contact time that absorption takes place and therefore the precipitation (resultant from reaction and subsequent supersaturation) is likely to take place in this region rather than in the bulk.

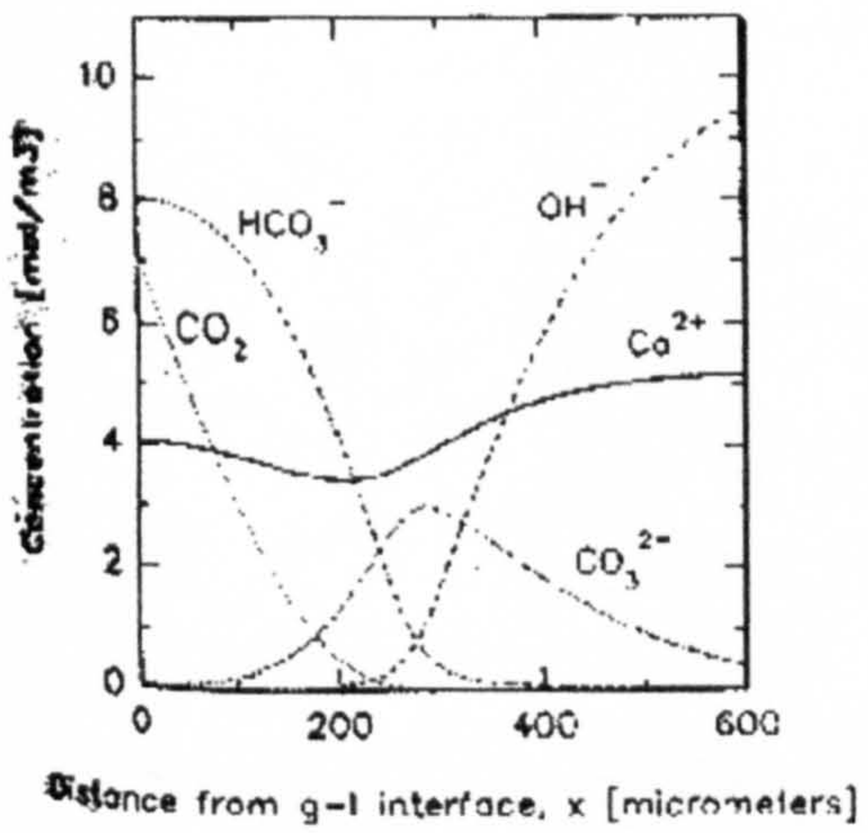


concentration profiles in the interfacial region at the end of the contact time, t=16.93s; $p_{CO2}$ = 0.25 bar; $[Ca^{2+}]_{bulk}$ = 52 mol.m$^{-3}$; $[OH^-]_{bulk}$ = 10.4 mol.m$^{-3}$

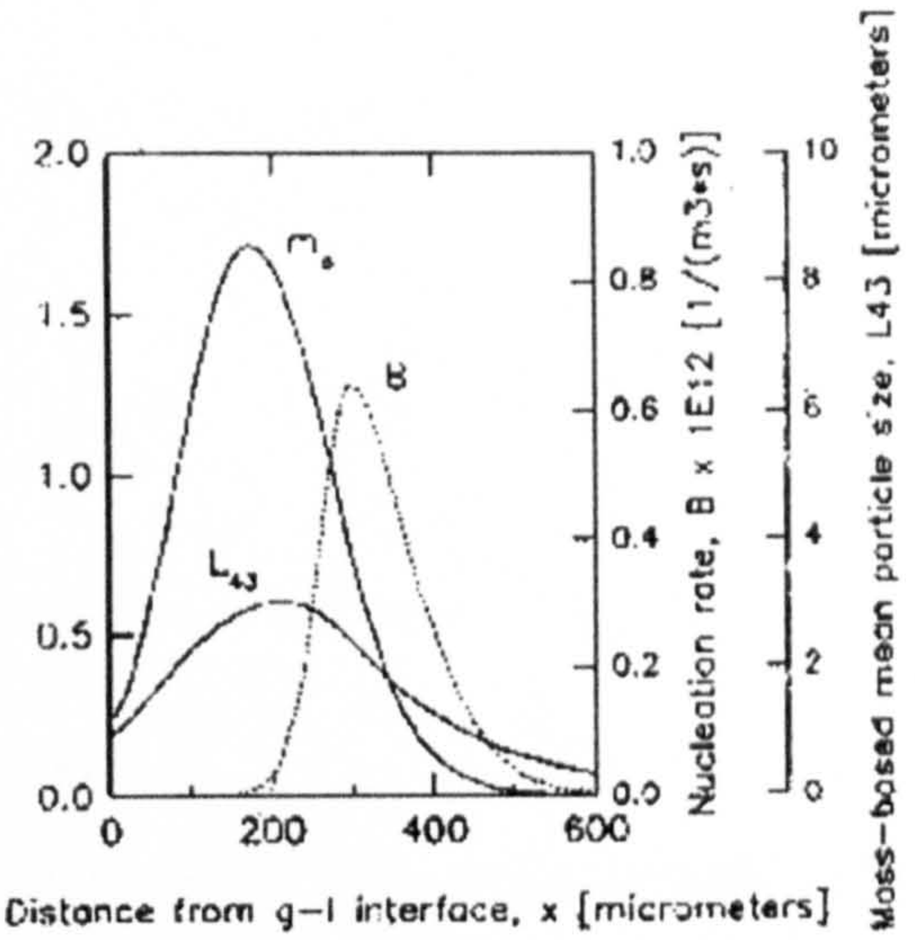


Particle number concentration, mo, nucleation rate and mass-based mean size $L_{43}$ at the end of the contact time

**Figure 3.21 (Hostomsky and Jones, 1995) penetration model concentration and crystallisation kinetic profiles for $CO_2$ diffusing into a flat-surface film**

In figure 3.21 above, carbon dioxide concentration decreases steeply with distance from the interface due to the effect of diffusion and reaction; similarly, hydroxyl ions diffuse from the bulk and deplete near the surface. The $CO_3^{2-}$ concentration, resulting from the acidobasic equilibrium between $HCO_3^-$ and $OH^-$ ions passes through a maximum with a position away from the interface.

Additionally, the level of supersaturation, i.e. the driving force of nucleation and growth (equal to $[Ca^{2+}]^{1/2} - K_{sp}^{1/2}$) also exhibits a maximum. This is reflected in the plots of nucleation rate, particle number concentration and mean particle sizes as a function of distance from the gas liquid interface. The maximum of the particle concentration, $m_0$, is located closer to the interface than the maximum of the nucleation rate, **B**.

At low contact times, the nucleation rate is suppressed by slow kinetics of reaction between $CO_2$ and $OH^-$, whereas the decreasing values of the nucleation rate for the faster kinetics at highest contact times are caused by the depletion of $Ca^{2+}$ ions in the interfacial region. The effect of contact time upon the integral nucleation rate is depicted in figure 3.22.

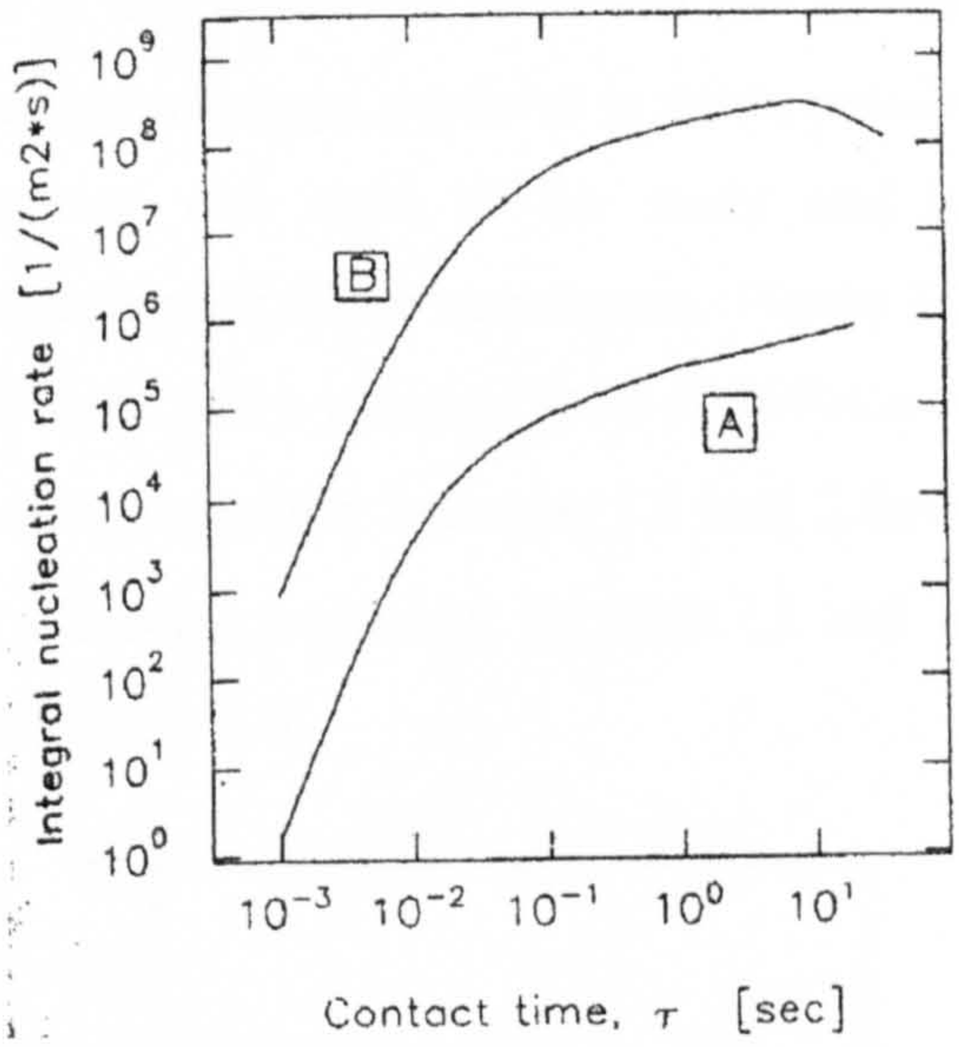


**Figure 3.22 Integral nucleation rates in the interfacial region versus contact time of two different sets of kinetic parameters (Hostomsky & Jones, 1995)**

From the simple model of a precipitator with gas absorption through a clear film of solution with precipitation occurring only in the bulk, Hostomsky and Jones concluded that the model predicted higher terminal values of median crystal sizes at lower mass transfer rates than those given by the penetration model, which considers the crystal nucleation in the interface.

(Jones, *et al*, 1992) observed an increase in the mean bulk crystal size as the rate of agitation in the batch was increased. This was attributed to an increase in the mass transfer coefficient due to the higher rate of mixing. They further noted the presence of agglomerates of dimensions greater than 10μm was predominant in solutions with a pH lower than 10. In this study, the initial $Ca(OH)_2$ concentration was approximately $5.2mol/m^3$ ($\cong 0.4g/l$), conducted in a batch reactor with a flat gas-liquid interface.

(Yagi *et al*, 1984) studied the crystallisation of calcium carbonate accompanying the absorption of a $CO_2$ and $SO_2$ mixture into limewater. They observed the presence of agglomerated particles in calcium hydroxide concentrations greater than $1mol/m^3$ in an MSMPR with a flat gas-liquid interface, with residence times in the range 210 to 840s.

(Wachi and Jones, 1991, 1992) observed the presence of a greater proportion of agglomerated particles (>60 wt%) that rapidly build up around pH 8.0. In explaining this, the authors relate the dependence of the agglomeration phenomena on the pH, with the amount of surface charge on the particles. For high calcium ion concentrations, the particles are negatively charged and the electrostatic repulsion prevents the formation of agglomerates, for lower pH values, the surface charge is neutralised so the formation of bigger particles is made possible. This behaviour was observed for every stirring rate used in the study and hence was regarded as independent of the local velocities in the suspension. Figure 3.23 below show the CSD for a stirrer speed of 200rpm and a reaction time of 3600s a bimodal distribution can be seen with a lower-size maximum between 1.8 and 2.8μm which corresponds to primary particles, and a second maximum between 13 and 16μm that relates to the agglomerates formed below pH 8.0.

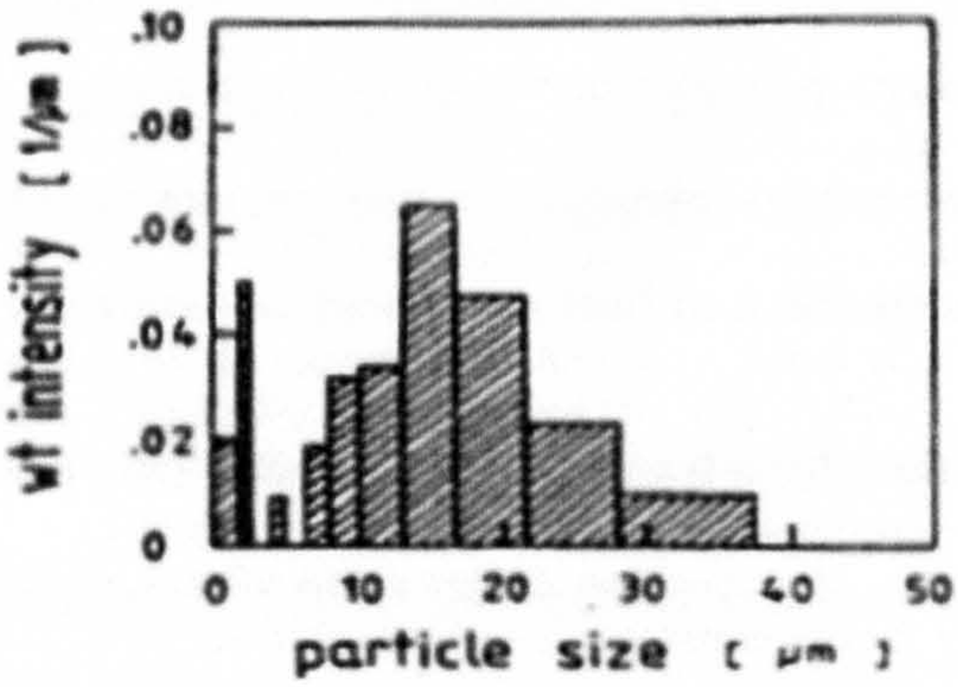


**Figure 3.23 CSD from the precipitation of $CaCO_3$ in a batch reactor (from Wachi and Jones, 1992)**

In further analysis of the reaction system, (Al-Rashed and Jones, 1999) and (Rigopoulos and Jones, 2001) have developed CFD models of semibatch and draft-tube bubble column carbonations.

(Yagi *et al*, 1984) mention that vaterite is formed at low temperature and high $Ca^{2+}$ concentration (from Wray and Daniels, 1957), yet in their own work vaterite is seen at low concentrations. They attribute that to a difference in excess species; $Ca^{2+}$ or $CO_3^{2-}$. They also noted a marked decrease in the absorption rate at high $Ca(OH)_2$ concentrations. As this process under study had a flat gas-liquid interface, this was attributed to agglomerated crystalline material in the interface surface disrupting the absorption. Further, they concluded in the case of combined $CO_2$-$SO_2$ absorption, the $SO_2$ affected the crystallisation of $CaCO_3$ by having a small effect on the rate of absorption ($SO_2$ is more soluble than $CO_2$) and dissolved $SO_2$ dissociates to form $SO_3^{2-}$

which acts as a habit modifier. The growth rate of the crystals considerably decreased with increasing $SO_2$ partial pressure.

Excess of one or other reactants can lead to a change in size and or shape of the product formed. (Jung *et al*, 2000) studied the effect of reactant concentration on the morphology of calcium carbonate in a Couette-Taylor reactor. In each of the experiments, calcite was formed, however the shape (and shape factor) of crystals varied with $OH^-$ concentration. Cubes were formed at 5mol/m$^3$ and as the concentration of $OH^-$ increased to 100 mol/m$^3$ the product shape morphed into spindle-like forms. The variation in morphology was explained in terms of excess $Ca^{2+}$ ions in the solution. Their conclusion was that excess $Ca^{2+}$ ions seem to absorb on the preferred faces of the cube-like calcium carbonate particle. Then the absorbed ion inhibits the face growth of the particle and brings about modification of the particle morphology. Conversely, with increasing the $CO_2$ flow to the reactor resulted in spindles changing to cubes as the concentration of $CO_2$ increased. Increasing $CO_2$ flow also lead to a smaller mean particle size. In a Couette-Taylor reactor, where toriodal vortices allow for intense mixing and engagement of the gas and liquid phases, it was seen that increasing the shear in the device lead to a decrease in mean particle size.

### 3.6.3.2 Gas-liquid-solid precipitation of calcium carbonate

To extend the reaction product from the solvent volume, milk-of-lime is used instead of limewater, creating a higher yield of crystals (Chen *et al* 2000). The extra step in the overall process is the dissolution of calcium hydroxide solid in the suspension as the carbonation process progresses. The dissolution of the calcium hydroxide particles adds an extra mass transfer resistance to the overall process, a limiting factor being its low solubility in water.

$$(A_1) \quad Ca(OH)_{2\,(s)} \Leftrightarrow Ca^{2+}_{(aq)} + 2OH^-_{(aq)}$$

$$(A_2) \quad CO_{2\,(g)} \Leftrightarrow CO_{2\,(aq)}$$

$$(B) \quad CO_{2\,(aq)} + OH^-_{(aq)} \Leftrightarrow HCO_3^-{}_{(aq)}$$

$$(C) \quad HCO_3^-{}_{(aq)} + OH^-_{(aq)} \Leftrightarrow CO_3^{2-}{}_{(aq)}$$

$$(D) \quad Ca^{2+}_{(aq)} + CO_3^{2-}{}_{(aq)} \Leftrightarrow CaCO_{3(s)}\downarrow$$

(Juvekar and Sharma, 1973) investigated this reaction route in bubble columns of 5 and 20cm diameter and a 12.5cm diameter mechanically agitated contactor. They presented the concentration profile of $CO_2$ and hydroxyl ion seen in figure 3.24.

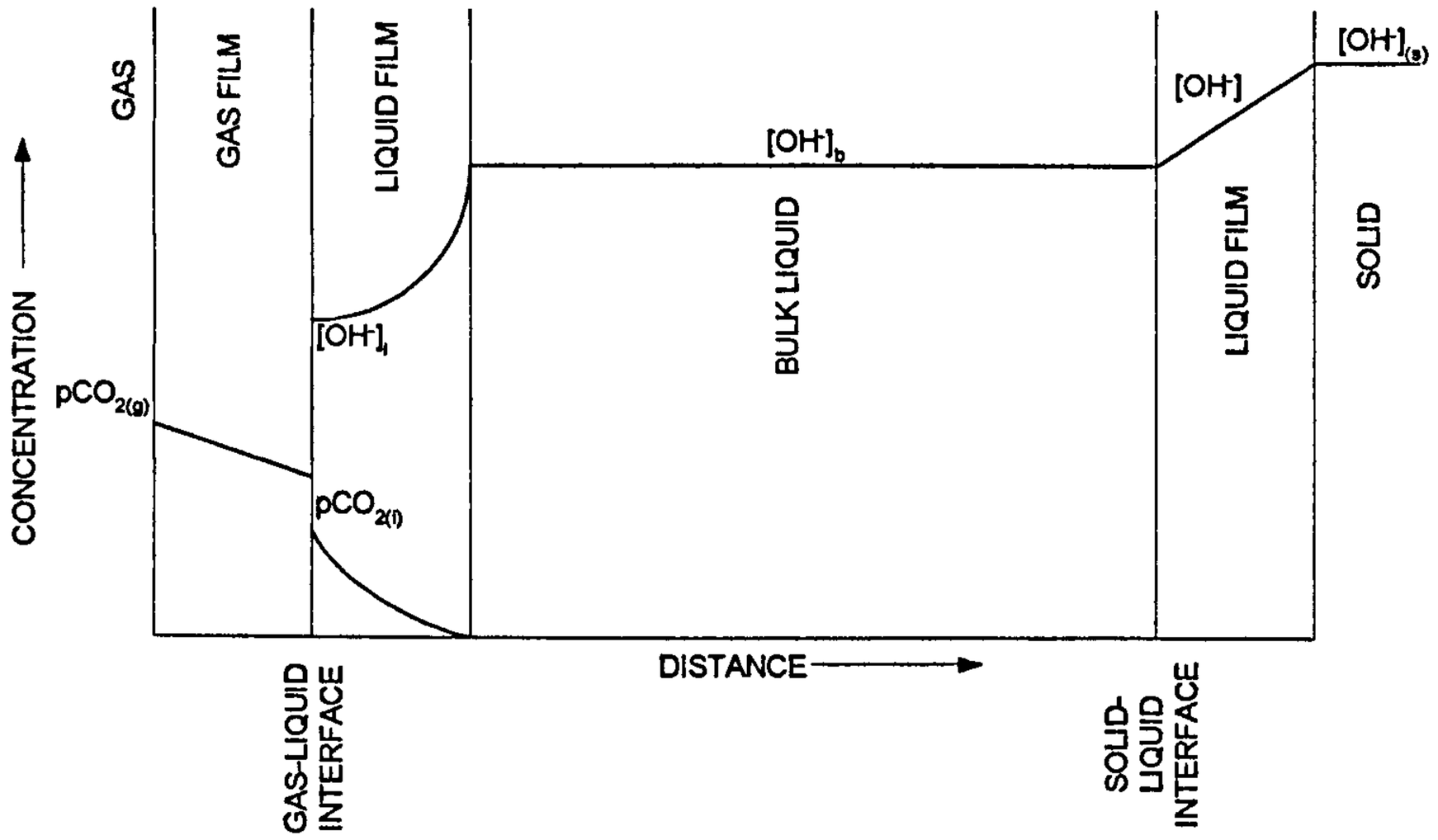


**Figure 3.24 Concentration profile for the carbonation of lime suspension (Juvekar and Sharma, 1973)**

The transport of $CO_2$ into the liquid phase is accompanied by fast reaction and the rate of absorption is enhanced by the fast reaction between $CO_2$ and the $OH^-$ ions (Danckwerts, 1970). According to (Juvekar and Sharma, 1973) the enhancement factor will be dependent on the liquid side mass transfer coefficient in the absence of chemical reaction, the concentration of $OH^-$ ions, the diffusivities of $CO_2$ and $OH^-$ in the liquid and the rate constant for the reaction between $CO_2$ and $OH^-$. Under certain conditions, the concentration of $OH^-$ ions at the gas-liquid interface may be the same as that in the bulk and the reaction may occur entirely in the film. (Juvekar and Sharma, 1973) carried out their experiments in a semibatch mode for each reactor configuration, using diluted $CO_2$ gas concentrations and particle loadings in the range 10-400g/l. They found that the carbonation had two distinct regions as each experiment progressed.

(i) A constant rate period during which the rate of absorption of $CO_2$ and the concentration of $OH^-$ ions in the solution remained essentially constant. In this period, the aqueous phase was always kept saturated with $OH^-$ ions.

(ii) A falling rate period, marked by the gradual decrease in the concentration of $OH^-$ ions in the liquid with time. During this period, the total surface area of the particles for dissolution reduces to an extent such that the resistance associated with the dissolution of calcium hydroxide particles becomes important.

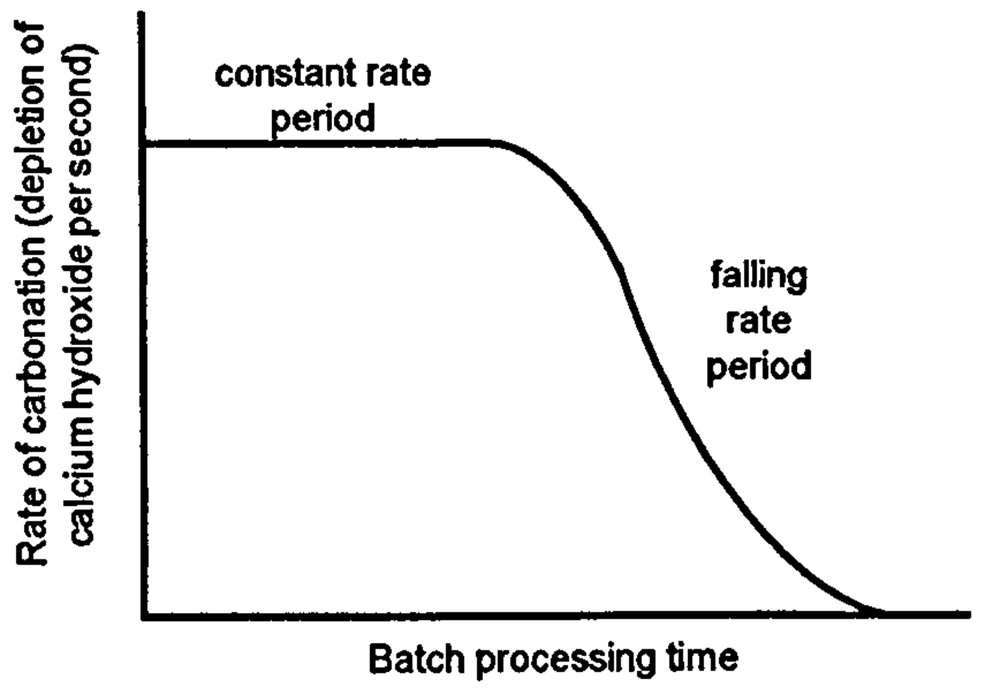


**Figure 3.25 Carbonation of lime: constant rate and falling rate periods**

(Juvekar and Sharma, 1973) observed during their experiments using bubble columns at high particle loadings that gas slugging occurred suggesting a decrease in the interfacial area for contacting. In their work with regards to a mechanically agitated contactor, they used impeller rotational speeds in excess of a critical speed beyond which the gas velocity had no effect on the interfacial contact area. From both these processes, it is shown that there are limitations in the process; the bubble columns being prone to gas flow slugging and the agitated vessel requiring high impeller speeds to disperse the gas (in excess of 600rpm in this case). Both cases were laboratory scale processes suggesting that full-scale operations might suffer similar restrictions. In all, they performed a comprehensive analysis of previous works on the absorption of $CO_2$ in aqueous alkaline solutions and concluded that the absorption of $CO_2$ into aqueous solutions containing hydroxyl ions is essentially liquid film controlled with the gas-liquid film resistance being negligible.

#### *3.6.3.2.1 Calcium carbonate precipitation in a RPB*

(Chen *et al*, 2000) used a rotating packed bed to precipitate calcium carbonate from slurries of lime (made up from tap water and quicklime – CaO). The slurry was circulated from a 3-litre batch vessel, through a RPB, ($d_i$=50mm, $d_o$=150mm, packing thickness =50mm) were it was contacted counter-currently with $CO_2$ gas and returned

back to the batch vessel. The recirculation was stopped when the batch pH reached 7.0 and this time regarded as the processing time. It was seen by increasing gas flow or by increasing the slurry circulation rate for a specific set of fixed parameters, that the processing time decreased. Furthermore, by increasing the rotational speed of the bed, the mean particle size decreased. The authors claim that these experiments were carried out in the absence of any chemical inhibitors. Their particle size analysis using TEM showed average particle sizes in the range of 30 to 80 nanometres. XRD analysis showed the crystals to be calcite. Average particle size was seen to decrease with increasing gas flowrate and slurry flowrate, but increased with slurry concentration.

No other workers have reported primary particles so small from this process route. The claims presented seem remarkable considering it is a semi-batch process whereby the slurry is circulated through the RPB and then back to the batch, product crystals mixing with unreacted slurry. There is no mention of agglomeration of the particles or the composition of the trace elements in the tap water used for the slurries. It might be possible that the tap water contains for example, lead, sulphate or magnesium ions, which may influence crystal growth/agglomeration. Other workers cited in the present study observe agglomeration of primary $CaCO_3$ particles. TEM micrographs at very high magnification might not be showing representative samples of the CSD. For these reasons, the particle size claims from the work by Chen *et al* is treated with caution, however the ability of the RPB's ability to contact and react the slurry more rapidly than conventional carbonation equipment is not brought into question since the high capacity for mass transfer has been shown by other workers, (Ramshaw, 1983) (Kelleher & Fair, 1996) (Balasundaram *et al*, 1990) (Trent *et al*, 2001). The RPB lends itself to high rates of mass transfer and allows for lower reaction times in the process, which would reduce operating costs.

### 3.6.3.3 Liquid-liquid precipitation of calcium carbonate

The precipitation routes to calcium carbonate by mixing two liquid reagents together have been investigated by many workers. (Wray and Daniels, 1957) studied the morphology of calcium carbonate precipitated at different temperatures from calcium nitrate and sodium carbonate solutions using a stirred semi-batch reactor. They found that at 40°C, the precipitate was predominantly calcite; at 45°C it was 30% calcite and 70% aragonite; at 50°C it was mostly aragonite; at 70°C it was all aragonite. Further,

aragonite tended to form at higher pH than calcite. The same results were essentially seen when calcium nitrate solution was substituted with calcium chloride solution. Although the aragonite transformed to calcite over a couple of hours, filtering and drying could stop the change. The authors attribute this effect of temperature on precipitating different phases to observing the inclusion of heavy ions (i.e. small quantities of co-ions in solution of $Pb^{2+}$, $Ba^{2+}$, and $Sr^{2+}$) into the crystal lattice due to the more rapid rate of crystallisation at high temperatures. At higher temperatures, the rate of crystallisation is accelerated rapidly and strontium ions do not have time to escape and thus they are incorporated into the $CaCO_3$ crystal lattice giving a larger structure - aragonite.

In observing calcite-seeded precipitations of calcium carbonate from the drop-wise addition of 0.02M sodium bicarbonate solution to $8 \times 10^{-4}$M calcium chloride solution, (Reddy and Nancollas, 1971) concluded that growth commenced immediately on the addition of seed crystals and the growth rate was found to be a linear function of the weight of seed crystals. They proposed that the growth of calcite from supersaturated solution was a surface-controlled second order reaction. Further, (Nancollas and Reddy, 1971) proposed that the rate of crystallisation was independent of stirring rate.

(Hostomsky and Jones, 1991) carried out experiments in a continuous flow crystalliser using equimolar calcium nitrate and sodium carbonate solutions under different conditions. A 0.3 litre vessel was used as the reactor with residence times in the range of 5 to 20 minutes, pH in the range 8.5 to 10.5 and reagent concentrations in the range 0.025 to 0.2 mol/l. All experiments were performed at 25°C. They observed for pH ≥ 9.5, mainly vaterite was precipitated in the form of agglomerates of spherical particles. At long residence times (20mins at pH 10.5) the agglomerates were made up of thin hexagonal vaterite platelets. High reagent concentrations yielded product that was of a very fine gelatinous nature without discernable shape. They concluded this to be amorphous calcium carbonate (ACC) as previously observed by (Ogino *et al* 1987) and (Brecevic and Neilsen, 1987). For suspensions of lower alkalinity (pH 8.5), agglomerates of calcite were formed. Further, in investigating the effect of agitation in the experiments where vaterite was formed, it was seen that increasing stirring contributed to an increase in the agglomeration rate. In modelling the crystallisation, they concluded that neglecting agglomeration would lead to overestimation of crystal growth rates. (Koga, *et al*, 1998) prepared ACC from an aqueous system of $CaCl_2$-

$Na_2CO_3$-NaOH in the range $11.2 \leq pH \leq 13.0$. Primary particles were formed of a diameter of approximately 0.05μm

Investigating the same reaction between calcium nitrate and sodium carbonate solutions, (Chakraborty *et al*, 1994) observed both calcite and vaterite in a MSMPR. They hypothesised that vaterite is originally nucleated but transforms during the time in solution, or during subsequent separation and drying before examination. They performed on-line examination of the suspension or examination of frozen samples by cryo-SEM. They report that the phenomenon of reactor scaling can shift the nucleation mechanism from heterogeneous to homogeneous due to reactor scaling mopping up the sites whereby heterogeneous nucleation can occur. Further, they suggest increasing the calcium to carbonate ion ratio inhibits the scaling of surfaces and also reduced aggregation, [which was confirmed later in the gas-liquid carbonation route described by (Jung *et al*, 2000)]. Using on-line techniques, they observed vaterite transforming into calcite within the reactor. At a high ratio of $Ca^{2+}/CO_3^{2-}$ (>7) there is a shift to the homogeneous nucleation of predominantly stable, well-formed vaterite with a slow transformation rate. In general, it was found that increasing the stirring rate increased the transformation rate. (Gomez-Morales *et al*, 1996) found from precipitation experiments of calcium chloride and potassium carbonate solutions that an excess calcium ion ratio in solution led to a decrease in the nucleation rate but an increase in the growth rate.

(Tai and Chen, 1995) investigating the calcium chloride – sodium carbonate route using a pH-stat method at low supersaturations ($1.53<\sigma<5.13$) - using both seeded and un-seeded methods - in MSMPR and semibatch experiments. At relative supersaturations below 2.91, rhombic calcite crystals were formed under well-controlled pH conditions (pH=10.6). Higher relative supersaturations yielded rosette agglomerates of aragonite in the pH range from 9.84 and 11.11. This work yielded morphologies akin to the work by (Swinney *et al*, 1982). Agglomeration was significant in most experiments with the agglomeration rate of calcite increasing with magma density and supersaturations under steady-state operation. No vaterite was observed in the experiments.

(Katsifaras and Spanos, 1999) found that small amounts of inorganic phosphate ions reduced the rate of vaterite crystallisation from the precipitation from calcium nitrate

and sodium bicarbonate solutions at low supersaturation by a pH-stat method. However, the phosphate ions stabilised the initially precipitated vaterite by blocking the active sites for dissolution and growth.

### 3.6.4 The effect of additives on $CaCO_3$ precipitation

A study of the patent literature yields a plethora of information on the additives used in the precipitation of calcium carbonate. Hence commercially sensitive knowledge of tailor-made $CaCO_3$ products is not forthcoming in developing intensified techniques in controlling particle size and shape.

The additives can be divided into organic and inorganic categories, be it individual ions such as magnesium or strontium, simple organic acids or more complex polymeric materials.

Incorporated strontium ions within the crystal lattice was attributed to the change in morphology seen in the experiments carried out at high temperature by (Wray and Daniels, 1957). Many studies have shown that the presence of $Mg^{2+}$ ions can inhibit the growth rate during the precipitation of $CaCO_3$. The rate reduction has been suggested to be approximately proportional to the concentration ratio of $Mg^{2+}$ ions with $Ca^{2+}$ ions in the solution (Morse and Mackenzie, 1990).

(Tracy *et al*, 1998a) demonstrated that spheres of calcite could be produced in the presence of $Mg^{2+}$ and $SO_4^{2-}$ ions. By altering the relative quantities of each of the ions – including the $Ca:CO_3$ ratio - the resulting sphere fraction could be tailored. Addition of $HPO_4^{2-}$ in the system was shown to significantly inhibit sphere formation. In describing the morphological development, (Tracy *et al*, 1998b) believe an amorphous precipitate forms with slightly higher magnesium content than the final spheres. After 10 minutes, the nano-phase disappears and rough spheres have appeared. Between 10 and 30 minutes, the spheres perfect their shape and remain stable. The $Mg^{2+}$ and $SO_4^{2-}$ ions in solution seem to interfere with initial precipitate formation and cause the amorphous phase to form. These change the precipitation pathways and pH of the system, causing the precipitation to proceed more slowly (over their control counterparts). Slower crystallisation is a hallmark of spherulitic growth in several systems.

(Zhang and Dawe, 2000) from seeded experiments - using both pH free drift and visual methods - investigated the influence of $Mg^{2+}$ on the precipitation and morphology of

calcite confirmed the higher the Mg/Ca ion ratio the lower the growth rate of calcite became in supersaturated solution. They attributed the growth inhibition to the non-uniform distribution of the $Mg^{2+}$ ion within the developing surfaces of the seed crystal. These slower growing surfaces dominate the morphology of the growing crystals. Further, (Meldrum and Hyde, 2001) citing other workers in that aragonite was the preferred crystalline phase in the presence of $Mg^{2+}$ ions when precipitating from solution. In investigating the role of $Mg^{2+}$ ions and malic and citric acid on the precipitation they produced a myriad of different particle shapes depending on the conditions. A range of lobes, dumbbells, ooids with convex external faces, and spherulitic and radially divergent calcites were observed. The organic additives influenced the precipitation of calcite rather than aragonite, probably by inhibiting nucleation and growth. The action of the organic additives was highly specific, adsorbing onto certain crystal faces during growth and producing crystals elongated along the [0 0 1] direction. $MgCO_3$ concentration within the lattice increased with Mg concentration in the working solution, but showed little correlation with the additive concentration. However for a given Mg concentration in solution, increasing the additive concentration induced a transition from single crystal to aggregate (up to 10% $MgCO_3$ content for single calcite crystals).

Organic compounds play an important role in creating structure during biomineralisation. From a physical chemistry point of view, the most important fact of biomineralisation is that the nucleation orientation of inorganics can be controlled by their functional groups. Owing to this fact, nucleation takes place at lower supersaturation than is necessary for homogeneous nucleation (Bunker *et al*, 1994). Under normal conditions, homogeneous nucleation of inorganics is not possible in organisms. Further, the solubility of $CaCO_3$ depends upon the organic additives within the system, hence the solubility and supersaturation of a particular system are dependent upon the additives involved (Kitano and Hood, 1965). For the growth of crystals, it is also important note that the surface energy is not the same for crystallographic faces. According to the Wulff theorem, each crystallographic face must grow at the rate proportional to its surface energy (Pamplin, in Pach *et al*, 1996). Minimising the total surface energy requires minimising the surface area of the face with the largest surface energy. In biomineralisation, this principle is altered by the adsorption of water-soluble polymers on some crystallographic surfaces.

In measuring ξ-potential - indicative of surface charge and surface area of the particles – (Agnihotri *et al*, 1999) showed the ξ-potential of $CaCO_3$ prepared in the absence of surface modifiers to be 30mV (c.f. >40mV (Jones *et al*, 1992)). The addition of anionic surfactants led to a decrease in the ξ-potential and depending on the surfactant used, could reverse the ξ-potential from positive to negative using Dispex N40V and Dispex A40. This suggested that the anions produced from dissociation in water are absorbed onto the crystal surface, thereby reducing the surface charge and facilitated agglomeration and growth of particles. Furthermore, due to lower electrostatic repulsion, nuclei aggregated at an earlier stage during crystal growth and resulted in an agglomerated particle with a more open pore structure. Increasing the surface modifier concentration beyond the point of surface neutrality imparted negative charge to the surface, increasing the repulsive forces and thus decreasing the aggregate size. These open-pore particles were developed for use in flue gas desulphurisation and showed excellent absorbency characteristics due to the high surface area and porosity as a result of surfactant addition during the carbonation process (Wei *et al*, 1997).

(Pach *et al*, 1996) examined the role of hydroxyethyl cellulose (HEC), colloidal silica and potato starch (PS) during the precipitation of $CaCO_3$ from the reaction between $Na_2CO_3$ and $CaCl_2$. Deionised water or 1%wt solutions of additives were used as working solutions at room temperature. Reactant concentrations of 0.01M were used. One reactant was fed drop-wise from burettes into 100ml of the other. It was observed that the shape of the calcite formed in water and the HEC solutions was similar, brick-shaped crystals in both cases, the size was consistently smaller in the presence of HEC (7μm in water compared with 3μm in HEC). The size of calcite crystals formed in the presence of PS was significantly decreased. In estimating the nucleation frequency of calcite, it was shown that the presence of starch increased the frequency by $2 \times 10^4$ over the water-only experiments.

It has been shown that organic modifiers may change the crystal habit. (Colfen and Antonetti, 1998) demonstrated that was possible to produce spherical calcite as well as producing vaterite and a number of different shapes in a double jet reactor using double-hydrophilic block copolymers. The copolymers used were synthesised with poly (ethylene glycol) (PEG) as the backbone by which functional groups were added. The functionalised block determined crystal size shape and modification, whereas the PEG block was necessary to keep the growing nuclei in solution. The samples were

aged in saturated $CaCO_3$ and polymer solution for a period of 12 months to allow Ostwald ripening. Spherical vaterite obtained remained stable over this time and samples adopted a hollow sphere morphology from certain copolymers.

Acidic proteins such as aspartic or glutamic acid are found in the marine environment precipitation of $CaCO_3$. (Manoli and Dalas, 2001) were able to produce thermodynamically stable vaterite spheres by a constant composition method in the presence of glutamic acid using calcite seeds to initiate the precipitation. They found that by increasing the amount of glutamic acid in the precipitation resulted in an acceleration of the crystal growth process. They report the dried vaterite to be stable after six months.

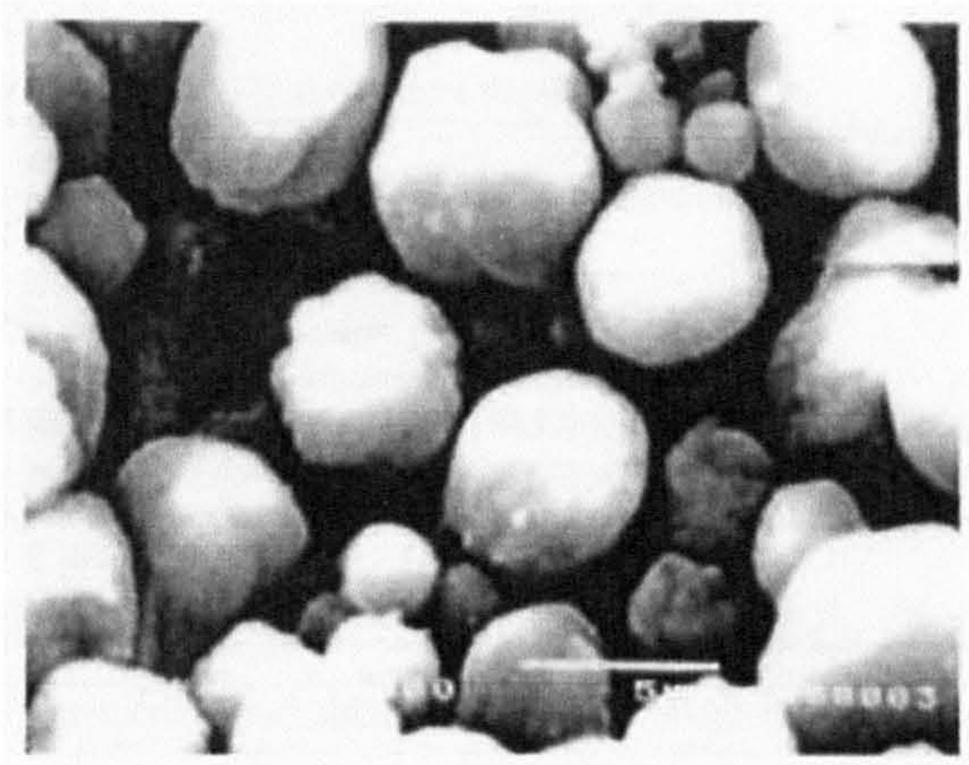

**Figure 3.26 SEM of vaterite grown on calcite in the presence of glutamic acid (Manoli and Dalas, 2001)**

(Thomas *et al*, 2002) have been able to use glutamic acid to stabilise the vaterite polymorph in their liquid emulsion membrane technique using calcium carbonate to encapsulate organic and inorganic substrates.

## 3.7 Precipitation on the spinning disc reactor

(Cafiero *et al*, 1999) proposed the spinning disc reactor as the first stage of a precipitation process. In their experiments concerning the precipitation of barium sulphate from aqueous solutions on an SDR of 0.5m in diameter, they found comparable mixing performance to that of a T-mixer. In the case of the SDR, the specific dispersed power is lower than that of the T-mixer. They state that when mixing conditions are incredibly intense, homogeneous nucleation will predominate with respect to heterogeneous nucleation. In order to achieve this, the mixing time, $t_m$, must be shorter than the induction time, $t_{ind}$ (also know as the characteristic reaction time or nucleation time). Furthermore, supersaturation ratios must be high such that intense mixing can allow this mechanism to predominate. Nucleation time is very fast at high supersaturation and the time elapsed between reaction and nucleation is negligible, hence they can be considered almost contemporary processes.

With high supersaturation ratios leading to high nucleation rates, a large number of particles per unit volume with a high surface area to volume ratio are produced. This leads to a high collision frequency between particles and hence fast agglomeration phenomena. (Heyer *et al*, 1999) observed that for particles in the nano-scale region, nucleation and agglomeration mechanisms predominate, whilst crystal growth does not play an important role.

In proposing the SDR as a continuous flow mixing device, (Cafiero *et al*, 1999) suggest that the scale-up of T-mixers and Y-mixers for the purposes of premixing feeds for stirred tank reactions are liable to high levels of energy consumption thus leading to the process becoming uneconomical. The SDR would not suffer from this restriction due to the centrifugal pumping effect on the fluid due to rotation; the disc inertia contributing to high shear forces on the liquid film and resulting in rapid mixing of the reactant fluids.

In carrying out precipitation experiments on the SDR, (Cafiero *et al*, 1999) mixed equivalent amounts of barium chloride and sodium sulphate solutions on the disc, discharged at a flowrate of 1.33ml/s from burettes. In changing the solution concentration, the maximum supersaturation ratio could be manipulated in the range $100<S_o<10000$. It was seen at the supersaturation ratios of 100, 2000 and 2500, fed onto a disc spinning at 1000rpm, that the number crystals per unit volume was higher

than the same supersaturation conditions in a T-mixer performed by (Nielsen, 1961) and (Mohanty *et al*, 1988). The latter had emphasised that homogeneous nucleation predominates at supersaturation ratios greater than 2000. However the former proposed that supersaturation had a significant roll to play with supersaturation ratios of 3000 and above.

At a supersaturation ratio of 2000, it was shown that in the rotational speed range 200-1000rpm, the average crystal size decreased from 3.0 to 0.7μm. Furthermore, at a rotational speed of 1000rpm, the size range of the crystals was very narrow (0.5 to 1μm). In conclusion, homogeneous nucleation was the predominating mechanism from the combination of intense mixing and high supersaturation. In comparing the power dissipation of T-mixers and spinning discs, it was shown that T-mixers typically would achieve values of 100kW/kg with significant pressure drop whereas the spinning disc could achieve the same mixing intensity for homogeneous nucleation with a power dissipation of 100W/kg with very little pressure drop.

(Jachuck *et al*, 2001) continued the experimentation of precipitation of barium sulphate on a spinning cone reactor (SCR). Here, the experimental parameters were extended to include initial supersaturation ratios of 500 and 5000, individual reactant flowrates in the range 2 to 8ml/s and rotational speeds in the range 2000 to 10000rpm.

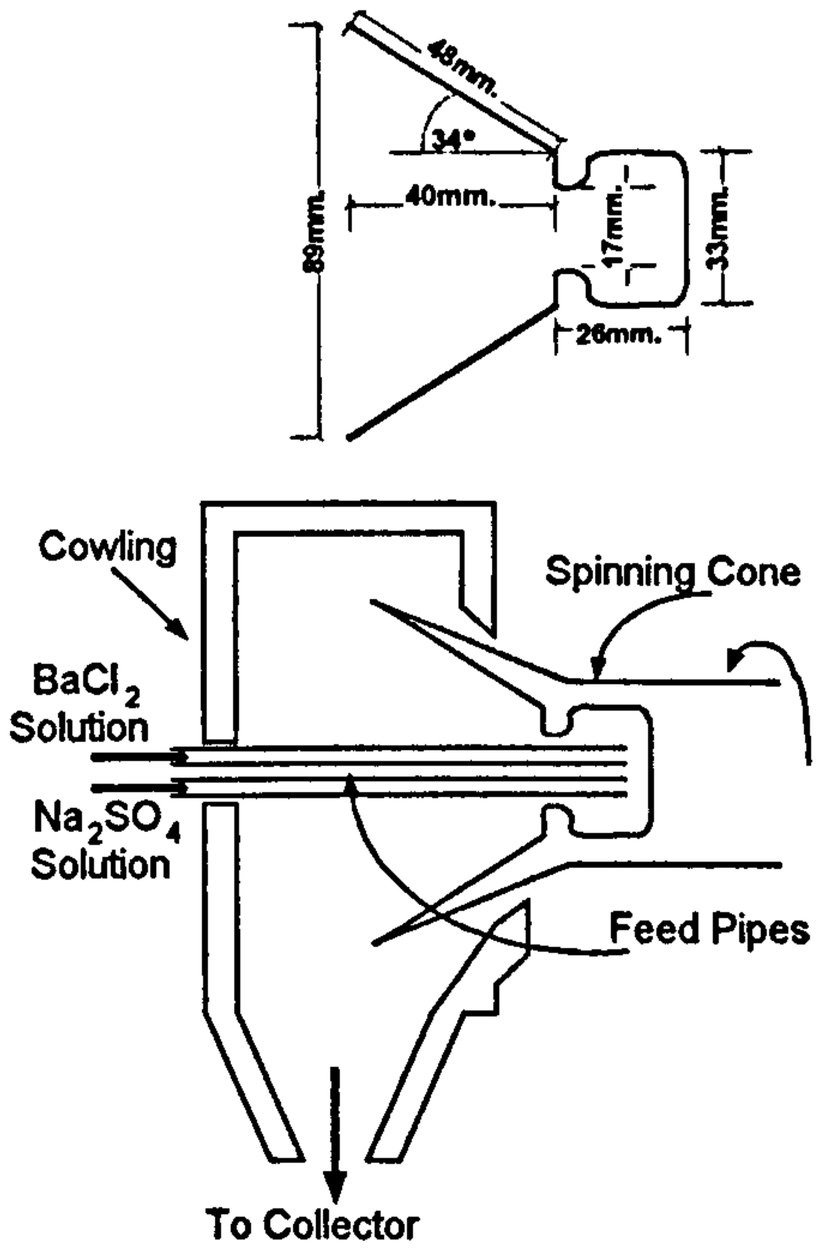


**Figure 3.27 Spinning cone schematic (Jachuck et al, 2001)**

A side view of the reactor set-up is show in figure 3.27 including dimensions of the cone.

The reactants were fed into the centre and the fluid was forced outward by the effect of the rotation. On exit from the periphery of the cone, the slurry is thrown against a cowling whereupon it drains to the bottom and into a collection vessel.

The spinning cone was used to primarily study the effects of higher flowrates and rotational speed. It was also noted that the work by (Cafiero *et al*, 1999) suggested that the low flowrates and large disc used led to film breakdown on the disc surface. Crystal size distribution (using a Malvern Mastersizer) and SEM imaging was utilised during the study. Results from the spinning cone were compared to a small batch reactor.

At a supersaturation of 500, it was found that the cone was capable of producing crystal product with a lower D[3,2] than that obtained in the batch. The batch produced crystals with D[3,2] = 6.85μm, the cone achieved it's lowest D[3,2] = 3.8μm at 6000rpm and 16ml/s. Despite the cone being capable of producing crystals with a smaller D[3,2] than the batch, the uniformity and span of the spinning cone data is higher in each experiment indicating a wider distribution than that of the batch at this supersaturation both on a number and volume distribution basis.

It was found at the higher initial supersaturation of 5000, the spinning cone provided a smaller mean crystal size based on D[3,2] than that obtained from the batch experiments. The batch yielded D[3,2] = 0.75μm whereas the cone was capable of an mean crystal size in the range $0.18 < D[3,2] < 0.32\mu m$ from all the experimental runs performed. Here, the spinning cone clearly demonstrated that it could make much smaller crystals compared to a batch technique.

At the lower supersaturation ($S_o$=500), the crystals obtained from the spinning cone were better defined than the batch reaction crystals, both reactors yielded crystals consisting primarily of platelet, pyramidal flowers and rose type structures determined from the SEM slides. At the higher supersaturation ratio of crystals formed on the cone at this supersaturation appeared to be smaller and more uniform than that of the batch experiment which appear to be much more irregular and agglomerated.

Experimental conditions at higher rotational speed favoured better performance in producing smaller crystal sizes. (Mohanty *et al*, 1988) emphasised that homogeneous

nucleation took place in their experiments at supersaturations of 2000 and higher. Therefore, it can be assumed that under initial supersaturation conditions of 500, homogeneous nucleation is not wholly responsible for the formation of small crystals whereas at $S_o$=5000, homogeneous nucleation predominates. At lower supersaturation, crystal growth is a factor. With such a high level of micromixing, very rapid rates of supersaturation depletion are experienced by the reactants on the surface of the cone but with intense mixing at lower supersaturation ratios, conditions arise for rapid crystal growth.

(Oxley *et al*, 2000) investigated the re-crystallisation of an Active Pharmaceutical Ingredient (API) on a spinning disc reactor. This API was removed from the solution by use of an antisolvent. This approach to crystallisation is similar to precipitation by reaction as it leads to rapid or 'crash' nucleation of the product involved due to the sudden onset of high supersaturation. In performing experiments on the SDR, they discovered that a stainless steel disc surface was liable to excessive encrustation by the crystallising material. A layer of PTFE was applied to the disc surface, which overcame this problem. The variables of temperature, rotational speed, feed rate and solvent/antisolvent ratio were all adjusted to investigate performance. In each case, recovery of material was in the region of 95% and for each set of variables, similarities in the CSD were seen. Rotational speed had the most effect on CSD. At high speed, there was a greater proportion of smaller crystals and agglomerates. In most cases, the $d_{50}$ was in the region of 3μm with the upper percentile, $d_{90}$ in the range 7-15μm. In comparing the SDR to optimised batch conditions, it was seen that the SDR produced very much smaller material with a tighter size distribution. The low surface wettability of the PTFE was seen in certain runs to lead to a breakdown in the continuity of the film. At low flowrates and high rotational speed, the film would degenerate into rivulets, which affected the quality of the crystalline product. However, the experimental data suggested that when film stability was maintained, particle size was small and the formation of agglomerates was suppressed. Rotational speed added an extra variable for reaction optimisation, with higher speeds giving better mixing, heat/mass transfer and shorter residence times. In conclusion, the SDR with suitable operating conditions demonstrated a capability of yielding a product with superior particle size definition over the batch process. A single 15cm diameter disc was estimated to be capable of producing 8.2 tonnes/year.

The work reported by (Trippa, Hetherington *et al*, 2002) represented the first examination of the carbonation of limewater on an SDR. The study evaluated the influence of flowrate, concentration, and rotational speed on the conversion rate and the particles size characteristics of the product. Experiments were performed using a 15cm diameter disc (the one also employed in the present study and the work reported by (Oxley *et al*, 2000)) with liquid flow rates in the range 4-20ml/s; rotational speeds in the range 500-2000rpm; $Ca(OH)_2$ concentrations of 8 and 16 mol/m$^3$. 95% purity calcium hydroxide solution was pumped into a 1cm dia. centre well on the disc before propagating across the disc surface under centrifugation. Gas was introduced by means of a nozzle such that it exited parallel to the disc surface. The initial and final pH of the solution was measured. The calcium carbonate product was analysed using a Malvern Mastersizer S to determine CSD and samples were prepared for SEM investigation.

The film conversion parameter, *M* (Levenspiel, 1972. p418), used to determine the location of the reaction was evaluated for the conditions present.

$$M = \frac{k[OH^-]D}{k_L^2} \qquad (3.53)$$

where *k* is the kinetic constant for the reaction $CO_{2(liq)} + OH^- \leftrightarrow HCO_3^-$, [OH-] is the hydroxyl ion concentration in solution, D is the diffusivity of $CO_2$ in the liquid and $k_L$ is the liquid side mass transfer coefficient.

If M >>1 all reaction occurs in the film, and the surface area is the controlling rate factor. If M<<1 no reaction occurs in the film, and bulk volume becomes the controlling rate factor. (Wachi and Jones, 1991) showed that in an agitated vessel, the reaction to be entirely completed in the liquid film and at lower mass transfer coefficients, a higher level of supersaturation is developed near the interface resulting in smaller primary particles. Using Moore's data for the mass transfer coefficient, it was estimated that the value of M to be in the range 1.6<M<14.6 suggesting the reaction to be completed entirely within the film. For a given calcium hydroxide concentration, the highest $k_L$ and therefore the lowest M value corresponded to the highest liquid flowrate and rotational speed.

The SEMs observed by (Trippa, Hetherington *et al*, 2002) showed a mixture of spherulitic and cubic crystals and in some cases only cubic crystals. The presence of

both shapes were seen in experiments where the highest concentration of calcium hydroxide and high $CO_2$ flowrates were used. Only cubic crystals were seen in the SEMs of experiments were low concentrations of calcium hydroxide and/or low $CO_2$ flows were used. Similar image were obtained by (Ogino *et al*, 1987) suggesting the possibility that both calcite and vaterite were present with calcite being the final product from the SDR.

The Sauter mean diameter, D[3,2] for each experiment was plotted for the experiments in the range 5-12μm. For each of the 3 flow rates of 4, 8 and 12ml/s, D[3,2] was seen to initially increase then decrease at higher rotational speed. Larger particle sizes were seen at 12ml/s. Comparing with a stirred batch carbonation experiment, it was seen that the SDR produced a tighter and smaller CSD than that of the batch.

In the case of the SDR – a high surface area to reaction volume contactor – the extent of the gas-liquid interface and mass transfer coefficients both influence the degree of uniformity of the supersaturation fields in the liquid phase and therefore govern the nucleation and growth kinetics ultimately determining the size of the primary particles. When the mass transfer resistance was high (low $k_L$), particles were larger in size. The trend obtained suggested that when the mass transfer resistance was lower, a higher level of supersaturation influenced the whole liquid phase leading to a lower particle size. This was analogous to the results obtained by (Wachi and Jones, 1991) for conventional stirred vessels.

## 3.8 State of the art in calcium carbonate precipitation – US patent review

A survey of recent USPTO patent literature reveals current developments of making precipitated calcium carbonate. These technologies centre on different methods of processing hydrated lime slurries.

Liu *et al* (US Patent no 6989142) reveal a process for making PCC by the simultaneous addition of $CO_2$ and lime slurry to a stirred vessel initially containing water. The slurry is 10 to 20wt% in concentration. The claim the authors make is for the formation of predominantly cubic calcite with a primary particles size of 1-4μm with an aggregate size of 3-10μm. The end point pH was controlled at 7.0. Once the reaction was complete, it was possible to dry the slurry by conventional methods such as filtration or spray drying. However, the final particle size was achieved by low

energy comminution techniques (either wet or dry). The product could be used in dentifrices due to its specific abrasive properties conducive to being effective in toothpastes.

In the process of Woode (U.S. Pat. No. 4,018,877), an aqueous suspension of calcium hydroxide at 25°C was agitated vigorously and reacted with a mixture of air and carbon dioxide. After 15 minutes (following the `primary nucleation stage`) a complex-forming agent, such as a hydroxy carboxylic acid (e.g., citric acid and malic acid) which complexes calcium ions. The complexing agent was added in a concentration range of 0.001 to 5 wt. %, preferably in the range 0.03 to 0.2 wt. % based on the weight of the calcium carbonate produced. The carbonation was stopped after about 50 minutes when the reaction mixture had just become acid to a phenolphthalein indicator. The mixture was then heated to 85°C. over a period of 20 minutes and was allowed to age for 30 minutes. Carbonation was restarted at a much lower rate, maintaining the temperature at 85°C. After 20 to 40 minutes the pH of the batch had fallen below 8.0. At this stage, 0.8% stearic acid in ammonia solution was added and the mixture was stirred at 85°C. for about 3 hours. The suspension was filtered. The filter cake was extruded through 5/16 inch diameter holes to yield "granules" which were dried in an oven overnight at 130°C on a gauze-tray to produce calcium carbonate having 0.72 relative granule hardness and 0.07μm ultimate particle size. The drawbacks of this process are that the total batch/production time is more than 5 hours during which time the temperature is maintained at 85°C for a period of 4 hours. In addition, the process requires drying of the product overnight at 130°C. This process is thus highly energy consuming.

(Hiroji Shibazaki *et al.* U.S. Pat. No. 4,133,894), disclose that precipitates of uniform particle size can be continuously produced by repeating the step of carbonation reaction. In the first step of the process, a suspension of calcium hydroxide having a solids concentration 0.1 to 10 wt % and a temperature of 15 to 30°C. is sprayed in the form of droplets of about 0.2 to 1.0 mm in diameter against a gas containing 10 to 40 vol% carbon dioxide in countercurrent contact therewith. The gas is passed at a specified superficial velocity of about 0.02 to 0.5 m/s. By this process, 5 to 15% of the calcium hydroxide is converted to calcium carbonate. In the second step of this process, the suspension resulting from the first step is sprayed in the form of droplets of about 1.0 to 1.5 mm diameter against a gas containing 15 to 35 vol% of carbon

dioxide and passed upward through the column at a superficial velocity of about 1.5 to 2.5m/s whereby growth of crystals is accomplished. In the third step of this process, the suspension resulting from second step is sprayed at a temperature of up to 30°C in the form of droplets of about 1.5 to 2.0 mm in diameter into a column in countercurrent contact at a superficial velocity of about 1.5 to 3.0 m/s whereby the carbonation is completed. Calcium carbonate having an average particle size of less than about 0.1 to 3.0 microns is produced. The main drawback of this process is that it requires control of number of parameters such as solids concentration, droplet size, temperature of suspension, gas velocity of carbon dioxide containing gas etc for three columns. Another drawback is the requirement of multi-step carbonation which is more expensive in terms of operating cost for columns and pumps than a single stage carbonation.

Bleakley, *et al.* (U.S. Pat. No. 5,342,600) describe a method of preparing precipitated calcium carbonate which comprises: (1) slaking quick lime in an aqueous medium, (2) subjecting the aqueous medium to continuous agitation during said slaking, (3) passing a suspension of calcium hydroxide obtained after slaking through a sieve having an aperture size of 40-70μm, (4) subjecting the suspension to high energy high shear agitation with an impeller having a peripheral speed of 40-70 m/s, so as to obtain finely dispersed calcium hydroxide, (5) terminating the said high energy high shear agitation on achieving finely dispersed slaked lime, (6) carbonating the finely dispersed slaked lime by passing through sufficient gas comprising carbon dioxide to neutralize the pH of the suspension during said carbonation step, (7) subjecting the suspension to continuous agitation with an impeller speed of 200-700 cm/s to maintain the suspension and (8) separating the precipitated calcium carbonate formed in the process. The disadvantage associated with this method is requirement for generating high-energy high-shear agitation during slaking and carbonation. The use of additives to control the morphology and particle size is also reported. Bleakley *et al.* (U.S. Pat. No. 5,558,850) disclose a process wherein 0.1 to 2.0 wt% of a reagent having one or more active hydrogen atoms e.g., polyhydric alcohol or phenol is added to the aqueous medium in which the quick lime is slaked.

Chapnerkar. *et al.* (U.S. Pat. No. 5,332,564) disclose a process wherein quicklime is slaked in an aqueous solution containing about 0.1 to 2.0wt% of a sugar for the production of rhombic shaped precipitated calcium carbonate. Bleakley *et al.* (U.S.

Pat. No. 5,232,678), disclose a process wherein 0.01 to 1.5wt% of triethanolamine, mannitol, morpholine and solid boroheptonate are employed in the preparation of clusters of calcium carbonate which give good light scattering properties when used as a paper filler or paper coating pigment.

Vanderheiden, (U.S. Pat. No. 4,714,603) discloses the use of polyphosphates in an amount of 0.1 to 1.0% by weight for generating precipitated calcite of substantially spherical morphology suitable for use in dull finish coated paper. The disadvantage associated with all these processes is the requirement of special reagents which add to the production cost.

Bleakley I*et al.* (U.S. Pat. No. 5,833,747), disclose a method for preparing precipitated calcium carbonate for use as a pigment in paper coating compositions. The method comprises the steps of (1) carbonating an aqueous medium containing lime, (2) at least partially dewatering the precipitated calcium carbonate-containing suspension using a pressure filter device operating at a pressure of 5 to 10 MPa and (3) subjecting the precipitated calcium carbonate-containing suspension to comminution by high shear attrition grinding with an attrition grinding medium such as silica sand having a median particle diameter in the range 0.1 to 4.0 mm. The product predominantly comprises aragonitic or scalenohedral crystals. The disadvantages of this method include the requirement of a device for high shear attrition grinding with a special grinding medium and a pressure filter device for dewatering the precipitated calcium carbonate containing suspension. Also, the grinding medium is not separated during the process.

Kroc *et al.*, disclose a process (U.S. Pat. No. 5,695,733) that comprises the steps of forming a reaction mixture containing seed material of a scalenohedral particles of aragonite type calcium carbonate and adding lime slurry into the reaction mixture while simultaneously introducing carbon dioxide. The flow rates of the lime slurry and carbon dioxide are adjusted to control the solution conductivity of the reaction mixture to from 2 to 4 milliSiemens to form the clusters of calcite particles. The drawback of this process is that it requires simultaneous addition of lime slurry and carbon dioxide to maintain the solution conductivity. Moreover, simultaneous control of flow rates of both liquid phase and gaseous phase reactants is difficult.

You Kyu Jae discloses a process for producing calcium carbonate particles having an average size of 0.1 to 1.0μm (U.S. Pat. No. 5,811,070). The process comprises the following steps. (1) Carbon dioxide is introduced into a milk of lime containing a first reagent, consisting of sodium glutamate, sugar, or a mixture thereof, to prepare an aqueous suspension containing calcium carbonate particles of 0.4 micron in average size. The concentration of the first reagent is from 0.1 to 2.0 parts per 100 parts of calcium hydroxide initially present in the milk of lime. (2) A milk of lime is added into the above aqueous suspension. (3) A carbonated solution is added to the aqueous suspension, which contains a second reagent comprising at least one of sodium polyacrylate and a bicarbonate in the range of 0.1 to 5.0 parts per 100 parts of calcium hydroxide present initially, calcium carbonate particles produced by the process are suitable as a filler for adhesives, paints, inks, papers and plastics, especially transparent polyethylene films. The drawback associated with this process is the addition of two different types of reagents in two stages, which makes the process complicated.

Vanderheiden discloses a process (U.S. Pat. No. 4,367,207). for preparing finely divided precipitated calcite. In the Vanderheiden process, carbon dioxide is introduced into an aqueous calcium hydroxide slurry containing anionic organo-polyphosphate polyelectrolyte at a temperature from about 7°C. to about 18°C. One disadvantage of this process is the requirement of an anionic polyelectrolyte which adds to the production cost. Another disadvantage is the required maintenance of a reaction temperature below ambient temperature. This requirement necessitates a chilling plant, which is energy consuming.

# 4 Experimental study overview

## 4.1 Reasons for the present experimental study

In reviewing the precipitation of $CaCO_3$ in the literature and with a general understanding of the current and future requirements of industry, process intensification techniques might facilitate better methods of precipitation of $CaCO_3$ and other products. As demonstrated by (Cafiero *et al*, 1999) and (Jachuck *et al*, 2001) the precipitation of barium sulphate on a spinning disc/cone yielded significantly smaller crystals than the batch technique. The predominant factor controlling this was the very high rates of mixing experienced on the cone, which lead to the rapid depletion of supersaturation, and much higher nucleation rates. Cafiero *et al* also demonstrated that the energy input in the spinning disc process was much lower than the use of a T-mixer arrangement, suggesting that operating costs would also be reduced along with attaining better control of crystal size.

With the understanding that the rapid mixing and high supersaturation leads to very small crystals being produced along with very short residence times and tighter CSD, it was hypothesised that a similar scenario could exist for calcium carbonate precipitation routes. An analogous liquid-liquid route would be chosen to investigate experimental parameters of rotational speed, flowrate and concentration. Furthermore, the SDR, with its ability to generate thin liquid films was conducive in rapid rates of gas-liquid absorption and could facilitate the carbonation of limewater and milk-of-lime reagents. Here the gas-liquid route to calcium carbonate could also be investigated.

The morphology of calcium carbonate is more complicated than that of barium sulphate, capable of forming three different crystal forms, and therefore emphasis on making the right size shape and form is important in the final product. Understanding the morphology from this rapid precipitation method is a factor in the present study.

Calcium carbonate is widely used in industry with established markets and well-developed processes competing worldwide. In carrying the industry forward to continue to be profitable, new processing methods might be required which are more economical should profit margins diminish with existing process technologies.

The further purpose of the experimental study is to demonstrate process intensification in new areas of process equipment, suggest new process routes and potential novel

economically viable processes. The SDR is one piece of equipment that may achieve this and in carrying out the present study, its suitability in this scenario is evaluated. The application of PI technologies in the field of crystallisation might allow for the more rapid development of products. In developing conventional stirred tank processes for crystallisation there is a marked difference between laboratory and plant conditions. For example, the circulation time and dispersed power within the vessel are orders of magnitude different for the same geometry (figure 4.1). If these process conditions were more closely matched, more laboratory development could be carried out and the problems associated with scale-up minimised.

**Figure 4.1 Variation of characteristic fluid circulation time $t_c$ and mixing time, $t_m$ in a Rushton geometry**

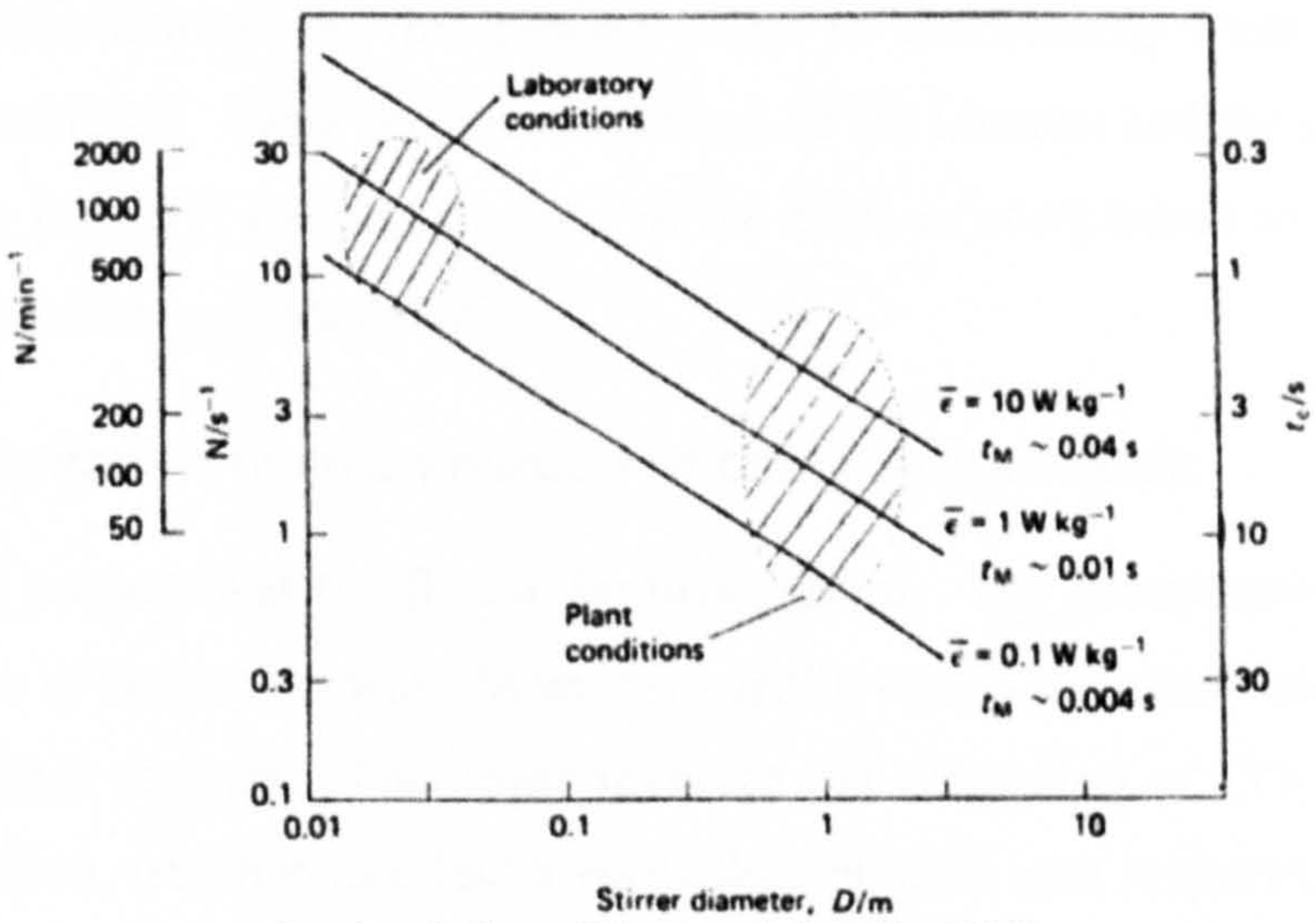


**stirred tank (from Sohnel and Garside, 1992)**

## 4.2 The scope of the experimental study

In reviewing the process routes in the literature, the possible scope for experimental investigation into the precipitation of calcium carbonate on the SDR was extensive to say the least. With the availability of items of equipment being something of a time constraint, the experimental study was broken down into smaller projects with a view to investigating and reporting each separately. For whichever process route was being investigated, a series of batch reactions were also undertaken to help in comparing data.

### 4.2.1 Gas-liquid reactions

The carbonation of calcium hydroxide is a commonplace industrial process. Academic research has also centred on this process route in determining mass transfer and crystallisation kinetics. From this understanding of the kinetics and the application of the reaction in industry, the performance of the SDR in comparison to a laboratory-scale batch operation was evaluated.

#### 4.2.1.1 Precipitation from a solution of calcium hydroxide

The gas-liquid process was the first to be investigated. The precipitation route from the carbonation of limewater was chosen principally as this had received considerable attention by other workers. This route involves the absorption of $CO_2$ into calcium hydroxide solution, which is in effect a very dilute process with respect to the calcium ions in solution and therefore not particularly intensive in respect to producing a high yield of crystals from the solution volume. However, this route is of importance since some basic process parameters can be measured easily (such as the change in pH) in order to determine mass transfer characteristics. As the SDR has been viewed as a mass transfer device for the absorption of gases into liquids, then data could be generated in order to determine its capabilities in this process. The parameters of gas composition and flowrate, liquid flowrate, calcium ion concentration and rotational speed could offer degrees of freedom in experimentation.

The carbonation of limewater on the SDR has already been reported by (Trippa, Hetherington, *et al*, 2002) whereby mass transfer and size data had been evaluated for the same equipment used here. A review of that work is contained within the literature section. The experiments performed in the present study are designed to compliment

the original data by providing further data and leads onto the study of absorption into a slurry of calcium hydroxide.

#### 4.2.1.2 Precipitation from a slurry of calcium hydroxide

The next route would investigate the gas-liquid solid reaction of the absorption of $CO_2$ into a suspension of calcium hydroxide. This process has been used in industry due to its capacity for much higher solids loading (1.5 to 30g/l) than simply using calcium hydroxide solution and therefore producing a much higher yield of crystal product. Some of the parameters are more difficult to measure, however a short study was employed to investigate the capability of the SDR for this process route.

From these studies, insight into the crystallisation process could be gained which may lead the way into promoting the SDR as a capable gas-liquid mass transfer device for these precipitation routes. Furthermore, no study of SDR technology so far has investigated the processes of gas absorption into a liquid, chemical reaction, crystal dissolution and crystal nucleation/growth simultaneously as would be the case here. In comparing intensified process technologies (Chen et al, 2000) used a RPB for manufacturing calcium carbonate by this process route.

### 4.2.2 Liquid-liquid precipitation reactions

The final study involved the liquid-liquid route to precipitation. The reagents of aqueous calcium chloride and sodium carbonate were used in the study. As this route was very similar to the barium sulphate precipitation on the spinning cone (i.e. two liquids mixing), the parameters of rotational speed, reactant flowrate and reactant concentration could be varied. This process is more simplistic in respect of the reduction of variable process parameters i.e. no gas phase concentrations and flowrates to consider. In addition, this route has the capacity of higher reactant loading in the working solutions giving the ability to test a wide range of supersaturation ratios and resultant products. Furthermore the role of the surface modifier, L-glutamic acid was investigated during this study to determine its effect on product morphology.

## 4.3 Experimental overview

### 4.3.1 Familiarisation work

Before any SDR experimentation was carried out, a familiarisation exercise was carried out to understand the reaction, to get a feel for the experimentation, make some measurements, get an idea of kinetics, crystal size etc. Understanding of the preparation of calcium hydroxide solution was garnered during this period. Here it was understood that the solution was susceptible to the vagaries of environmental conditions. In making saturated solution, exposure to the atmosphere resulted in precipitates forming on the surface of the liquid due to the absorption of atmospheric $CO_2$. Furthermore, in preparing a saturated solution, undissolved crystals of calcium hydroxide remained in the solution. In order to remove this variability, the solution was stored in flasks and flushed with nitrogen before sealing and storing before imminent use. Prior to placing in sealed reagent bottles, the solution was filtered in order to remove particulate solids suspended in the solution above 0.2μm. The precipitate was removed in order to create homogeneous conditions within the solution for nucleation. The presence of particles would lead to heterogeneous nucleation influencing the precipitation kinetics. This would not be a factor in the calcium hydroxide slurry experiments, however, the same care was taken in the liquid-liquid experiments to remove particulate material from the solutions prior to experimentation. It could be argued that particles will still exist within the solution no matter what is done to the solution to remove them. However filtering and storing solution under nitrogen would go a long way in assuring consistent reagent properties occurred throughout the experimental study. Details of the preparation of solutions are contained later.

The author's understanding of precipitation processes involving PI technologies was nurtured by participation in the precipitation of $BaSO_4$ on a spinning cone (Jachuck *et al*, 2001). This initial work showed promise for the research into calcium carbonate precipitation using an SDR. In that study, it was shown that high supersaturation coupled with high rates of mixing lead to product with lower mean size and tighter size distribution being produced using a centrifugally accelerated liquid film technique like that of the SDR. Other workers at the time, including (Oxley *et al*, 2000) reported tighter size distributions using crystallisation techniques on the SDR.

### 4.3.2 Planning experimental sets with the availability of CSD analyser

The previous reported results of the absorption of $CO_2$ in calcium hydroxide solution on the SDR (reported by Trippa et al, 2002) did not have the use of a wet particle sizing technique. The only method available to classify the crystal size distribution (CSD) was by scanning electron microscope (SEM). This was an incredibly laborious task of taking a picture at suitable magnification and determining the crystal size by measuring the Feret diameter (the characteristic particle length parallel to a given dimension) of each individual crystal in the picture. This was also an expensive method due to the cost of SEM time, resulting in a number of experiments being omitted due to time and cost constraints. Thirdly, there was significant period of time between experimentation and analysis suggesting the possibility of secondary kinetic effects upon the precipitate could become a factor and hence effect the size distribution of the precipitate. During the barium sulphate investigation, the use of a Malvern Mastersizer S - on a loan period from the EPSRC Engineering Instrument Pool - had allowed almost immediate analysis of the CSD of slurry samples obtained. The instrument was capable of a quick turn around such that it could be ready for use for another sample within 5 minutes or less. This allowed the study to proceed such that experimental results could be interrogated almost immediately and action taken upon them. Delays in performing experiments arose due to the availability of the instrument. There could be a wait of 9 months to a year between loan periods. These loan periods were between 5 to 7 weeks in length. For each of the experimental studies undertaken, careful planning had to be taken beforehand. This plan also took into account the requirements of other workers on projects requiring some time with the analyser. With this work being entirely new, contingencies had to be made as each study progressed. This would be due to unforeseen outcomes in the work regarding various factors, explained in more detail later. However to give an idea of why the plans were altered, for example, observations made on one or two experiments in a series showed that a certain line of investigation would not be worth pursuing in the context of the entire study. As a result, the experimental plans were adjusted to make what was regarded as best use of the Mastersizer instrument's time in the laboratory.

### 4.3.3 The spinning disc reactor employed in the present study

For all experiments in this study, the same 15cm diameter spinning disc reactor rig was employed. This rig's availability suited the study, as it would be best matched to the flowrates of reagents intended. Liquid product was collected through drains in the bottom of the SDR's shell and the rig could be dismantled by one person for cleaning and routine maintenance. The larger rigs available at the time would perhaps be prone to poor surface wetting and required more personnel each time it needed cleaning. Very short residence times could be established on the 15cm diameter rig which suited the short induction and reaction time of the precipitation process.

#### 4.3.3.1 SDR layout, dimensions and operation

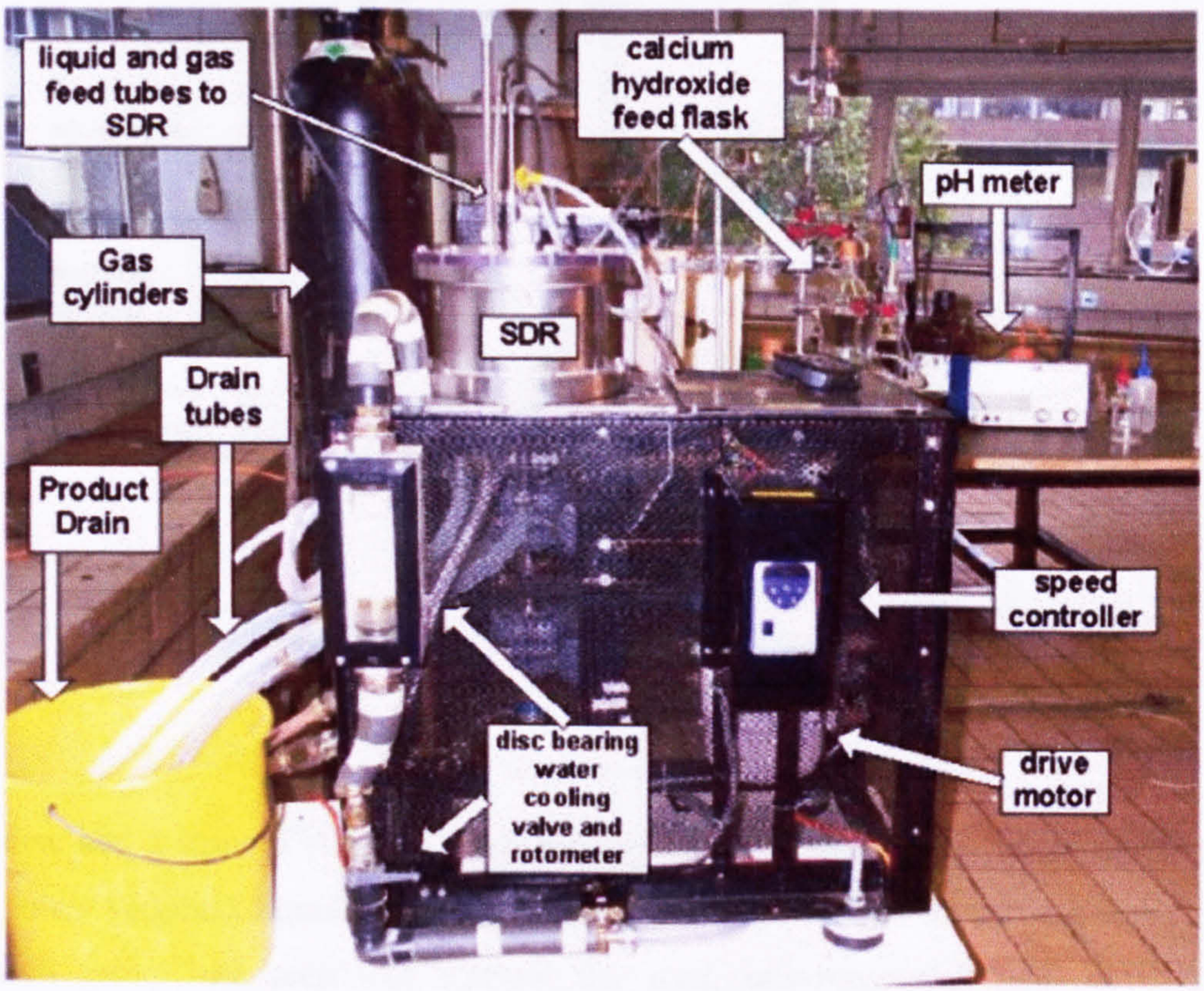


**Figure 4.2 General layout of SDR rig employed in present study**

Figure 4.2 shows the general layout of the SDR and ancillary equipment used in the gas-liquid reactions. The disc was driven by an electric motor. The rotational speed was controlled by an electronic speed controller in the range of 300 to 4000rpm. Water supplied through the sealed rotary union into the shaft allowed for cooling of the bearings and internal workings. This fluid could also be used for heating or cooling of the underside of the disc surface, however this facility was not used during the present

study. A heating/cooling circuit was also available for the shell, this was not required for the precipitation experiments. The disc and the shell were constructed from stainless steel. The disc surface was a stainless steel plate attached by stainless steel screws.

A schematic of the SDR, showing fluid inlet and outlet configurations is shown in figure 4.3.

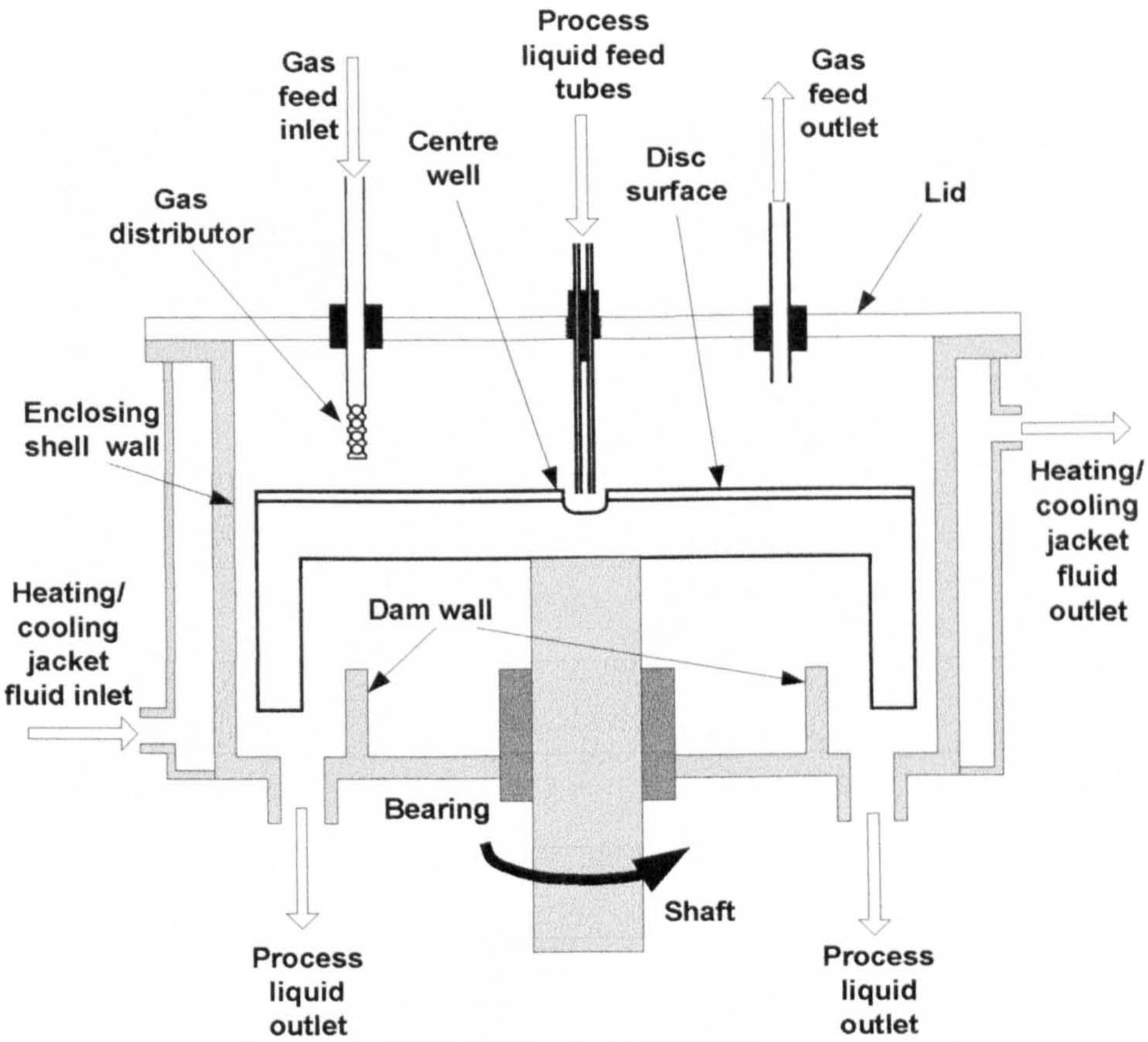


**Figure 4.3 schematic of the SDR**

The disc had a smooth stainless steel surface with a centre well where two 'shotgun' feed tubes supplied liquid reactants to the disc. Previous observational work in the research group had seen that without the well, unsymmetrical flow fields could develop on a smooth disc, the small well acted as to equalise the flow fluctuations before it propagated across the surface. An additional ring feeder (not shown in figure 4.3) for a second liquid feed was constructed. It fed liquid onto the disc from 16 1mm holes at a radius of 12.5mm from the disc centre.

A gas inlet feed pipe was employed to deliver gas into the space between the lid and the disc surface. The pipe had holes drilled in the side with the end blocked off with a bung to allow the gas to flow out in all directions parallel to the disc surface. In early

experiments, the gas exited the end of the pipe which effected the liquid film by blowing a dry spot on it, hence the holes drilled in the side of the tube allowed the gas to exit parallel to the disc and at a much reduced velocity such that it would not effect the liquid film.

The polycarbonate lid was held in place by twelve Allen bolts around the circumference. A circumferential dam wall was employed to keep process liquids away from the shaft bearings.

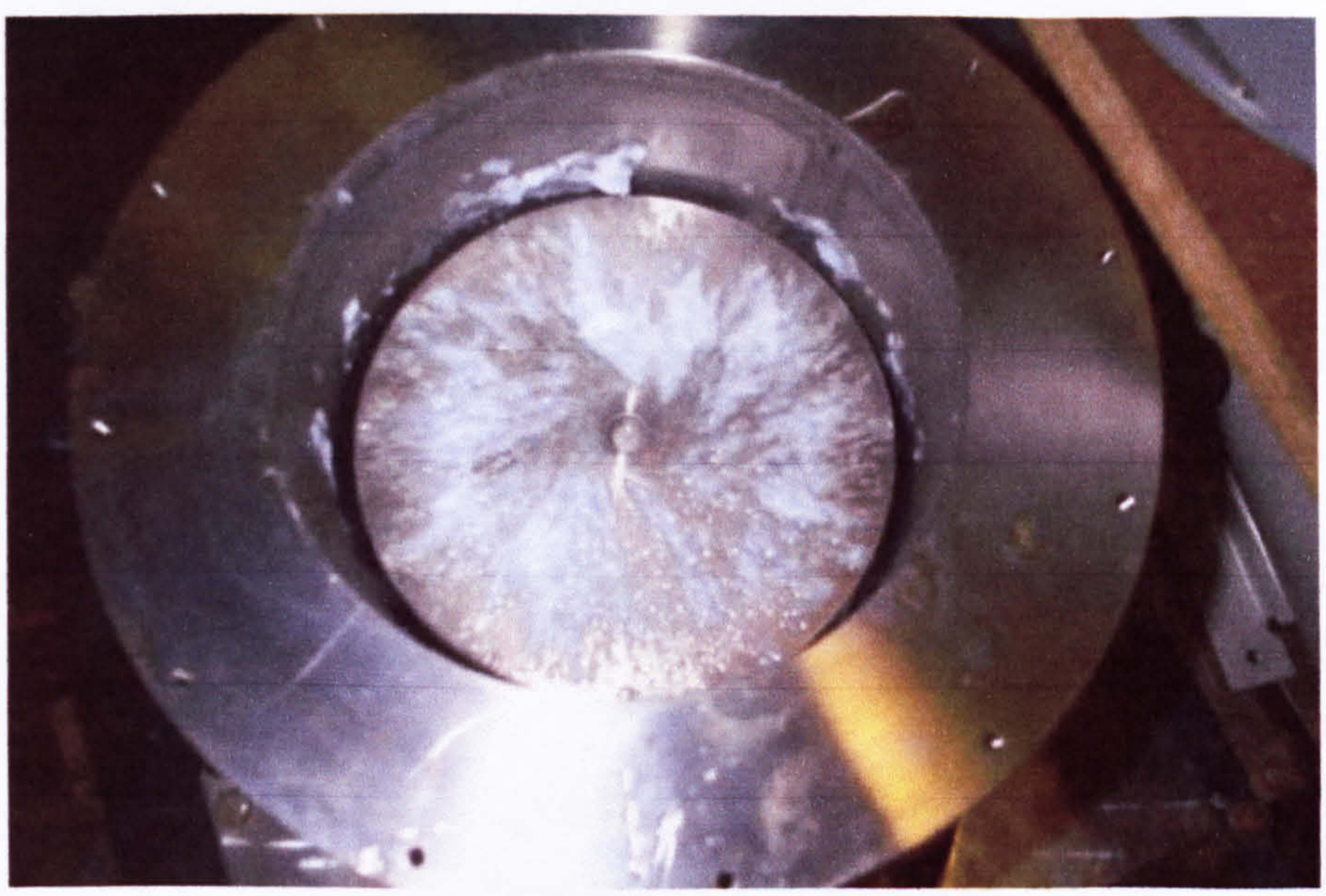

**Figure 4.4 View of the disc and enclosing shell**

In figure 4.4 above, the lid has been removed so that the surface of the disc can be seen. The picture was taken after an experiment performed with very high supersaturation from a liquid-liquid reaction. The precipitation caused severe fouling of the SDR and the subsequent experiments at this supersaturation were abandoned. The centre well can be seen with the enclosing shell wall.

# 5 Gas-liquid solution experimental study

## 5.1 Introduction

The experimental work in this part of the present study is a continuation and amplification of the work described by (Trippa *et al*, 2002). The carbonation of calcium hydroxide solution is studied on the SDR and in the batch. Firstly, the characteristics of the reaction are established from a batch reaction. Secondly, mass transfer parameters, crystal size distribution and morphology for both processing methods are evaluated and compared.

## 5.2 $CaCO_3$ precipitation from the carbonation of limewater

In these experiments, saturated calcium hydroxide solution was used a reactant. Calcium hydroxide is sparingly soluble in water and its solubility is inversely proportional with temperature. As a result, fluctuations in ambient temperature affect the solubility limit and therefore its saturation concentration. The maximum theoretical supersaturation ratio is dependent on the concentration of the calcium ion in solution and the absorption rate of $CO_2$ hence this ratio is susceptible to temperature and local fluid conditions. Upon carbonating the limewater, the supersaturation will develop slowly as the gas is absorbed incrementally into the solution. With low supersaturation, heterogeneous nucleation is likely to occur followed by a predominance of crystal growth over nucleation. Furthermore, the polymorphic nature of $CaCO_3$, and variances in supersaturation may result in more than one crystal shape forming from the reaction.

## 5.3 Scope of the experimental study

The experiments in the present work regarding the carbonation of calcium hydroxide solution were performed in a stirred 1-litre batch reactor and the 15cm diameter SDR rig. The batch reactions performed were used to measure the change in pH of the solution as the carbonation process progressed. From measuring the change in pH, the rate of change of $OH^-$ concentration could be estimated, this ultimately being used to calculate the overall rate of absorption of $CO_2$ into the liquid. The $CaCO_3$ product obtained was sampled, CSD analysis of the product was taken as well as slides prepared for SEM analysis.

# 5 Gas-liquid solution experimental study

## 5.1 Introduction

The experimental work in this part of the present study is a continuation and amplification of the work described by (Trippa *et al*, 2002). The carbonation of calcium hydroxide solution is studied on the SDR and in the batch. Firstly, the characteristics of the reaction are established from a batch reaction. Secondly, mass transfer parameters, crystal size distribution and morphology for both processing methods are evaluated and compared.

## 5.2 $CaCO_3$ precipitation from the carbonation of limewater

In these experiments, saturated calcium hydroxide solution was used a reactant. Calcium hydroxide is sparingly soluble in water and its solubility is inversely proportional with temperature. As a result, fluctuations in ambient temperature affect the solubility limit and therefore its saturation concentration. The maximum theoretical supersaturation ratio is dependent on the concentration of the calcium ion in solution and the absorption rate of $CO_2$ hence this ratio is susceptible to temperature and local fluid conditions. Upon carbonating the limewater, the supersaturation will develop slowly as the gas is absorbed incrementally into the solution. With low supersaturation, heterogeneous nucleation is likely to occur followed by a predominance of crystal growth over nucleation. Furthermore, the polymorphic nature of $CaCO_3$, and variances in supersaturation may result in more than one crystal shape forming from the reaction.

## 5.3 Scope of the experimental study

The experiments in the present work regarding the carbonation of calcium hydroxide solution were performed in a stirred 1-litre batch reactor and the 15cm diameter SDR rig. The batch reactions performed were used to measure the change in pH of the solution as the carbonation process progressed. From measuring the change in pH, the rate of change of $OH^-$ concentration could be estimated, this ultimately being used to calculate the overall rate of absorption of $CO_2$ into the liquid. The $CaCO_3$ product obtained was sampled, CSD analysis of the product was taken as well as slides prepared for SEM analysis.

Where the batch vessel reaction was (obviously) a batch process, the SDR reaction was performed on a continuous basis whereby the calcium hydroxide solution was fed onto the disc on a continuous basis with $CO_2$ gas being fed to the space above the disc at a predetermined flowrate. The initial pH of the solution prior to being fed onto the disc was measured, the pH of the product exiting the disc was also measured in order to determine the change in the $OH^-$ concentration and estimate the rate of $CO_2$ absorption in the short residence time the fluid experiences on the disc. Again, the $CaCO_3$ product was sampled for CSD and SEM analysis. Disc experimental parameters could be altered to determine the effect of rotational speed, liquid flowrate, gas-liquid flow ratio, gas component composition and calcium hydroxide solution concentration.

## 5.4 Experimental set-up

### 5.4.1 Preparation of calcium hydroxide solution

Calcium hydroxide powder was taken from a 95% pure 1kg supply (Calcium hydroxide GPR, BDH product code 27599 5C) and added to de-ionised water. The product label lists Arsenic as 0.0003%, Heavy Metals (as Pb) as 0.004% and Magnesium and Alkali Salts as 4.8%. The powder was added in excess of the equilibrium concentration, with a ratio of approximately 2g of powder per litre of water. This mixture was gently agitated in a 5-litre flask mounted on a magnetic stirrer unit. The top of the flask was sealed to prevent the ingress of air and therefore atmospheric $CO_2$. The mixture was agitated for approximately 1 hour and then left for a period of 48 hours for the suspended particles to settle and the solution concentration to reach equilibrium. The time allowed for settling improved the filtration rates in the next stage of the process. Using this process, several 5-litre flasks at different stages in this preparation process were used to maintain solution stock for the duration of the experimental period.

The resultant suspension was decanted from the flask into a 1-litre Nalgene vacuum filter unit with a 0.2μm membrane. The filtered solution was collected under vacuum in a 2-litre reagent bottle. Once the bottle was full, nitrogen gas was sparged into the solution for approximately 2 minutes to remove any $CO_2$ gas in the solution and to deplete $CO_2$ levels in the space above the liquid level. Experience had shown that precipitate could form in the liquid surface after a period of 1 to 24 hours if this was not carried out. Therefore, it was important to reduce the possibility of this happening

by removing and excluding as much $CO_2$ from the reagent flasks as possible and thus stop the precipitate forming. Solution storage under this inert atmosphere could be guaranteed for several days without the appearance of particulates. Assuming any precipitate observed in the flasks was calcium carbonate, then this would have some erroneous effect on the precipitation study as these particles would have some influence on nucleation, growth and subsequent size analysis. On another matter, the pH and therefore reactant concentrations of the solution would be affected by the ingress of $CO_2$ leading to differing initial reactant conditions from the stock solutions.

### 5.4.2 Ancillary equipment set-up

#### 5.4.2.1 $Ca(OH)_2$ solution pumping system

Calcium hydroxide solution was contained within a flask prior to pumping onto the disc. Nitrogen gas was supplied to the flask via a length of tubing as and when required to reduce the atmospheric carbon dioxide levels in the flask to help prevent precipitation occurring during downtime and turnaround. A bung was used to prevent air leaking back into the flask when the pump was switched off. The bung had to be removed before pumping started to equalise pressure in the flask and to take solution pH measurements as required. See figure 5.2 for the set-up.

The outlet in the bottom of the flask was connected by 6mm bore Tygon tubing via a peristaltic pump (Watson-Marlow 505S) to the two centre feed tubes (2mm bore) on the SDR rig. The pump rotational speed was previously calibrated to flowrate using a stopwatch and a measuring cylinder allowing known flowrates of 4 to 20ml/s to be pumped from the flask. The feed tubes passed the solution to the centre well on the spinning disc.

#### 5.4.2.2 Gas distribution and control system

Both carbon dioxide and nitrogen gas was used for gaseous reactant feed from regulated cylinders supplied by BOC Gases. These were fed through plastic tubing to a flowmeter panel. Two Platon rotometers (approx 20-200ml/min and 50-1800ml/min) were placed in the flow line for each gas and were used to regulate the individual gas flowrates at NTP. Both gas flows could be measured in the range of 20 to 2000 ml/min. After passing through the flowmeters, the individual gas streams

where combined to allow the gas to mix along a long length of tubing to be fed to the gas distributor on the SDR rig or the glass sparger in the batch.

The pressure of the gas in the reactor was impossible to measure due to it being an open system. The flowrates were too low to detect pressure drop through the system. However, it was assumed that the reaction occurred under a very low positive pressure from inside the rig to outside due to the flow of gas.

#### 5.4.2.3 pH meter

A BDH standard glass pH probe was used to measure the pH of the solution. The meter used was an analogue type. The pH meter/probe was calibrated before each experiment using standard buffer solution of pH 9.2 since the reaction took place in the alkaline region of pH 7 to 13, then this seemed the most suitable. The buffer solution was made fresh once per week. In calibrating the probe, the tip was washed in dilute acid and then distilled water to remove a built up of crystals on the glass before immersing it into the buffer. The same meter/probe was used for every measurement to reduce variance.

#### 5.4.2.4 Mastersizer S set-up

The Mastersizer, on loan from the EPSRC Engineering Instrument Pool was the primary instrument for sampling the CSD of each experiment. The instrument worked by means of laser light diffraction of the particles passing through a carrier fluid projected in front of a CCD detector. The instrument software then calculates the size distribution of the particles based on the Mie theory of light scattering from the particles producing a diffraction pattern on the CCD. It determines the size of particles based on the projected area of a sphere from the diffraction patterns detected as the sample is run through. Inaccuracies creep in when particles deviate from spherical. This is especially exacerbated when long needles are the dominant form. Some shape factor correction maybe used but since shape may change from sample to sample it is difficult to factor correctly. Knowing the refractive indices of the particles and the fluid are also important, these are well known for calcium compounds and water. The instrument was capable of measuring sizes in the range 0.05 to 1000μm.

In setting up the instrument, its PC was turned on; the instrument was turned on and allowed to warm up for 30 minutes prior to calibration. Using the dedicated software,

the instrument was calibrated to remove background optical interference prior to sampling the product. This was done by circulating clean water through the flow cell and a sample taking to allow this 'background reading' to be taken away from sample measurements. The appropriate sampling presentation model (which best suited the dispersion of $CaCO_3$ in water) was loaded into the software. A small sample dispersion unit was used to circulate the sample through the optical window of the instrument. After every experiment, the dispersion unit was flushed thoroughly to remove the sample. Periodically the sampling circuit had to be washed with dilute acid to remove possible $CaCO_3$ scale deposits, it was then rinsed with distilled water and recalibrated.

Samples were taken and analysed from each experiment and a microscope slide of the sample was taken for possible SEM study later. Each sample analysed using the Mastersizer was calculated on a volume percent basis, which calculates the CSD data based on the area projected by an equivalent sphere. Mastersizer data was saved for each of the experiment samples; this data was later transferred to Microsoft Excel spreadsheet format for interpretation.

### 5.4.3 Batch reactor experimental set-up and procedure

The batch reactor set-up is seen in figure 5.1.

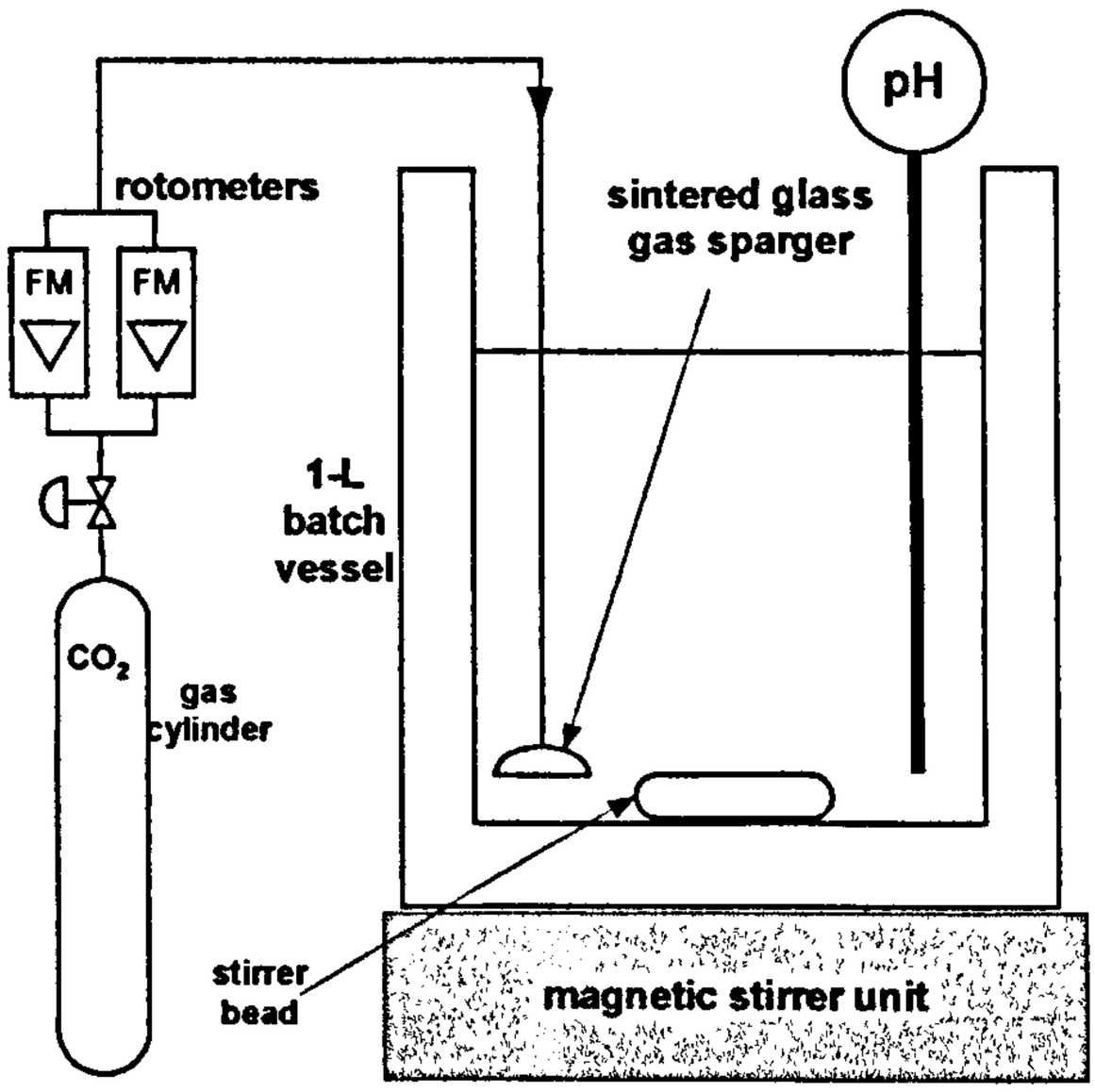


**Figure 5.1 Schematic of batch reactor set-up for gas-liquid reactions**

Batch experiments were performed with reaction volumes of 200ml, 1litre and 2 litres but for mass transfer and CSD evaluation in this part of the present study, a 1 litre vessel was the primary reactor used in the experiments. Each size of reactor was set up

in the same way. A 1 litre Pyrex vessel was used to evaluate the rate of mass transfer from a conventional batch reactor. 1 litre of saturated calcium hydroxide solution was placed in the vessel at the beginning of the experiment. For all the batch experiments 100% $CO_2$ was fed to the bottom of the vessel via two rotometers through 6mm bore PVC tubing to a sintered glass sparger where the gas bubbles disengaged into the solution. The tubing was made rigid by taping it to a 10mm diameter metal bar and clamped in place.

The liquid was agitated using a magnetic stirrer unit set to the maximum speed setting. Agitation began before the gas flow was started to allow the solution to reach steady-state. A pH probe, clamped to a retort stand, was immersed in the solution to monitor pH as the reaction progressed. The effect of immersing the pH probe and the sparger tubing near to the edges of the reactor lead to them acting as flow baffles within the vessel, which reduced the likelihood of cavitation vortices from the stirrer bead.

Once the gas flow was started, pH was measured and recorded at different time intervals. When the gas flow was stopped (at a predetermined pH), the agitation of the liquid was continued whilst a slurry sample was removed using a pipette for CSD analysis and prepared on a microscope slide.

When sampling and analysis was complete, the batch reactor vessel, gas tubing, stirrer bead and pH probe were washed with dilute acid then distilled water to remove scale deposits.

### 5.4.4 SDR experimental set-up and procedure

The 15cm diameter SDR rig previously described was used for the experimental study. The calcium hydroxide solution pumping system and gas supply were connected to the SDR as seen in figure 5.2 below.

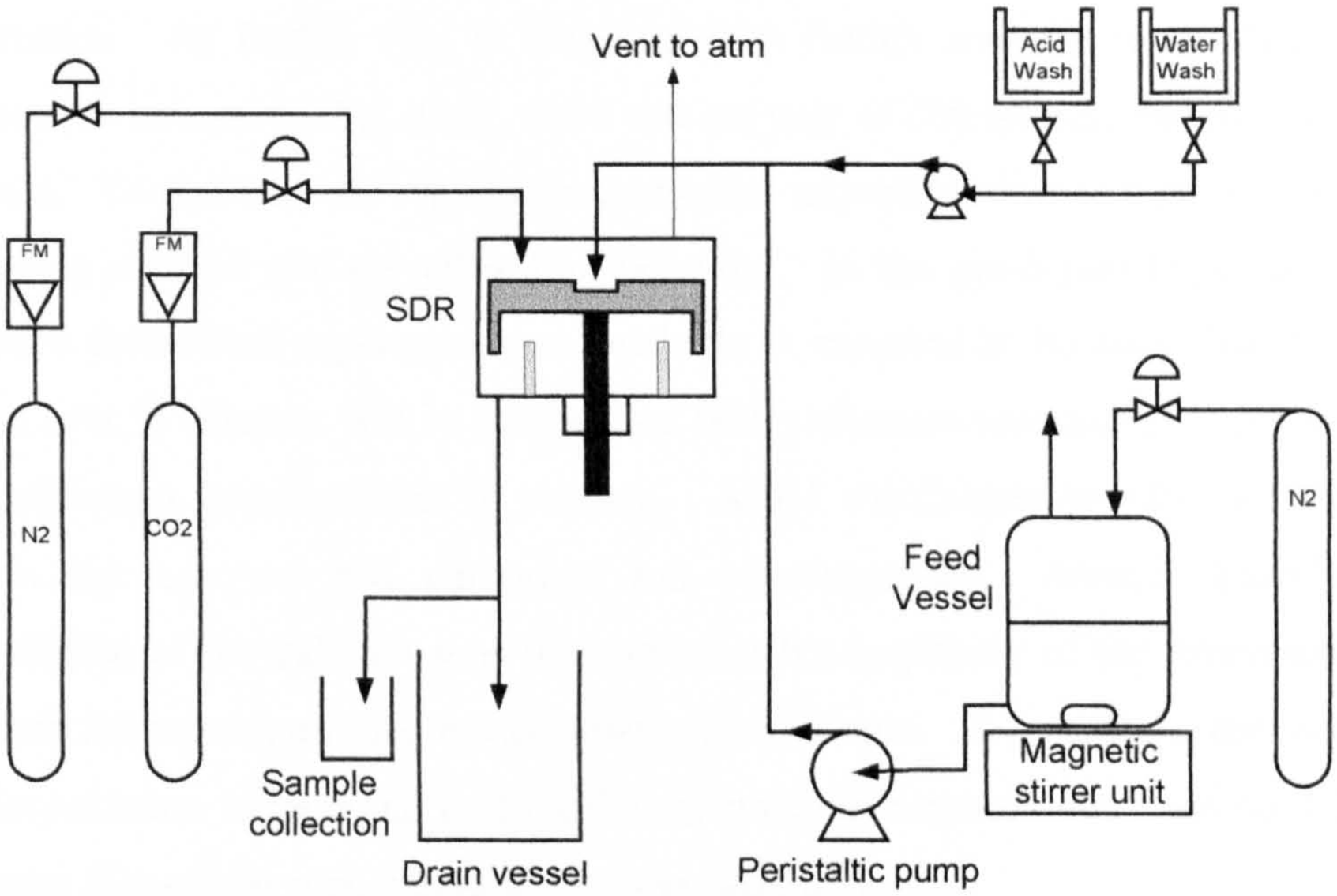


**Figure 5.2 Schematic of SDR set-up for gas-liquid reaction experiments**

The experiments were set up to emulate a process run on a continuous basis. Firstly, the gas flow to the SDR was established; the proportions of $CO_2$ and $N_2$ set on the rotometers for the required conditions. The disc rotational speed was set and allowed to run up to speed. The pH of the calcium hydroxide solution in the feed vessel was measured and recorded. The peristaltic pump (previously calibrated for flowrate by timing volumes into a measuring cylinder) was started to supply solution to the disc at the required flowrate setting. The solution was fed to the disc centre through both shotgun tubes into the centre well. Approximately 100ml of reactant was pumped onto the disc to allow steady-state flow conditions to be established and the product was allowed to flow freely out of the drain tubes and into a bucket. Once this state was established, a 50ml beaker of slurry was collected from the drain tubes for sampling purposes. The pH of the product was measured, the CSD measured and microscope slides prepared. After the sample was taken, the liquid and gas flow was stopped with the disc allowed to rotate to drain any remaining reactants. A dilute acid wash was then pumped onto the disc to remove any scale deposits followed by a rinse with distilled water. The SDR was then ready for another experimental run.

## 5.5 Results

### 5.5.1 Determination of the maximum supersaturation ratio

During the batch process or as it passes over the spinning disc, $CO_2$ is absorbed incrementally into solution which forms an amount of supersaturation and hence precipitation. As further $CO_2$ is absorbed then further solution supersaturates and precipitation occurs. In this study, there was no way of determining the rates of these processes. To that end, the maximum theoretical supersaturation is used as a measure of solution strength and crystallisation potential. In the gas-liquid experiments, the maximum theoretical supersaturation available is assumed to be such that all of the calcium ions in solution will be mopped up with carbonate ions and precipitated until the equilibrium concentration is reached. A 1:1 stoichiometric ratio would exist between the calcium and carbonate ion concentrations. Hence, knowing the concentration of the calcium ions in solution at the beginning of the experiment will determine the maximum theoretical supersaturation ratio. If we assume the carbonate ion concentration to be equal to the calcium ion concentration then from eq 3.51, the maximum theoretical supersaturation for the system, $S_{max}$ is;

$$S_o = \left( \frac{[Ca^{2+}][CO_3^{2-}]}{K_{SP}} \right)^{1/2} \qquad 3.51$$

$$S_{max} = \left( \frac{[Ca^{2+}]^2}{K_{SP}} \right)^{1/2} \qquad 5.01$$

From (Perry, 1997), the solubility of calcium hydroxide solution is inversely proportional to its temperature.

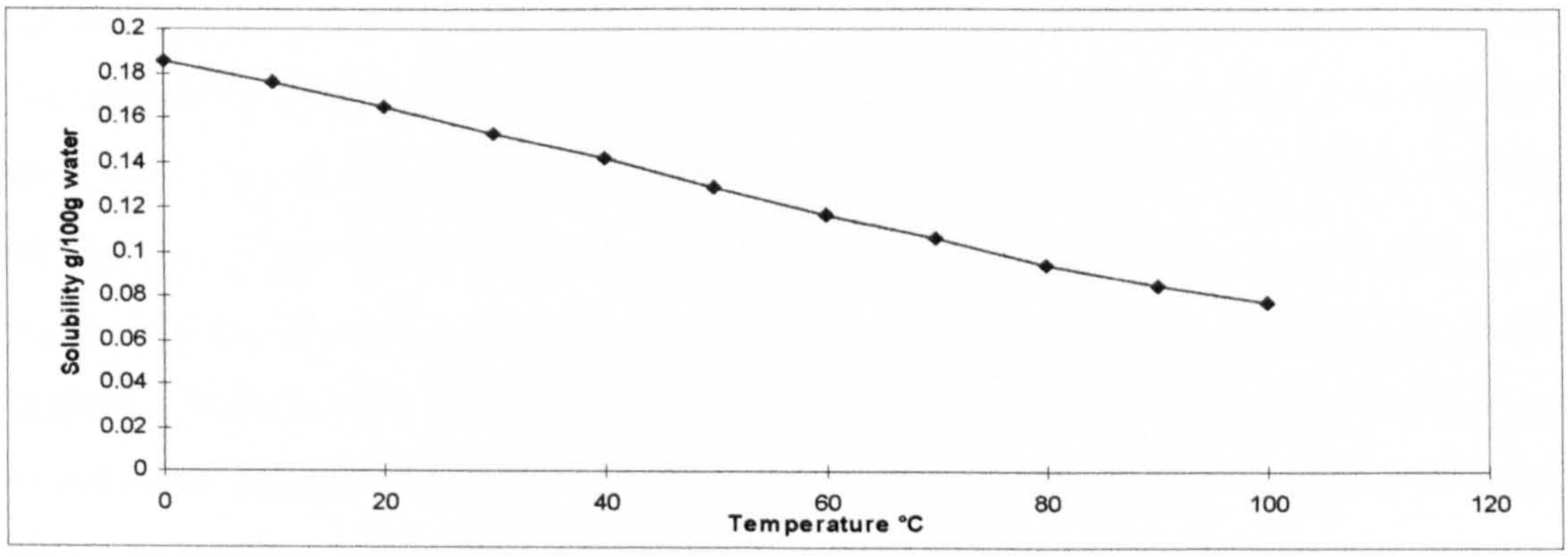


**Figure 5.3 solubility of calcium hydroxide in water (Perry, 1997 pp3.98 table 3.120)**

At 20°C, which was the average temperature for laboratory, conditions the solubility of calcium hydroxide is 1.65g/l (0.0223mol/l) from fig 5.3.

The solubility product for calcium carbonate in water is been reported by (Hostomsky and Jones, 1995): $3.47*10^{-3}$ $mol^2/m^6$ (Plummer and Busenberg, 1982) and $4.01*10^{-3}$ $mol^2/m^6$(Langmuir, 1969). Multiplying by $10^{-6}$ converts these figures into $mol^2/l^2$. Then in equation 5.01, $S_{max}$ at 20°C is 351 or 378.

However, the initial pH of the solution normally used is between 12.4 and 12.5, back calculating, this makes the calcium ion concentration to be (using $K_{sp} = 3.47*10^{-3}$ $mol^2/m^6$).

| pH | $[OH^-]$ mol/l | $[Ca^{2+}]$ mol/l | $S_{max}$ |
|---|---|---|---|
| 12.4 | 0.025 | 0.0125 | **213** |
| 12.5 | 0.032 | 0.016 | **268** |

The maximum initial supersaturation lies between 213 and 268 for reactions starting with a 'saturated solution' of calcium hydroxide. At this level of supersaturation, the nucleation mechanism is thought to be homogeneous (see table 3.2). In practice however, this supersaturation will be much lower as it is not instantaneously formed in solution.

### 5.5.2 Determination of the rate of absorption

#### 5.5.2.1 Considerations for mass transfer analysis

In the present study of the gas liquid reaction, methods of inferring the overall mass transfer rate of $CO_2$ into solution by different measurement techniques were considered. These would include gas chromatography, gas sensing electrodes, gravimetric and tritimetric methods and pH/alkalinity sensing techniques.

For the experimental set-up employed, chromatographic determination of exit gas through the drain tubes was deemed to be more sensitive to air ingress at lower flow rates. Air ingress would cause error in the determination of gas composition exiting the reactor. Measurement of gas flow (and therefore estimation of composition) was gleaned from the rotometer readings. Likewise, analysing gas composition in the chamber above the disc surface would be pointless due to the assumption that this gas composition is that of the bulk (and also approximated to the composition of the feed gas). No method of determining exit gas concentrations was employed directly, so attention was made to measurements based on the liquid side.

Titrimetric analysis of the amount of $CO_2$ absorbed into solution was considered. The total alkalinity of solution can be determined by the use of phenolphthialien indicator. This method is described in (Kotaki and Tsuge, 1990). However, when attempting to complete experiments within a short turn-around time to facilitate the optimum use of the Mastersizer whilst it was in the lab, carrying out titrimetry for each experiment would have slowed down the experimentation considerably. A bias was formed toward the number of experiments performed rather than the use of multiple analysis techniques. Retrospectively, some titrimetric analysis along the way should have been carried out in order to cross reference the data and provide validity of the pH metering.

The technique employed using pH probes was deemed the fastest way to carry out analyses of relative mass transfer. The $CO_2$ absorbed into the liquid is effectively locked up into a solid as formation of $CaCO_3$ particles. By using the same probe to measure the pH of the feed and the product, with adequate rinsing in-between, the error incurred by employing two pH-sensing instruments is removed. The probe could be immersed into the feed vessel and reach an equilibrium reading within a few seconds. Rinsing and immersing the probe into the product collection vessel did not take much longer to accomplish. Samples could then be taken from the product vessel for particle size analysis and the pH of the product sample monitored to check if there was change over a period of minutes.

### 5.5.2.2 The effect of pH and associated conversion

In considering the change in the measured pH from the batch and SDR data it is noted that a reduction of 1.0 pH units would be the equivalent of a 10-fold reduction in hydroxyl concentration (or 90% conversion). 2.0 pH units would be the equivalent of a 100-fold reduction in hydroxyl concentration (or 99% conversion). From a starting pH of 12.5 and an end pH of 10.5 there will be a 99% conversion of the [$OH^-$] in the solution. In the batch data, it can be shown how the pH changes with time. From the measured pH we can infer the concentration of the remaining hydroxyl ions in solution. As the change in the hydroxyl ion concentration is related to the $CO_2$ absorption rate (assuming that the all the $CO_2$ in solution combines with OH ions to form $HCO_3^-$ ions only), then the rate of absorption mass transfer can be determined.

### 5.5.2.3 Inferring mass transfer from pH

By measuring the pH at initial conditions and final conditions i.e. inlet and outlet on the SDR and at intervals in the batch, the rate of $CO_2$ absorption may be attained.

In the overall reaction:

$$Ca(OH)_2 + CO_2 \rightarrow CaCO_3 + H_2O$$

1 mole of $CO_2$ reacts with 2 moles of OH-

The pH of a solution represents the concentration of $H^+$ ions (and corresponding $OH^-$ ions) in the solution (Harris, 1999). The approximate definition of pH is the negative logarithm of the $H^+$ concentration

$$pH \approx -\log[H^+] \qquad (5.02)$$

In pure water at 25°C with $H^+ = 1.0*10^{-7}$ M, pH = $-\log(1.0 \times 10^{-7}) = 7.00$

If the concentration of OH- is $1.0 \times 10^{-3}$ M, then $[H^+] = 1.0 \times 10^{-11}$ M and the pH = 11.0

The relationship between the $H^+$ and $OH^-$ concentrations is;

$$pH + pOH = -\log(Kw) = 14.00 \text{ (at 25°C)} \qquad (5.03)$$

By example, if the pH = 3.58 then pOH = 14.00 – 3.58 = 10.42

and the $[OH^-] = 10^{-10.42} = 3.8 \times 10^{-11}$ M

Therefore by measuring the change in pH we can determine the change in hydroxyl concentration and therefore infer the amount of $CO_2$ absorbed. By measuring the change in pH with time, we may infer the rate at which $CO_2$ is being absorbed into solution.

### 5.5.2.4 pH measurement and determination of mass transfer in the batch

With the pH probe immersed in the calcium hydroxide solution, pH was measured at the beginning of the experiment. As carbonation begins, the time was noted as the pH changed in 0.1 or 0.2 pH intervals. The hydroxyl concentration could be determined for the pH and hence, the average mass transfer rate at the midpoint between the time intervals was determined by the relationship;

$$\frac{d[OH^-]}{dt} = \frac{[OH^-]_1 - [OH^-]_2}{(t_1 + t_2)/2} \qquad (5.04)$$

This allows for the rate of mass transfer to be determined as the carbonation progresses.

#### 5.5.2.5 pH measurement and determination of mass transfer from the SDR experiments

The pH of the solution was taken from the feed flask before the beginning of the experiment and from the product collection beaker as it exited the reactor, hence the inlet and outlet conditions are know but there was no method available to determine the change in pH as the solution flowed across the disc. The residence times of the fluids on the disc are extremely small, estimated by the Nusselt model to be in the range to 0.04 to 0.32s for the experiments on the present study. Using this estimate of residence time, the rate of change of the hydroxyl ion was calculated by;

$$\frac{d[OH^-]}{dt} = \frac{[OH^-]_{inlet} - [OH^-]_{outlet}}{t_{res}} \qquad (5.05)$$

It was assumed that the carbonation process takes place only on the disc so that the residence time may be used in determining the mass transfer rate. However it is feasible that gas-liquid mass transfer will take place as the liquid drains down the shell walls and through the drain tubes since the positive pressure of the gas flow exerts itself out through the liquid drain as well as the gas outlet. This mass transfer rate is impossible to quantify for the variable process conditions within the equipment but is assumed the liquids draining in this way would have greater film thickness than that generated on the disc and would perhaps experience mass transfer rates orders of magnitude lower. Appendix section 9.14 shows the film thickness, mean film velocity and residence time of a continuous film flowing down the shell wall for the conditions in the present study.

If the Nusselt model is regarded as unreliable for determining the residence time and considering the inaccuracies feasible due the absorption into the liquid on other surfaces within the reactor, the mass transfer performance of the SDR may only be generalised. The measurement of pH at the inlet and outlet allow for the change in concentration of the hydroxyl ion to be determined (molar concentration per unit volume), this figure also infers the amount of $CO_2$ in solution absorbed by the solution. Also the liquid flow rate is known from the pump calibration (unit volume per unit

time). Hence, by multiplying these two parameters together, the rate at which $CO_2$ is absorbed in the SDR may be estimated as follows:

$$N_{CO2,SDR} = Q\left(\frac{d[OH^-]}{2}\right) \qquad (5.06)$$

where $N_{CO2,SDR}$ is the overall rate of $CO_2$ absorption within the SDR (mol/s).

Retrospectively, an experimental method could have been employed by which sample was collected at the disc periphery by a tube and thus be removed from being exposed to gas inside the shell. This method would have been difficult to employ in practice since there is only 5mm between the edge of the disc and the shell wall with the risk of collision with the rotating disc at high speed being a safety issue.

### 5.5.3 Batch mass transfer experiments

#### 5.5.3.1 Initial batch work

Early batch experiments in the batch reactor centred on acquiring data on the effect of agitation and of the effect of increasing the flowrate of $CO_2$. In studying these effects, a smaller batch reactor containing 200ml of calcium hydroxide solution was used whereby it was agitated (or not) with a magnetic stirrer at the nominal speed setting with the gas sparger and pH probe being immersed in the liquid. For these experiments, the change in pH with time is plotted for each run. This process was used to study the general characteristic effect of carbonation on the solution pH.

In considering the effect of agitation it was seen in each case that pH dropped more quickly when the batch was agitated than when it was not. This was seen by (Wachi and Jones, 1991) who saw a faster decrease in pH with increasing stirrer speed in the batch carbonation of limewater.

In the two cases illustrated below for $CO_2$ flowrates of 225 and 500 ml/min, the comparison is made to show the effect of agitation.

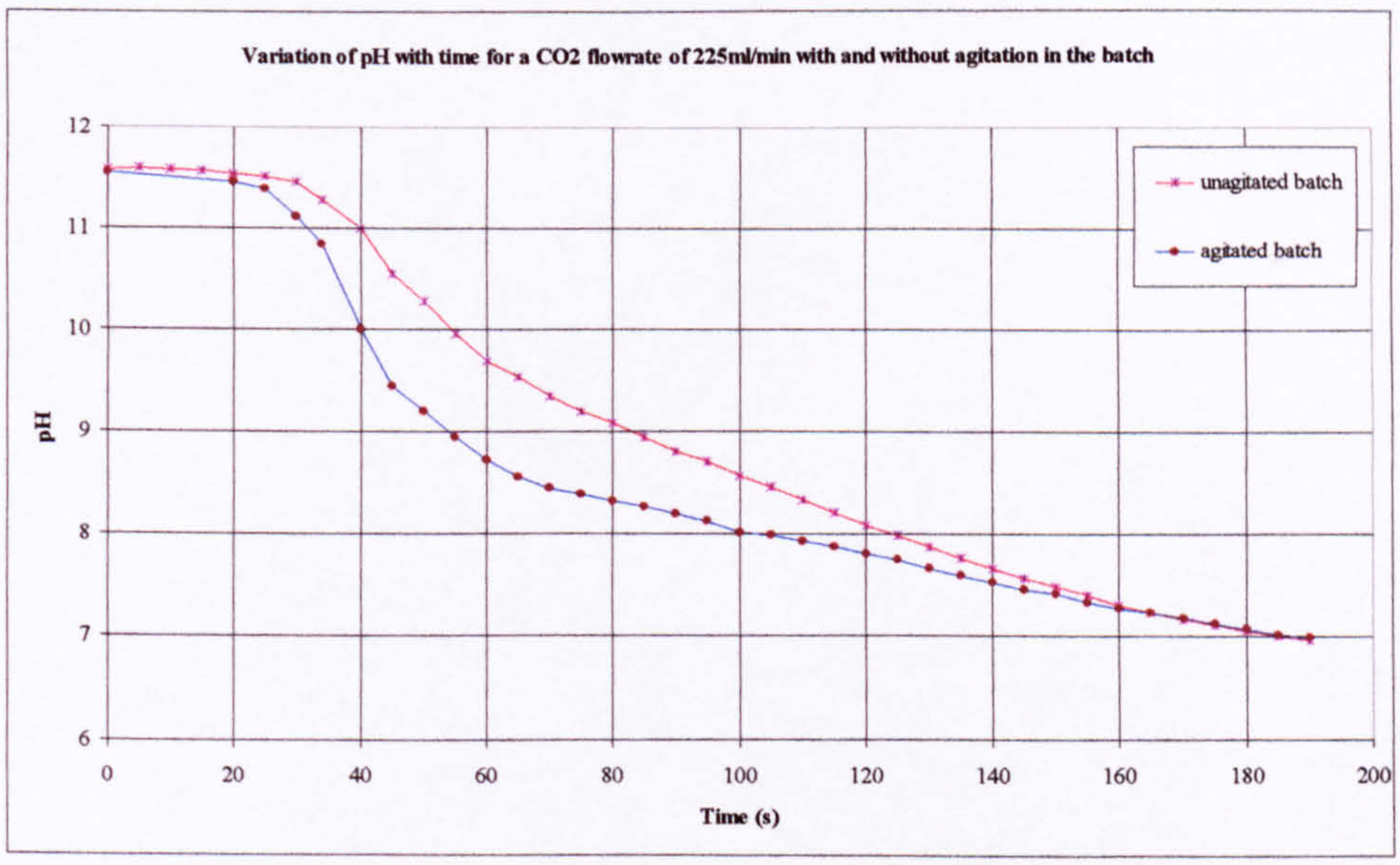


**Figure 5.4 Variation of pH with time for a $CO_2$ flowrate of 225ml/min with and without agitation in the batch**

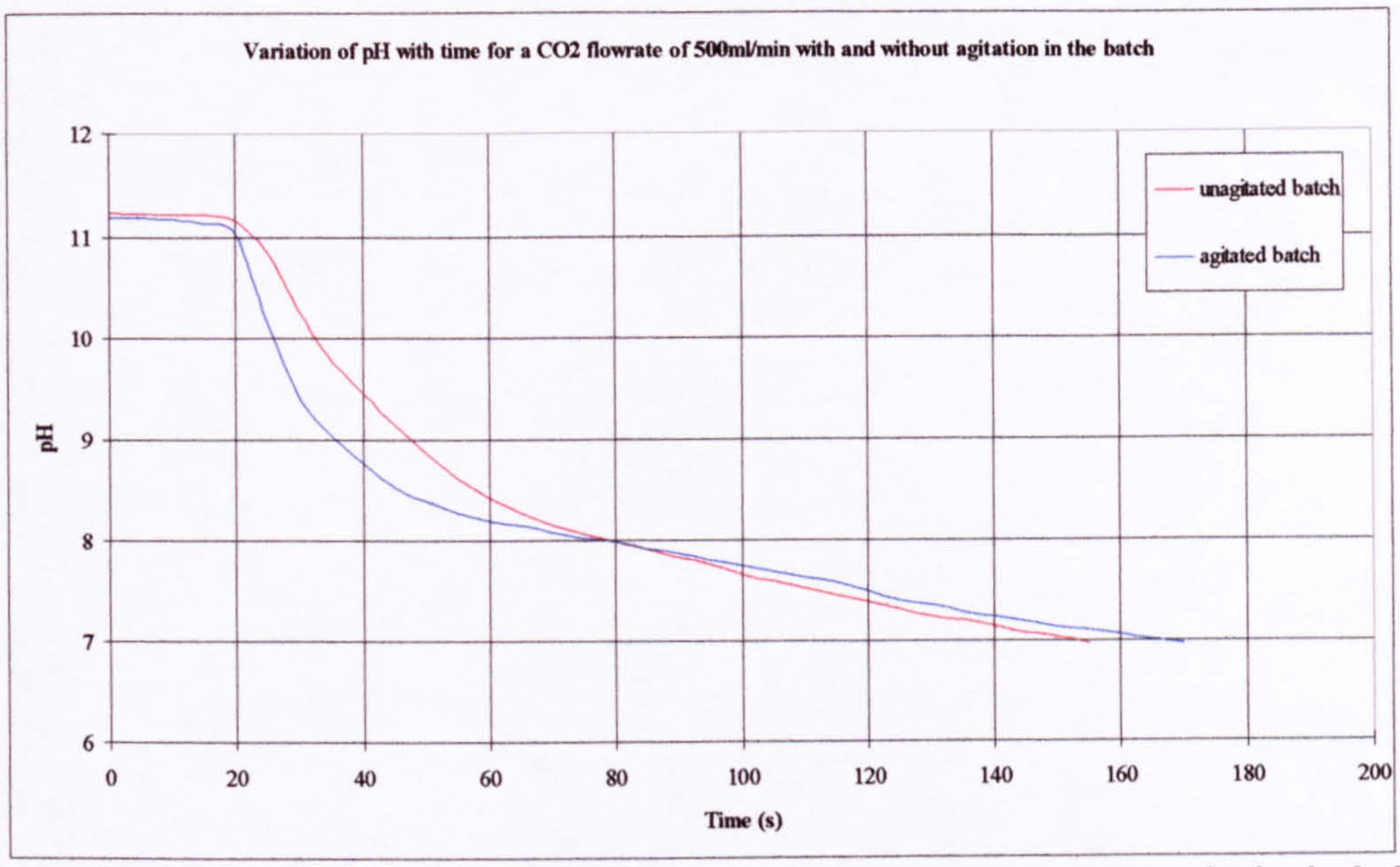


**Figure.5.5 Variation of pH with time for a $CO_2$ flowrate of 500ml/min with and without agitation in the batch**

In the two cases illustrated and in all cases, the change in pH with time was higher when the batch was agitated. This was always prevalent near the beginning of the reaction, the fall in pH being the most rapid early in the carbonation. In fact this is a characteristic of the carbonation, higher rates of mass transfer occur at higher pH, this is because there is an enhancement to mass transfer brought about by the chemical reaction. From a change in the logarithmic scale over 3 pH units, the $OH^-$ concentration has reduced 1000 fold and would signify a 99.9% depletion of the available $Ca^{2+}$ for the precipitation. At lower pH, the physical of absorption of $CO_2$ into solution will be the dominant process as opposed to the chemical reaction enhanced process at higher pH. Further carbonation results in the formation of carbonic acid as the pH passes into the acidic region, the formation of carbonate ceases and the formation of bicarbonate begins. Calcium carbonate is dissolved by the acidic conditions and bicarbonate forms.

In considering the effect of $CO_2$ flowrate on the rate of depletion of solution pH, the effect can be seen in figure 5.6.

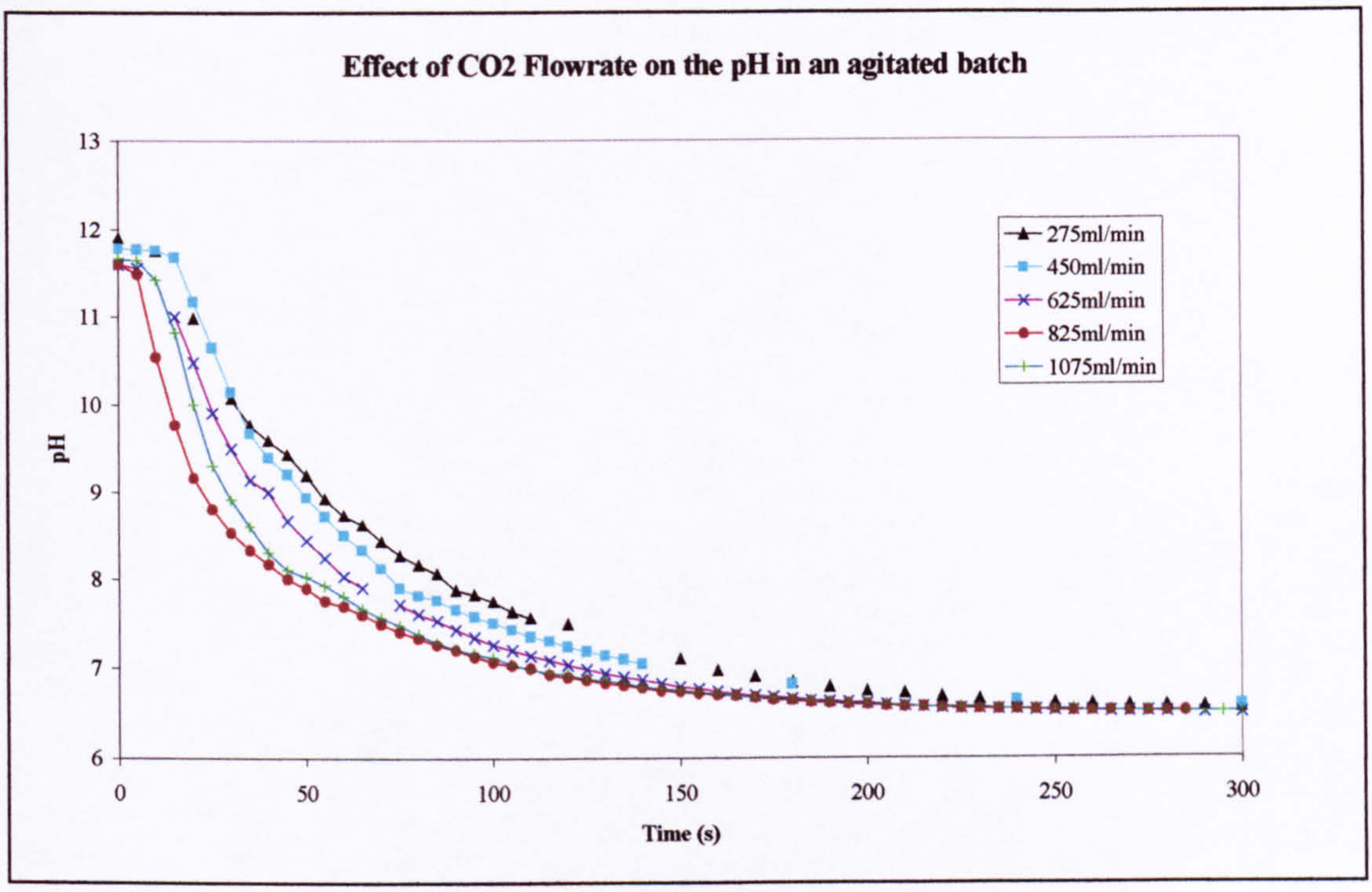


**Figure.5.6 Effect of $CO_2$ flowrate on the pH in an agitated batch**

The effect of increasing the $CO_2$ flowrate in the batch reaction led to a faster depletion of solution of pH. Intuitively, by increasing the number of bubbles transmitted in the solution with time by increasing the gas flow, the available surface area of the bubbles in the solution volume increase and thus facilitate an increase in the overall rate of mass transfer. This was prevalent up to 825ml/min. Increasing the flowrate further actually led to a slightly slower carbonation rate suggesting that there was a reduction in effective bubble area/residence time or a reduction in the agitator performance to effectively mix due to the large number of bubbles to further enhance mass transfer in this 200ml vessel. Essentially, the impeller could have become flooded with gas at the higher $CO_2$ flowrate and therefore be less effective at dispersing the gas.

In conclusion from these initial experiments, it was seen that agitating the batch and increasing the gas flowrate could increase the rate of carbonation. This would lead to faster rates of reaction, developing higher supersaturation and affecting the crystallisation kinetics. In the initial batch work as no facility for CSD evaluation was available, this effect could not be studied.

### 5.5.3.2 Determination of mass transfer in the batch reactor

From the initial experiments, the characteristics of the carbonation rate process were understood. In using the batch reaction as a benchmark for the SDR experiments, the

batch reaction was scaled up to the 1-litre vessel as described earlier and the Mastersizer had become available. In the initial batch work, there had been no facility for particle categorisation. Using a larger vessel increased the experimental run time for a given gas flowrate and each batch was agitated as the product was seen to settle without agitation. Keeping the crystals in suspension was important as these experiments concerned the nature of the precipitate, agitation would facilitate a well-mixed reactor synonymous with batch crystallisers in industry. In these experiments, the change in pH was used to determine the rate of change in hydroxyl concentration as well as collecting product samples for categorisation. A single experiment was repeated several times to develop more confidence in the mass transfer data. The same agitation and $CO_2$ flowrate were chosen. $CO_2$ was pumped into the batch at a rate of 1000ml/min and the magnetic stirrer was set to its maximum setting. With the gas tube and the pH probe rigidly set in the vessel, they acted like baffles and prevented the stirred solution from developing cavitation vortices.

The three experiments are labelled A1, A2 and A3. The three experiments are plotted on the same axis in charts to show the change in pH with time, the change in the hydroxyl concentration with time, and the rate of change in the hydroxyl concentration with time.

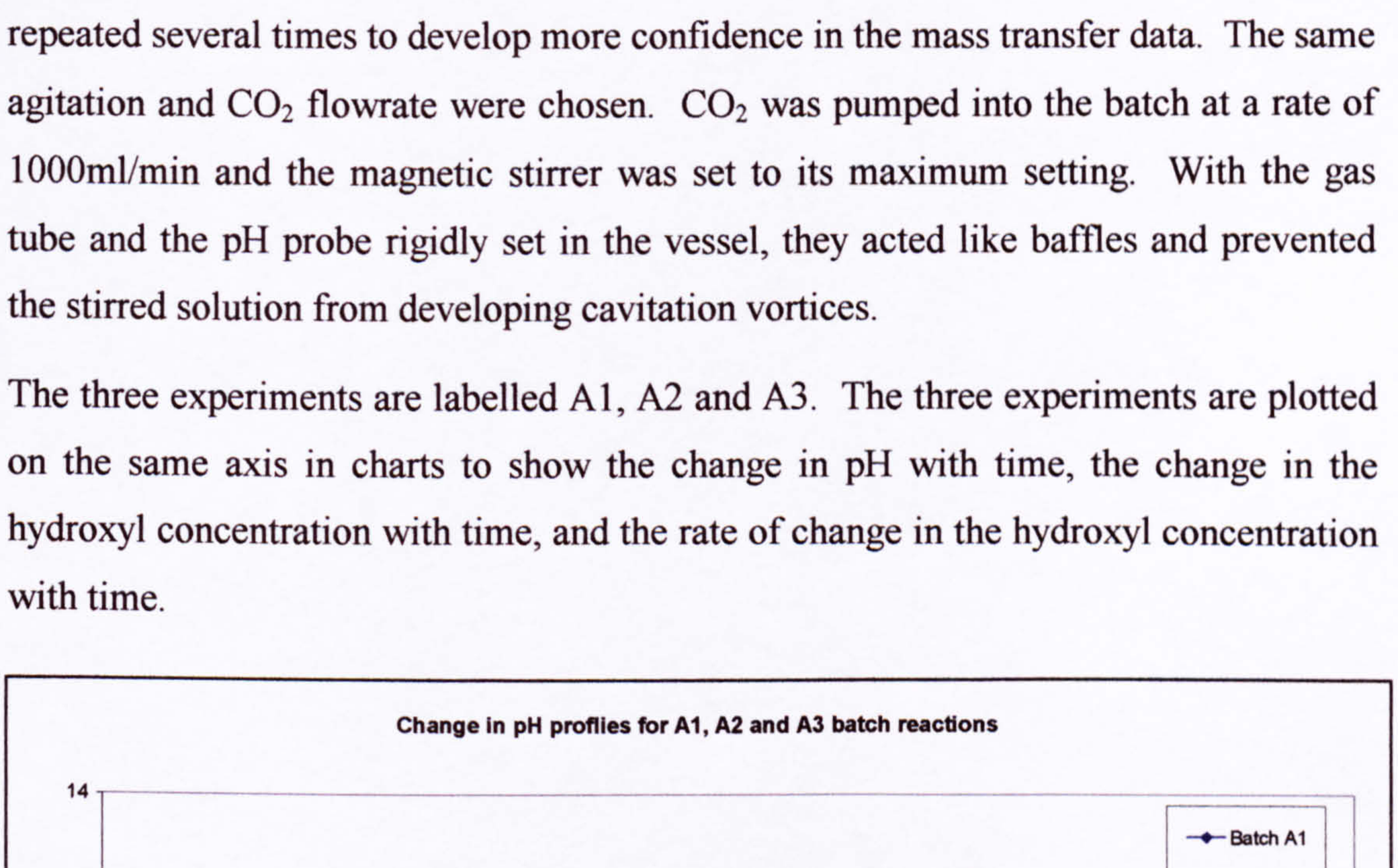


**Figure 5.7 Change in pH profiles for A1, A2 and A3 batch reactions**

From the pH profiles of the experiments in figure 5.7 above, it is seen that there is a spread of data between the experiments. The profiles match each other quite closely at the beginning of the experiment, but around pH 12 the profiles of A1 and A2 diverge with A3 being somewhere in the middle. It is seen that there is some experimental variability for identical conditions. It was noted that the initial pH of A1 and A2 was 12.5 whereas A3 had an initial pH of 12.6. The batches might have been stored in different reagent bottles; the three experiments were carried out over 2 days and therefore the solution might be subject to variability in concentration. Furthermore, variances in temperature between lab sessions may have led to measurement variability.

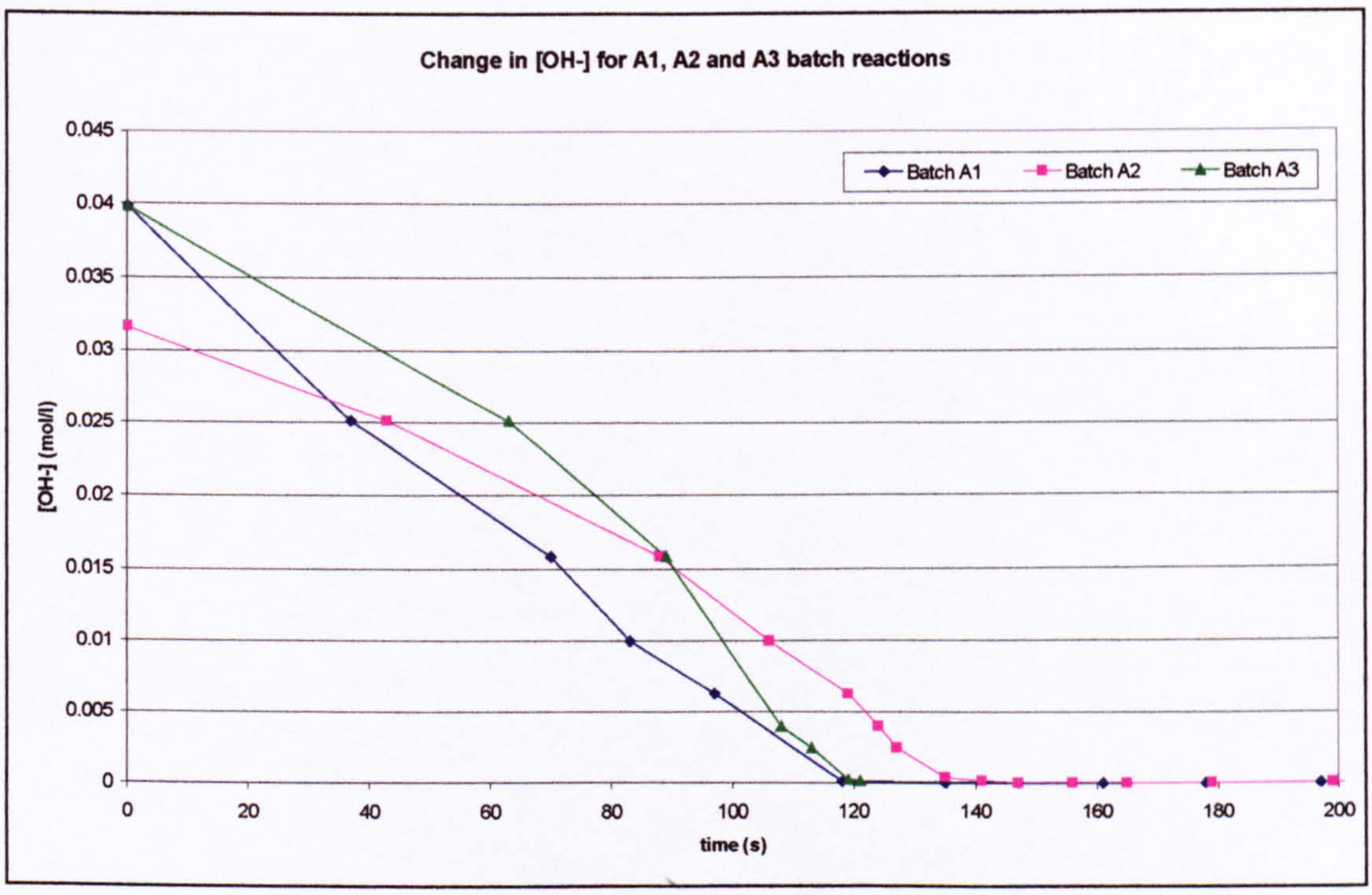


**Figure 5.8 Change in [$OH^-$] for A1, A2 and A3 batch reactions**

In figure 5.8, the variability is shown in the change in hydroxyl concentration with time. The profiles are all approximately linear with time until the hydroxyl concentration is almost depleted (this is around pH 10 for each experiment). The change in the hydroxyl concentration then becomes almost zero. This is the limit whereby the reactants are almost used up - approximately 99.4% depletion in the hydroxyl concentration from the starting conditions- and the limit of the enhancement of mass transfer by chemical reaction.

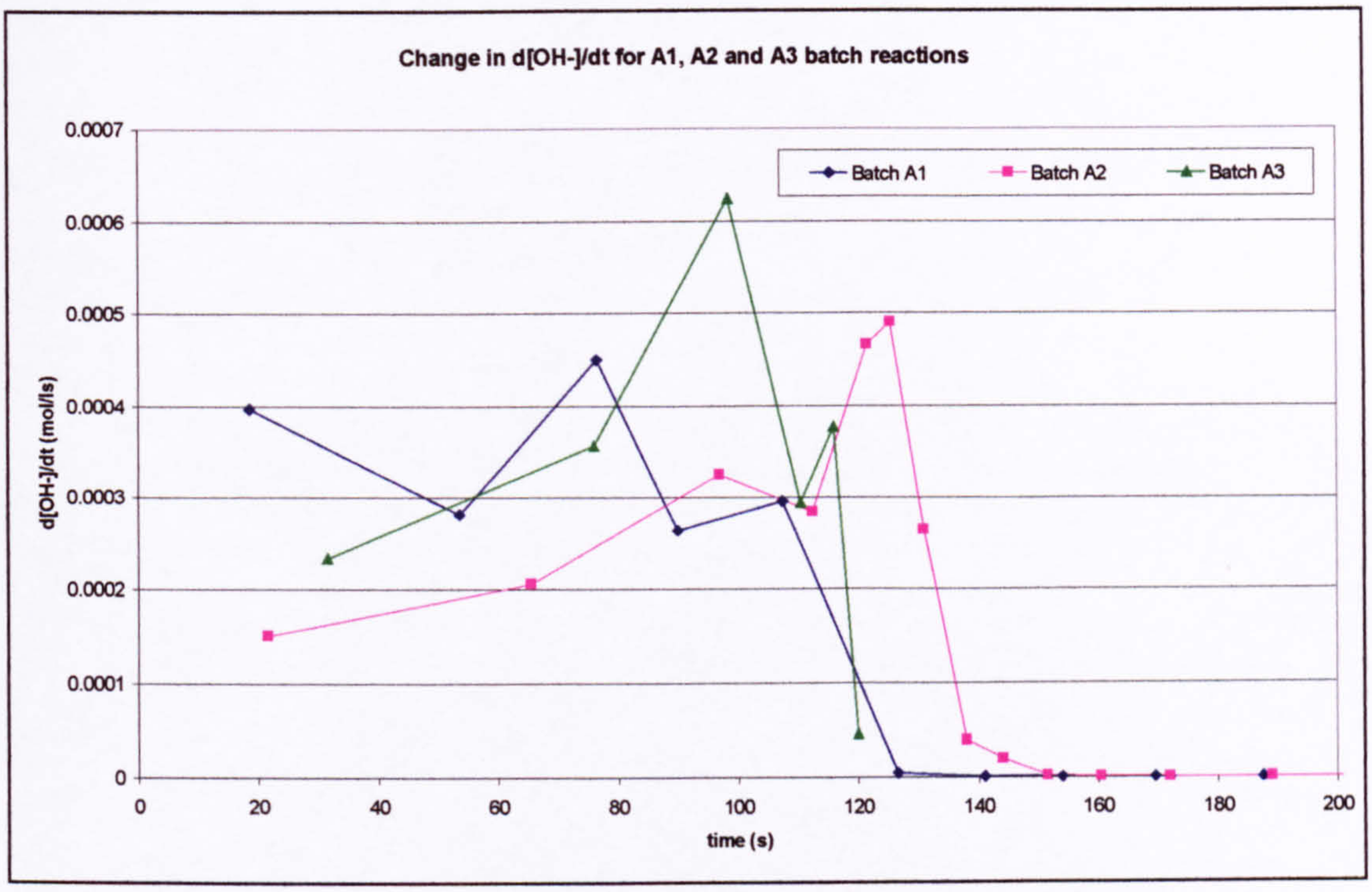


**Figure 5.9 Change in d[OH-]/dt for A1, A2 and A3 batch reactions**

In considering the change in the rate of hydroxyl depletion, data was calculated for $d[OH^-]/dt$ at intervals and then plotted in figure 5.9. Slight variations in the $d[OH^-]$ data led to fluctuations in the plots, again, $d[OH^-]/dt$ falls to very low levels at around 120-140 seconds representing pH 10.0 in each experiment.

If an average for $d[OH^-]/dt$ is taken for each experiment between the beginning of the experiment and the time at which it falls to pH 10, a table of the average $d[OH^-]/dt$ can be seen below. Following, in the overall reaction:

$$Ca(OH)_2 + CO_2 \rightarrow CaCO_3 + H_2O$$

1 mole of $CO_2$ reacts with 2 moles of $OH^-$

From this, we can estimate the rate of $CO_2$ absorption in the batch between pH 12.6 and 10.0. The rate of $CO_2$ absorption is half the rate of depletion of the hydroxyl ion and therefore can be calculated.

| | Batch A1 | Batch A2 | Batch A3 | Average for all 3 batches | Standard deviation |
|---|---|---|---|---|---|
| Average d[OH-]/dt between starting pH and pH 10 (mol/ls) | 0.000337 | 0.000312 | 0.000322 | 0.000324 | 1.3E-05 |
| Rate of $CO_2$ absorption in the batch (mol/ls) | 0.000169 | 0.000156 | 0.000161 | 0.000162 | 6.4E-06 |

**Table 5.1 $CO_2$ absorption rates in the batch reaction experiments**

Table 5.1 shows that the average values for the $CO_2$ absorption rate are very similar for the batch experiments performed under the same conditions.

### 5.5.4 SDR mass transfer experiments

In determining the $CO_2$ absorption rate on the SDR, the pH of the inlet and outlet conditions was measured. From that, the concentration difference of the hydroxyl ion was inferred. The absorption rate of $CO_2$ by the solution was calculated from the concentration difference and the liquid flowrate in equation (5.06).

The first set of absorption experiments were performed on the SDR to determine mass transfer rates. This set of experiments was named "A-set". 5 disc rotational speed and 5 liquid flowrates were employed. For each of these experiments, 100% $CO_2$ was used. The flow ratio was fixed so that the molar flowrates of calcium ion in the liquid to $CO_2$ in the gas were 1:3. The flowrate parameters are shown in table 5.2 below. The rotational speeds used were 500,750, 1000, 1500 and 2000rpm.

| Calcium hydroxide solution flowrate (ml/s) | Corresponding $CO_2$ flowrate (ml/min) |
|---|---|
| 4 | 240 |
| 8 | 480 |
| 12 | 720 |
| 16 | 960 |
| 20 | 1200 |

**Table 5.2 A-set gas and liquid flow parameters for SDR absorption experiments**

During these experiments, CSD analyses of the samples were taken to determine what the possible effect the mass transfer rate had upon the product distribution. The crystal size distribution data will be described and discussed later.

#### 5.5.4.1 Effect of rotational speed and liquid flowrate on the SDR

From the A-set experiments performed on the SDR, the change in pH was measured and the $d[OH^-]$ determined. This data was put into experimental plots to determine the effect of changing rotational speed. The rotational speeds are shown in rad/s corresponding to the rpm of the disc. The $d[OH^-]$ numerical data from the experiments is tabulated in table 5.3.

| | Disc rotational speed | | | | |
|---|---|---|---|---|---|
| | 52.4 rad/s | 78.0 rad/s | 103.6 rad/s | 156.0 rad/s | 207.2 rad/s |
| 4 ml/s | 0.0282 | 0.0316 | 0.0235 | 0.0151 | 0.0190 |
| 8 ml/s | 0.0251 | 0.0251 | 0.0251 | - | - |
| 12 ml/s | 0.0282 | 0.0316 | 0.0251 | 0.0211 | 0.0216 |
| 16 ml/s | 0.0251 | 0.0251 | 0.0251 | - | - |
| 20 ml/s | 0.0251 | 0.0251 | 0.0251 | 0.0226 | 0.0253 |

**Table 5.3 d[$OH^-$] (mol/l) obtained from A-set SDR experiments**

The blank cells in table 5.3 were experiments not performed, hence no data was available. It is noted for several experiments that the value of [$OH^-$] was the same, 0.0251. The effect of rotational speed at different solution flowrates on the change in hydroxyl ion concentration is plotted in figure 5.10 below.

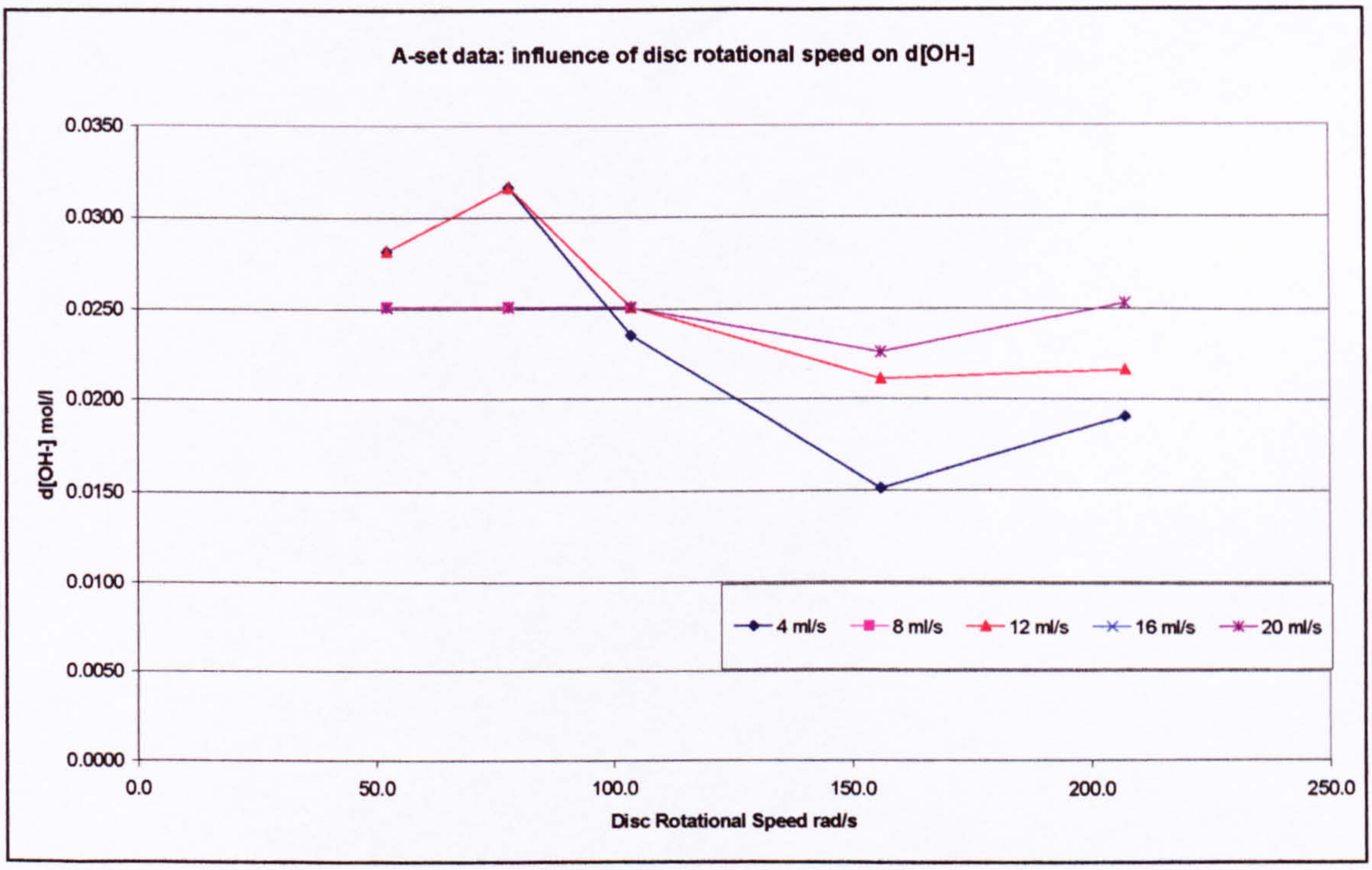


**Figure 5.10 A-set data: influence of disc rotational speed on d[OH-]**

It is seen in figure 5.10 that d[$OH^-$] increases at low rotational speed for 4 and 12 ml/s, the other flowrates show no effect between 52.3 and 104.6rad/s (500 and 1000rpm). Above this rotational speed however, at 4, 12 and 20 ml/s, d[$OH^-$] decreases at 156 rad/s (1500rpm) then has an increase at 207.2 rad/s (2000rpm).

The effect of flowrate at different rotational speeds on the change in hydroxyl ion concentration is shown in figure 5.11 below.

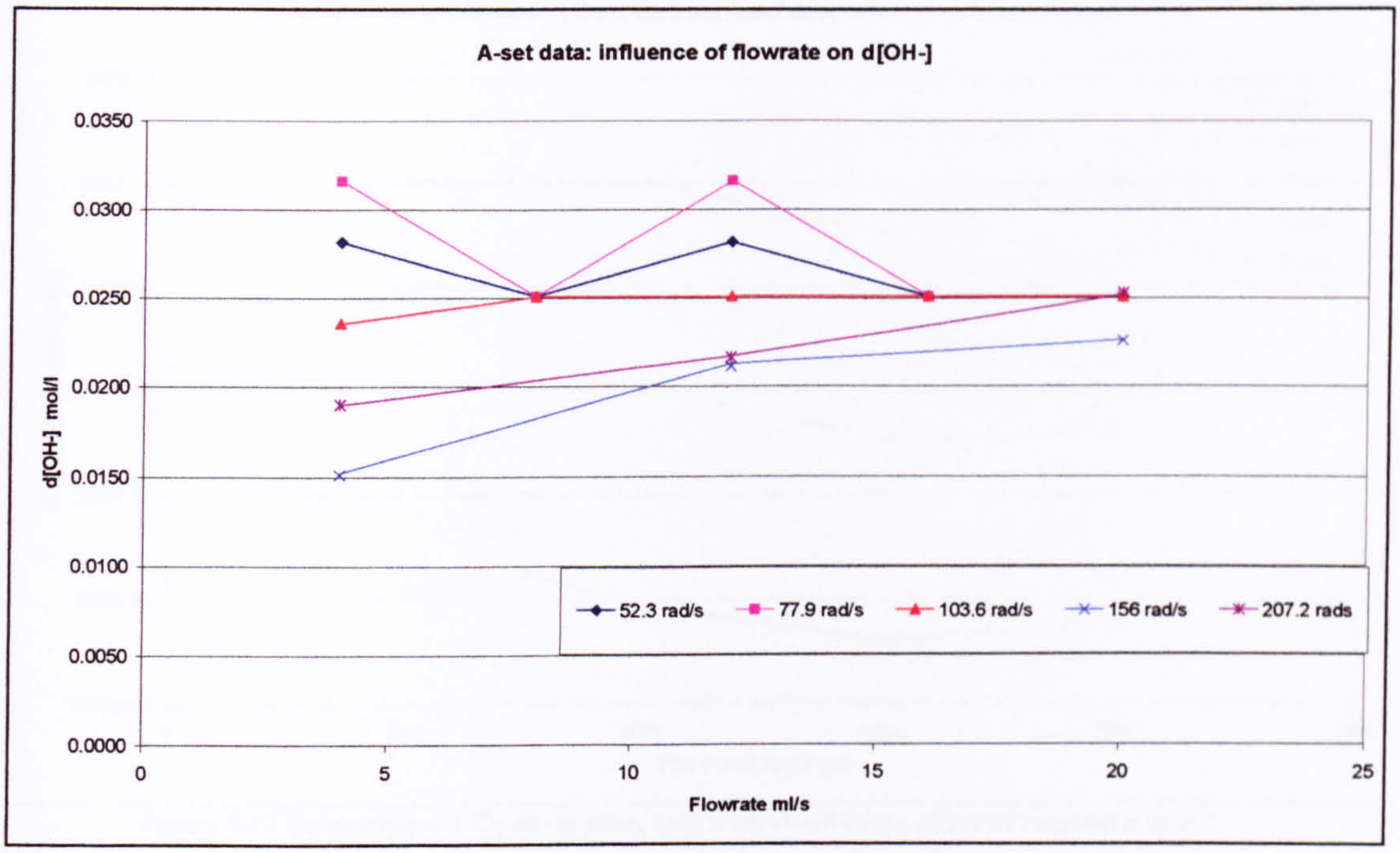


**Figure 5.11 A-set data: influence of flowrate on d[$OH^-$]**

At 103.6 rad/s (1000rpm) there is almost no effect of flowrate on the change in hydroxyl ion concentration. At the higher rotational speeds of 156 and 207.2 rad/s (1500 and 2000rpm), the change in hydroxyl ion concentration increases with increasing flowrate. The change in hydroxyl ion concentration does not have a strong dependence on the flowrate however as the flowrate increases, this will have an effect on the amount of liquid absorbing the $CO_2$ as more liquid/gas and therefore reactant is available for mass transfer.

In determining the mass transfer rate of the A-set data, it can be envisaged that even if the disc rotational speed was set to zero, then gas absorption would occur in an atmosphere of $CO_2$ as the fluid moved under its own inertia as it was pumped onto the disc and drained down the vertical surfaces and out through the drain tubes. It is for this reason that the mass transfer performance, based on the absorption rate of $CO_2$, is evaluated as a function of the liquid flowrate and the change in hydroxyl ion concentration as previously set out. The absorption rate of $CO_2$ is calculated using equation (5.06). The effect of rotational speed on the absorption rate of $CO_2$ is shown in figure 5.12 and the effect of flowrate on absorption rate of $CO_2$ is shown in figure 5.13.

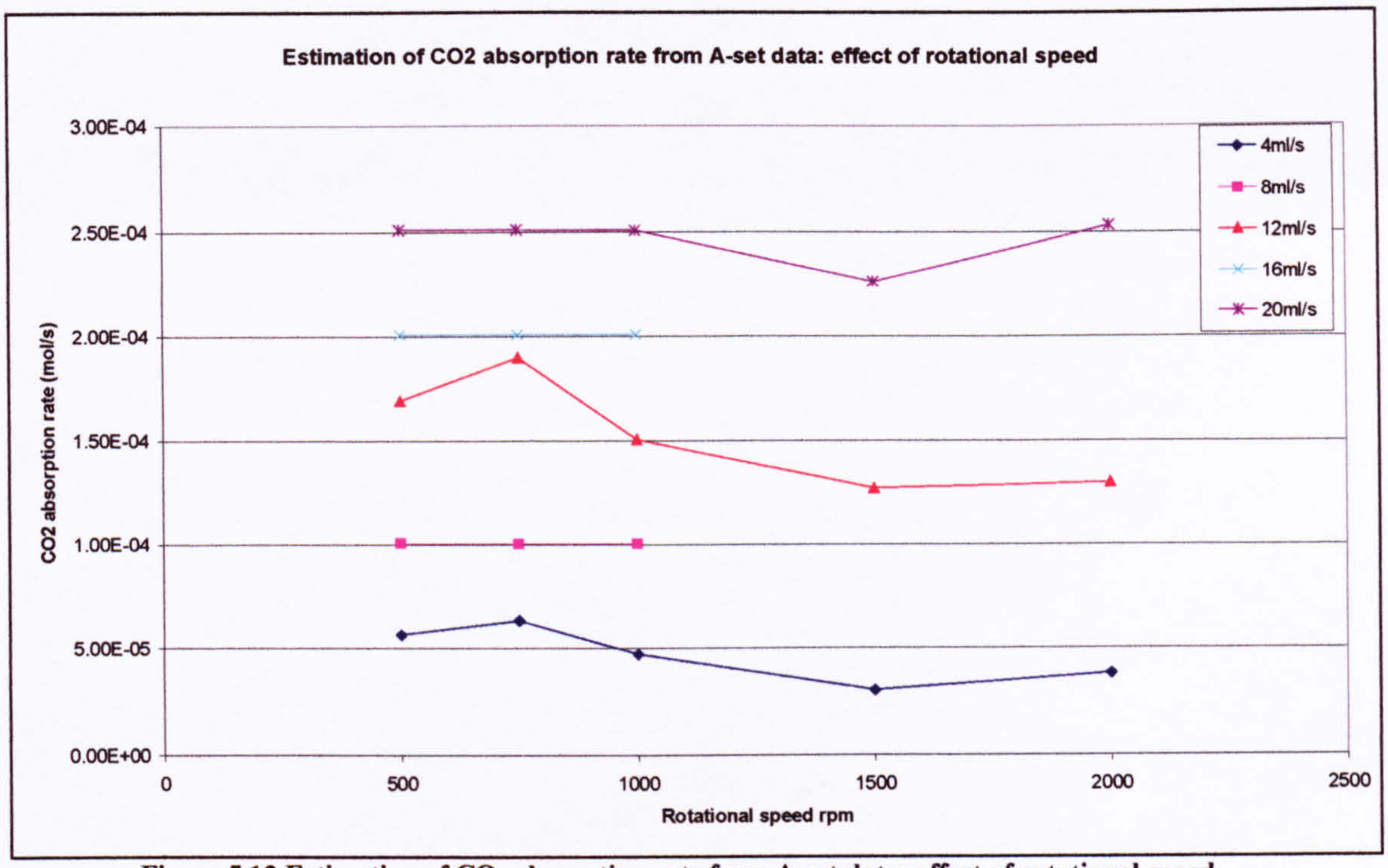


**Figure 5.12 Estimation of $CO_2$ absorption rate from A-set data: effect of rotational speed**

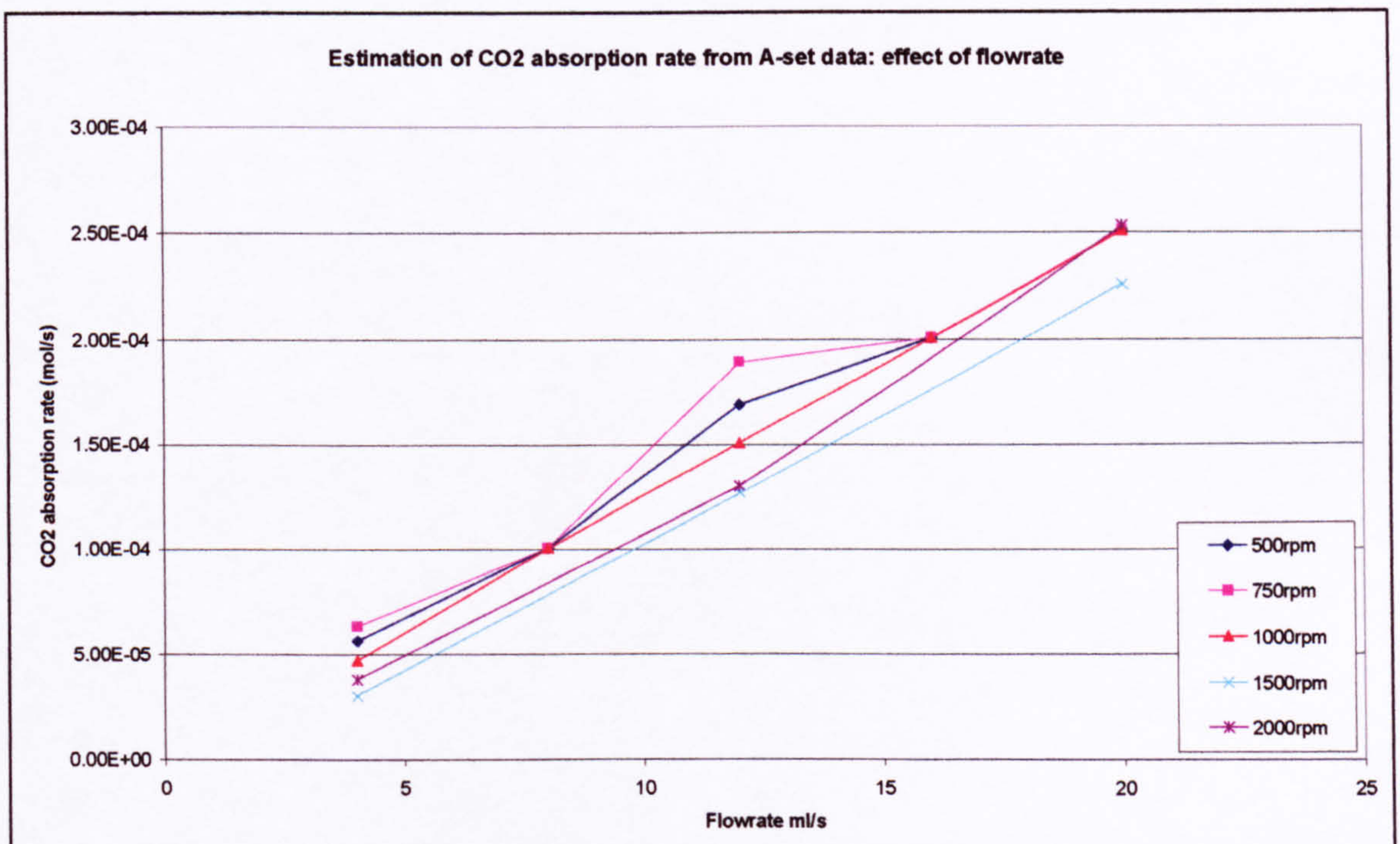


**Figure 5.13 Estimation of $CO_2$ absorption rate from A-set data: effect of flowrate**

From figures 5.12 and 5.13 above it is seen that the overall rate of $CO_2$ absorption is a very weak function of rotational speed whereas in the case of the effect of flowrate on the overall rate of $CO_2$ absorption, there is an almost linear dependence within the experimental range. The liquid to gas flow ratio was fixed so hence, with increasing liquid flowrate, there was a corresponding increase in $CO_2$ flow.

The rotation of the disc acts to distribute the liquid into a film on the surface of the disc and then distributes this flow circumferentially to form a free draining film or rivulets running down the walls of the shell. It is on these interfacial areas that the absorption process occurs. In estimating the surface area of a 15cm diameter disc to be 176cm$^2$, estimating the shell walls to be 16cm in diameter and 10cm in height, this wall would provide a free draining surface area of approximately 502cm$^2$.

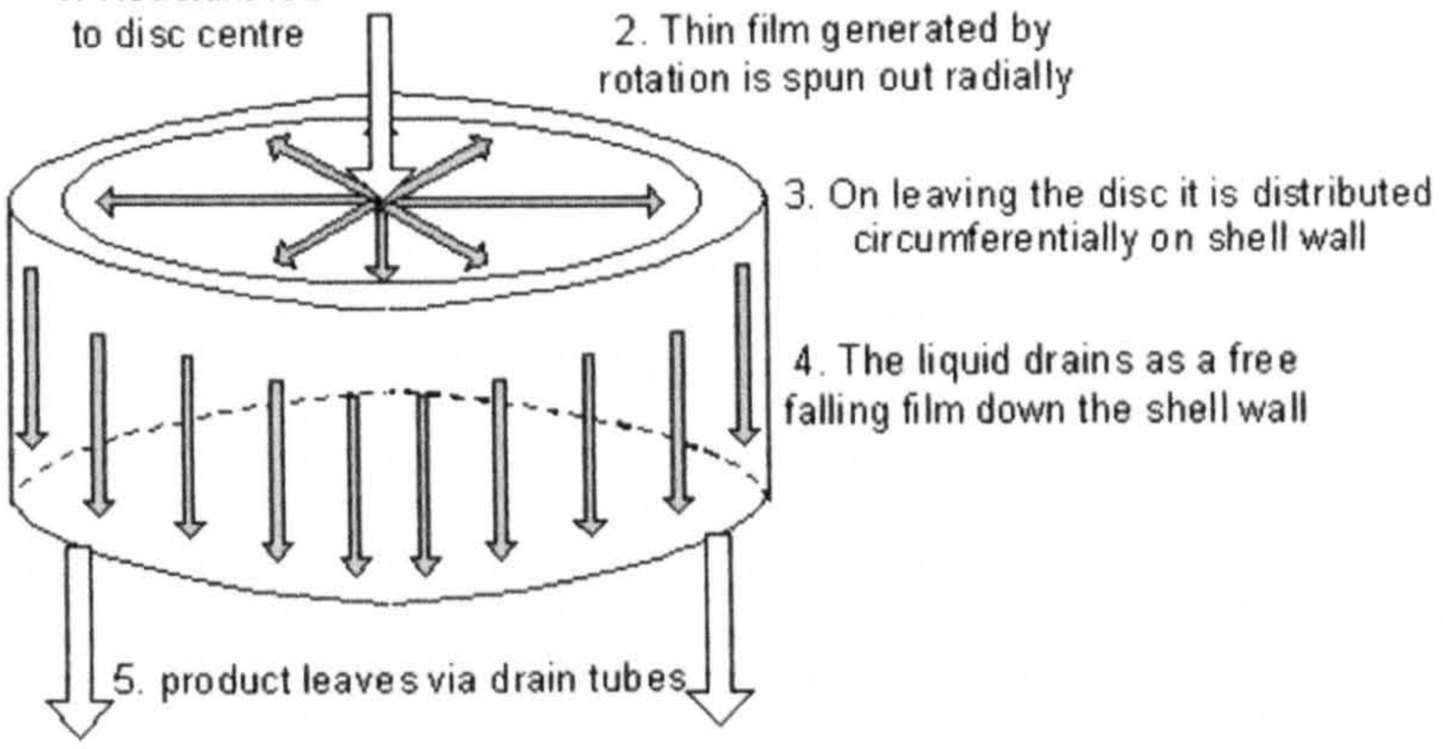


**Figure 5.14 mass transfer areas within SDR rig in present study**

Not taking into account other surfaces (e.g. the drain tubes), this is approximately three times the surface area than that provided by the disc surface alone. It is suggested that the flowrate of liquid in contact with the gas as it flows on each of these surfaces all contribute to the overall rate of absorption of $CO_2$ and therefore this represents a mass transfer rate for the whole configuration of the SDR and not just the disc surface. This is further complicated by the spray droplets which form at the periphery of the disc which will be in contact with the gas for a finite time determined by their radial velocity. In order to evaluate the disc alone, product samples should have been taken from the disc periphery as well as from the product drain. Any difference in the periphery sample and a drain tube sample from the same experiment would illustrate the effect of the disc and the effect of the wall as individual mass transfer surfaces. Mass transfer rates on the disc surface may be significantly higher than in a falling film but the disc surface contributes less than 25% of the total interfacial area where contact between phases occurs. The effect of rotation produces a much thinner film on the disc surface along with greater mixing giving an enhanced rate of mass transfer per unit area than that of the film draining on the shell wall, however, their relative rates cannot be specifically determined upon here without experimental measurement but a crude numerical estimation was carried out.

### 5.5.5 Mass transfer approximation of disc, droplet and wall contributions

A model was produced to predict physical absorption of the 3 mass transfer zones to first estimate their relative contributions. As a crude approximation, only physical absorption without reaction was considered. This model and discussion can be found in Appendix 9.3. The model suggested that a relatively low contribution of surface area and residence time of the droplets led to there being little contribution to the overall mass transferred from gas to liquid. However, the film falling down the shell wall could contribute in the range 2.18 to 9.36% of the total mass transferred.

### 5.5.6 Effect of gas flow ratio on mass transfer on the SDR

Data was obtained from experiments performed at different gas flow conditions to determine the performance. For this study, the top rotational speed of 2000rpm was chosen as it represented the shortest residence time and the thinnest films generated on the disc for a range of flowrates.

Alongside the A-set experimental data for flowrates at 2000rpm, two other experimental sets were performed. The first set used double the $CO_2$ ratio than the A-set, this was named the 'B-set'. The second set ('D-set') was operated at the same total gas flowrate as the A-set however the $CO_2$ had been diluted with nitrogen so that it formed 40% of the total gas flow. The gas flow conditions for a given solution flowrate are shown in table 5.4 below.

| Calcium hydroxide solution flowrate ml/s | A-set | | B-set | | D-set | |
|---|---|---|---|---|---|---|
| | $CO_2$ flowrate ml/min | $N_2$ flowrate ml/min | $CO_2$ flowrate ml/min | $N_2$ flowrate ml/min | $CO_2$ flowrate ml/min | $N_2$ flowrate ml/min |
| **4** | 240 | 0 | 480 | 0 | 100 | 140 |
| **8** | 480 | 0 | 960 | 0 | 200 | 280 |
| **12** | 720 | 0 | 1440 | 0 | 300 | 420 |
| **16** | 960 | 0 | 1920 | 0 | 400 | 560 |
| **20** | 1200 | 0 | 2400 | 0 | 500 | 700 |
| | | | | | | |

**Table 5.4 Gas flow conditions for solution flowrates**

The B-set experiment at 20ml/s could not be performed because the rotometers could not measure higher than 2l/min. Based on the measurement of inlet and outlet pH, the

change in hydroxyl concentration was inferred. The data from the experiments performed were plotted in figure 5.15 .

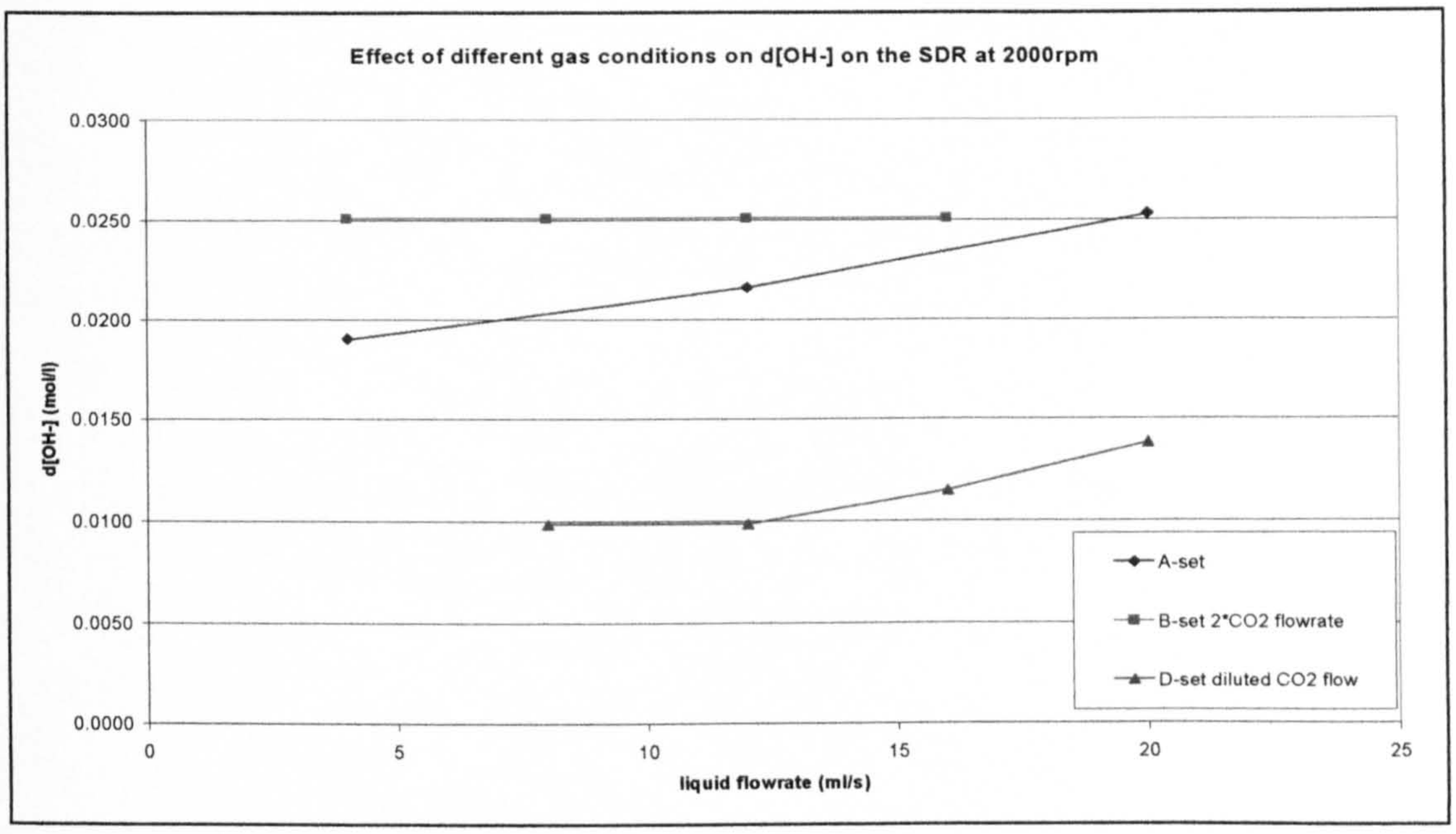


**Figure 5.15 Effect of different gas conditions on d[$OH^-$] on the SDR at 2000rpm**

Doubling the gas flowrate for a given liquid flowrate is seen to increase the rate of mass transfer. The data show that the conversion of hydroxyl ion remained constant for the 4 flowrates investigated. This is because the conversion does not change much below pH 10 and the conversion of reactants below this figure is greater than 99.9% so small variations in pH below pH 10 will not have an effect upon the conversion calculated. In the case of diluting the gas with nitrogen, it is seen that the conversion of hydroxyl ion is lower than the A-set and B-set. Hence it is seen that the relative flowrate of the $CO_2$ affects the absorption rate by the liquid. With this in mind, the use of the Venkataraman model to predict the absorption rate is inappropriate when trying to predict gas-liquid mass transfer in a system where the gas conditions are variable since the model does not factor for gas conditions above the disc (i.e. counter/co-current flow and pressure).

There were a large number of permutations of experiments that could have been performed on the SDR to develop a bigger picture of the mass transfer capabilities, however the present study is more emphasised toward crystallisation and the experiments performed were done so to study the effect they have on the products of

precipitation by this reaction route. However the relative mass transfer rates of the batch and SDR have been established and can therefore be compared. This will be useful in understanding how supersaturation develops and its effect on the CSD.

### 5.5.7 Comparison of batch and SDR mass transfer

The rate of $CO_2$ absorption determined from the 1-litre batch experiments was estimated to be $1.6*10^{-4}$ mol/l.s for a $CO_2$ flowrate of 1000ml/min and at maximum agitation provided on the magnetic stirrer (table 5.1). . As these experiments were performed in a 1-litre batch, then their mass transfer rate would be $1.6 \times 10^{-4}$ mol/s.

The SDR showed that mass transfer rates were strongly dependent on the liquid flowrate. The gas flowrate was increased to be in the same molar proportion as the liquid at each liquid flow. The highest rate of $CO_2$ transfer on the SDR from the A-set experiments was seen to be $2.5 \times 10^{-4}$ mol/s at 20ml/s (figure 5.15). This occurred at liquid flowrates of 20ml/s and for rotational speeds of 500, 1000 and 2000rpm. This is 56% higher than the rate determined for the batch experiments. It is feasible that the mass transfer rate on the SDR could have been higher if the experimental range for the liquid flowrate had been extended.

#### 5.5.7.1 Processing rates

The SDR was shown capable of generating higher rates of mass transfer than the batch. If we consider the length of time it would take to process the batch from its starting pH of 12.5 to about 10 (representing a 99.95% conversion of the [$OH^-$]), batches A1, A2 and A3 took 118, 141 and 121 seconds respectively. At 20ml/s, the SDR is capable of continuous carbonation as a once-through reactor configuration, hence at 20ml/s, it would take 50 seconds to pump 1 litre of solution through the SDR rig. The SDR in this case is approximately 2.2 times faster than the 1-litre batch vessel in the carbonation of calcium hydroxide solution.

### 5.5.8 CSD of $CaCO_3$ produced on the SDR

The crystal size distribution of the product obtained from the SDR for each experiment was analysed using the Mastersizer S. The CSD of each experiment was taken immediately from the product sample obtained. CSD profile data of each experiment were obtained from the analysis along with summary data such as the Sauter mean diameter, D[3,2], and the standard deviation of the crystal size. The summary data was

useful as it allowed plots to be made to see what process parameters had an influence on product quality. The A-set experiments, previously described, were used to determine the effect of rotational speed and flowrate on the product quality.

Individual CSD profiles have been grouped together to show the CSD of the 5 rotational speeds at three different flowrates of 4, 12 and 20 ml/s from the A-set data. Likewise, CSD profiles of 5 experiments carried out at 500rpm, 5 carried out at 1000rpm and 3 at 2000rpm have been plotted as groups. These charts have been plotted in Appendix section 9.1.3. The Sauter mean diameter for all the A-set experiments performed is plotted below to show the effect of rotational speed and flowrate.

### 5.5.8.1 Effect of SDR rotational speed on the CSD

If the Sauter mean diameter for the effect of rotational speed is plotted for all the A-set data, the result is seen in figure 5.16 below.

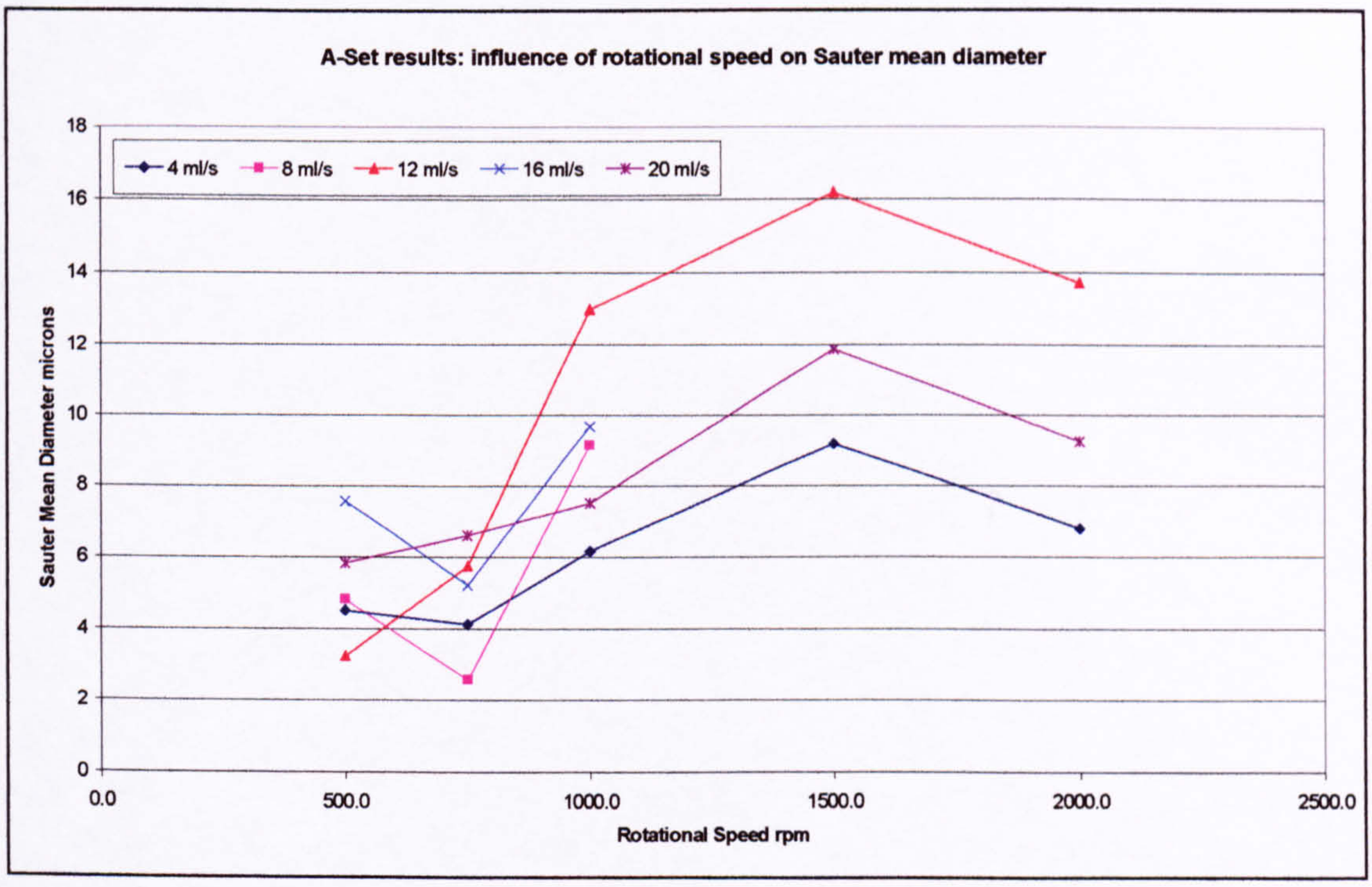


**Figure 5.16 A-Set results: influence of rotational speed on Sauter mean diameter**

These A-set experiments were documented by (Trippa *et al*, 2002). In considering the effect of SDR rotational speed on the D[3,2], it is seen that in each of the cases of the flowrates at 4, 12 and 20ml/s, the D[3,2] increase from a minimum at low rotational speeds to a maximum at 1500rpm the drops at 2000rpm.

These trends are reflected in the figures 9.1, 9.2 and 9.3 where the CSD profiles are plotted for the flowrates of 4, 12 and 20ml/s. In figure 9.1 at 4ml/s, crystals are seen between 1 and 3μm for rotational speeds of 500 and 750rpm. At higher rpm, the crystals are no smaller than 3μm. In general, it is seen that increasing rotational speed shifts the CSD to larger sizes. Similar effects are observed for 12ml/s and 20ml/s (figure 9.2 and 9.3) in that the CSD increases as the rotational speed is increased, being at its largest at 1500rpm with a slight reduction in size as the speed increases to 2000rpm.

The increase in the mean diameter with rotational speed might be attributed to the higher rate of mixing imparted by the disc to the fluid as the speed is increased. At low initial supersaturation as is experienced here, rapid absorption would facilitate higher growth rates after nucleation had occurred. It was seen that the rotational speed had little effect on the absorption rate, however, it is known that the rate of mixing is significantly increased as rotational speed is increased. In equation (3.8 and 3.9),the kinetic energy given to the liquid by the disc was equal to the frictional power dissipated by the fluid given by;

$$P_f = \frac{1}{2} Q \rho \varpi^2 \left( r_o^2 - r_i^2 \right) \qquad \text{(eq 3.8 and 3.9)}$$
$$or \approx \frac{1}{2} Q \rho \varpi^2 r_o^2$$

Hence the energy given to the fluid is proportional to the square of the rotational speed but only a proportional relationship with the flowrate.

In the case where crystals are in relative motion with the surrounding solution i.e. under agitation or sedimentation, the diffusion field will be disturbed by the supply of solution with higher concentration, resulting in a higher growth rate. The critical crystal size at which such convective processes begin to influence diffusion to crystals growing under sedimentation or gentle stirring conditions were estimated by (Nielsen, 1980):

$$r_{crit} = \left( \frac{9.D.\mu}{2.a.|\Delta\rho|} \right)^{\frac{1}{3}} \qquad (3.46)$$

If the is crystal greater than the critical crystal size, the influence of convection for diffusion controlled growth becomes significant. This can normally be ignored for

crystals smaller than 5 to 10μm, however, in the present study where the solution and crystals are under high accelerations due to the rotation of the disc (say for simplicity that the $a$ term is substituted with $r\omega^2$), the critical size may become much smaller; the high rates of energy transfer and accelerating particles in the rotating field leading to a reduction in the diffusion layer thickness. Hence it is feasible that the spinning disc may contribute to higher crystal growth rates than that experienced in conventional precipitation equipment.

The effect of the D[3,2] reducing as the speed increases from 1500 to 2000 might be attributed by the reduction in residence time. It is also feasible that agglomeration is more pronounced at higher rotational speeds - perhaps linked to the lower conversion and higher pH. If the final pH of the product is considered, a similar trend is seen in

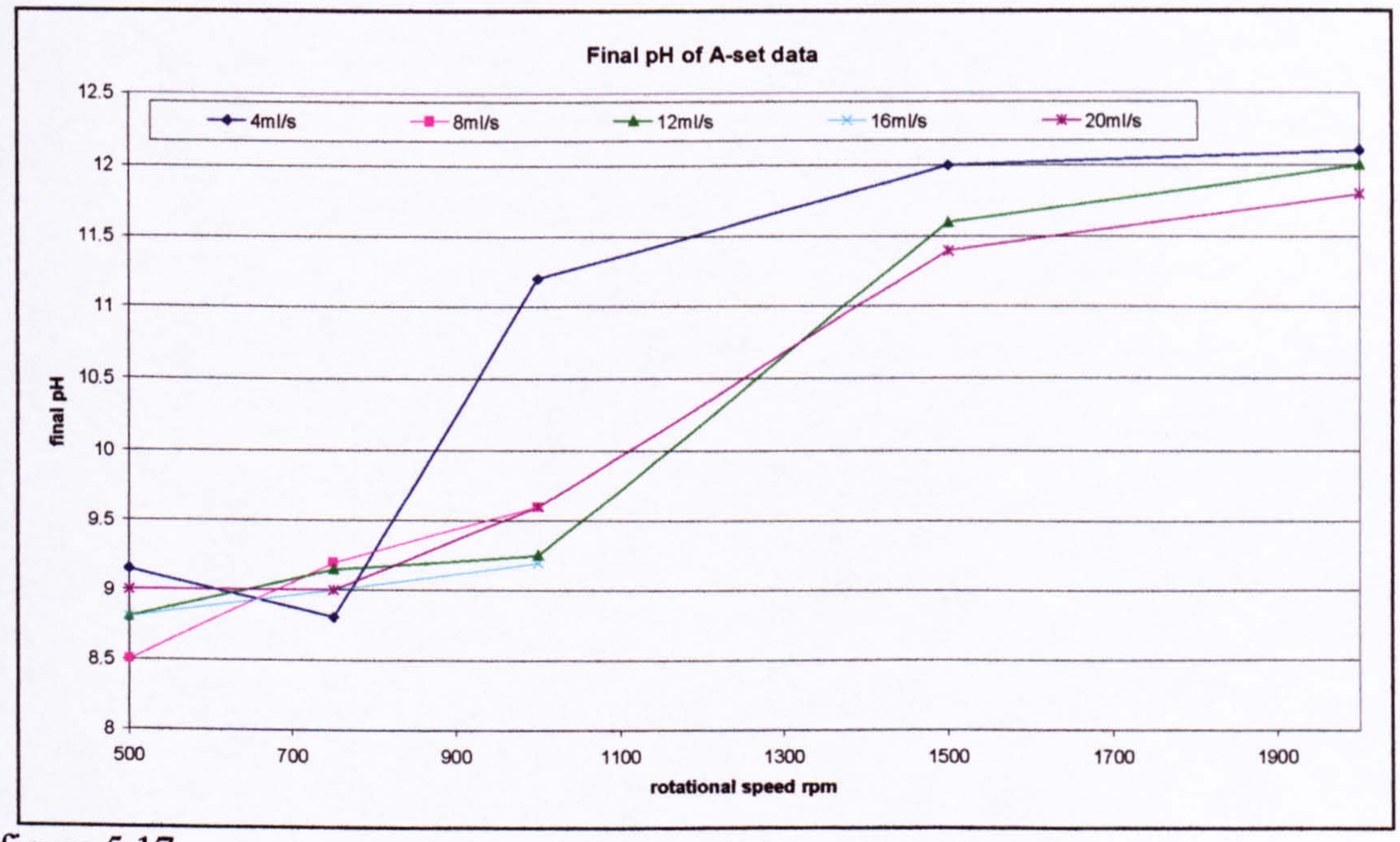


figure 5.17.

**Figure 5.17 Final pH of A-set data**

Agglomeration can be a function of the solution pH as the ionic charge in the solution affects the surface charge on the crystals. Agglomeration may be more prevalent at higher pH. If this is the case, then the primary particles produced from the initial precipitation and having a higher final pH became agglomerated immediately before sampling and formed larger particles represented in the CSD.

Contradictory to this theory, (Wachi and Jones, 1991 and 1992) observed agglomerated at pH levels around 8.0 and suggest there is little agglomeration at

higher pH due to there being high calcium ion concentrations and the particles being negatively charged – hence electrostatic repulsion prevents agglomerate formation. At lower pH the surface charge is neutralised and hence agglomeration occurs.

However, there is possible evidence for bigger primary particles resulting and not agglomeration. At higher final pH, the potential supersaturation developed within the solution would have been lower hence it was more likely that nucleation rates would be lower and crystal growth would be the more dominant process. (Jones *et al*, 1992) noted that there was an increase in the mean particle size as the rate of agitation increased. In figure 5.16, larger particle sizes are seen at the higher rotational speed i.e. from higher rates of mixing. This would further influence the system into producing larger crystals with the lower supersaturation from the high final pH

### 5.5.8.2 Effect of SDR liquid flowrate on the CSD

The effect of flowrate on the D[3,2] is shown below in figure 5.18

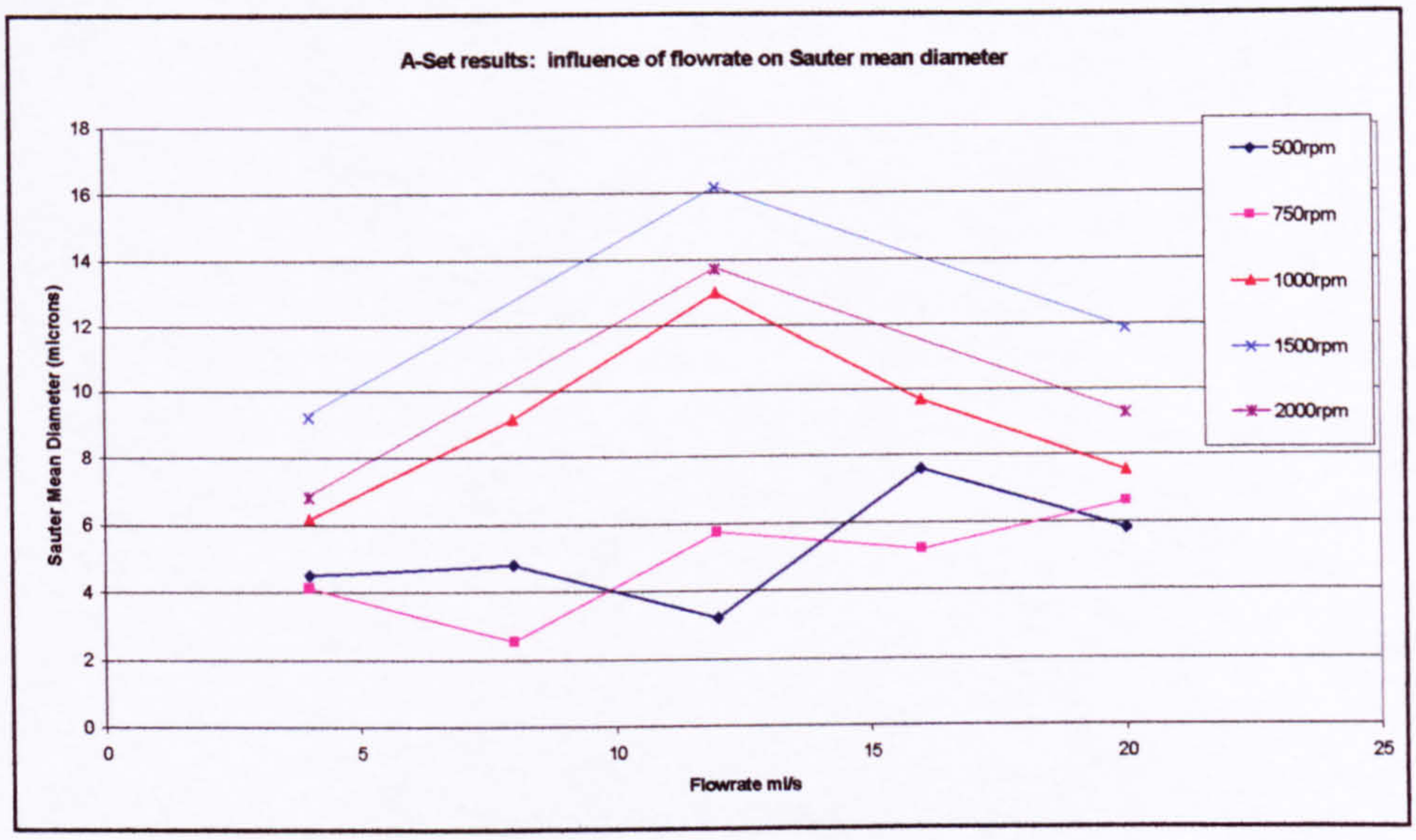


**Figure 5.18 Influence of flowrate on Sauter mean diameter**

The flowrate of 12ml/s yielded the highest mean diameters in the range 1000 to 2000rpm. In noting the possible relationship between the mean size and the final pH as seen with rotational speed, the same final pH data is plotted with respect to flowrate in figure 5.19 below.

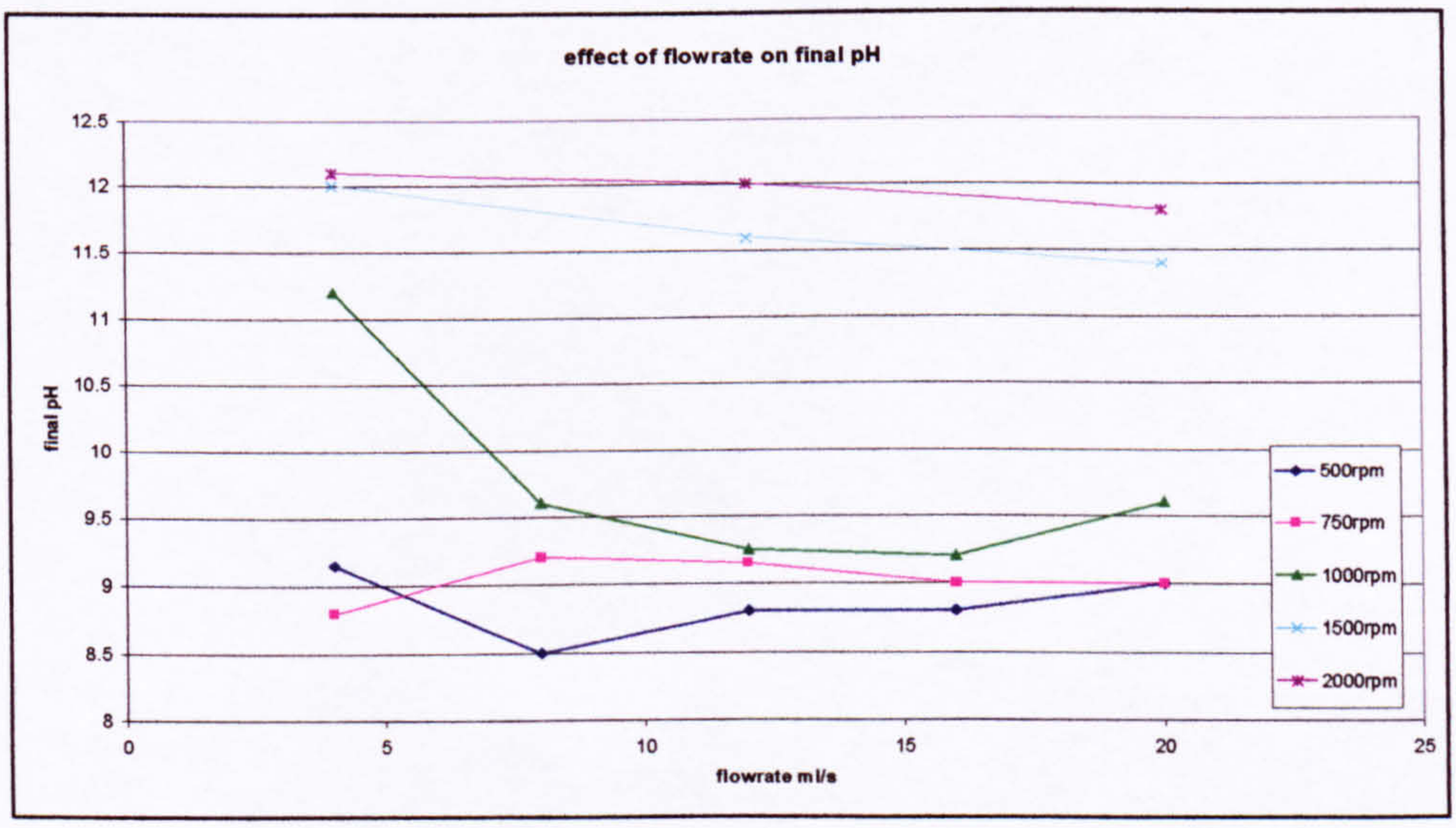


**Figure 5.19 Effect of flowrate on final pH**

As flowrate is increased, there is little effect on changing the pH at 1500 and 200rpm. At the higher rotational speeds, the final pH is higher and hence having the effect on

increasing the mean size. The lower mean diameters being prevalent at lower final pH, reflected in the data from the lower rotational speed.

### 5.5.8.3 Summary of disc conditions on the effect on the CSD

Rotational speed had a major influence on the CSD. The higher product pH generally seen at high rotational speeds lead to a larger size. It appears to be a major factor in determining D[3,2] prior to analysis. A higher product pH leads to agglomeration of smaller primary particles. Evidence to support the hypothesis was gleaned from visual inspection; the product appeared to flocculate in the product collection beaker. As agglomerates were hypothesised and appeared to be loosely bound, likely to be separated by gentle agitation, seen by shaking the beaker, the product was tested in the analyser over a period of minutes to see if these agglomerates would breakdown. It was originally thought the flocked material would immediately have broken up in the dispersion unit in the time it took to add the sample to achieve the correct obscuration and starting the analysis - this was not the case.

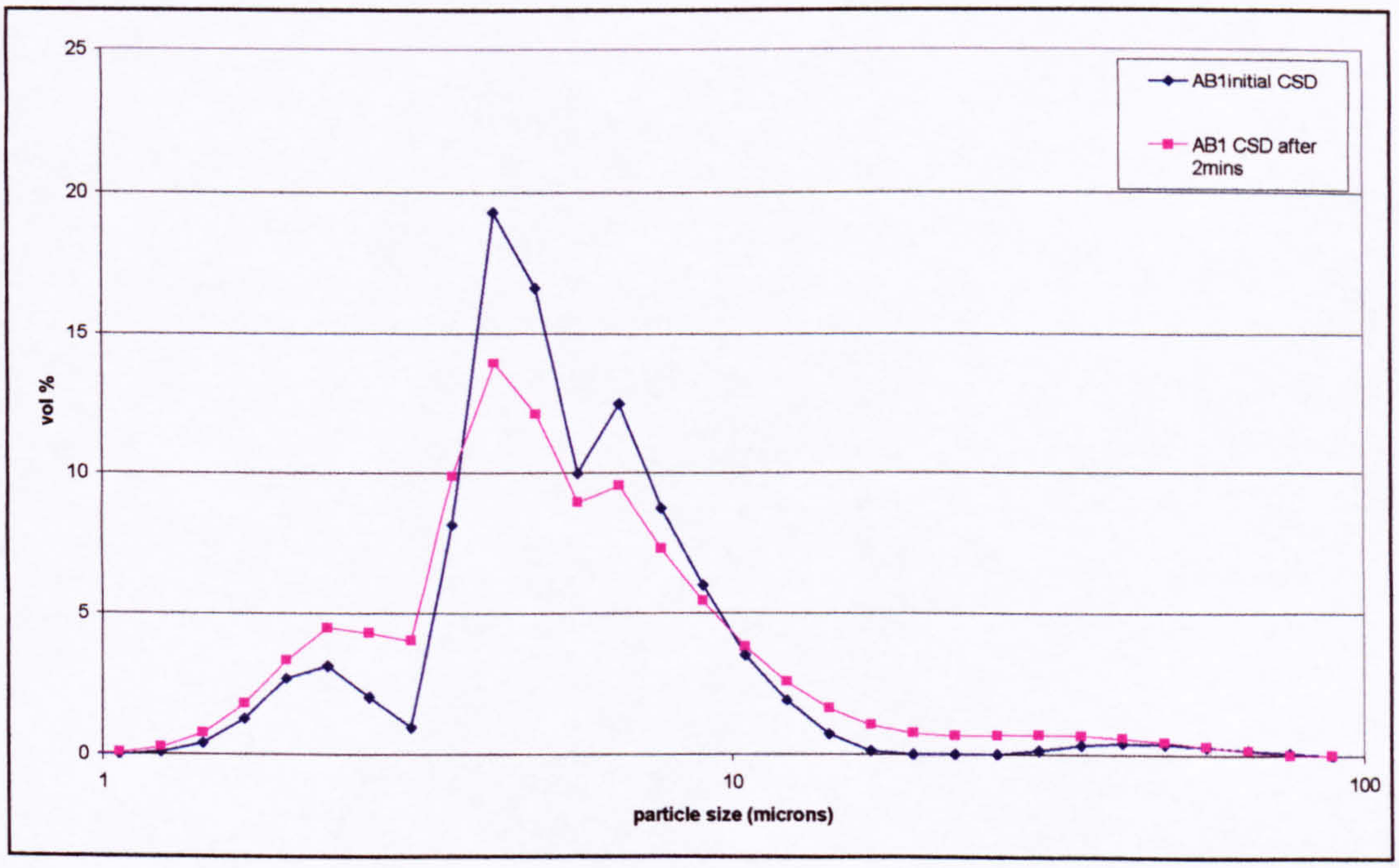


**Figure 5.20 Change in CSD after a period of 2mins**

As an example, the experiment at 750rpm and 8ml/s (experiment AB1) had the sample in the analyser ran again after 2 minutes, seen in figure 5.20 . This showed a decrease in the size seen in the first CSD. Although agglomerates were deemed less of an issue in this particular experiment, it shows that the product does agglomerate after exiting

from the disc and that after a period of time in the Mastersizer dispersion unit leads to a breakdown in agglomerates.

This change has been seen in other experiment CSDs that have been repeated after a period of time. The second CSD shows a decrease in the size after time suggesting some breakdown in agglomerates in the interval between analyses.

### 5.5.9 Morphology of calcium carbonate produced on the SDR

From some of the experiments carried out, SEM micrographs were taken of sets of experiments to determine the effects of rotational speed and flowrate on the morphology of the $CaCO_3$ product.

#### 5.5.9.1 The effect of disc rotational speed on $CaCO_3$ morphology

For each of these experiments, the liquid and gas flowrate were held constant. The liquid flowrate was 8ml/s with a corresponding $CO_2$ flowrate of 480ml/min. For each of these experiments, the initial pH of saturated $Ca(OH)_2$ solution was measured at 12.45. The experimental parameters and morphologies obtained are summarised in figure 5.21 below.

| $Ca(OH)_2$ flow ml/s | $CO_2$ flow ml/min | Disc rotational speed rpm | Initial $Ca(OH)_2$ pH | Final $Ca(OH)_2$ pH | Crystal morphologies |
|---|---|---|---|---|---|
| 8 | 480 | 500 | 12.45 | 8.7 | Rhombic/spherical |
| 8 | 480 | 750 | 12.45 | 8.2 | Rhombic/spherical |
| 8 | 480 | 1000 | 12.45 | 8.4 | Rhombic/spherical |
| 8 | 480 | 1500 | 12.45 | 9.0 | Rhombic/spherical |
| 8 | 480 | 2000 | 12.45 | 9.6 | Rhombic/spherical |

**Figure 5.21 Crystal morphologies with changing rotational speed**

From these experiments, the outlet pH of the transformed $Ca(OH)_2$ solution was seen to be higher at high rotational speeds than lower rotational speed. This would indicate that there is lower conversion to $CaCO_3$ as rotational speed is increased. However the mass transfer rate is not necessarily lower due to the residence time decreasing with increasing rotational speed. For each of the experiments studied under the SEM, it was seen that the morphologies were the same in each case. This suggests that the liquid and gas flowrate parameters had the most influence over the morphology rather than the changing rotational speed.

SEM micrographs of each of the experiments examined here are shown in figure 5.22 below.

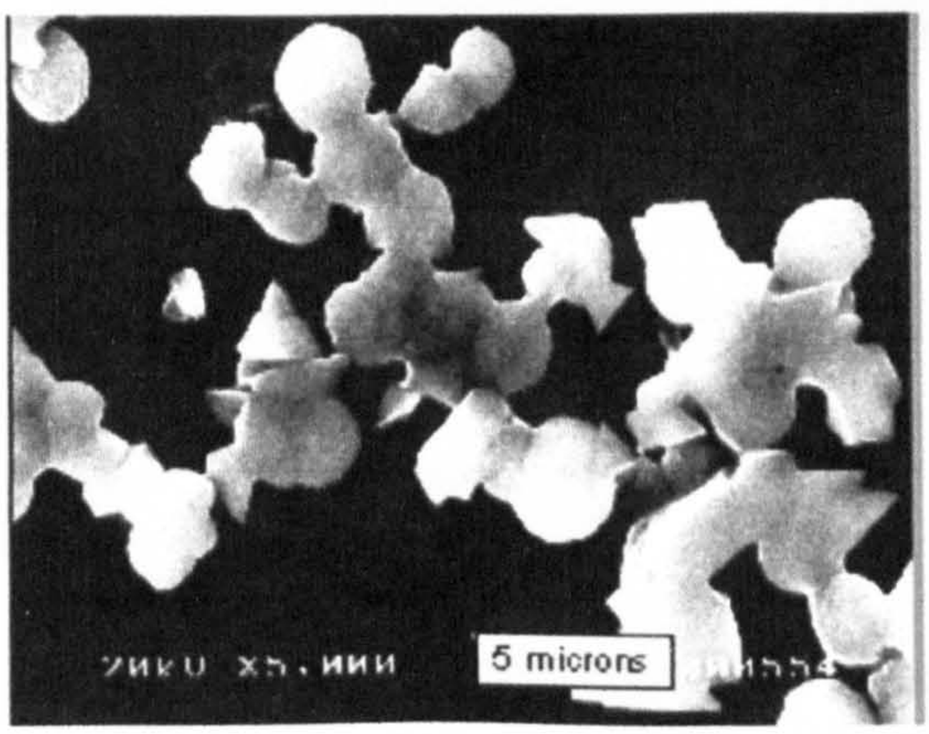


500rpm

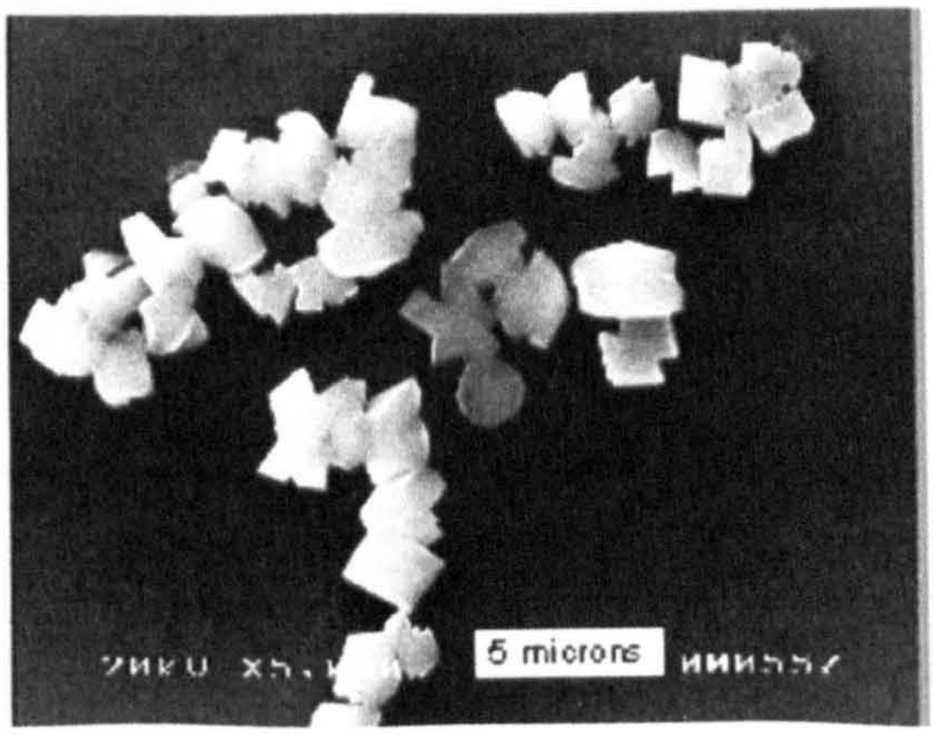


750rpm

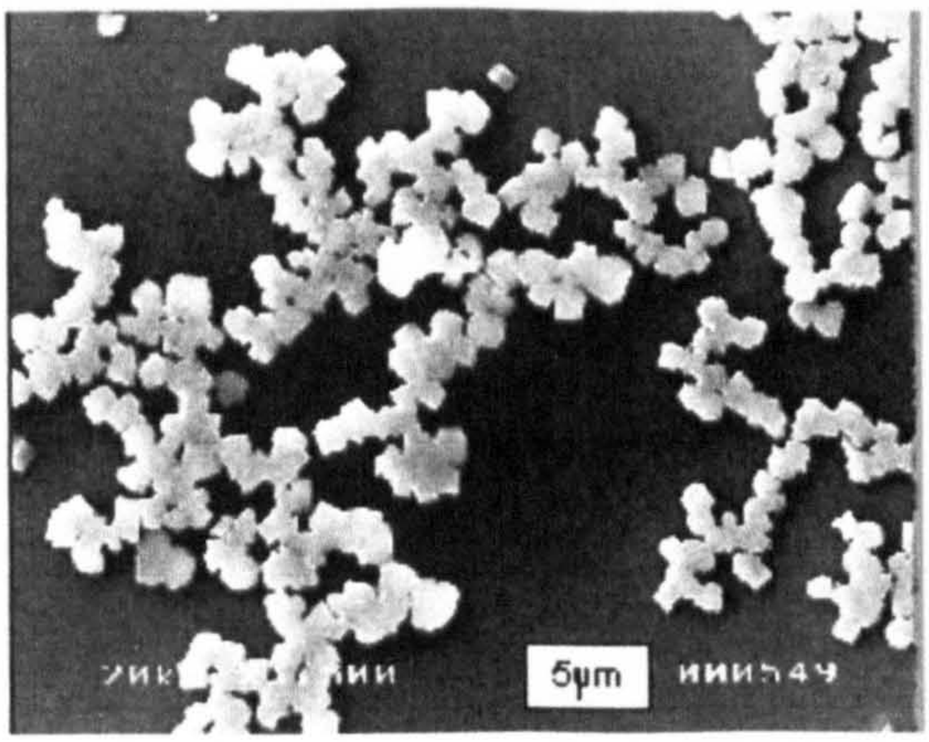


1000rpm

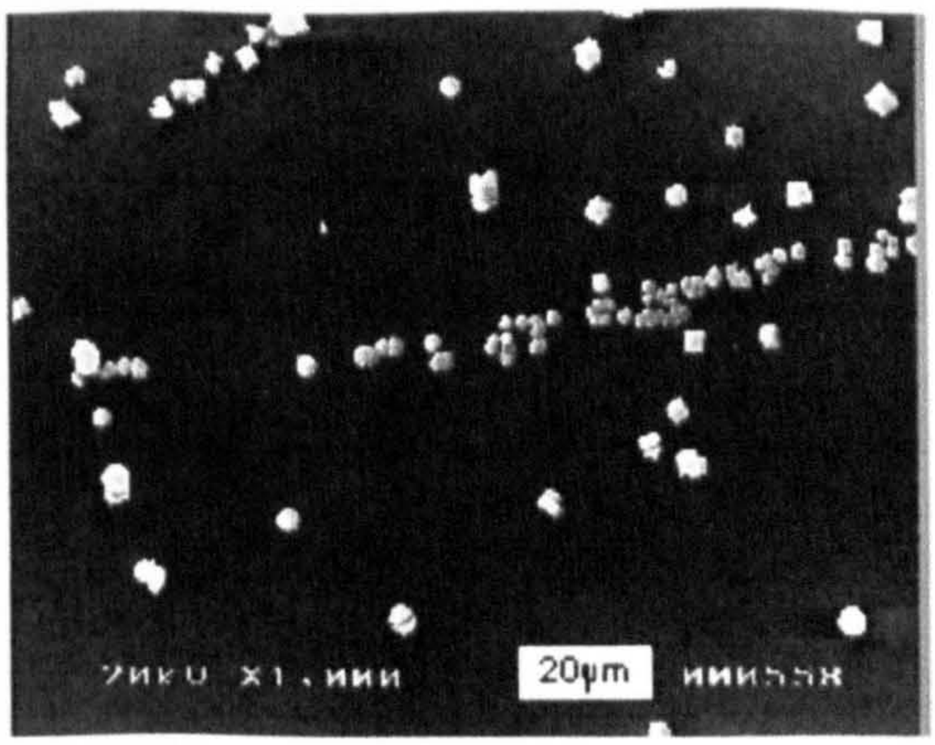


1500rpm

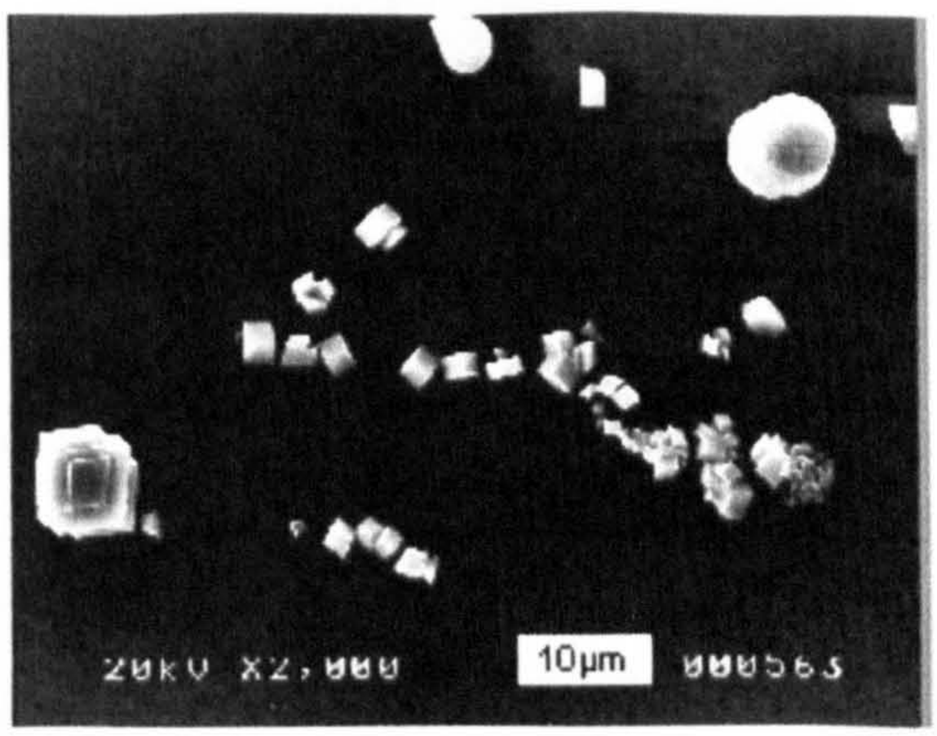


2000rpm

**Figure 5.22 Effect of rotational speed on morphology**

From each of the micrographs in figure 5.22, the size and morphology in each of the slides look very similar, suggesting the precipitation of both calcite (cubic/rhombic) and vaterite (spheres). Individual crystals appear to be in two sizes, suggestive of the

bimodal distribution of the CSD, there are crystals in the size range of 2-3μm and 10μm, both shapes appear in both size classes. There will be however, some variation in the relative quantities of each shape of crystal and therefore relative quantities of each polymorph. It would be impossible to determine the quantities from the SEM alone since each slide is not wholly representative of the sample quantitatively. X-ray diffraction analysis might have confirmed the relative amounts of each polymorph.

### 5.5.9.2 The effect of liquid flowrate on $CaCO_3$ morphology

Each of the experiments studied for the effect of flowrate on the SDR operated at a disc speed of 1000rpm. The liquid flowrate was altered with the $CO_2$ flowrate adjusted to maintain the same ratio with the liquid flowrate. For these experiments, the initial pH of saturated $Ca(OH)_2$ solution was 12.5. The five experiments chosen for SEM analysis are summarised in the table below.

| $Ca(OH)_2$ flow ml/s | $CO_2$ flow ml/min | Disc rotational speed rpm | Initial $Ca(OH)_2$ pH | Final $Ca(OH)_2$ pH | Crystal morphologies |
|---|---|---|---|---|---|
| 4 | 240 | 1000 | 12.5 | 11.9 | Rhombic |
| 8 | 480 | 1000 | 12.5 | 8.8 | Rhombic/spherical |
| 12 | 720 | 1000 | 12.5 | 8.3 | Rhombic/spherical |
| 16 | 960 | 1000 | 12.5 | 8.7 | Rhombic/spherical |
| 20 | 1200 | 1000 | 12.5 | 7.8 | Rhombic/spherical |

**Figure 5.23 Crystal morphologies with changing liquid flowrate**

It was observed that at the lowest flowrate of 4ml/s that only rhombic crystal forms were present. This also corresponds to the lowest pH conversion within the reactor. It is feasible for the gas flowrate for this experiment to be low enough that the $CO_2$ atmosphere is not fully developed above the disc surface and air ingress might create dilution effects not directly measurable within the reaction chamber during the experiments. The combination of low liquid and low gas flowrate/concentration would lead to the supersaturation developing relatively slowly and hence only the rhombic calcite form being present. For each of the other experiments, which have lower final pH, both spherical and rhombic forms are present.

The micrographs depicting the crystal forms at different flowrates are shown in figure 5.24 below.

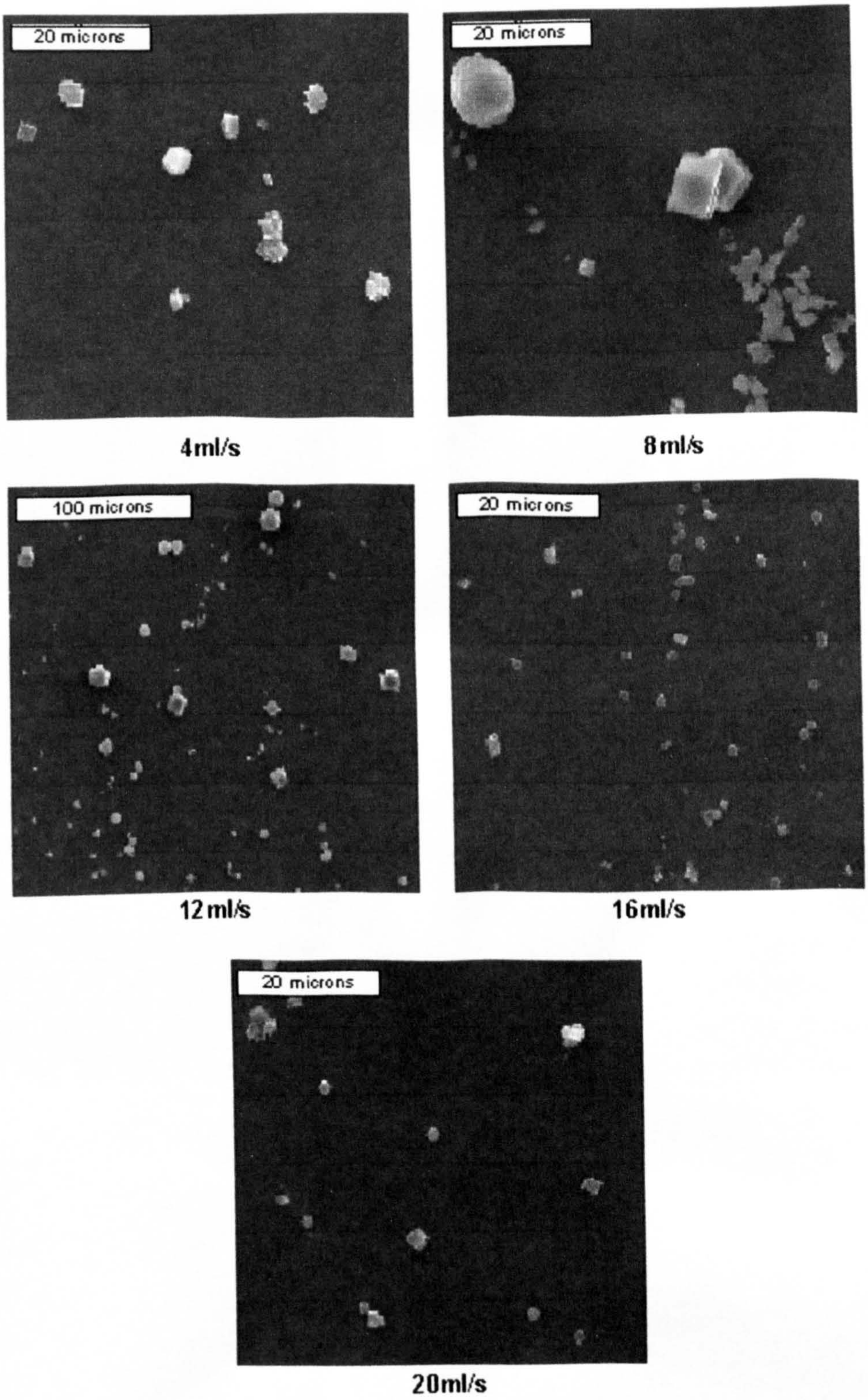


**Figure 5.24 Effect of flowrate on morphology**

### 5.5.10 Comparison of SDR and batch product quality

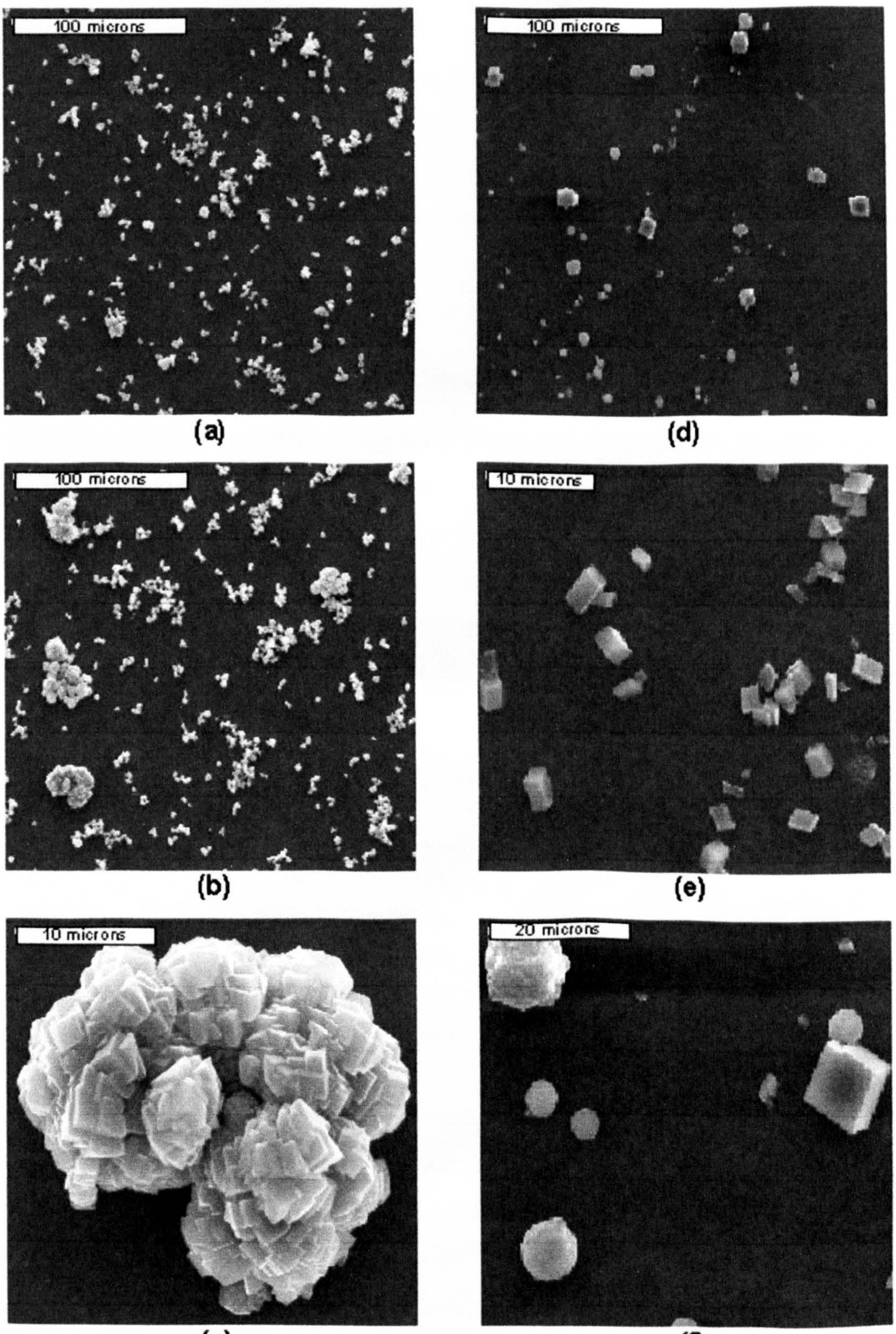


**Figure 5.25 SEM micrographs of batch and SDR calcium carbonate product**

In figure 5.25 above, the product from the batch and the SDR from the carbonation of calcium hydroxide solution can be seen. The product from the SDR was taken from an experiment operated at 12ml/s and 1000rpm. The batch product was imaged from a magnetically stirred 1-litre batch carbonated with $CO_2$ at 1 litre/min. As seen in the SDR morphology, the product consisted of both spheres and rhombohedral shaped crystals. The batch consisted exclusively of rhombohedral shaped crystals. It is seen that some of them can grow into complex shapes of sizes in excess of 30μm. The SDR produced crystals that were either spheres or rhombs which appear to be much more defined and in general, smaller than the batch. This is due to faster absorption/reaction, leading to higher nucleation rates and therefore smaller crystals.

### 5.5.10.1 CSD comparison of batch and SDR

It has been seen in the SEMs of the batch and the SDR that the product size is smaller on the SDR, however this can be further examined by the CSD data. As discussed earlier, it was suggested that the final product pH had an effect on the CSD at high product pH there was a greater tendency for agglomeration to take place. With this in mind, a batch reaction (Batch A3) was matched with SDR runs from the A-set of experiments with similar final pH. The SDR runs chosen were for flowrates of 4, 8, 12 ,16 and 20ml/s at 500rpm.

The final pH of the experiments is summarised in the table below:

| Experiment | Final product pH |
|---|---|
| **SDR: 500rpm 4ml/s** | 9.15 |
| **SDR: 500rpm 8ml/s** | 8.5 |
| **SDR: 500rpm 12ml/s** | 8.8 |
| **SDR: 500rpm 16ml/s** | 8.8 |
| **SDR: 500rpm 20ml/s** | 9.0 |
| **Batch A3** | 9.2 |

**Figure 5.26 Final product pH of batch and SDR experiments compared CSD**

The summary chart plotted shows the additional CSD parameters of D[v,0.1] – particle size on the $10^{th}$ percentile by volume, D[v,0.5] - particle size on the $50^{th}$ percentile by volume, D[v,0.9] - particle size on the $90^{th}$ percentile by volume. The results can be seen in figure 5.27 below.

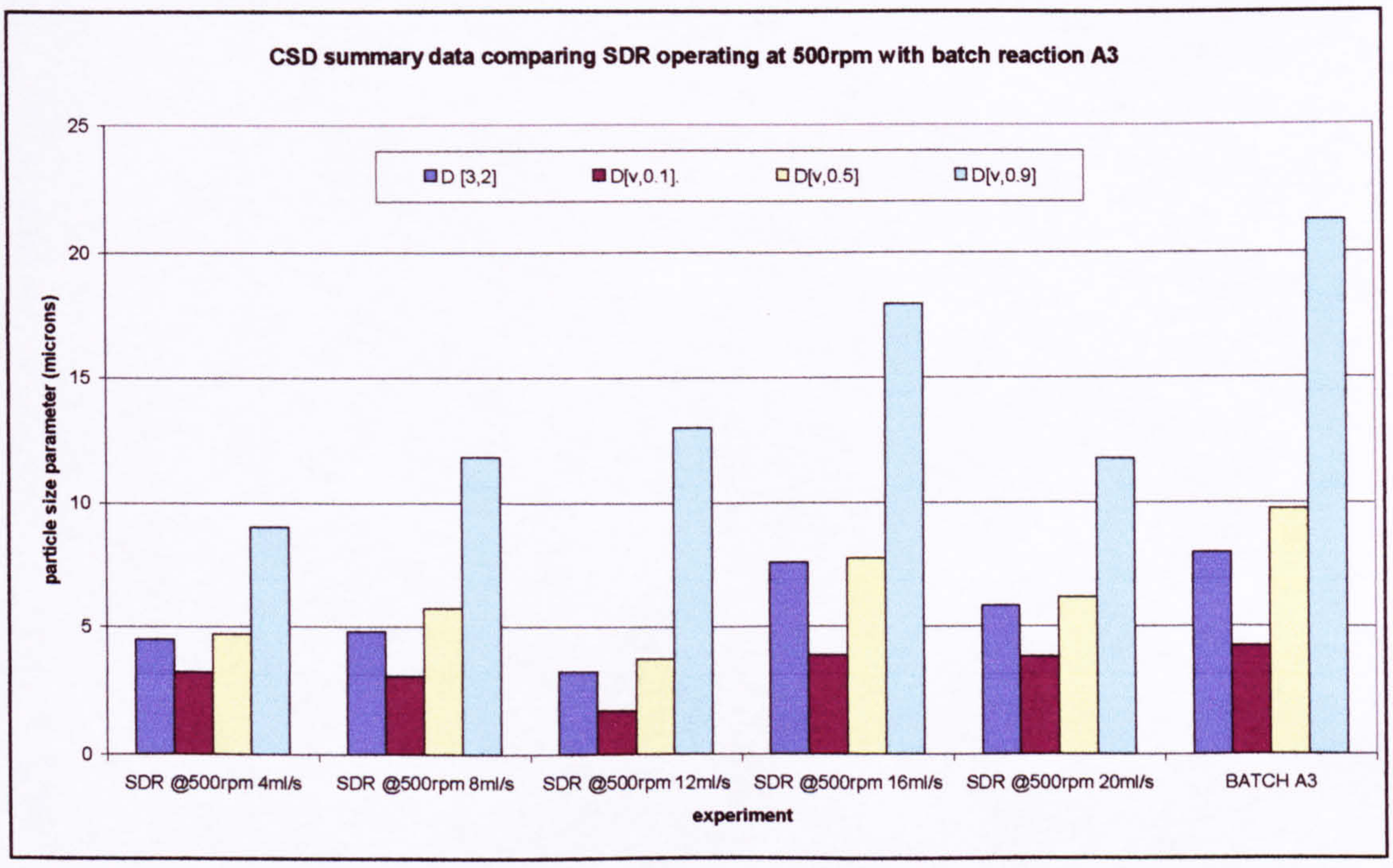


**Figure 5.27 CSD summary data comparing SDR operating at 500rpm with batch reaction A3**

It can be seen from the CSD summary data that the batch reactor yielded a larger particle size than each of the SDR experiments plotted. The SDR having higher mass transfer ability displays this evidence in these CSDs above. Under these process conditions, the higher rate of $CO_2$ absorption and fast mixing yields small crystals than the 2-litre batch vessel. Supersaturation is developed more quickly in the thin film leading to higher nucleation rates which in turn contribute to smaller crystals.

## *5.6 Discussion*

### 5.6.1 Experimental technique

The short time that was made available with the Mastersizer during this study meant that some aspects of the experimentation were rushed and experiments were unable to be repeated. There are such a large number of permutations of experiments that could have been investigated for the present study. In rushing through experiments when the Mastersizer was around, less diligence was taken in backing up experimental techniques with other methods. This was compounded by the slow process of filtering the calcium hydroxide solution to remove suspended particles prior to experimentation. Titration of the product is one example; this would have allowed a secondary method to verify the ion concentration in the liquid. Some gas samples could have been taken for chromatography to verify gas composition in the disc enclosure. Gravimetric analysis of product might have confirmed some yield data but

with such dilute solutions being used (1g of $Ca(OH)_2$ per litre), weighing accurately the dry crystal mass to compare with the slurry mass it came from would have been difficult to do without encountering large errors.

With the data available from the change in PH and the Mastersizer and SEM micrographs, it was possible however to make estimates on the magnitude of the mass transfer processes involved and to determine the crystal product quality.

### 5.6.2 Mass transfer

#### 5.6.2.1 The batch-wise absorption of carbon dioxide in calcium hydroxide solution

The small batch work carried out initially showed that by increasing the stirring rate, the carbonation rate increased. Likewise, by increasing the $CO_2$ flowrate to the vessel, the carbonation rate increased. However, too high $CO_2$ flowrate in the batch can lead to mass transfer performance dropping off.

The rate of change of absorption is approximately constant between the initial pH of the saturated solution (approximately pH 12.4) and about pH 10 whereby 99.4% of the hydroxyl ion concentration is depleted. Below this pH level, chemical enhanced absorption ceases and physical absorption will begin to be the predominant mechanism of mass transfer.

In 1-litre stirred batch experiments, the carbonation of saturated limewater had an average mass transfer rate of $0.162 \times 10^{-3}$ mol/s (between pH 12.4 and 10.0).

#### 5.6.2.2 The absorption of carbon dioxide in calcium hydroxide solution using an SDR

For the set of conditions chosen for the SDR experiments, it was seen that increasing rotational speed had little effect on the overall $CO_2$ absorption rate whereas by increasing flowrates to the disc (liquid and gas being fed at the same ratio), absorption rates were correspondingly increased.

There was concern that in the SDR that there is a degree of absorption as the liquid drained down the shell walls after leaving the disc edge. This could drain as either a continuous film or as rivulets. As there was no sampling of the product leaving the disc edge, there is no way of telling what this contribution might be. There must have

been a reasonable degree of absorption and corresponding crystallisation on the disc because a thin layer of crystals formed on the disc surface was observed.

It was seen that SDR had overall a 56% higher absorption rate than the 1-litre batch when supplying the reactants with the same flow of $CO_2$. This meant that the processing time was 2.2 times faster using the SDR over the batch. This could lead to a significant process time saving potential should this technology be developed.

It was shown that by increasing the gas:liquid flow ratio, the rate of absorption could be increased. A diluted $CO_2$ stream was used in some of the experiments and was shown to be able to absorb into the film at lower rates than pure gas stream. Extrapolating this work might allow flue gas streams (with $CO_2$ concentrations in the region of 10-15%) to be absorbed into thin rotating films. Development of this technology might lead to carbon sequestration processes whereby a useful product is made during the process

Overall, this particular 15cm diameter rig could have had greater capacity for processing calcium hydroxide. By developing a counter-current flow system whereby gas enters at the edge of the disc and transits inward over the film surface, better mass transfer performance might be achieved (especially for diluted $CO_2$ streams). Likewise, finding the optimum contacting conditions (rotational speed, liquid-gas flowrate and ratio) for a given disc diameter have yet to be determined.

### 5.6.3 Size distribution

It was seen that high rotational speeds, the rate of absorption was increased. Further, overall mass transfer would be improved by the increased energy input into the fluid. However these advantages were offset by there being a much lower residence time on the disc at higher rotational speed (at a given flowrate). It appeared that at lower rotational speeds (500 and 750rpm) the mean particle diameter was generally smaller (2.5 –7.7μm) and with a lower final pH (8.5 – 9.6) than at higher rpm (1500 and 2000rpm) which had larger mean diameters (6.8 –16.1μm) with higher final pH (11.4 – 12.1). This is illustrated in figure 5.28 below.

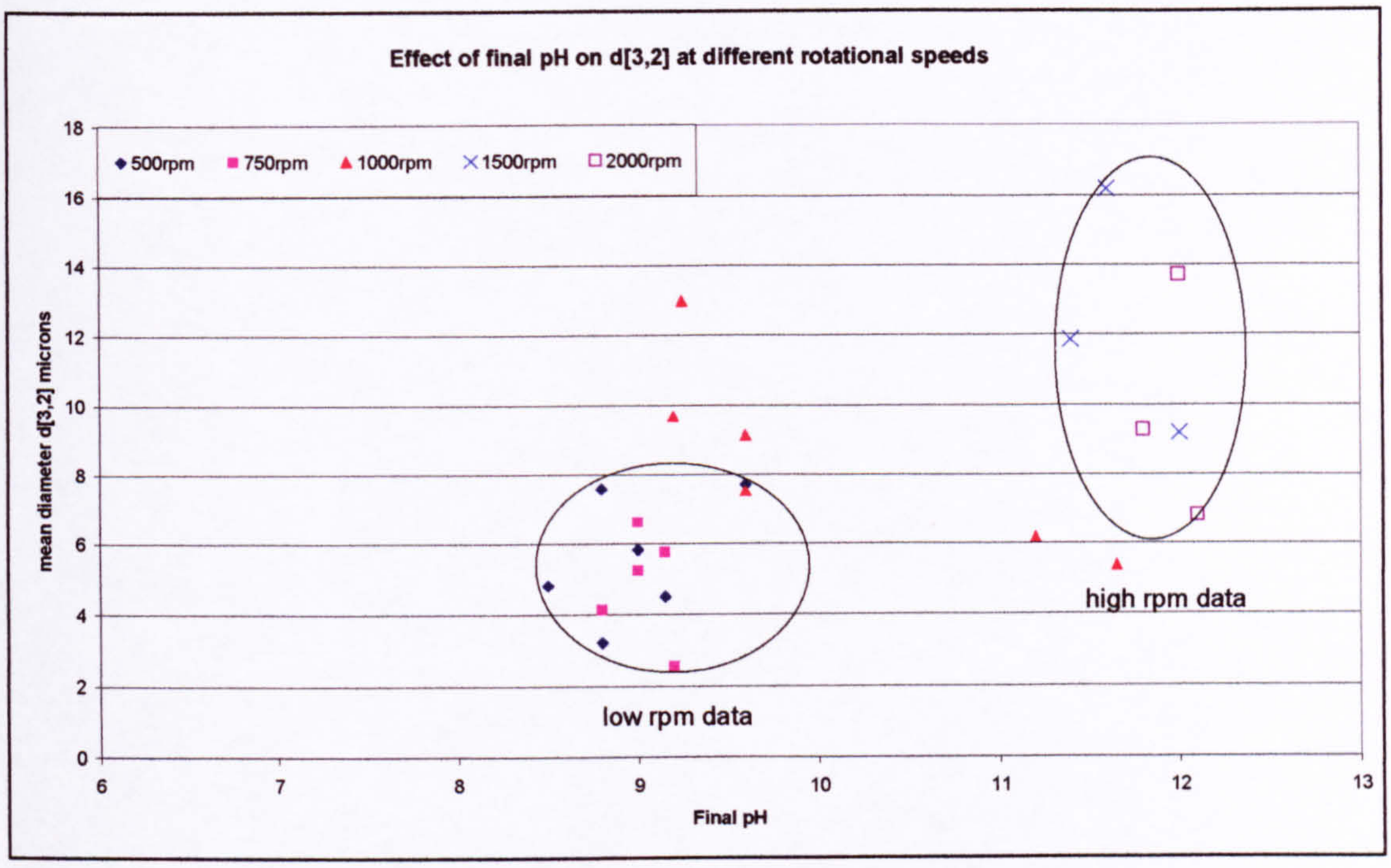


**Figure 5.28 Effect of final pH on d[3,2] at different rotational speeds**

In determining the reason for producing larger crystals at higher rotational speed is not certain as to whether or not agglomeration plays a part at higher pH although flocculation of product was noticed of higher pH products. Applying classic crystallisation kinetic theory, lower supersaturation resulting from higher final pH would lead to lower nucleation rates and higher growth rates and hence larger particle sizes would result. A further contributing factor to larger crystals on the SDR at lower supersaturation would be the effect of high rotational sped on mixing. Rapid mixing of the film means that the diffusion field around a crystal will continually be disturbed by the flow of fresh ions to it, resulting in a faster growing crystal than under lower mixing intensity.

It was seen that by reanalysing a CSD sample 2 minutes after the first one that the CSD shifted towards slightly smaller crystals. This suggests that some dissociation of agglomerates can occur in that time whilst being in the dispersion unit of the Mastersizer. Later discussions with Malvern Instruments (the makers of the Mastersizer) revealed that the crystal product could be dispersed better by the use of anionic surfactants and several analyses carried out until the CSD stabilises to give the final product distribution. There would be concern that if there was vaterite present in the sample, it could be subject to Ostwald ripening during its time in the analyser.

In comparing the batch and SDR products it was seen that the SDR can produce smaller sized crystals than the batch. This due to the once-through plug flow nature of the SDR flow regime with faster mass transfer contributing to faster and higher supersaturation developing. Nucleation rates in the SDR would be higher than the batch and resulting growth rates lower.

### 5.6.4 Morphology

The SEMs do confirm that smaller crystals are formed using the SDR as opposed to the batch.

During crystallisation on the SDR, at higher supersaturating conditions (resulting from high pH changes), spherical crystals were seen in these runs alongside rhombic/cubic shaped crystals. These spherical crystals according to the literature could be vaterite. For lower supersaturations (resulting from low pH changes) only rhombic shaped crystals were seen. For the present study, there was no available X-ray diffraction analysis available to determine the presence of vaterite or indeed its relative quantity with respect to calcite.

No spherical crystals were seen in the batch SEM analysis suggesting both aging and/or low supersaturation in the batch precludes vaterite from forming and/or being present at the end of the experiments. An initial sample of the batch slurry early in the experiment may have confirmed vaterite formation – i.e. does the system nucleate as vaterite first then transform into calcite. If this is the case then the SDR with such a short residence time will have a degree of residual vaterite in the product. In tailoring crystal shapes it may be possible to precipitate entirely vaterite and keep it stable in solution (Manoli and Dala, 2000).

In both the SDR and the batch, there appeared to be a bimodal size distribution for the products. (Wachi and Jones,1992) noted a bimodal distribution during their work on batch absorption (see figure 3.23). In the present study, these where seen to be primary crystals, either well-defined cubes or rhombs, rough spheres and large multifaceted types. In some of the SEMs some of the crystals are clustered together on the slide hinting at agglomeration when they were in suspension.

Slides were taken of every experiment performed but only a small percentage underwent SEM analysis. In order to have a more complete picture of the morphology

across a greater range of conditions, more slides needed to be analysed. However, this was not possible due to the high cost of SEM time.

## 5.7 Conclusions to gas-liquid study

In the present study, the SDR has demonstrated itself as being able to continuously absorb $CO_2$ into calcium hydroxide solution. For runs of approximately 400ml, the 15cm diameter SDR showed that by defining the process parameters, control of the final pH of the solution might be attained. Further, these parameters may also define the resultant product size distribution. Short residence times and rapid absorption lead to higher nucleation rates and smaller product size than what might be obtained in a 2-litre batch vessel.

This process has no real relevance to an industrial process other than providing a fundamental study of some of the underlying process parameters such as mass transfer rate. An industrial PCC process from absorbing into clear saturated solutions of calcium hydroxide would not be cost-effective. However, this once through technique using SDR is superior to the batch in delivering mass transfer. An SDR overall equipment size for 15cm disc takes up approximately the same space a 2-litre batch vessel arrangement. Neither the batch nor SDR systems have been optimised in the present study; however, it will be interesting to have some form of full performance comparison at the laboratory scale. Increasing $CO_2$ flow in the batch eventually leads to gas slugging and ineffective mixing – the gas bubbles eventually becomes difficult (or more specifically energy intensive) to disperse with an impeller. The SDR does not suffer from this problem, as the two phases remain separate within the reactor. This may become advantageous when scaling up such a process to industrial scale.

In the present study, a maximum flowrate of 20ml/s onto the disc was regarded as the maximum; any higher flow resulted in too much splashing – this was also close to the limit of the peristaltic pump speed. The lower product size was achieved at lower rotational speeds, longer residence times allowed for higher overall mass transfer to be achieved and thus resulted in higher supersaturation. The higher supersaturation allowed for lower product size to be achieved.

The extra interfacial area of free falling film on shell wall provided a surface for mass transfer. In acquiring more accurate data of the disc performance, any future study should consider this area and take samples from the disc periphery in determining

relative mass transfer rates on both the disc and the walls. An experimental method should employed by which sample was collected at the disc periphery by a tube and thus be removed from being exposed to gas inside the shell. In the present study, this method would have been difficult to employ in practice since there is only 5mm between the edge of the disc and the shell wall and with the risk of collision with the rotating disc at high speed.

The present study did not employ a gas-liquid contacting regime that was either co-current or counter-current. The gas was allowed to develop above the liquid film effectively being of uniform concentration throughout. As most of the reactions carried out in the SDR used 100% $CO_2$, this would have little effect on the mass transfer. However if future studies were to consider dilute $CO_2$ streams such as flue gases, a co/counter-current mode of contacting in the SDR might prove useful to determine how best to deplete the $CO_2$ from the gas mixture. Process intensified gas cleaning devices may be considered to be employed to meet future environmental regulation whereby some derivative SDR technology is adapted for such a purpose.

In further studying the SDR as a gas-liquid contactor, non-precipitating chemical systems should be used first e.g. the absorption of $CO_2$ in sodium hydroxide. In studying precipitating systems, more analysis techniques should be employed in greater depth than the present study. These techniques would include total alkalinity titration, gas chromatography and X-ray crystallography.

These techniques along with perhaps some on-disc sampling method of fluid conductivity or product distribution might allow the reactor to modelled using advanced techniques such as computational fluid dynamics to determine mass transfer and population balance modelling of the crystallisation. Combining these techniques would lend great insight into the processes on the disc and lead to better design of processes based upon SDR technology.

# 6 Calcium hydroxide slurry experimental study

## 6.1 *Introduction to the study*

The reason for performing these experiments was to ascertain the capability of the SDR as a viable reactor for this process. The carbonation of lime slurry is commonplace in industry for the production of calcium carbonate. High $Ca(OH)_2$ suspension concentrations are employed in this process resulting in high yields of $CaCO_3$ product. This reduces the hydraulic loading of plant equipment and makes the process more cost effect than using calcium hydroxide solutions alone. Since the solubility of calcium hydroxide in water is quite low (approximately 1.85 g/l in cold water), suspension densities in excess of 50g/l are employed in industrial applications. The process is usually carried out in batch mode but sometimes it is processed in a counter-current spray or packed tower whereby the suspension is contacted with gas.

### 6.1.1 Calcium hydroxide reaction mechanism

The $Ca(OH)_2$ particles in suspension partially dissolve to form a suspension with a pH of around 12.5. As the carbonation of the suspension progresses, the dissolved $Ca(OH)_2$ reacts with the dissolved $CO_2$ to form $CaCO_3$ particles. This creates a dissolution driving force allowing for the continual depletion of $Ca(OH)_2$ particles and formation of $CaCO_3$ through nucleation and growth of existing crystals. During this time, Ostwald ripening may occur resulting changes in morphology and size distribution. The conversion to $CaCO_3$ stops once all $Ca(OH)_2$ has dissolved and the concentration has been depleted in the suspension. Continual carbonation will lead to bicarbonate formation and begin to dissolve the $CaCO_3$.

## 6.2 *Advantage of the SDR?*

(Juvukar and Sharma, 1973) investigated particle loadings in the range 10-400g/l. They observed that when using bubble columns at high particle loadings, gas slugging occurred, suggesting a decrease in interfacial area and when using mechanically agitated vessels they observed increasing impeller speeds above a critical speed had no effect of improving the bubble interfacial area. These were laboratory scale processes suggesting industrial units may share the same problems.

In the present study, it was suggested that the SDR might have a potential benefit to this process. If the gas absorption rate is seen to be higher in the SDR than in the batch

sparging process, then the processing time for a given volume of $Ca(OH)_2$ slurry would be reduced. Likewise, high agitation achieved on the disc surface would allow for rapid dissolution of the $Ca(OH)_2$ particles. Coupled with higher absorption, higher supersaturation can occur and would perhaps lead to smaller mean particle size with a tighter distribution. Overall the SDR should improve all mass transfer processes, however the effect on crystal size distribution would need to be established.

## 6.3 Batch slurry experiments

Initial batch experiments were carried out to determine the time it took for 2 litres of $Ca(OH)_2$ suspension of a known concentration to change to a measured pH of around 10 (this was not always possible to measure accurately due rapidly changing meter displays close to the end-point). The pH remains high whilst there are $Ca(OH)_2$ particles still in the suspension. These continuously dissolve to maintain the $OH^-$ concentration in solution. Once all $Ca(OH)_2$ particles have completely dissolved, the system will behave like the $Ca(OH)_2$ solution experiments whereby the calcium ion concentration in solution will begin to drop as the carbonation continues although there will be a significant crystal mass of $CaCO_3$ particles in the suspension at this point.

### 6.3.1 Preparation of calcium hydroxide slurry

Slurries were made up just prior to experimentation so that $CO_2$ absorption from the atmosphere was minimised. These slurries were made in the same way as the solution but without the filtration process. To prepare slurry with X grams/litre of calcium hydroxide, X grams were added to de-ionised water and then made up to the total desired volume. The slurries were stirred in the charging vessel before pumping onto the SDR or stirred in the batch vessel before any experimentation. This stirring maintained homogeneity of slurry density throughout the bulk and prevented settling of particulates.

### 6.3.2 Batch experimental procedure

Five batch experiments were carried out, four runs with a suspension of undissolved calcium hydroxide particles and one with saturated calcium hydroxide solution. Carbonation of a saturated solution was included so that the same agitation and sparging conditions as the slurry could be evaluated in this equipment to allow comparison. The concentration of $Ca(OH)_2$ slurry was altered for each experiment, the concentrations are shown below.

| Slurry Batch Experiment | $Ca(OH)_2$ suspension concentration (g/l) |
|---|---|
| 1 | 15.0 |
| 2 | 7.5 |
| 3 | 5.0 |
| 4 | 2.0 |
| 5 | saturated solution |

**Table 6.1 Summary of batch reaction slurry concentrations**

Each run was performed with 2 litres of slurry agitated at the same stirrer speed and sparged with the same flowrate of gas. The slurry was prepared by adding a measured weight of calcium hydroxide powder and added to the agitated known volume of water and left for several minutes for the slurry to properly mix. A flat-blade impeller was used for the agitation. $CO_2$ was fed via 6mm PVC tubing into the bottom of the vessel through a sintered glass sparger at a rate of 2 litres/min. A pH probe was immersed in the slurry and the stirrer speed for the experiment was selected. The pH probe and the $CO_2$ line into the bottom of the vessel were placed in the vessel in such a way as to act as baffles on the stirring action of the vessel i.e. they worked toward breaking any large vortices caused by the impeller shaft. The experiment was timed from when the $CO_2$ flow was started and the pH at given times was recorded as the experiment progressed. Upon completion of the reaction the $CO_2$ was stopped and agitation of the suspension was continued. Slurry samples were taken via the tap in the bottom of the vessel and CSD analysis was performed using the Mastersizer. For each sample, 4 CSDs were taken at 2-minute intervals.

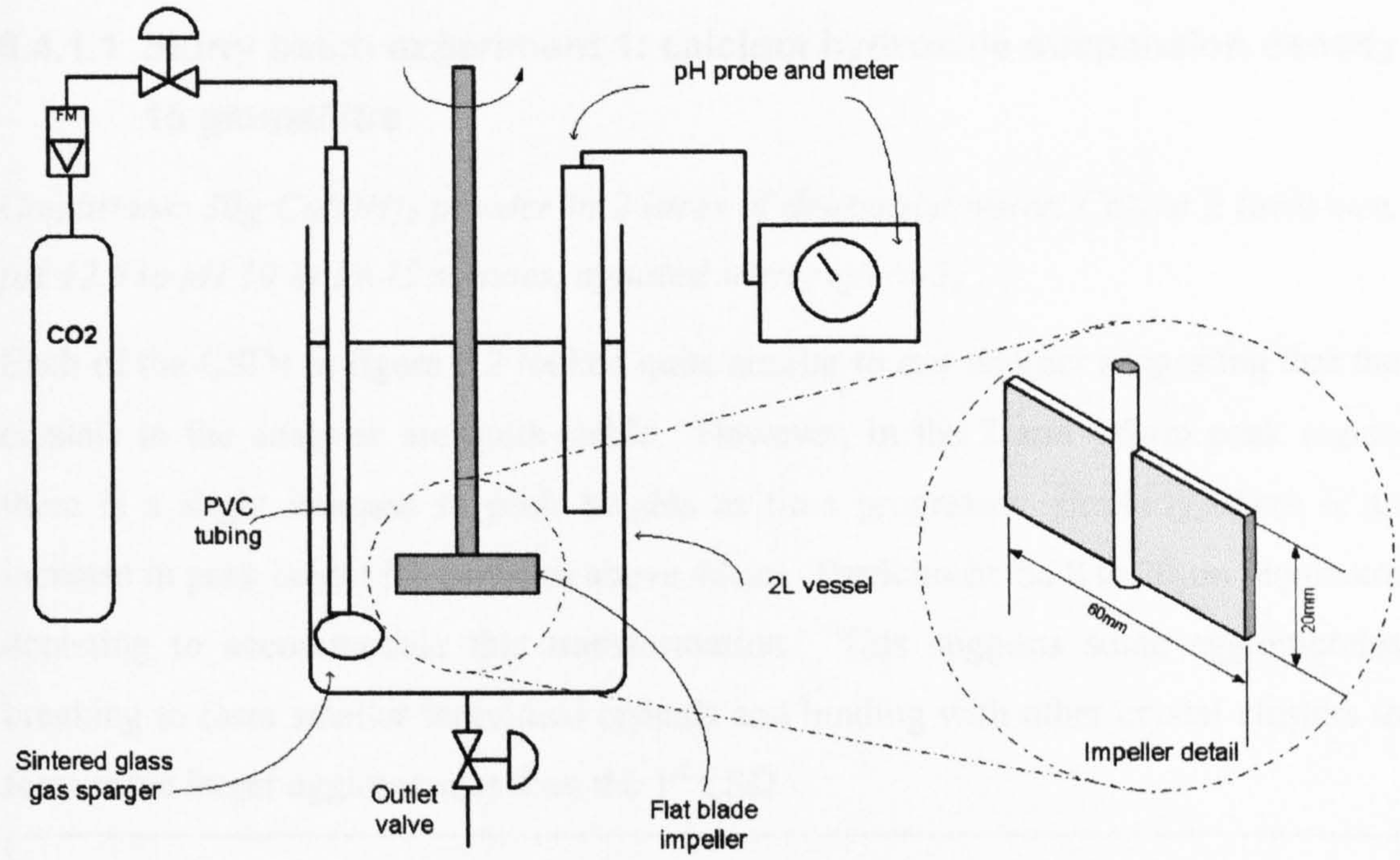


**Figure 6.1 2-litre batch reactor set-up**

## 6.4 Batch results

### 6.4.1 Crystal size distribution analysis of each experiment

The Mastersizer CSD data records for each experiment were analysed. All CSD for an experiment was plotted graphically to see what change occurred in the CSD over time, this would allow for interpretations to be made as to whether or not secondary crystal processes were occurring in the product. The Mastersizer determined the size of all particles in suspension regardless of what material they where made of and sized them using the assumed model for the refractive index of $CaCO_3$.

In these experiments, no SEM imaging was available due to cost constraints so all data interpretation have had to be made on the Mastersizer data alone. Once each experiment has been examined individually, CSD comparisons were made between the experiments to see what trends can be seen in changing the calcium hydroxide suspension density.

### 6.4.1.1 Slurry batch experiment 1: calcium hydroxide suspension density 15 grams/litre

*Conditions: 30g $Ca(OH)_2$ powder in 2 litres of de-ionised water, $CO_2$ at 2 litres/min, pH 12.5 to pH 10 in 19.45 minutes, agitated stirrer speed 3.*

Each of the CSDs in figure 6.2 looked quite similar to one another suggesting that the crystals in the analyser are quite stable. However, in the 2 and 4.5μm peak region there is a slight increase in peak heights as time progresses, similarly, there is an increase in peak height for particles above 40μm. Particles in the 8 to 20μm region are depleting to accommodate this transformation. This suggests some agglomerates breaking to form smaller individual crystals and binding with other crystal clusters to form some larger agglomerates than the 1st CSD.

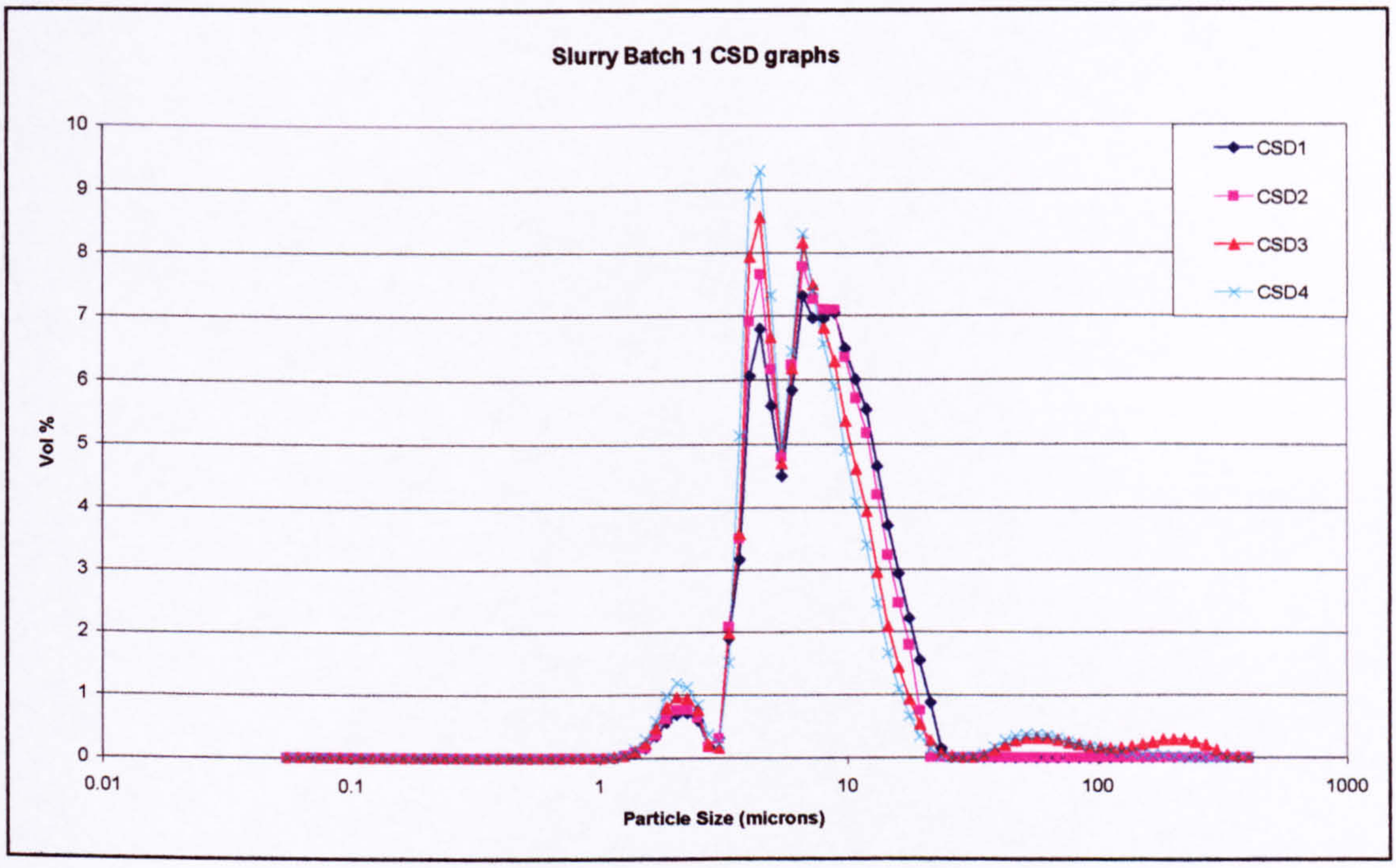


**Figure 6.2 Slurry batch 1 CSD graphs**

### 6.4.1.2 Slurry batch experiment 2: calcium hydroxide suspension density 7.5 grams/litre

*Conditions: 15g $Ca(OH)_2$ powder in 2 litres of de-ionised water, $CO_2$ at 2 litres/min, pH 12.6 to pH 10 in 7.34 minutes, agitated stirrer speed 3.*

All CSDs seen in figure 6.3 are very similar to each other over the analysis period suggesting a stable product. In comparison to Slurry batch 1 CSD, this experiment produced a mono-modal distribution whereas the 1st experiment had 3 distinct peaks.

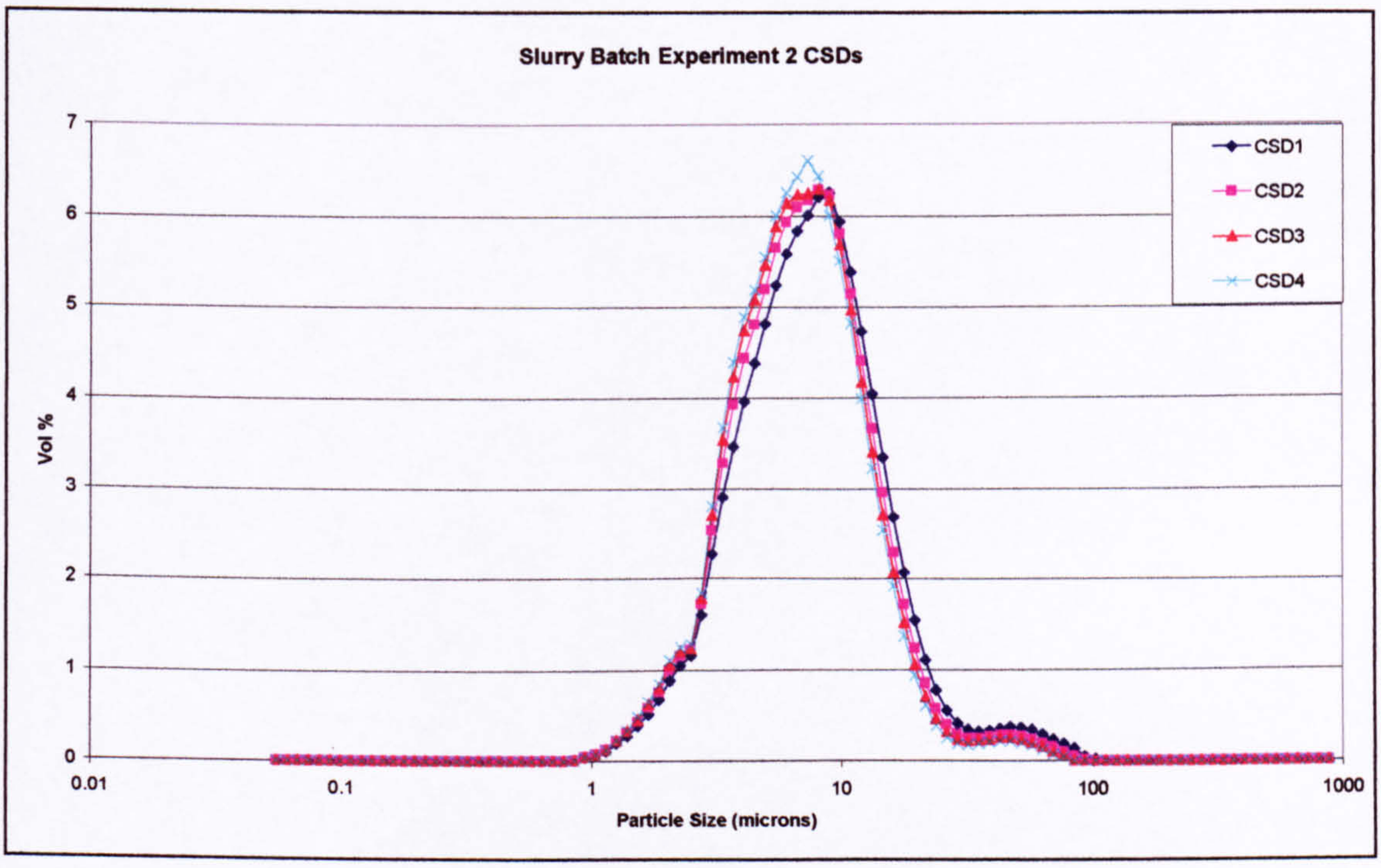


**Figure 6.3 Slurry batch 2 CSD graphs**

### 6.4.1.3 Slurry batch experiment 3: calcium hydroxide suspension density 5.0 grams/litre

*Conditions: 10.0g $Ca(OH)_2$ powder in 2 litres of de-ionised water, $CO_2$ at 2 litres/min, pH 12.5 to pH 10 in 4.51 minutes, agitated stirrer speed 3.*

Again, all CSDs seen in figure 6.4 are very similar to each other over the analysis period suggesting a stable product. The small peak between about 30 and 100 microns suggests some of the calcium hydroxide large particles had not broken down by the end of the experiment or there were some air bubbles entrained within the dispersion unit.

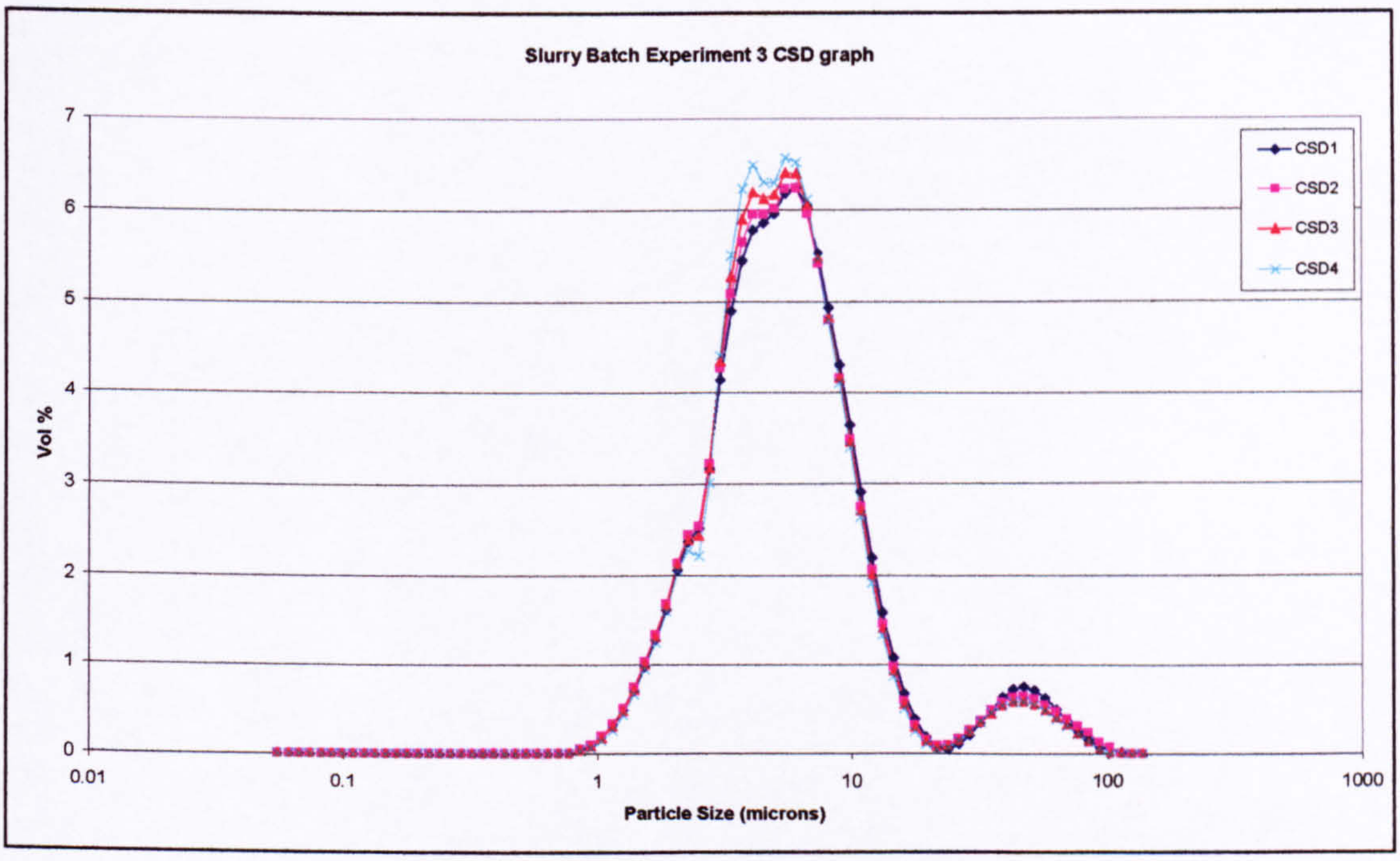


**Figure 6.4 Slurry batch experiment 3 CSD graphs**

#### 6.4.1.4 Slurry batch experiment 4: calcium hydroxide suspension density 2.0 grams/litre

*Conditions: 4.04g $Ca(OH)_2$ powder in 2 litres of de-ionised water, $CO_2$ at 2 litres/min, pH 12.5 to pH 10 in 1.52 minutes, agitated stirrer speed 3.*

6 CSD analyses were taken for this experiment seen in figure 6.5. The data suggests some slight drift toward smaller particle size as time progresses. The percentage of particles above 10μm appear to decrease resulting in a small increase in smaller particles. This suggests there are some agglomerated particles breaking up during the analysis period.

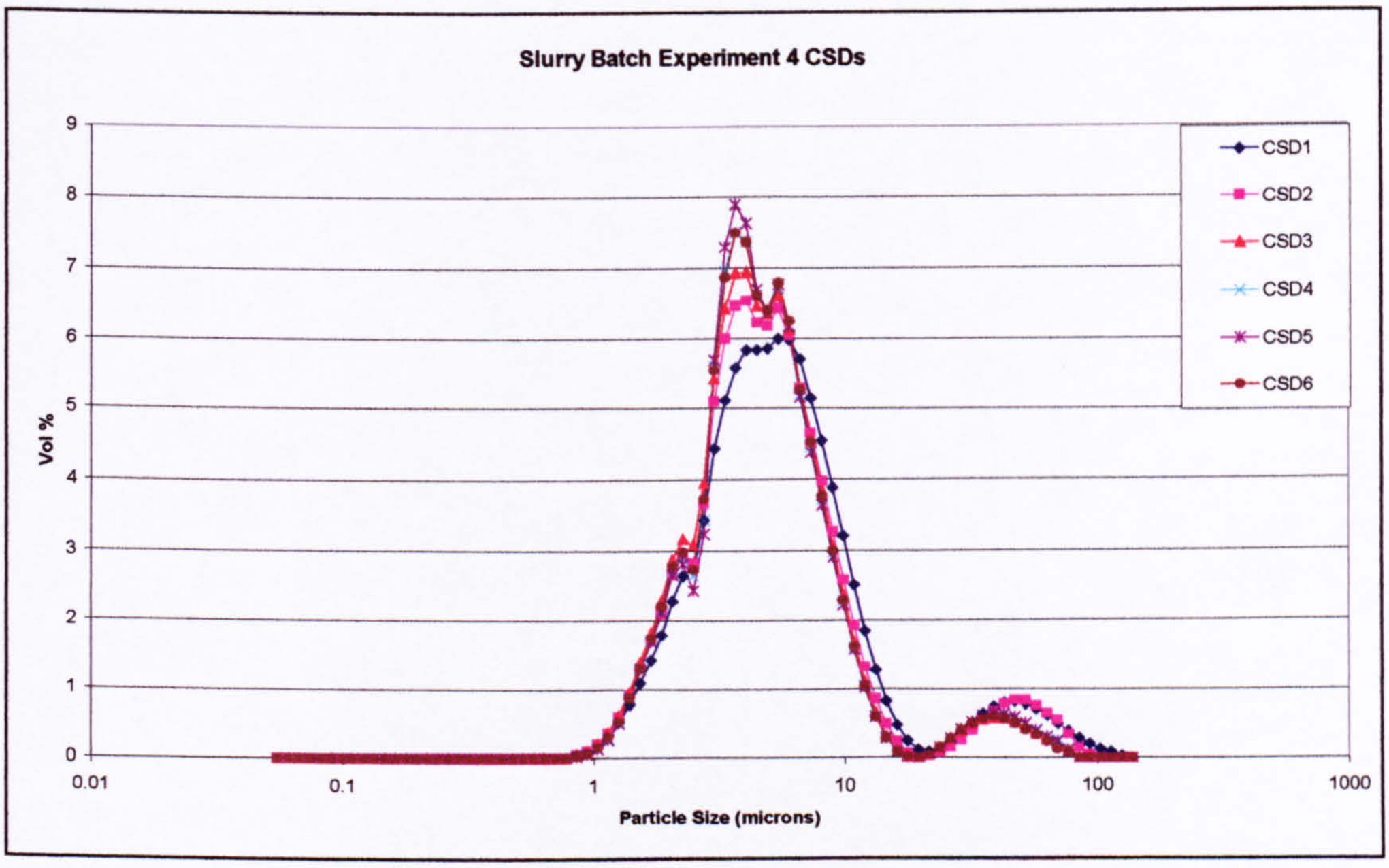


**Figure 6.5 Slurry batch experiment 4 CSD graphs**

### 6.4.1.5 Slurry batch experiment 5: calcium hydroxide saturated solution

*Conditions: approx 3.7g $Ca(OH)_2$ powder in 2 litres of de-ionised water, solution filtered and degassed with nitrogen before use. $CO_2$ at 2 litres/min, pH 12.4 to pH 10 in 1.08 minutes, agitated stirrer speed 3.*

Although 3.7g of $Ca(OH)_2$ powder was added to make up the solution, after filtering etc, the starting pH read 12.4 when in the reaction vessel. By calculation this suggested that the actual concentration was 0.93 g/l, approximately half the value stated in the literature [Perry's table 2-120 p2.121 solubility = 0.165g/100ml water @ 20°C]. If the pH meter read 12.5, the inferred concentration would be 1.17 g/l and if it read 12.6 the inferred concentration would be 1.47g/l. So a 0.1 change in pH denotes an approximately 20% change in calcium hydroxide concentration between pH 12.5 and 12.4. Obviously, any inaccuracy in this measurement would lead to significant errors in determining calcium ion concentration. It can be assumed that the solution is saturated due to excess material settling out after a 48-hour period but the exact concentration is difficult to determine by pH measurement alone. Without constant temperature in the lab, precise analysis and measurement of the solution concentration is inordinately difficult especially since calcium hydroxide solubility is inversely soluble with temperature. For the purposes of this work we will assume the initial concentration is that estimated via the pH measurement, 0.93g/l.

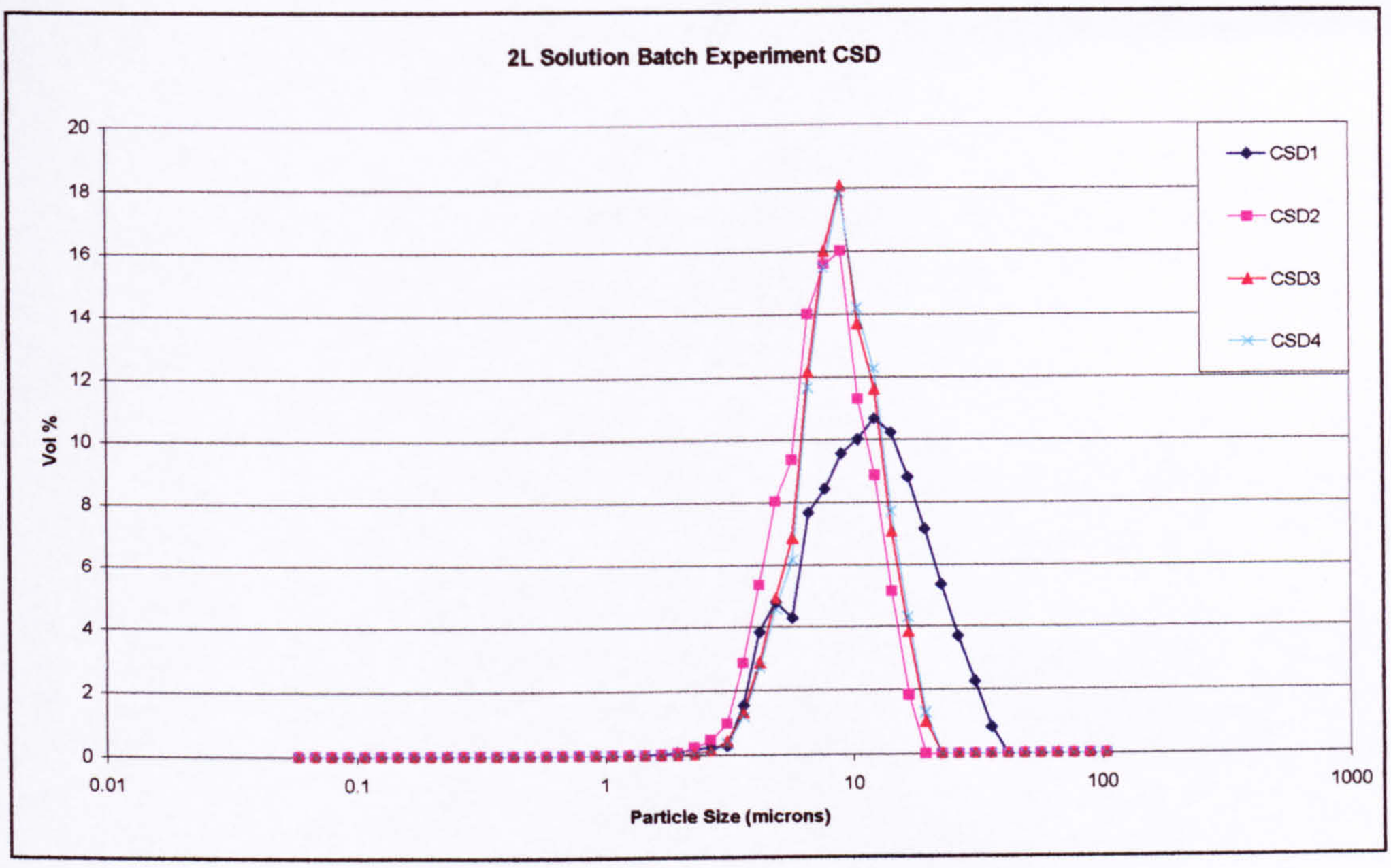


**Figure 6.6 2-litre solution batch experiment CSD graphs**

In the 2-litre batch solution experiment, the CSD data seen in figure 6.6 suggests that from the 1st to the 2nd CSD there is a decrease in particle size, implying there is a breakdown of agglomerates. Particle size increases for the 2nd to the 3rd and 4th CSDs perhaps suggesting Ostwald ripening. The 3rd and 4th CSD have no change in them suggesting stable material.

### 6.4.2 The effect of calcium hydroxide slurry concentration on crystal size distribution in the batch

A comparison was made between the CSD of each experiment to see what effect the calcium hydroxide slurry concentration had upon the CSD. The first CSD of each experiment was plotted on the same graph and a CSD statistical characteristic chart was prepared for interrogation.

From the graph of 1st CSD for each experiment, figure (6.7), it was seen that there is a increase in particle size as the $Ca(OH)_2$ density increases in the slurry experiments. In batch carbonation, (Juvekar and Sharma, 1973) state that with an initial slurry concentration at 10g/l the mean diameter was 25μm whereas at 100g/l it was 50μm suggesting the mean diameter does increase with increased particle loading. The solution experiment has a higher mean size that any of the slurry experiments due to lower nucleation and higher growth rates from lower available supersaturation.

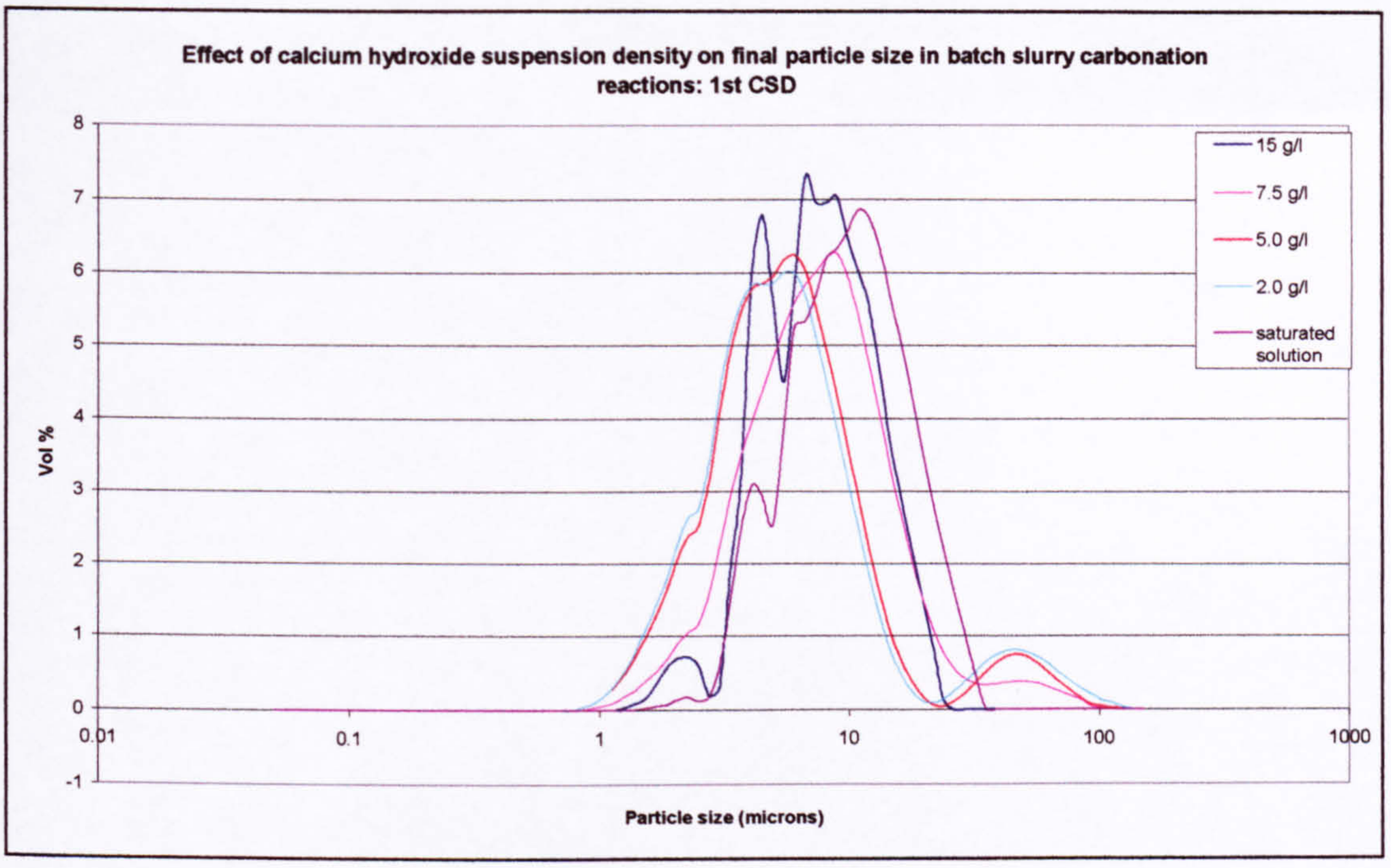


**Figure 6.7 Effect of calcium hydroxide loading on CSD in batch experiments**

This trend is seen in the Sauter mean diameter, D[3,2] in figure 6.8. For slurry concentrations of 2.0, 5.0 and 7.5 g/l there are distribution peaks in the 10 to 100μm region. With the higher proportion of small particles in these experiments, it is suggested that these peaks come from agglomeration of some of the product. These 'tails' have an effect on D[4,3] so the relationship becomes invalid when considering this mean diameter expression, however, the solution result still has a higher mean D[4,3] than the slurry results.

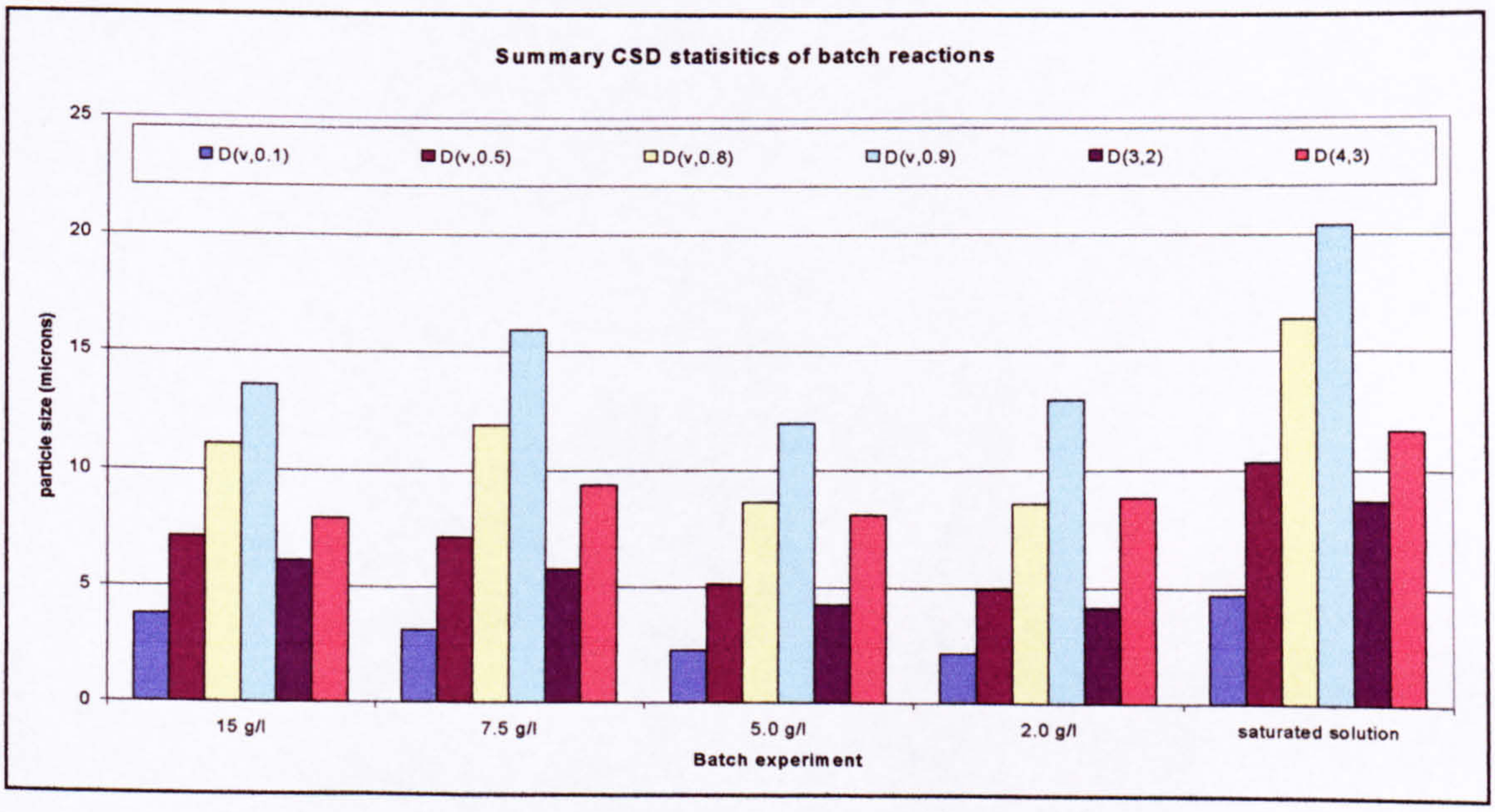


**Figure 6.8 1st CSD summary statistics for slurry batch experiments**

### 6.4.3 Batch: discussion of crystal size distribution

***Slurry vs solution***

In considering slurry reactions against the precipitation from clear solution, then the particles in the slurry will effect nucleation processes by creating a large surface area by which primary heterogeneous nucleation will occur at a much higher rate than that of a solution relying on primary nucleation from a 'particle free' solution (homogeneous) and the surfaces of the crystalliser (heterogeneous). In the solution case, the supersaturation begins to deplete immediately and cannot be maintained by fresh dissolution of $Ca(OH)_2$ this means that the maximum supersaturation ratio and subsequently nucleation rate will begin to fall as soon as the carbonation begins hence growth dominates over nucleation more quickly. The slurry allows for supersaturation level to be maintained until all the $Ca(OH)_2$ has been depleted in solid form, hence the nucleation rate will be higher than from the saturated solution experiment.

***Slurry experiments only***

In considering the slurry experiments only, it can be hypothesised that the mean diameter of the particles increases due to the processing time and therefore the longer dissolution time allowing for the continuous growth of crystals from the continually supersaturating solution. The more concentrated the slurry density, the more calcium ions that are available for growth. In this case, the level of supersaturation is relatively low due to the low concentration of calcium ions in solution, such that growth processes will predominate over nucleation. The longer processing times for higher suspension densities also allows for small crystals of $CaCO_3$ to redissolve. These might have been the metastable vaterite form and hence have the opportunity to transform to calcite during the processing time.

### 6.4.4 Batch processing time

From the five batch experiments performed here, the time taken for the slurry to convert to the end point of pH 10 was measured. This was designated the processing time. From the slurry density, we can determine the processing rate on a mass and molar basis. Since the stirring rate and gas flowrate were identical for each experiment, the effect of calcium hydroxide slurry concentration on processing time can be evaluated.

The intial mass of the $Ca(OH)_2$ was assumed to be converted to >99% $CaCO_3$ when the pH of 10 was attained. Using the slurry loading of $Ca(OH)_2$ on a molar and mass ratio and dividing it by the processing time gave the processing rates seen in table 6.2 below.

| Experiment | Starting pH | End pH | Calcium Hydroxide Conc (g/l) | Calcium Hydroxide Conc (mol/l) | Processing time (s) | Processing rate (g/s) | Processing rate (mol//s) |
|---|---|---|---|---|---|---|---|
| **Slurry Batch 1 (15g/l)** | 12.4 | 10 | 15 | 0.2024 | **1185** | 0.0126 | 0.000171 |
| **Slurry Batch 2 (7.5g/l)** | 12.6 | 10 | 7.5 | 0.1012 | **454** | 0.0165 | 0.000223 |
| **Slurry Batch 3 (5g/l)** | 12.5 | 10 | 5 | 0.0675 | **232** | 0.0215 | 0.000291 |
| **Slurry Batch 4 (2g/l)** | 12.5 | 10 | 2 | 0.0270 | **114** | 0.0175 | 0.000237 |
| **Solution Batch (0.93 g/l)** | 12.4 | 10 | 0.93 | 0.0126 | **68** | 0.0136 | 0.000185 |

**Table 6.2 Processing Time and Rates for Batch Slurry Experiments**

In table 6.2 we see that higher processing rates are achieved for lower slurry concentrations. At 15g/l, the lowest processing rate is achieved. Low slurry concentrations also have a higher rate than the solution experiment. The solution batch processing rate may have been lower that the slurry batches at lower concentration due to there being a large number of particles in the slurry initially facilitating heterogeneous nucleation, whereas with the solution batch, many orders of magnitude less particles were available for this to occur. A larger number of particles would also have facilitated a greater area for mass transfer to occur and thus increase the overall rate. However, at increasing slurry densities, the processing rate begins to slow due to the higher viscosity of the suspension, this becoming a barrier to mass transfer. Gas slugging in bubble columns at higher slurry concentrations was experienced by (Juvekar and Sharma, 1973) and likewise the same effect could have been happening in the present study – it being more difficult to disperse bubbles in concentrated slurries.

In considering the pH of the solution, the starting pH varied between 12.4 to 12.6. It could be hypothesised that this might influence the absorption rate. A detailed pH measurement with time was performed on a repeat of slurry batch experiment 1 where the pH was record with as many readings as possible during the course of the run this resulted in obtaining the data seen in figure 6.9 below. The slurry pH fluctuates with time, reaching peak values of 12.85. The pH begins to drop towards the end as the $Ca(OH)_2$ particles become depleted in suspension and only $Ca(OH)_2$ in solution

remains. At the beginning of the reaction, the $Ca(OH)_2$ particles in the slurry may be quite large and agglomerated resulting in them having lower surface area for dissolution. As the experiment proceeds, the agglomerates break up under agitation and the particles get smaller due to dissolution resulting in faster dissolution and higher pH.

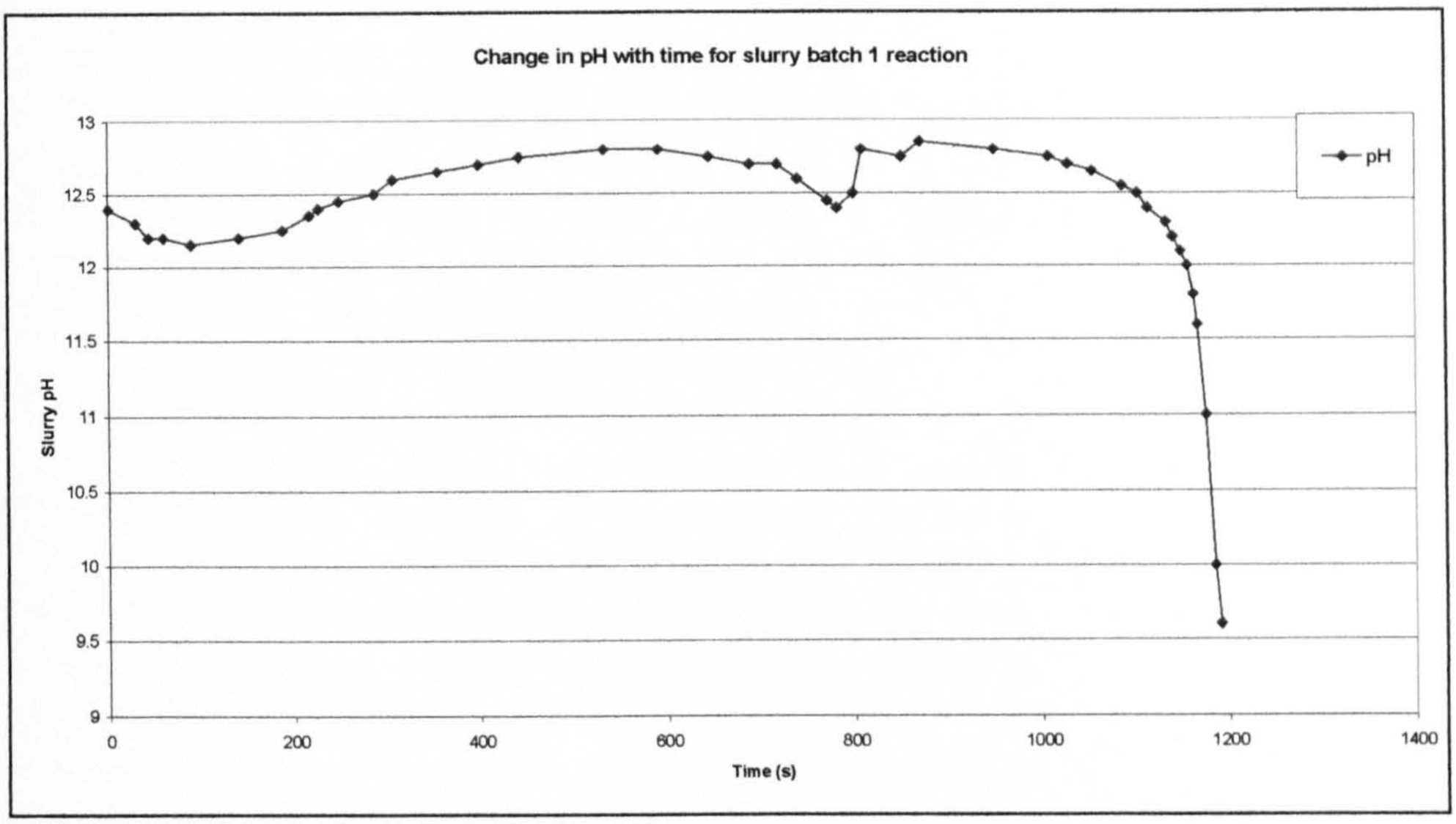


**Figure 6.9 Change in pH with time for slurry batch 1 reaction**

The reason for the dip and then rise in pH between 700 and 900 seconds is not fully understood however it could be hypothesised that during this time, there is a large number of small $CaCO_3$ crystals in the suspension which are effecting the viscosity and/or the conductivity of the solution, so that there is an effect upon the dissolution rate and/or the pH measurement. This is happening toward the end of the experiment where the $Ca(OH)_2$ particles will be almost depleted and the formation of $CaCO_3$ will be nearing completion. These particles by their nature affect the membrane of the pH probe by blocking the surface of the glass and the meter has the potential to 'drift'.

Detailed pH monitoring of the other experiments was not undertaken so understanding this effect at other slurry densities is not possible without such data.

## 6.5 Spinning disc experiments

Four experiments were performed on the SDR to evaluate its capabilities in processing calcium hydroxide slurries. For each experiment, the calcium hydroxide suspension density was maintained at 15g/l. It was seen that the higher slurry concentrations should be focused on in order to best evaluate the SDR in these experiments, as high slurry densities would be used in industrial equipment. The SDR employed was that used in all the other experiments with a diameter of 150mm. For all SDR slurry experiments, the reactant was fed into the centre well on the disc surface.

### 6.5.1 SDR slurry recirculation experiments

The first method was to employ the SDR as the absorber and circulate 2 litres of slurry from the bottom of the 2-litre batch vessel to the SDR and back to batch vessel. The batch vessel was stirred during the reaction to maintain an even distribution of the suspension. The configuration can be seen in figure 6.10 below.

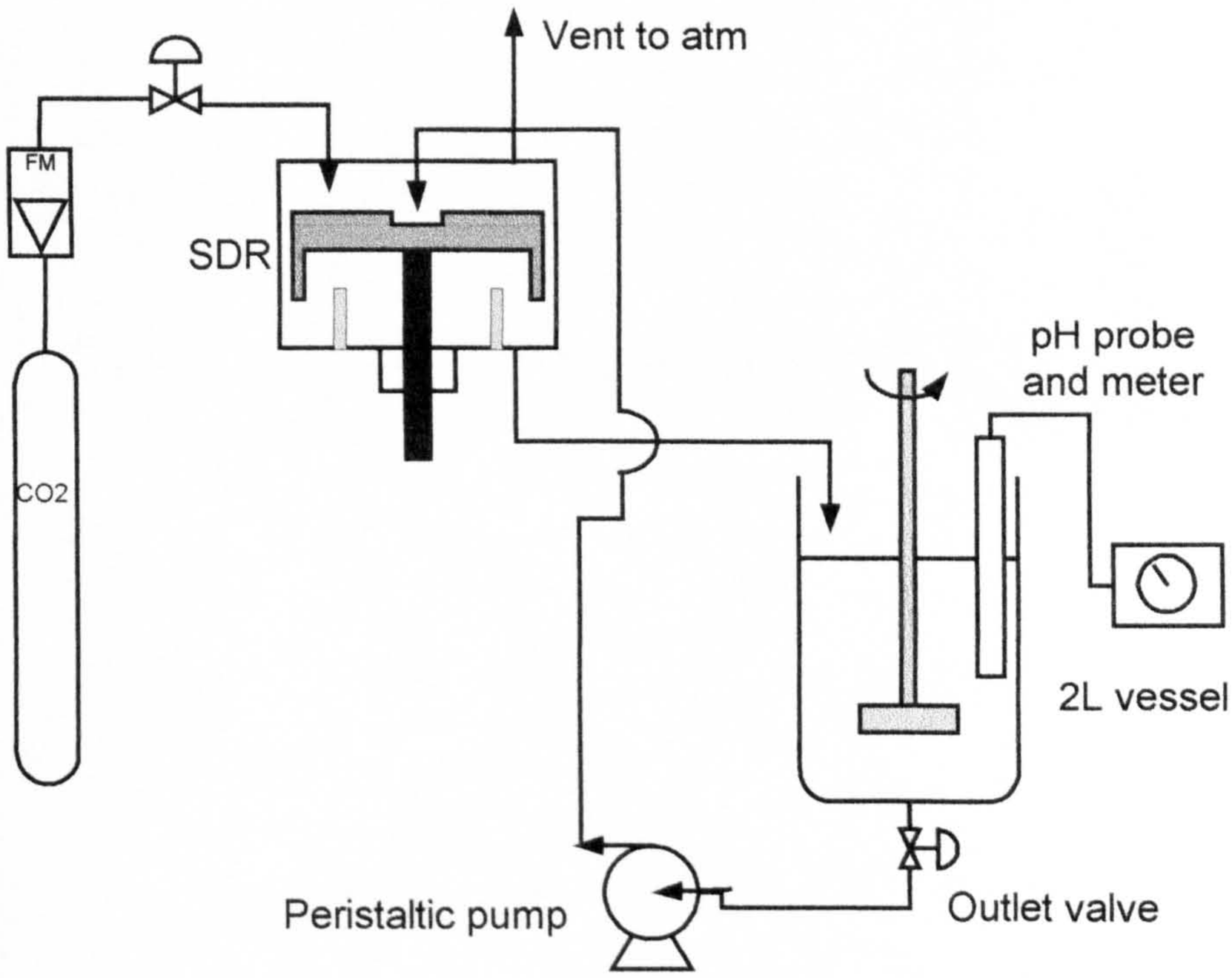


**Figure 6.10 SDR-batch slurry recirculation experimental set-up**

In each of the two runs performed in this way, the disc rotational speed was set at 1000rpm and the slurry circulated at 15ml/s (calibrated by timing a known volume). The agitator was initially calibrated to run on the lowest setting for each of the experiments. Using a strobe light, this was seen to be running at 210rpm when

calibrated in water. The strobe light was not available to check rotational speed during experimentation. The $CO_2$ flowrate was set at 2.0 litres per minute. So in comparing the batch to the SDR-batch, the batch volume, $CO_2$ flowrate and the slurry density remain constant. For these two experiments, the pH in the vessel was monitored with time so a comparison of processing time could be made between the batch and SDR-batch experiments. Once the pH reached 10, the circulation and the $CO_2$ flow was stopped but the stirring in the batch vessel was continued to maintain even distribution of the suspension density. The CSD was taken of the product once the circulation to the SDR had stopped. The two runs performed had identical condition to see if there was any deviation of processing time.

### 6.5.2 SDR individual disc pass experiments

The second equipment configuration was set up to determine the number of disc passes required for the slurry to be processed if it were to be imagined the process was operated with a cascade of discs all with the same diameter, gas and liquid flowrate and rotational speed. In order to do this with a single disc, the stirred batch vessel was used to hold 2 litres of slurry. The slurry was then pumped onto the disc at approximately 15-19ml/s (this was calculated by timing how long it took for the 2 litres of slurry to empty from the batch vessel and then calculating the mean flowrate during that time). The disc was run at 1000rpm and fed with $CO_2$ at a rate of 2 l/min. On exit from the disc, the slurry was collected in a second vessel where it was then returned to the stirred batch vessel were the pH was recorded. The configuration can be seen in figure 6.11 below.

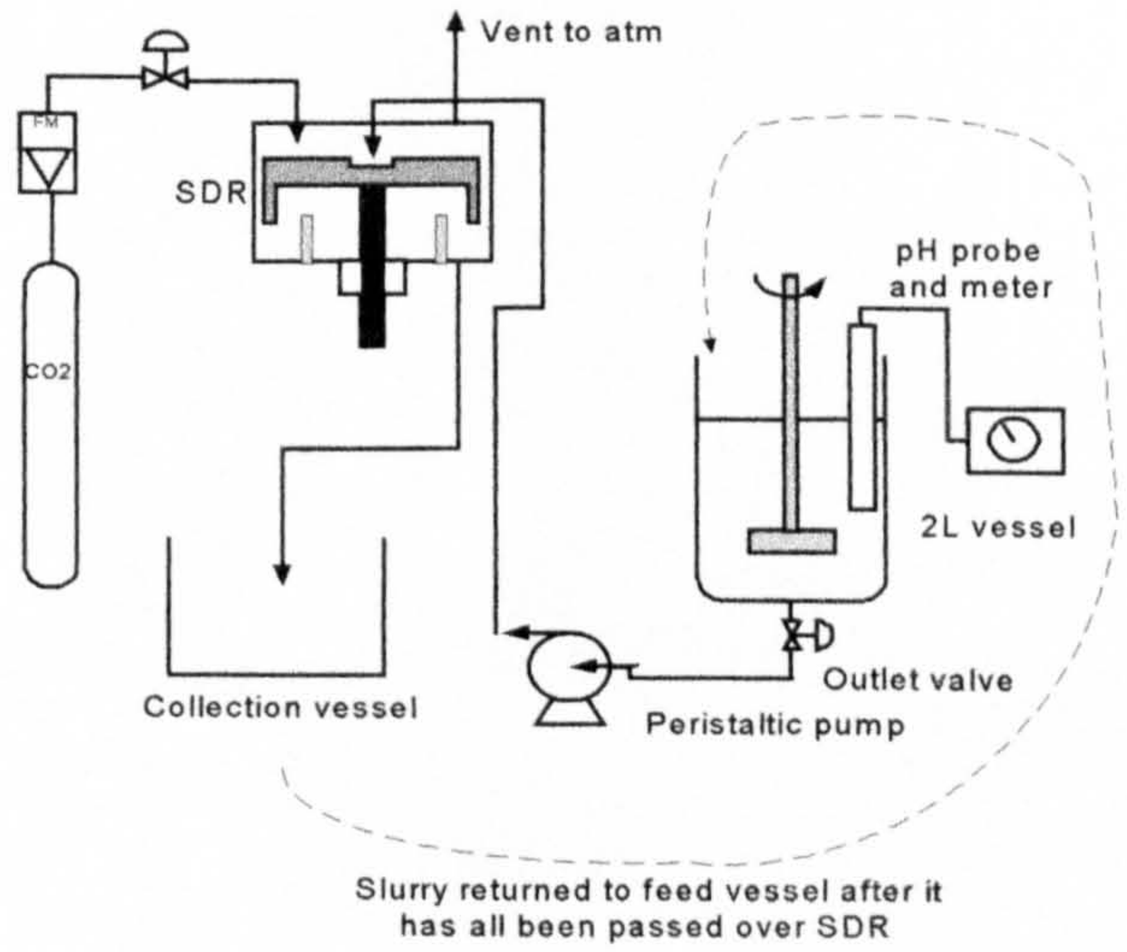


**Figure 6.11 SDR slurry disc pass experimental set-up**

This process of passing the slurry over the disc to a second vessel was repeated until the pH dropped below 10. For each pass, the pH and the time for the vessel to empty were recorded. The final product CSD was analysed using the Mastersizer S. This experiment was repeated but this time, the CSD was taken of a small sample of slurry after each pass to evaluate what happened to the CSD with time/pass. The processing time could be worked out by adding the times for each pass of the 2 litres of slurry.

## 6.6 SDR slurry experimental results

### 6.6.1 Processing time and processing rate

The time was noted for each of the recirculation experiments for the pH to reach 10 For the disc pass experiments, the number of passes and the pass time were summed to find the time taken for the pH to fall below 10 i.e. if the pH was 12.2 after 8 passes and 8.4 after 9 passes then 9 passes were taken to be the time to process the slurry, the times for each of the passes were then added up to give the processing time. For both disc pass experiments, it took 9 passes for both runs for the pH to drop below 9. The processing times were then compared to the 2-litre batch operation for the 15g/l. The processing time and rate data is summarised in table 6.3 below.

| Experiment | Starting pH | End pH | Ca(OH)2 conc. (g/l) | Ca(OH)2 conc. (mol/l) | Processing Time (s) | Processing rate (g/s) | Processing rate (mol/s) |
|---|---|---|---|---|---|---|---|
| Slurry Batch 1 repeated (15g/l) | 12.4 | 10 | 15 | 0.2024 | 1185 | 0.012658 | 0.000171 |
| SDR Slurry 1 RUN 1 (15g/l) | 12.6 | 10 | 15 | 0.2024 | 1008 | 0.014881 | 0.000201 |
| SDR Slurry 1 RUN 2 (15g/l) | 12.65 | 10 | 15 | 0.2024 | 1016 | 0.014764 | 0.000199 |
| SDR Slurry 2 "disc pass expt 1" (15g/l) | 12.8 | 9.5 | 15 | 0.2024 | 1010 | 0.014851 | 0.000200 |
| SDR Slurry 3 "disc pass expt 2" (15g/l) | 12.6 | 8.4 | 15 | 0.2024 | 997 | 0.015045 | 0.000203 |

**Table 6.3 Processing time and rate for slurry reactions of a density of 15g/l**

What is interesting in the SDR processing times is that for both configurations, the processing times are almost the same. In comparing the SDR operation with the batch operation, the SDR has a processing rate approximately 12.4% faster than the batch method so some advantage can be made of the SDR to be used as the absorber for the process.

### 6.6.2 SDR disc pass experimental results

The time for 2 litres of slurry to pass over the disc was recorded in the SDR disc pass experiments. It was noted that there is a difference in time for the passes; this would result in a change in the flowrate for each pass. The pass time data and flowrate is presented in table 6.4 below.

| | Disc pass experiment 1 | | Disc pass experiment 2 | |
|---|---|---|---|---|
| Disc Pass | Time (s) | Flow rate ml/s | Time (s) | Flow rate ml/s |
| 1 | 132 | 15.15 | 129 | 15.50 |
| 2 | 118 | 16.95 | 113 | 17.70 |
| 3 | 115 | 17.39 | 110 | 18.18 |
| 4 | 112 | 17.86 | 114 | 17.54 |
| 5 | 106 | 18.87 | 113 | 17.70 |
| 6 | 105 | 19.05 | 107 | 18.69 |
| 7 | 106 | 18.87 | 102 | 19.61 |
| 8 | 106 | 18.87 | 104 | 19.23 |
| 9 | 110 | 18.18 | 103 | 19.42 |
| Total | 1010 | | 995 | |
| Average | | 17.91 | | 18.18 |
| Std Dev | 8.700 | 1.271 | 8.293 | 1.273 |

**Table 6.4 Disc pass times and flowrates**

In table 6.4 it can be seen that the changing time taken per pass effects the flowrate. It was assumed that the viscosity of the slurry is affected by the extent of the carbonation. The change in particle size and number with time will affect the viscosity of the slurry. Since pH is only affected towards the end of the carbonation then this may not affect the solution viscosity. The change in flowrate will affect the hydrodynamic parameters of the fluid on the disc. The new flowrate can be determined and assuming the slurry bulk density remains the same then the only parameter not known is the viscosity. As seen in the second disc pass run, the trend that the time per pass decreases with each pass, the viscosity has a tendency to decrease as the carbonation proceeds. In both experiments, the viscosity is lower at the end than at the beginning of the experiment.

With hindsight, the same pumping set-up should have been carried out with water as well as slurry. The relative pumping times could then allow for the slurry viscosity to

be determined. However, after the slurry experiments had been completed, the tubing and pumping equipment were quickly cannibalised for other projects and experiments. Without the viscosity of the slurry, it is difficult to determine the exact hydrodynamic parameters on the disc.

*Comments further to the above: This argument did not take into account the small sample of product taken from the batch after each disc pass thus reducing the slurry volume. This was only performed for the second disc pass experiment. However it is estimated that each sample required no more than 3 to 5 millilitres of sample to perform the analysis so by the 9$^{th}$ pass (say) 30 to 40 millilitres would have been taken from the batch, which would equate to approximately 2 seconds of flow at this pumping rate. The rate at which the time changed from above is greater than this estimate alone so the effect of a viscosity change can still be concluded from the data especially since the first disc pass experiment was not subject to sampling after each pass and the trend is seen in that as well.*

### 6.6.3 SDR CSD data for slurry experiments

CSD analysis was performed on the final product for the second disc circulation experiment and for both of the disc pass experiments. In the second disc pass experiment, a CSD was taken from a small sample after each pass to chart the accompanying change in CSD.

**SDR-batch circulation experiment 2**

From the CSD graph in figure 6.13 each CSD appears almost exactly the same as each other suggesting that the final product is stable over the analysis period. Three peaks are seen suggesting a tri-modal distribution of product.

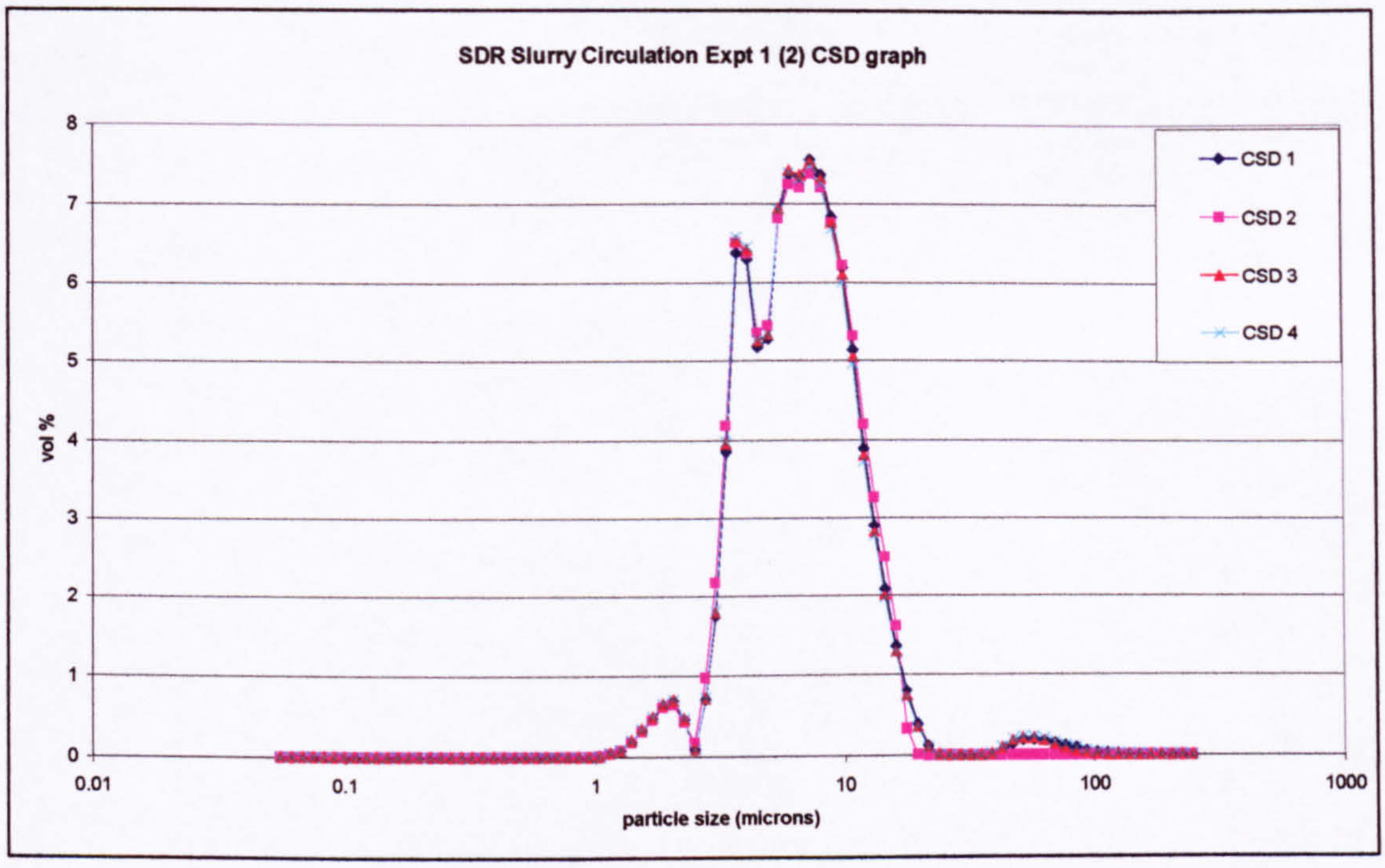


**Figure 6.12 SDR slurry recirculation experiment CSD**

## SDR disc pass experiment 1

In figure 6.14 again the final product sample CSD analysis suggests a stable product.

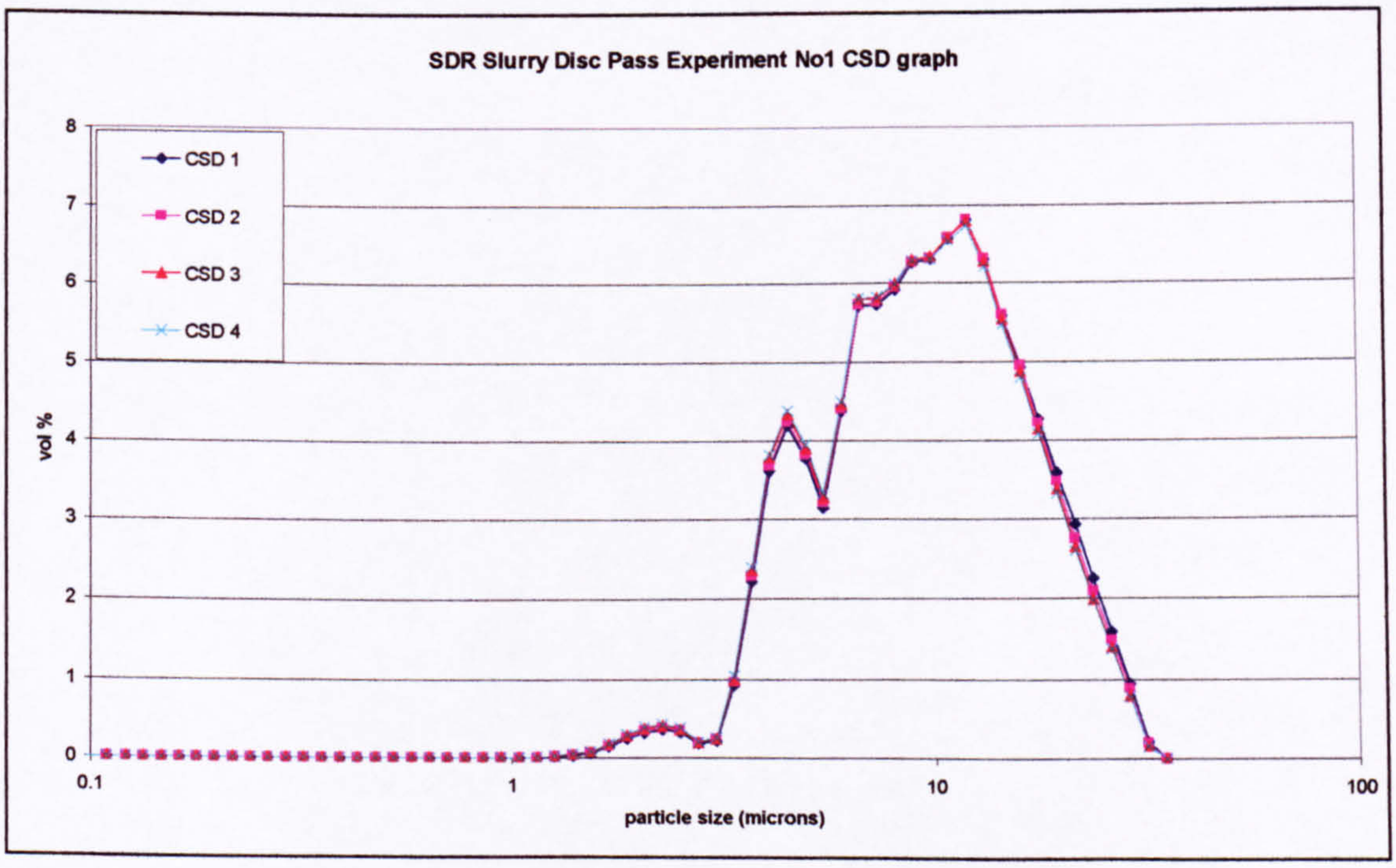


**Figure 6.13 SDR disc pass experiment 1 final product CSD**

### 6.6.4 SDR disc pass experiment 2: the change in CSD with each disc pass

A small sample of the slurry was taken out of the batch after each pass and a single CSD analysis was performed upon it. The Mastersizer was rinsed and prepared for the next sample during each pass. The CSD of the initial slurry was also performed.

Below is the CSD summary data plotted for each pass in figure 6.14 It represents the change in 6 CSD characteristics with each pass.

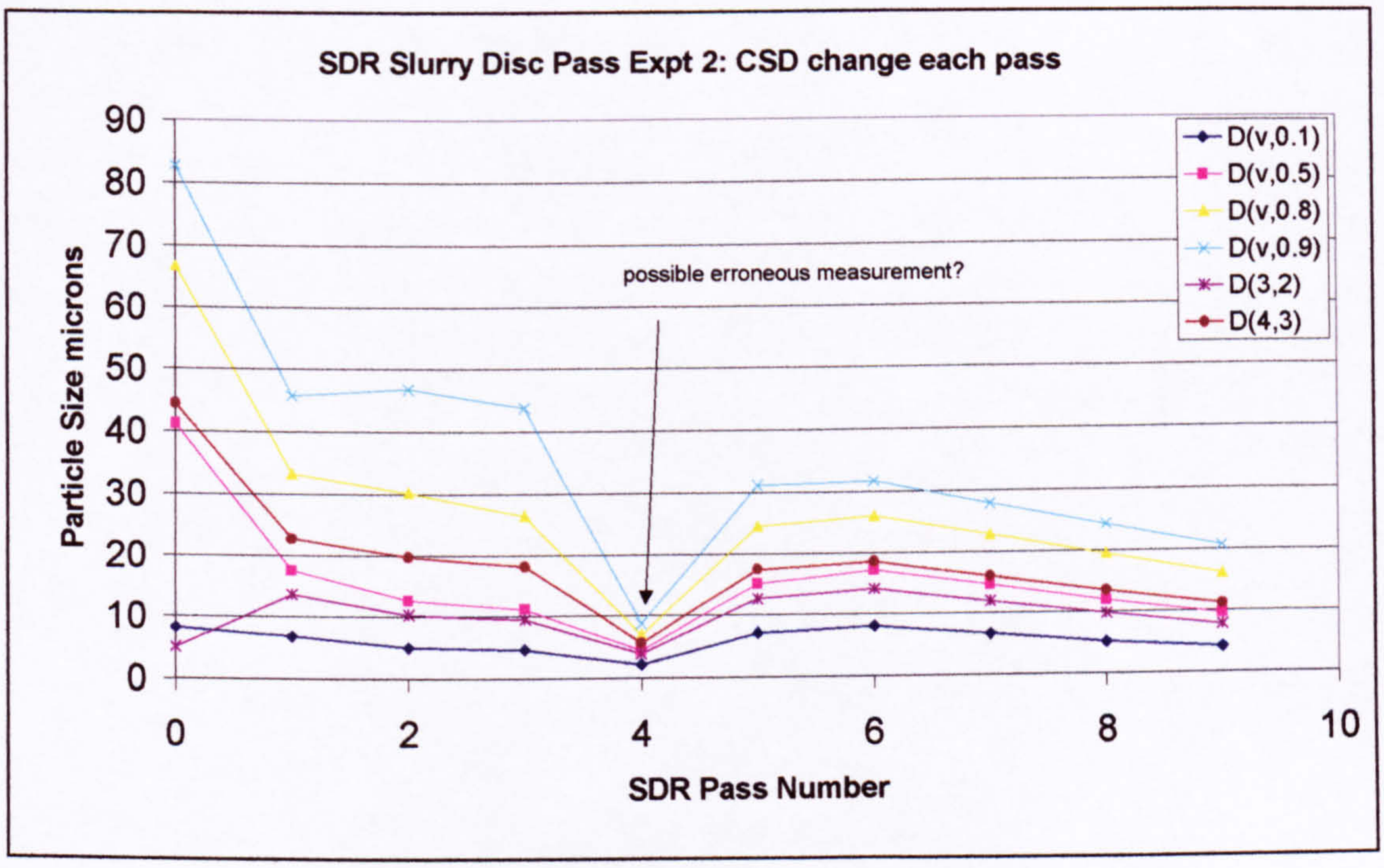


**Figure 6.14 Change in CSD with each pass over the disc**

In general it is seen that there is a reduction of particle size with each pass. However, it is suggested that disc pass 4 might be an erroneous analysis result due to its much smaller size than the data for the passes either side. It was noted on pass number 5 that the slurry appeared to becoming more viscous and then seemed to thin again after pass number 8, suggesting that there might be a lot of small particles in the slurry after pass number 4 and this in turn effected the viscosity.

The large agglomerated particles of $Ca(OH)_2$ in the slurry initially were broken down and small $CaCO_3$ particles formed from the carbonation. The biggest shift in the CSD is after pass 1. This would be due to the high shear conditions on the disc breaking agglomerated $Ca(OH)_2$ powder.

## 6.7 SDR/batch slurry CSD comparison

The CSD from the batch experiment is compared to that taken from the 2nd circulation experiment on the disc and the two disc pass experiments. The CSD graphs are seen in figures 6.15and the average particle size values are presented in table 6.5 below.

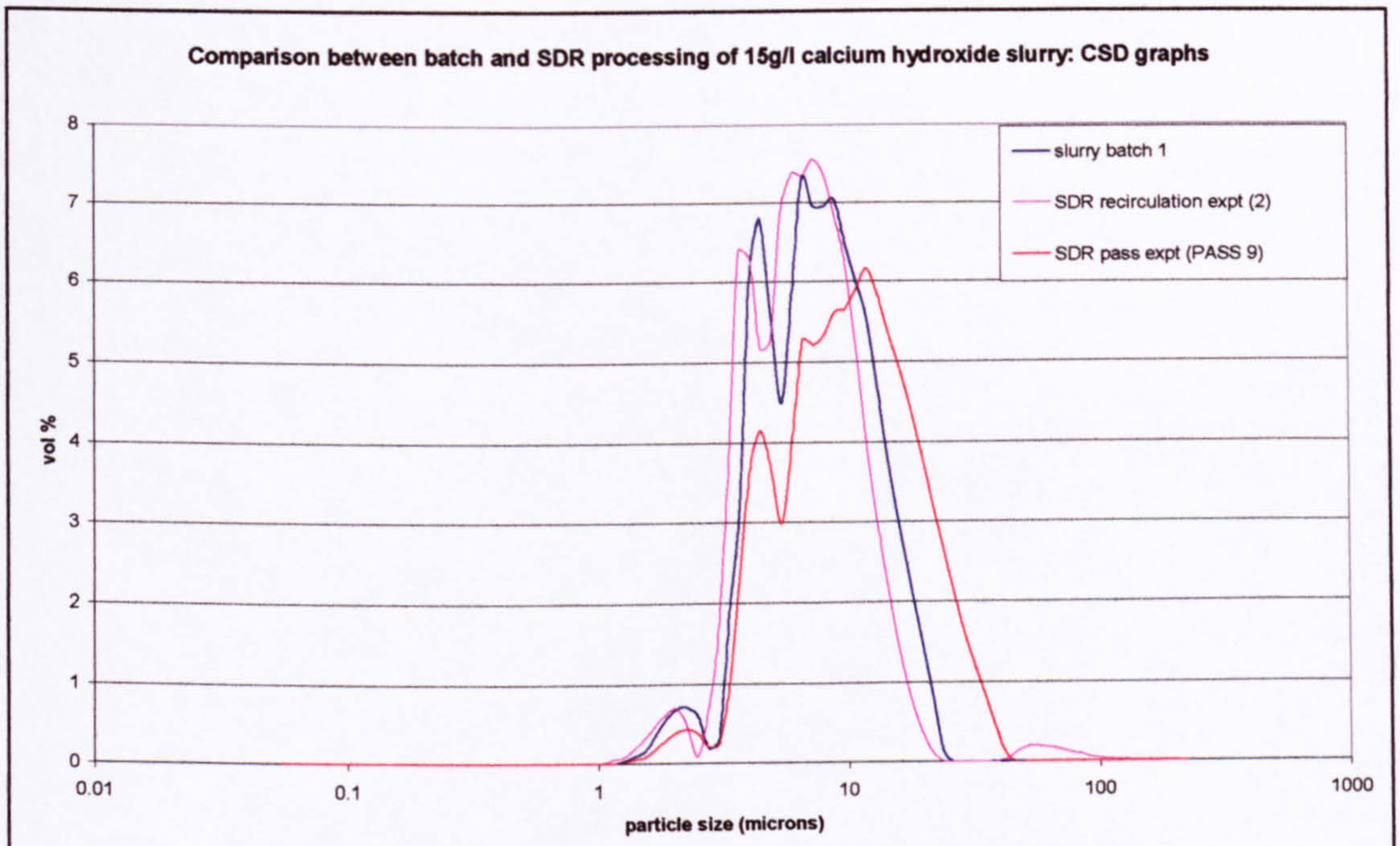


**Figure 6.15 CSD of batch and SDR 15g/l slurry experiments**

| | slurry batch 1 | SDR recirculation expt (2) | SDR pass expt (PASS 9) |
|---|---|---|---|
| **D(v,0.1)** | 3.77 | **3.38** | 4.13 |
| **D(v,0.5)** | 7.12 | **6.28** | 9.59 |
| **D(v,0.8)** | 11.11 | **9.47** | 16.16 |
| **D(v,0.9)** | 13.61 | **11.57** | 20.73 |
| **D(3,2)** | 6.1 | **5.45** | 7.74 |
| **D(4,3)** | 7.95 | **7.58** | 11.21 |

**Table 6.5 Summary CSD data of batch and slurry experiments**

The SDR recirculation experiment yields a smaller mean particle size than that in the batch, however for the disc pass experiment, the mean size is slightly larger than that of the batch. In all of the CSDs of batch and SDR in the figure 6.15, the shape of the distribution curves have the same 3-peak characteristics suggesting that the final product is very similar.

The reason for the larger CSD in the pass experiment may be described by the way the experiment was carried out. In both the batch and recirculation experiments, the carbonation was operated continuously such that the carbonation process is constantly changing the bulk volume CSD condition, as it is a continuous experiment. In the disc pass experiment, the product from the pass was collected in a separate vessel then dumped back in the feed tank for the next pass, the pH was taken and then the pumping started again. Overall, the processing time was longer than just the pass time due to these pauses in the process each time a pass was complete. This may have lead to the larger mean size of the product in the disc pass experiment. Agglomeration and/or growth from morphological transformation could be more prevalent during these pauses whereby vaterite crystals are dissolving, creating low supersaturation, which leads to growth and agglomeration of primary calcite crystals.

## 6.8 Comparison with other workers

(Chen et al, 2000) used a rotating packed bed (RPB) for the carbonation of lime. They found that increasing gas flow or slurry flow rate or rotational speed all contributed to reducing the carbonation time. Further, by increasing gas flowrate and slurry flowrate, the mean particle size was reduced. Increasing the initial slurry concentration led to an increase in the mean size. The RPB is a complementary and competing intensified device to the SDR, it's main benefit being the high liquid and gas loadings which can be applied to it without it flooding or low turndown it can operate at under normal conditions. Chen's work processed 3 litres of slurry in a recirculating operation using a torus with a depth of 50mm, 150mm outer diameter and 50mm inner diameter. Nominal conditions were 2980rpm, with a $CO_2$ flow of 7 l/min and a slurry flow of 83 ml/s. In the present study, the 150mm diameter disc rotated at 1000rpm and had a gas flow of 2 l/min (limited by the flow meters) and a slurry flow of approximately 17ml/s. Chen's lowest slurry concentration was 35g/l whereas in the present study, 15g/s was the highest. Carbonation times are compared below in figure 6.16 (the SDR was carbonation time was adjusted to account for processing 3 litres of slurry like the RPB).

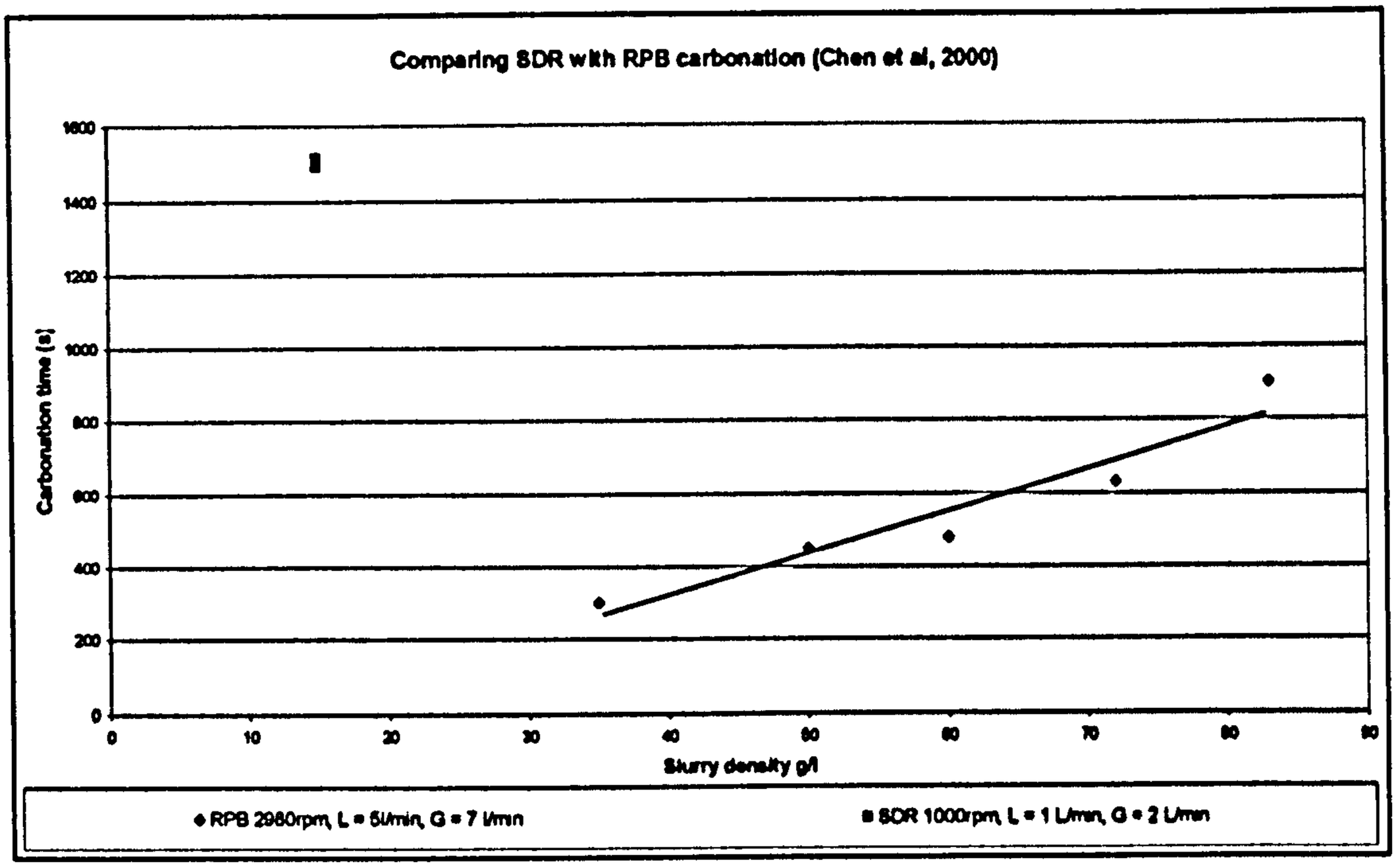


**Figure 6.16 Comparison of SDR and RPB (Chen *et al*, 2000) carbonation times**

The RPB in Chen's study appears to produce much lower carbonation times than the SDR did in the present study, however the SDR used lower liquid and gas flow rates and lower rotational speed than the RPB. With lower rotational speed the film thickness would be greater and therefore the mass transfer rate would be lower. Further work would be required to more closely compare relative carbonation rates of both devices. To scale up to an industrial unit, the RPB is scaleable by increasing the bed depth and torus diameter, the SDR can be scaled by increasing its diameter and by stacking discs on the same shaft. Both offer high mass transfer capability but it is difficult to compare like-for-like especially as the RPB has different packing types and the SDR surface may be enhanced by grooves etc to improve mass transfer.

Chen *et al* claim that these experiments were carried out in the absence of any chemical inhibitors. Their particle size analysis using TEM showed average particle sizes in the range of 30 to 80 nanometres. XRD analysis showed the crystals to be calcite. In the present study, the SDR yielded particles with a d[3,2] of 5.45μm. No other workers have reported primary particles so small from this process route. The claims presented seem remarkable considering it is a semi-batch process whereby the slurry is circulated through the RPB and then back to the batch vessel, product crystals mixing with unreacted slurry. There is no mention of agglomeration of the particles or the composition of the trace elements in the tap water used for the slurries. It might be possible that the tap water contains for example, lead, sulphate or magnesium ions,

which may influence crystal growth/agglomeration. Other workers cited in the present study observe agglomeration of primary $CaCO_3$ particles. TEM micrographs at very high magnification might not be showing representative samples of the CSD. It from these reasons that the particle size claims from the work by Chen *et al* is treated with caution.

## 6.9 Conclusions and recommendations to the slurry work

Several experiments have been performed in order to draw comparison between a batch carbonation of $Ca(OH)_2$ slurry and the same operation utilising an SDR as the absorber/mixer. In comparing the 2-litre batch operation with two SDR configuration there are perceived advantages the disc may have:

- In the circulation and disc pass experiments, it is suggested that the processing time is reduced or to put it another way, the carbonation rate has been increased. This could have great benefit in reducing production costs and increasing plant output.
- From the second disc pass experiment, it is seen that there is a large shift in particle size when the initial slurry is contacted on the disc. The spinning disc acts as a high shear device which breaks up the powder agglomerates and allows for faster dissolution of $Ca(OH)_2$.
- In the SDR-batch circulation experiment, not only was there a reduction in processing time over the batch but also it produced a smaller mean size of crystals.

The narrow range of experiments performed was due to restricted experimental time available when the Mastersizer was present. However, the SDR has performed favourably over the batch vessel for like-for-like operation parameters of batch volume, $CO_2$ flowrate and slurry concentration. A much bigger study would allow for performance to be better evaluated over a greater range of conditions and perhaps indicate what kind of intensified technology would suit the processing of precipitated calcium carbonate.

The SDR employed was only 150mm in diameter. This rig was not designed with optimised performance for gas-liquid mass transfer in mind but as the project progressed, ways of making improvement to mass transfer performance were

envisaged. These will be discussed in detail later. Its small size offered low residence time and a small area for mass transfer not ideally suited for these mass transfer operations. In considering using this disc diameter, it would require 9 of them to perform a once-through continuous approach to processing. This seems a little impractical in design especially when trying to design a cascade with gas flow to each disc in mind. In considering a SDR device for industrial applications, higher slurry densities would have to be considered along with larger disc diameters. Higher $CO_2$ flowrates could be considered; here the set-up was limited to a maximum measured flow of 2 litres/min Disc rotational speed could be considered as a performance parameter. Disc residence time and film thickness govern mass transfer characteristics so further enhancements could be made. Perhaps 2 or 3 passes would all that would be required for an industrial sized device of say 500mm in diameter with optimised process parameters.

Any further study would look at varying more parameters and in greater range. A larger diameter SDR rig would be useful to determine scale up performance. Light scattering CSD analysis is incredibly useful to determine product characteristics however some SEM analysis of samples would compliment any CSD data.

A study to further compare SDR with RPB performance would allow for better evaluation of the technologies as gas absorption/reactor devices.

# 7 Liquid-liquid experimental study

## 7.1 Introduction

According to (Mersmann, 1999), there is a case for precipitating small, uniform particles by inducing high supersaturation ratios with high rates of meso and micro mixing of the reagent fluids. (Cafiero *et al*, 1999) investigated $BaSO_4$ precipitation on the SDR from the combination of $BaCl_2$ and $Na_2SO_4$ solutions in equimolar quantities. In his work, he used very small flowrates (approximately 0.5ml/s from burettes) of reactants on a relatively large diameter disc (0.5m) at moderate rotational speed (200 to 1000rpm). His observations suggested higher nucleation rates than that obtained by (Nielsen, 1961) using a T-mixer for a supersaturation ratio of 100. In his experimental work with supersaturation ratios of 2000, he observed a reduction in mean crystal size as the rotational speed increased. In comparing with (Mohanty *et al*, 1988), he estimated that at a supersaturation ratio of 2000, the SDR increased the number of particles produced per unit volume by an order of magnitude over the T-mixer. At this level of supersaturation (Mohanty *et al*, 1988) stated that for supersaturation ratios over 2000, homogeneous nucleation predominated in this system.

From the author's repetition of Cafiero's work on the same equipment, the precipitation was seen to occur on the disc, however it was observed that the disc was not fully wetted by the reactants due to such a small flowrate from the burettes on a relatively large disc leading to film breakdown within a few centimetres of the feed points. A breakdown in the continuity of the film would make certain disc parameters such as residence time and film thickness impossible to determine by current model equations.

In the work carried out by (Jachuck, Hetherington *et al*, (2001), it was seen that in the case of $BaSO_4$ precipitation, by inducing very high rates of mixing for highly supersaturating conditions ($S_o$=5000), that very small particles can be obtained in a spinning cone reactor. Here, the experimental parameters of rotational speed (2000 to 10000rpm), reactant flowrate (4 to 20ml/s) and supersaturation ($S_o$=500, 5000) were widened. This was achieved using a much smaller spinning cone to provide the surface for film with a cone aperture of 89mm. This work also benefited from the use of a Malvern Mastersizer for determining crystal size distribution. The aim of the

experimentation was to induce very high rates of mixing within a very short reactor residence time.

In conclusion of the $BaSO_4$ investigations, it was shown that parameters such as reactant concentration, rotational speed and flowrate could influence precipitate size and shape when processed on a spinning cone/disc reactor. High rates of mixing led to rapid depletion of supersaturation and therefore smaller particles were produced. At lower supersaturations it was seen that the higher mass transfer rates developed on the cone would increase the crystal growth rate when homogeneous nucleation was not the dominant mechanism.

The preceding investigations by the PIIC research group in the precipitation of $BaSO_4$ encouraged the author into extending this experimental work into the precipitation of $CaCO_3$ by liquid-liquid process routes on an SDR. One of the hypotheses was 'could the spinning disc reactor produce particles of $CaCO_3$ on the sub-micron scale of a consistent quality?' as had been seen with $BaSO_4$ precipitation.

By investigating the process conditions of this reaction route to calcium carbonate it was hypothesised as to whether such control of particle size could be obtained. The case for particle size control of $CaCO_3$ is more complex than that of $BaSO_4$. $CaCO_3$ has 3 crystalline polymorphs whereas $BaSO_4$ only has one. It would be ideal to have one particular polymorphic form and shape from the $CaCO_3$ precipitation. In the present gas-liquid work on $CaCO_3$, the supersaturation ratio was limited by the $Ca^{2+}$ ion concentration in solution and the rate at which $CO_2$ could be absorbed to create supersaturation in solution. In the present study of liquid-liquid reactions it is possible to create a calcium ion carrying solution and a carbonate ion carrying solution of such concentration that by mixing them together, they will create very high supersaturation ratios for the precipitation of $CaCO_3$.

## 7.2 Process route

### 7.2.1 Choice of reagents

There are many combinations of solutions containing calcium and carbonate ions separately, which may be mixed together to form a supersaturating solution and thus go on to precipitate $CaCO_3$. With an exhaustive list of component combinations, it was important to decide which might be most suitable. A major factor in the decision was the availability of laboratory and more importantly analysis time. The hypothesis

to be tested was the influence of mixing and supersaturation on the particle size so a single process route had to be followed to reduce the number of variables and therefore experiments. In considering which solutions to use, it was reasoned that precipitating $CaCO_3$ from calcium chloride ($CaCl_2$) and sodium carbonate ($Na_2CO_3$) would be interesting to look at for the following reasons.

- The reagents are relatively cheap to obtain from suppliers suggesting that it would be a cost effective process to produce $CaCO_3$ from this route.
- They combine in 1:1 stoichiometric ratios from solutions of the same molar concentration.
- The ions left in solution are $Na^+$ and $Cl^-$ which can be recovered as common salt or reprocessed as a brine in electrolysis to generate more reagents by creating NaOH to absorb $CO_2$ and generate more $Na_2CO_3$ solution and to dissolve $Ca(OH)_2$ (or limestone) in hydrochloric acid to form more $CaCl_2$ solution. The recycling of solution ions is an element of green chemistry philosophy and good economic practice, as it will aid in the reduction of waste treatment and raw material input.

Other liquid-liquid routes were considered but due to time constraints on laboratory and analyser time, they had to be omitted from the final experimental plan. One other route omitted was the reaction between $Na_2CO_3$ and $CaNO_3$. This is obviously similar to the chosen route but with $NO_3^{2-}$ ions being in solution instead of $Cl^-$.

Another route that could be considered is the reaction between $Na_2CO_3$ solution and calcium hydroxide solution/slurry. It is feasible that slurry could be processed on the disc if the mass transfer rate was high enough and the residence time long enough. Here, the $CO_2$ would have already been absorbed to form the carbonate so the reactants are already there in solution rather than carrying out the carbonation process on the disc simultaneous to the precipitation. Research could then be carried out as to the most suitable equipment for the carbonation of NaOH solution to form $Na_2CO_3$ (or $NaHCO_3$) solution, the SDR only being required for the precipitation step. Here, very much higher concentrations of carbonate in solution can be achieved as the solubility of NaOH is very much greater than $Ca(OH)_2$.

Overall, it was seen with the liquid-liquid route that the initial supersaturation could be more easily controlled and calculated because the concentrations are known from solution concentration whereas the supersaturation cannot be determined for the gas-liquid work on this disc due to the gradual carbonation of the solution (and thus incremental supersaturation) occurring.

### 7.2.2 Additives

There are many possible chemical additives that could be used in influencing the size and shape of the crystals (e.g. starch, malic acid, citric acid, ascorbic acid and glutamic acid). Having control of the shape would allow better control of the product properties. In order to control morphology of the product, experiments were to be carried out with the presence of L-glutamic acid added to one of the solutions. (Manoli & Dalas, 2001) have demonstrated that L-glutamic acid can exclusively precipitate $CaCO_3$ in the spherical vaterite form. Glutamic acid was added to the working solution in their experiments of a concentration of $6.8 \times 10^{-4}$M. Their constant composition technique used calcite seeds to initialise the precipitation and pH control by pipetting potassium nitrate into the precipitator during the experiment. In the experiments in the present study of glutamic acid in the role of precipitation, pH was measured but not controlled and no seeding experiments were undertaken.

### 7.2.3 Further considerations

If more experimental time had been available, several possible routes could have been evaluated to see which would be most suited to the fast processing on the SDR. Accordingly, investigations into the role of additives and surface modifiers could have been carried out to determine what chemistry would be involved in providing the best conditions for controlling particle size and shape on the SDR.

In trying to prove the hypothesis that high rates of mixing coupled with high supersaturation can yield small uniform crystals then experimental planning was conducted with this foremost in mind.

## 7.3 Overview of the liquid-liquid experimentation

The two reactants where of equimolar concentrations such that it required the same reactant volume of each to mix to complete the reaction.

For this study, both SDR and batch reaction work was carried out. A 1-litre batch vessel was employed for this study. The batch reaction was operated in semi-batch mode whereby one of the solutions was charged into the flask initially and then agitated. The second reagent was pumped in at a know flowrate until an equal volume of each reagent existed within the vessel and the precipitation was deemed complete.

For the experimentation performed on the SDR, both reactant feeds were pumped onto the disc with equal flowrate and the product collected from the drain tubes. Rotational speed and flowrate could be manipulated to allow two degrees of freedom alongside reactant concentration.

In order to examine the effect of the supersaturation ratio on the product size and shape, 3 reactant concentrations were used that would correspond to 3 levels of supersaturation when mixed together in equivalent volumes. These supersaturations were determined from solubility data of the $CaCO_3$ and the solution concentration giving supersaturation ratios of 180, 720, and 1800, the solution concentrations being 0.05, 0.2 and 0.5M respectively. Higher solution concentrations than this would lead to a precipitate that was so viscous, it was impossible to process in the batch or on the disc and hence the supersaturation ratio achievable for the system was limited.

The effect of glutamic acid was studied for each of the supersaturation ratios. Glutamic acid was added to the calcium chloride solution in a ratio of 1:2 with the calcium ion concentration. This was the smallest ratio used by (Manoli & Dalas, 2001) during their experiments in precipitating vaterite.

#### 7.3.1.1 Preparation of reagents

Both $CaCl_2$ and $Na_2CO_3$ solutions were made up in 5 litre batches in large flasks. The correct amount of powder was weighed corresponding to molar concentrations of 0.05, 0.2 and 0.5M to produce supersaturation ratios of 180, 720 and 1800 respectively when the two solutions were mixed in equal volumes during the reaction run. The powder was added to 4.8 litres of de-ionised water and allowed to dissolve. Once the powder

had completely dissolved the volume of solution was made up to 5 litres with de-ionised water.

In preparing the reagent solutions for the experimental work, it was observed that in preparing solutions of $CaCl_2$, solid impurities were discovered in the solution. These particles, red in colour, were thought to be iron oxide. The colour was more predominant in solutions of high concentration and once it was determined that these particles were in the chemical feedstock (Calcium Chloride hexahydrate RECTAPUR BDH cat no 22311297), then steps were made to remove them. It was deemed necessary to try and remove the particles from the solution as it was seen that they could act as nucleation sites during reaction and cause error in size analysis. The particles were filtered from the reagent solution by passing the solution through 0.2μm Nalgene filter membranes.

When making calcium chloride solution containing glutamic acid. The acid powder was added after the calcium chloride powder had dissolved and filtered, the solution made up to its full volume once the glutamic acid had dissolved.

### 7.3.2 Experimental setup

For this set of experimental work, two Cole-Parmer gear pumps had been made available. In the previous work involving the gas-liquid reaction experiments, peristaltic pumps had been used. It was known that these exhibit a degree of pulsing in their delivery of flow and therefore can lead to inaccuracies in the flowrate entering a vessel or propagating across the surface of a disc. The gear pumps deliver flow at a much more constant (and therefore accurate) rate. Both had control boxes that allowed for proper calibration and setting of flowrate.

### 7.3.2.1 The batch reactor experimental set-up

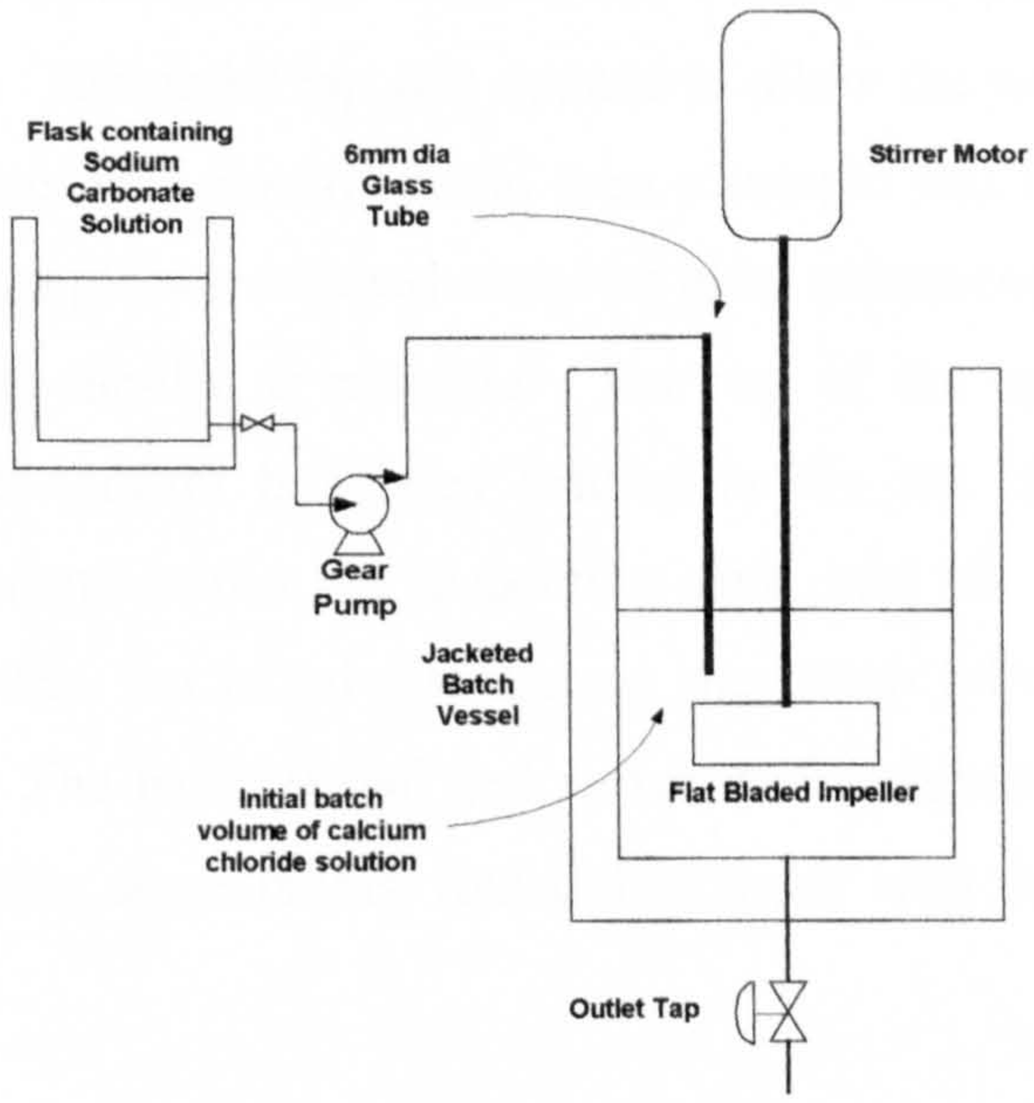


**Figure 7.1 Batch reactor set-up for liquid-liquid experiments**

Figure 7.1 represents the batch reactor equipment set-up. These experiments are preformed in semi-batch mode whereby one reactant is in the reactor vessel at the beginning of the run whilst the other is added at a predetermined flowrate. The flow is stopped once equal volumes of both reactants are in the reactor vessel.

Sodium carbonate solution charged in a separate flask is pumped using a gear pump through PVC tubing where it connected to a length of glass tubing, 6mm in diameter, whereby the fluid is delivered into the reactor vessel at a height of 10mm above the stirrer blade tip. This region is considered to be where the highest turbulence is created within the vessel and therefore the highest mass transfer. The stirrer is a flat blade paddle 60mm long and 20mm high. The reactor vessel was 120mm internal diameter and made of Pyrex.

The rotational speed of the stirrer for each of the experiments performed was set at 210rpm. This was calibrated using a stroboscope with the stirrer motor set on the first position on the control dial. The rotational speed was kept low due to shaft vortices being produced at higher rotational speed settings on the dial. 500ml of calcium chloride solution was contained within the batch vessel at the beginning of the experimental run. Care was taken as to prevent any sodium carbonate entering the vessel before pumping began. The glass tube was removed from the reactor and

washed before each run and the tube clamped to stop fluid leakage into the vessel. Agitation was started 20 seconds before the sodium carbonate flow was started. Once 500ml of sodium carbonate had entered the vessel, the pumping was stopped but stirring continued. The outlet tap was opened to allow the product out. The first 100 millilitres of product was discarded and then a sample was collected in a beaker. A few drops of the sample were spread onto two glass microscope slides and placed on a hot plate to dry as rapidly as possible. The rest of the sample was used in CSD analysis. The Mastersizer had been readied before the start of the run. A few millilitres were pipetted into the dispersion unit until the obscuration was within recommended levels. An initial distribution was taken followed by four more at 2-minute intervals. The batch vessel and stirrer were washed with weak hydrochloric acid to dissolve scale deposits then rinsed thoroughly with de-ionised water ready for the next run.

### 7.3.2.2 The spinning disc reactor experimental set-up

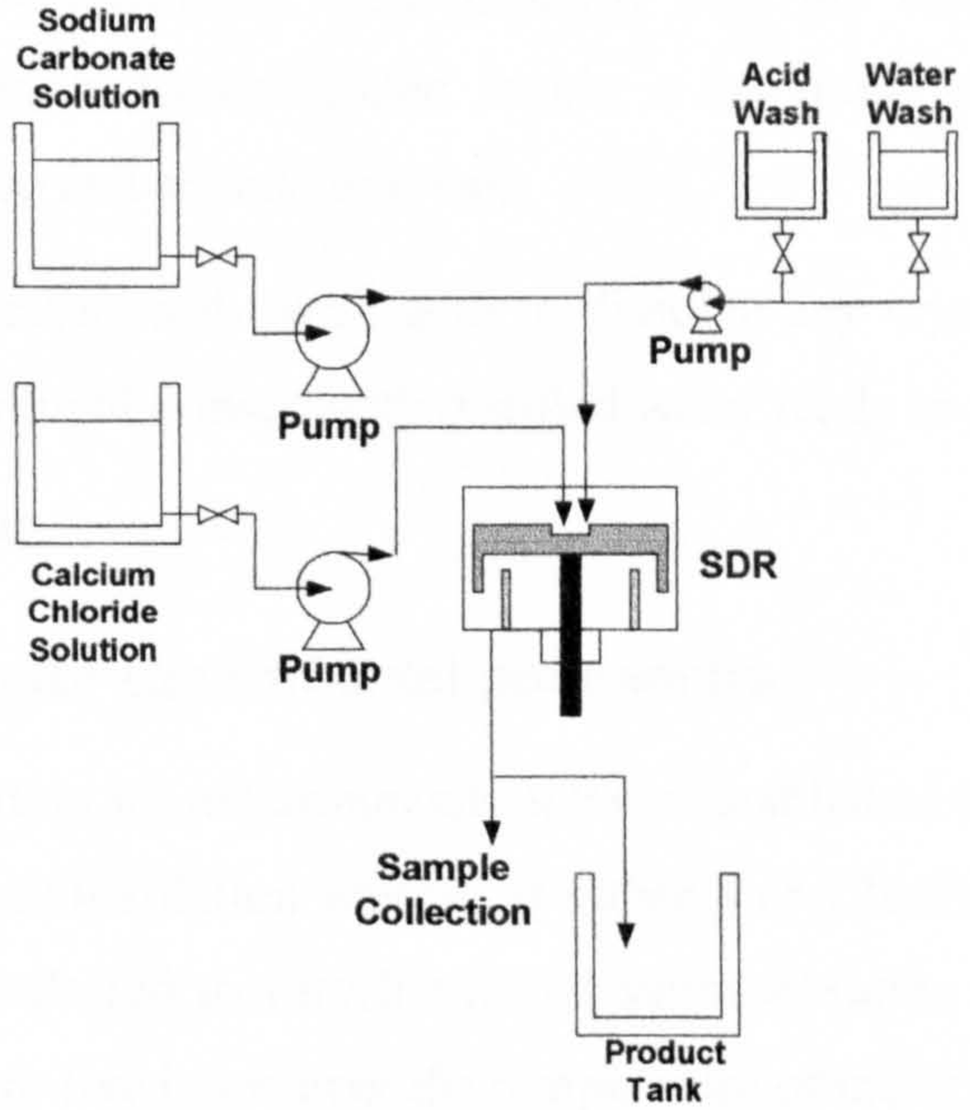


**Figure 7.2 SDR experimental set-up for liquid-liquid reactions**

Figure 7.2 shows the experimental set-up for the SDR experiments. The SDR rig was the same 15cm diameter disc used in the gas-liquid experiments. The reactants were stored in a flask before being pumped using a gear pump for each. A separate feed for acid washing and water rinsing and delivered by peristaltic pump. The gear pumps delivering the reactants were calibrated and tested.

The feed of the two reactants could be delivered in two ways. The first set-up had one feed into the centre well on the disc through a single 3mm diameter pipe The second feed went into a ring feeder which had sixteen 1mm holes in it at a radius of 12.5mm from the centre to distribute the flow. The second arrangement had the two feeds directly fed into the centre well, each through a 3mm diameter pipe. This allowed for the effects of feed position upon product quality to be investigated.

On performing a run, the disc rotation was started followed by the lubricating water to the bearings. The flowrates of the reagents was selected on the gear pump controllers and the pumps started. The first 100ml of product flowing out of the drain tube was allowed to drain into a bucket to allow for start up variances. A 50ml beaker was used to collect product for sampling. The flow of the reactants was then stopped.

As with the batch reactions, a few drops of the sample were spread onto two glass microscope slides and placed on a hot plate to dry as rapidly as possible. The rest of the sample was used in CSD analysis. The Mastersizer had been readied before the run started. A few millilitres were pipetted into the dispersion unit until the obscuration was within recommended levels. An initial distribution was taken followed by four more at 2-minute intervals.

The rig was first washed with weak acid to dissolve any crystal residues within the reactor and then thoroughly rinsed with distilled water ready to perform another run.

### 7.3.3 Experiments

#### 7.3.3.1 Batch reactor experimental parameters

Two degrees of freedom for experimentation were established for these batch runs; the flow rate of the $Na_2CO_3$ solution was set at either 8 or 12ml/s and the initial reagent concentrations were altered to vary the initial supersaturation ratio. Reactor volume and stirrer speed were fixed, however the temperature of the reactants/equipment were subject to the vagaries of the weather since there was no heating in the pilot plant laboratory during this study. The temperature of the reactants was measured using glass thermometers to an accuracy of 0.25°C. Temperature of the reactants fluctuated between 15 and 19°C. Heated water baths for the reactants and reactor vessel had been considered but no equipment capable of performing the task was available during this research period.

### 7.3.3.2 SDR experimental parameters

Three degrees of freedom were examined in the SDR experiments. The reagent concentrations, disc rotational speed and reactant flowrate were all varied to achieve this. The reagents were taken from the stock solutions made up as previously outlined to achieve three different supersaturation ratios. The rotational speed had three settings of 500, 1000 and 2000 rpm. The reagent flowrate was set at 4, 8 and 12ml/s for each reactant.

### 7.3.3.3 Other experimental parameters

For experiments performed on the disc at the lower supersaturation ratio of 180, the effect of feed point location was examined. The experiments were performed on the SDR using the arrangement of one feed into the centre of the disc and the other through a ring feeder. Four of the runs were repeated with both the reagent feeds being fed into the centre well of the disc. By examining the feed points on the SDR, information might be gleaned as to how best to get the two reactants mixed in order to achieve the tightest product CSD.

The addition of L-glutamic acid to one of the feeds was also examined in order to discover any effect it might have on the morphology of the crystals. For chosen runs experiments on the SDR or in the batch, the experiment was repeated with glutamic acid dissolved in the $CaCl_2$ solution.

## 7.3.4 Sample analysis and data collection

Each experiment had product samples collected for analysis. A slurry sample was taken and analysed using the Malvern Mastersizer to determine CSD characteristics and any change they might experience over several minutes. Microscope slide samples were also taken of each experiment. Some of these slides were examined under SEM to scrutinise crystal shape and size and to compliment the CSD analysis.

## 7.4 Crystal size distribution results of L/L experiments

In carrying out the experimental investigations for the liquid-liquid reaction route to $CaCO_3$, the use of the Mastersizer was available. From the previous study into the gas-liquid route, it was seen that there was a change in the CSD with time. It was thought that perhaps agglomeration and/or Ostwald ripening was occurring during these analysis periods. Since $CaCO_3$ is capable of forming as calcite, aragonite and vaterite in these experiments, then the use of the analyser to look at the change in CSD was seen as a useful tool in determining product size and stability. In the analysis with this study it was decided to take multiple CSD analyses for each experiment in order to gain insight the possible change in CSD over time, usually taking 4 or more CSDs at 2-minute intervals for each sample collected from an experiment for analysis. The CSDs for each experiment were plotted on the same axis in order to view any change that might occur during the analysis period. This allows us to see what happens with the crystals over time to see what effects might happen to the product. All the graphs for the results here are contained within the Appendix section 9.2.

### 7.4.1 The change in CSD during analysis of experiments with $S_0$=180

Four experiments from the disc were chosen at random and one from the batch for the initial supersaturation, $S_o$=180. Each of the graphs was interrogated.

**180FMRH (SDR: flow @ 8ml/s for each reactant, rotational speed @ 2000rpm)**

It appears that the 1st CSD has larger particles than subsequent ones, suggesting that agglomerates break up in dispersion unit after the first analysis. There is a small increase in particle size after second CSD (figure 9.7).

**180FHRH (SDR: flow @ 12ml/s for each reactant, rotational speed @ 2000rpm)**

There is a decrease in particle size after 1st CSD followed by increase from 2nd to 3rd/4th/5th CSD (figure 9.8).

**180FLRH (SDR: flow @ 4ml/s for each reactant, rotational speed @ 2000rpm)**

There is a decrease in particle size after 1st CSD followed by increase from 2nd to 3rd/4th/5th CSD. There are some large particles >100microns, these could be gas bubbles in the dispersion unit (figure 9.9).

Note: SEM shots are available for this experiment

**180FHRM (SDR: flow @ 12ml/s for each reactant, rotational speed @ 1000rpm)**

There is a decrease in size from 1st to 2nd CSDs. The amount of smaller particles diminishes in 3rd/4th/5th CSDs. The proportion of large particles in 50-100 micron range increase as result. Particles in 10-micron region remain approximately the same in 2nd-5th CSD. This suggests agglomeration of small particles over time (figure 9.10).

**180BATCH-FM (stirred batch containing 500ml $CaCl_2$ with $Na_2CO_3$ added at 8ml/s, stirrer speed 210rpm)**

There is a decrease in particle size after the 1st CSD followed by an increase from 2nd to the 3rd/4th/5th CSD (figure 9.11)

**180BATCH-FH (stirred batch containing 500ml $CaCl_2$ with $Na_2CO_3$ added at 12ml/s, stirrer speed 210rpm)**

There is an increase in particle size from 1st to 2nd CSD then a decrease to 3rd (but with larger tails), then an increase to 4th and 5th. Tails above 100microns suggest air bubbles in analyser (figure 9.12).

Note: SEM shots are available for this experiment

### 7.4.2 The change in CSD during analysis of experiments with $S_0$=720

The comparison of CSD data is repeated here for three SDR experiments chosen at random and two batch experiments with an initial supersaturation ratio of 720.

**720FHRM (SDR: flow @ 12ml/s for each reactant, rotational speed @ 1000rpm)**

There is a reduction in particle size from 1st to 2nd CSD. Progressively larger tails occur on 3rd to 4th to 5th CSD as result of a decrease in smaller ones, suggesting agglomeration (figure 9.13).

**720FMRM (SDR: flow @ 8ml/s for each reactant, rotational speed @ 1000rpm)**

It appears that the 4th CSD data is overlaid by the 5th. The 3rd, 4th and 5th CSDs have peaks with very large particle sizes indicative of air bubbles in the analyser. Considering the distribution of crystals below 100 microns in each CSD, there is a reduction in size from 1st to 2nd. The 2nd to subsequent CSDs have a decrease in peak height around 2 microns (figure 9.14).

**720FLRH (SDR: flow @ 4ml/s for each reactant, rotational speed @ 2000rpm)**

There is a decrease in particle size from the 1st to the 2nd CSD suggesting a break down of agglomerates. There are increases in the 3rd to 4th and 5th CSDs particle size (figure 9.15).

Note: SEM shots are available for this experiment

**720BATCH_FM (stirred batch containing 500ml $CaCl_2$ with $Na_2CO_3$ added at 8ml/s, stirrer speed 210rpm)**

There is a decrease in the particle size until it reaches an almost constant analysis result after the 5th CSD. In the 5th, 6th and 7th results there is a two peaks, a small peak at around 0.3 microns and another at around 10 microns (figure 9.16).

**720BATCH_FH (stirred batch containing 500ml $CaCl_2$ with $Na_2CO_3$ added at 12ml/s, stirrer speed 210rpm)**

The 1st to 2nd to 3rd CSDs shows a decreasing particle size leading to a slight increase in CSD in 4th and 5th due to quantity of smaller particles (approx 0.5 microns) diminishing (figure 9.17).

Note: SEM shots are available for this experiment

### 7.4.3 The change in CSD during analysis of experiments with $S_0$=1800

The comparison of CSD data is repeated here for 3 SDR experiments chosen at random and 1 batch experiments with an initial supersaturation ratio of 1800.

**1800BATCH_FH (stirred batch containing 500ml $CaCl_2$ with $Na_2CO_3$ added at 12ml/s, stirrer speed 210rpm)**

The 1st and 2nd CSD seem to show agglomerates which separate in the 3rd, 4th and 5th. The 4th/5th show trimodal distributions (figure 9.18).

Note: SEM shots are available for this experiment

**1800FLRH (SDR: flow @ 4ml/s for each reactant, rotational speed @ 2000rpm)**

There is a decrease in size 1st to 2nd to 3rd/4th/5th. This is probably due to breakdown in agglomerates. There is a bimodal distributions in 3rd/4th/5$^{th}$ (figure 9.19).

Note: SEM shots are available for this experiment

**1800FLRL (SDR: flow @ 4ml/s for each reactant, rotational speed @ 500rpm)**

There appears to be a breakdown in agglomerates from 1st to 2nd to 3rd CSD. There is a trimodal distribution in later CSDs (figure 9.20).

**1800FHRH (SDR: flow @ 12ml/s for each reactant, rotational speed @ 2000rpm)**

There appears to be a breakdown in agglomerates from 1st to 2nd to 3rd. There is a bimodal distributions in latter CSDs (figure 9.21).

### 7.4.4 Overview of the CSD analysis results

In each of these experiments examined at initial supersaturation ratios of 180, 720 and 1800 there was the common effect of the 1st CSD having a larger particle size than the 2nd. This would suggest that there is some break up of agglomerates/aggregation or perhaps some Ostwald ripening during the 2 minutes between analyses. Agglomeration/aggregation/flocculation was observed whilst samples were being collected during each of the runs. This was obvious when agitation/flow had stopped i.e. when the product was sat in the sample beaker. The sample was gently swilled around in order to keep the product dispersed as much as possible, however, it is assumed that the crystals simply had a tendency to group together. The process that is happening here suggests a break up of agglomerates/aggregates/flocs during this initial 2-minute period in the analyser. Looking at the 3rd and subsequent CSD of each experiment, there maybe some ripening here as in quite a few cases with $S_o$=180, the peak of smaller crystals (<1μm) diminishes and the larger crystal peak shifts slightly to the right suggesting growth of larger crystals with the demise of small ones.

In conclusion, the CSD data suggests the formation of a product, which has a tendency to agglomerate upon exiting the spinning disc or batch reactor. This agglomerated product when in the analyser will break apart over a couple of minutes. Further time in the analyser shows a depletion of smaller crystals and growth of larger ones.

### 7.4.5 Effect of spinning disc parameters on final CSD mean crystal size

For each of the supersaturation ratios in the liquid-liquid study it was decided to trend the Sauter mean diameter, D[3,2], from the final CSD of each experiment to see what influence rotational speed and flowrate might have upon the final product size. Although it is argued that the product might still be undergoing Ostwald ripening

during this time, most experiments suggested that agglomeration was minimised at this time and that growth and aging was relatively slow. This is suggested by 4$^{th}$ and 5$^{th}$ CSD samples showing profiles that are very close to one another. Accordingly, any air bubbles in the analyser would be most likely to have disengaged with the sample at this time leading to more accuracy in the product sampling. Therefore, the last CSD of each experiment was deemed most suitable to trend in this way

## 7.4.5.1 SDR experiments performed at So=180

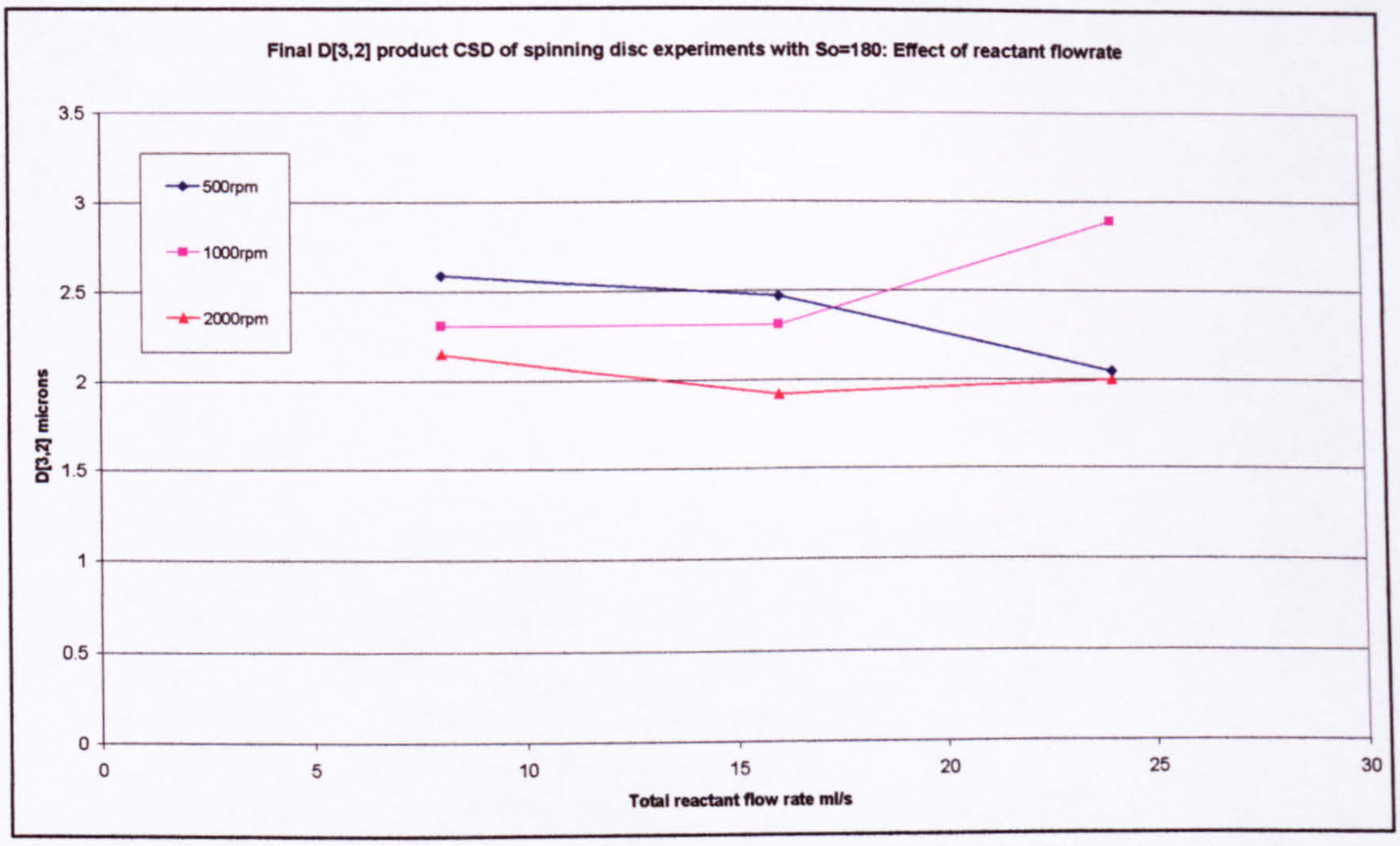


**Figure 7.3 Final D[3,2] product CSD of spinning disc experiments with So=180: Effect of reactant flowrate**

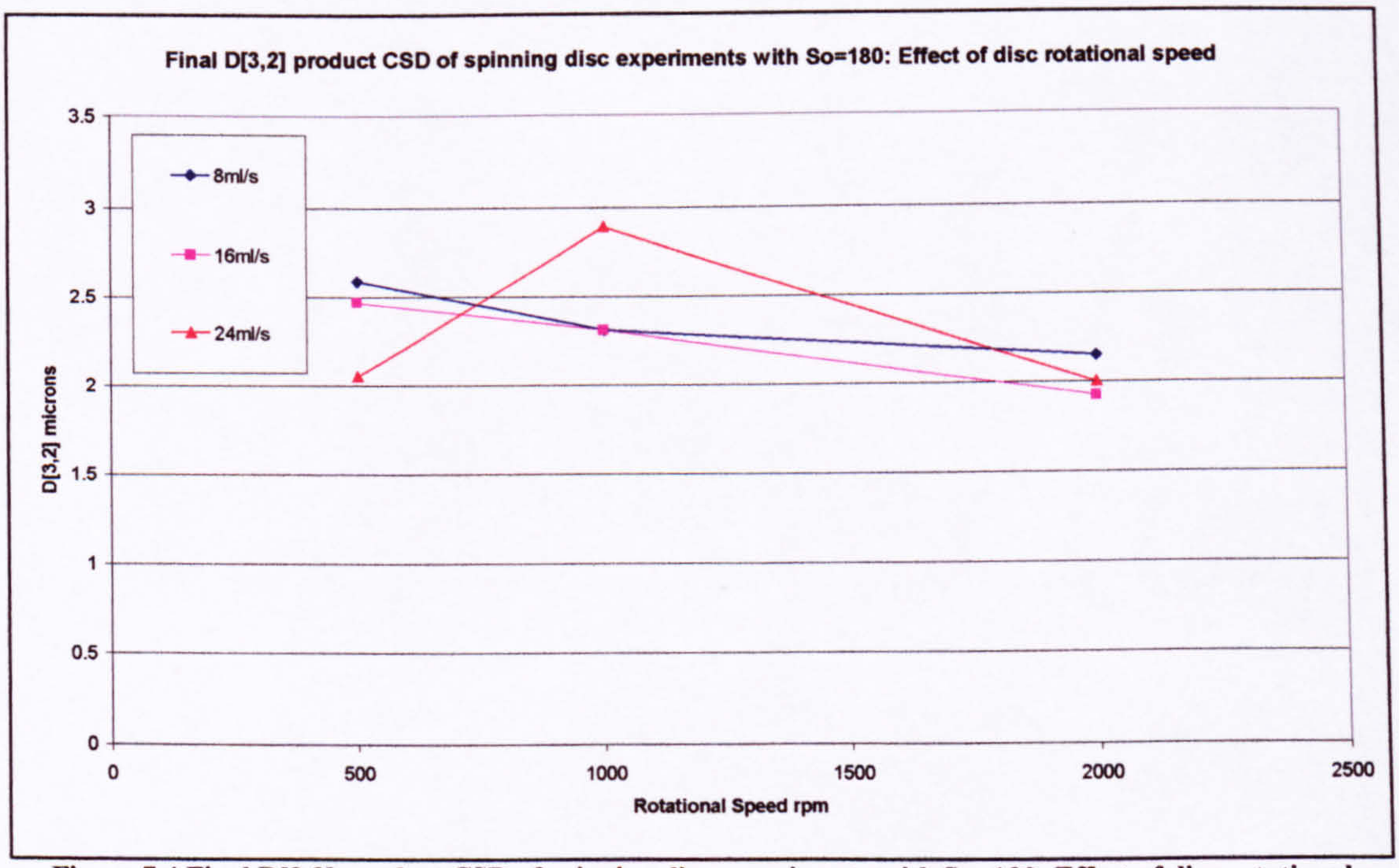


**Figure 7.4 Final D[3,2] product CSD of spinning disc experiments with So=180: Effect of disc rotational speed**

Experiments performed on the disc at So=180 yielded a D[3,2] in the range 1.92 to 2.89μm. In the case of total reactant flowrates of 8 and 16ml/s it is seen that increasing rotational speed decreases the final mean size.

## 7.4.5.2 SDR experiments performed at So=720

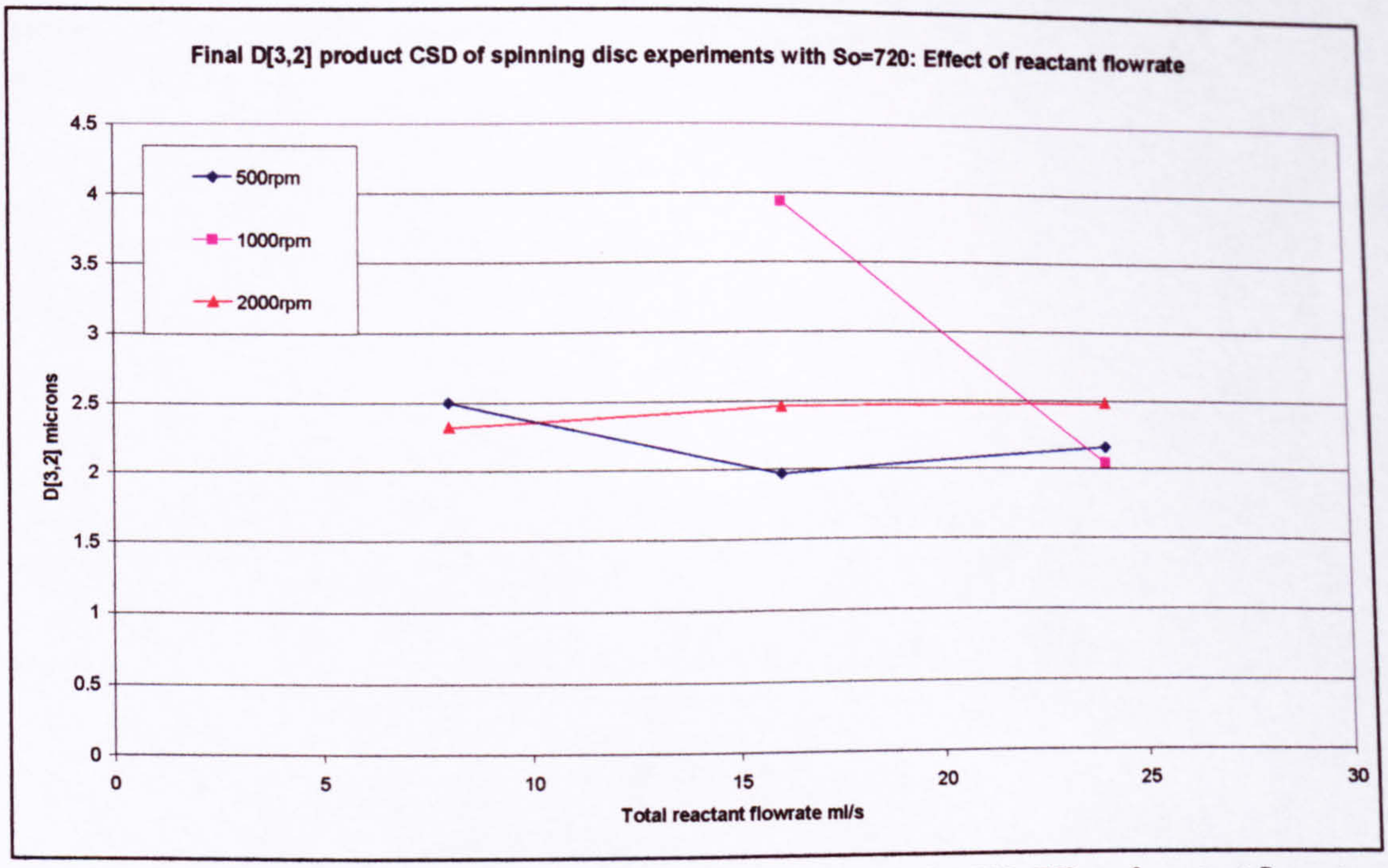


**Figure 7.5 Final D[3,2] product CSD of spinning disc experiments with So=720: Effect of reactant flowrate**

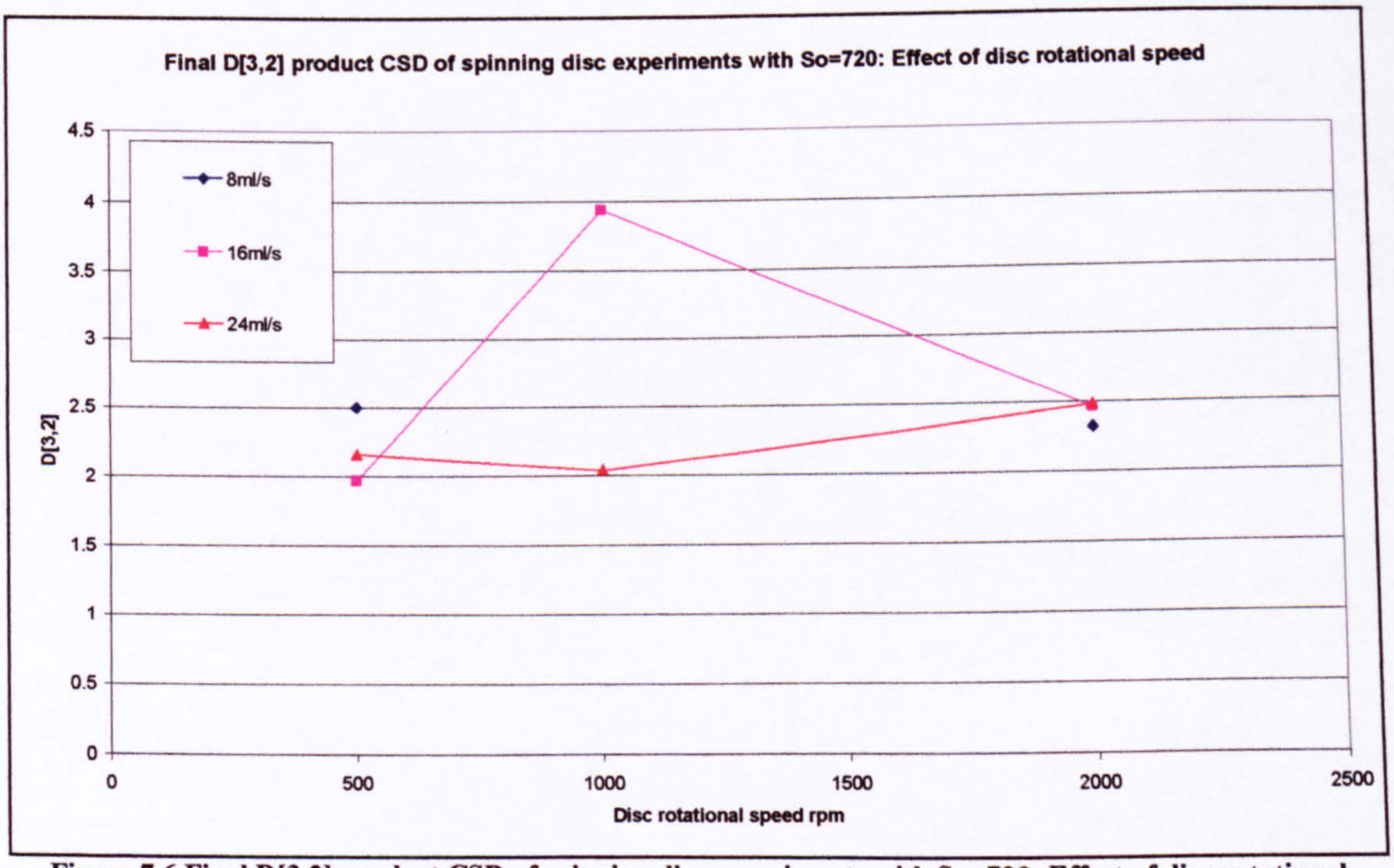


**Figure 7.6 Final D[3,2] product CSD of spinning disc experiments with So=720: Effect of disc rotational speed**

Experiments performed on the disc at So=720 yielded a D[3,2] in the range 1.97 to 3.94μm. In examining the CSDs of the experiment (8ml/s 1000rpm) that yielded the higher value of 3.94μm shows a peak around 100μm suggesting that there was air

bubbles present in the analyser. It may be concluded that this higher limit on the range is therefore erroneously high due to the skewing of the data due to the inclusion of the air bubbles. In considering the other experiments, it appears than changing the rotational speed and flowrate within these ranges have negligible effect upon the final mean size.

## 7.4.5.3 SDR experiments performed at So=1800

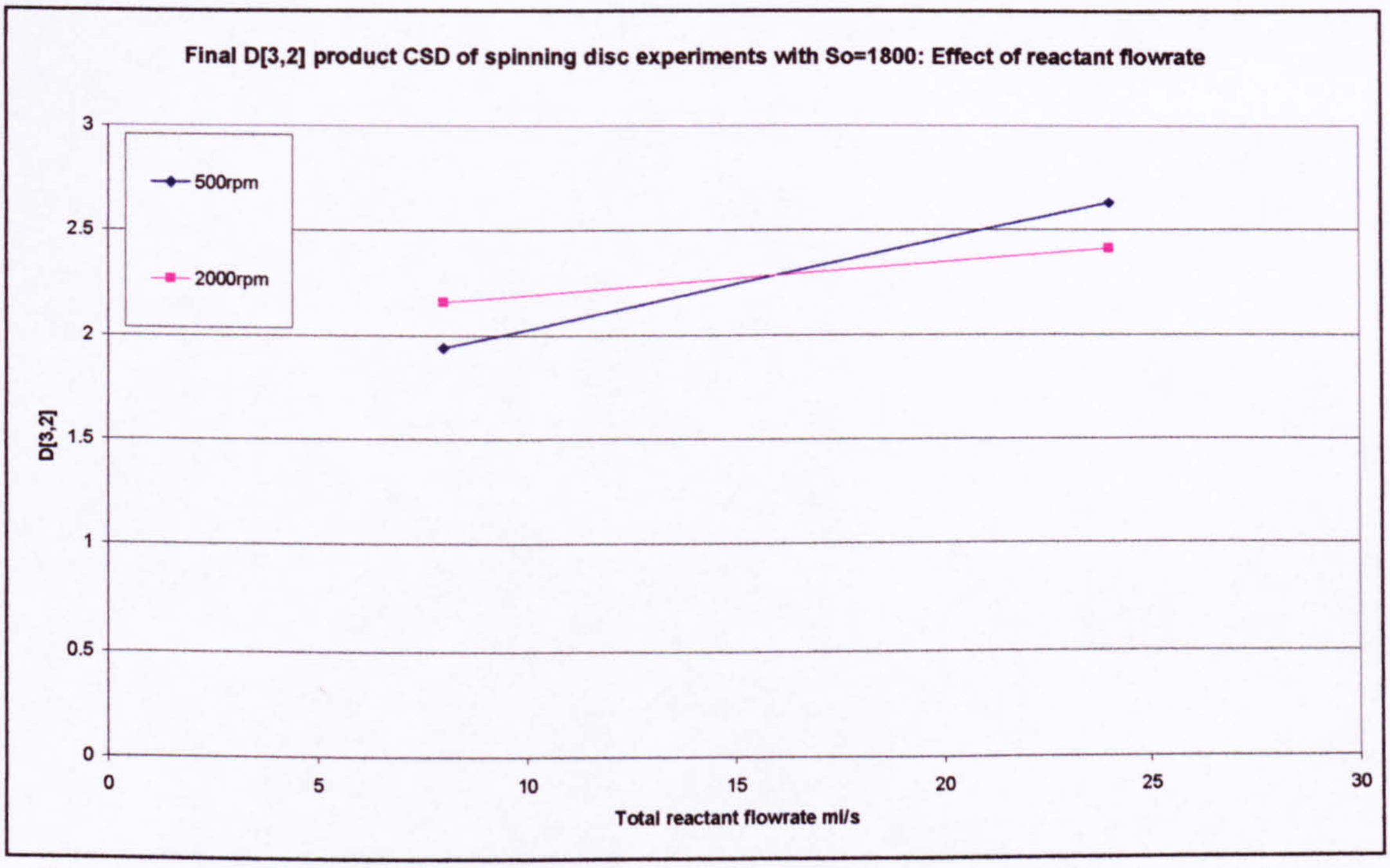


**Figure 7.7 Final D[3,2] product CSD of spinning disc experiments with So=1800: Effect of reactant flowrate**

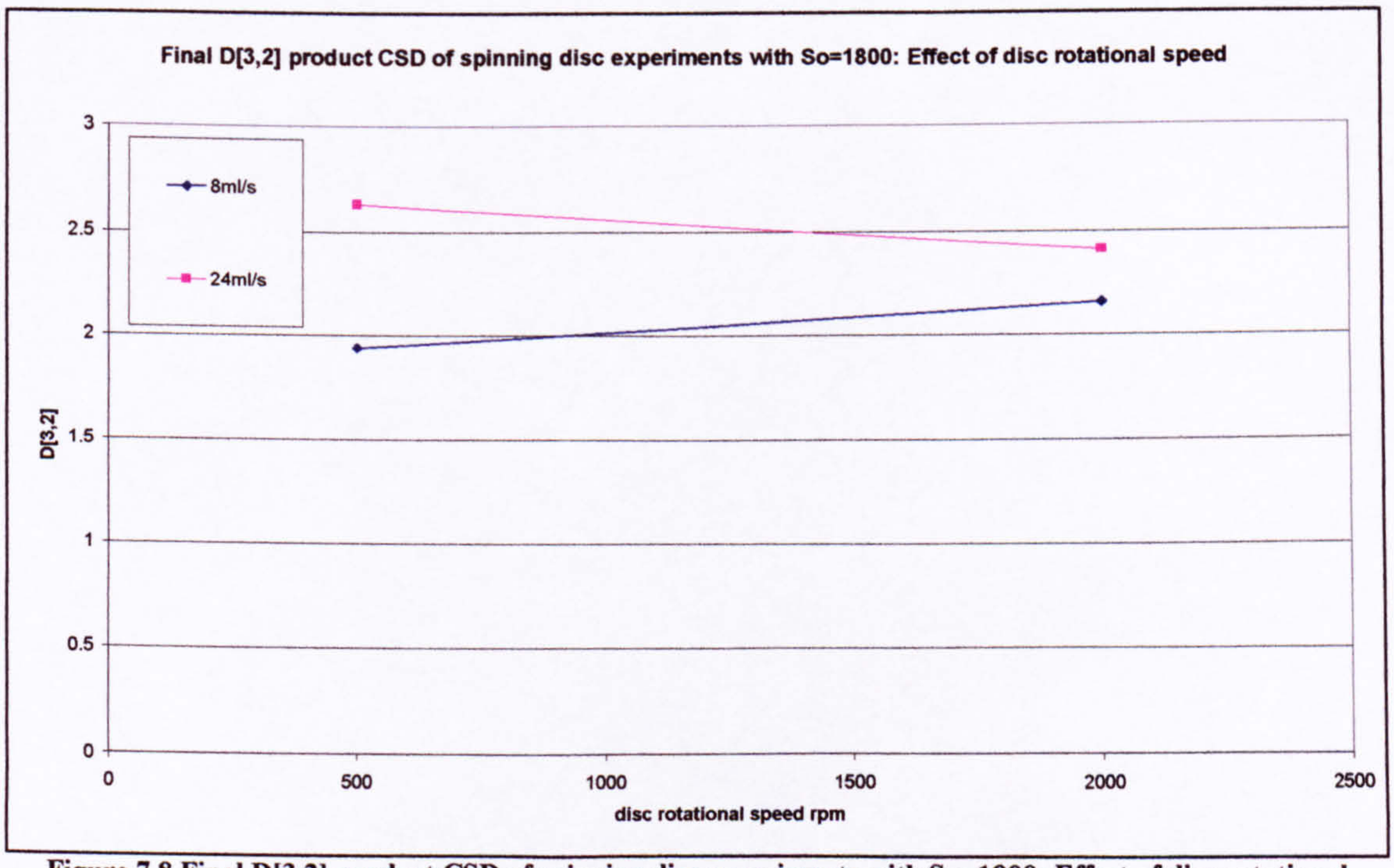


**Figure 7.8 Final D[3,2] product CSD of spinning disc experiments with So=1800: Effect of disc rotational speed**

In considering the trends produced for the experiments performed on the disc at So=1800 (figures 7.7 and 7.8), it is difficult to draw conclusions from just four experimental data points. It was seem that in increasing the flowrate for each

rotational speed led to an increase in the mean size. The experiments performed yielded mean sizes in the range 1.94 to 2.63μm.

### 7.4.5.4 Comments on the size distribution for all supersaturations

From the figures 7.3 to 7.8 for each the supersaturation ratios, although there are trends in the figures, it was unwise to come to immediate conclusions about parametric effects upon the final D[3,2]. This was because no experiments were repeated which would bring the validity of the data points into question. However, since similar CSD curves have been seen in the individual experiments, it can be suggested that the products are very similar from each experiment performed on the disc at the given supersaturation. Variation of product distribution and therefore mean size is a result of disc parameters, erroneous air bubbles being trapped and the formation of agglomerates. Further experimentation would have lead to more confidence in the data.

For all the experiments performed, it has been seen that the mean size is approximately in the same range for each supersaturation. However, with different crystal morphologies (see SEM work) existing at the different supersaturations lending to different CSD profiles being created, it should not be concluded from the final CSD data that the mean size parameter D[3,2] is not influenced by supersaturation.

### 7.4.6 Preclusion of further data analysis and interpretation

Having examined the CSD data for the liquid experiments, it seemed a futile exercise in gleaning more information from further trend analysis of experimental sets using derived variables such as residence time from such a small data-set. Development of good model data was incredibly difficult and therefore ruled out. For example, the precipitate was formed almost instantaneously on the disc surface where the two reactants mixed, so therefore would estimating the residence time on the entire disc, so that growth parameters could be estimated, be of any use? Furthermore, the precipitate resulting from the high supersaturating reactions was gelatinous when formed but appeared to thin into a free flowing liquid after a couple of minutes, any estimation of it's viscosity on the disc (by measurement) would not have any accuracy. An inaccurate set of physical properties for the precipitate would lead to errors in the hydrodynamic model. Since the onset of precipitation appears to take place in a small

annulus near the feed points in the centre, the hydrodynamic model for the whole disc would seen irrelevant to compute for this study since it is impossible to determine;

1. accurate physical properties for model estimates
2. further model inaccuracies due to the inertial mixing and flow effect of the fluids being fed onto the disc
3. where and when the growth of crystals starts and/or stops on the disc (assuming the process is complete on the disc).

If we split the precipitation mechanism up, then nucleation might occur at the boundary of the mixing fluid elements with growth occurring in a well-mixed low supersaturation zone, all of this in a small annulus close to the feed points and within (say) microseconds of reagent contact. The agglomeration and aging processes take minutes and hours and proceed outside the SDR's influence.

In all cases examined, the CSD analyses of each experiment were multi-modal. In the case of the experiments performed at initial supersaturations of 180 and 720, at least two crystal forms were seen in the SEM micrographs. Assuming these are different polymorphs (i.e. with different physical properties) then each would have it's own nucleation and growth rate models. The CSD mean crystal size is somewhat meaningless as it refers to a conglomeration of two separate products, the mean size representing somewhere between the two. Coupled with the agglomeration when first analysed, any crude estimation of nucleation rate using the mean crystal size is ruled out since this is dependent on having a meaningful mean size for the estimate. Furthermore, variation in the CSD for each experiment varied significantly between analysis intervals. In many experiments, the CSD appears to stabilise by the 3$^{rd}$ and subsequent analyses, i.e. after 4 minutes in analyser, but in other experiments, the CSDs do not produce a stable product after the period of time analysed. Analysing the final CSD from each experiment was the best method of determining SDR parametric effects since this would allow the longest time for primary agglomerates to break up which seemed to have the biggest impact on the early CSD results from each experiment.

As each experiment was performed only once then there is further uncertainty in the CSD data. A better understanding would have come from repeating the same experiment several times, however lack of laboratory time ruled this out. After the

pressures of trying to work in a laboratory, constantly interrupted by construction workers during that period, hindsight is a wonderful thing.

## 7.5 SEM micrograph results and analysis of liquid-liquid reactions performed during batch and SDR experiments

A limited number of SEM pictures were obtained after the experimental period was completed. SEM analysis of all runs was impossible due to cost constraints hence a careful selection of samples taken in order to tray and be as representative of the experimental work as possible. Slide samples for the 3 initial supersaturation ratios, for both SDR and batch and the addition of L-glutamic acid are compared. These micrographs serve as a qualitative tool by which the morphology of the crystals can be determined.

### 7.5.1 SEM analysis of batch and SDR crystals formed at an initial supersaturation ratio of 180

In figure 7.9 below are a set of micrographs showing the product of both batch and SDR operations at a supersaturation ratio of 180.

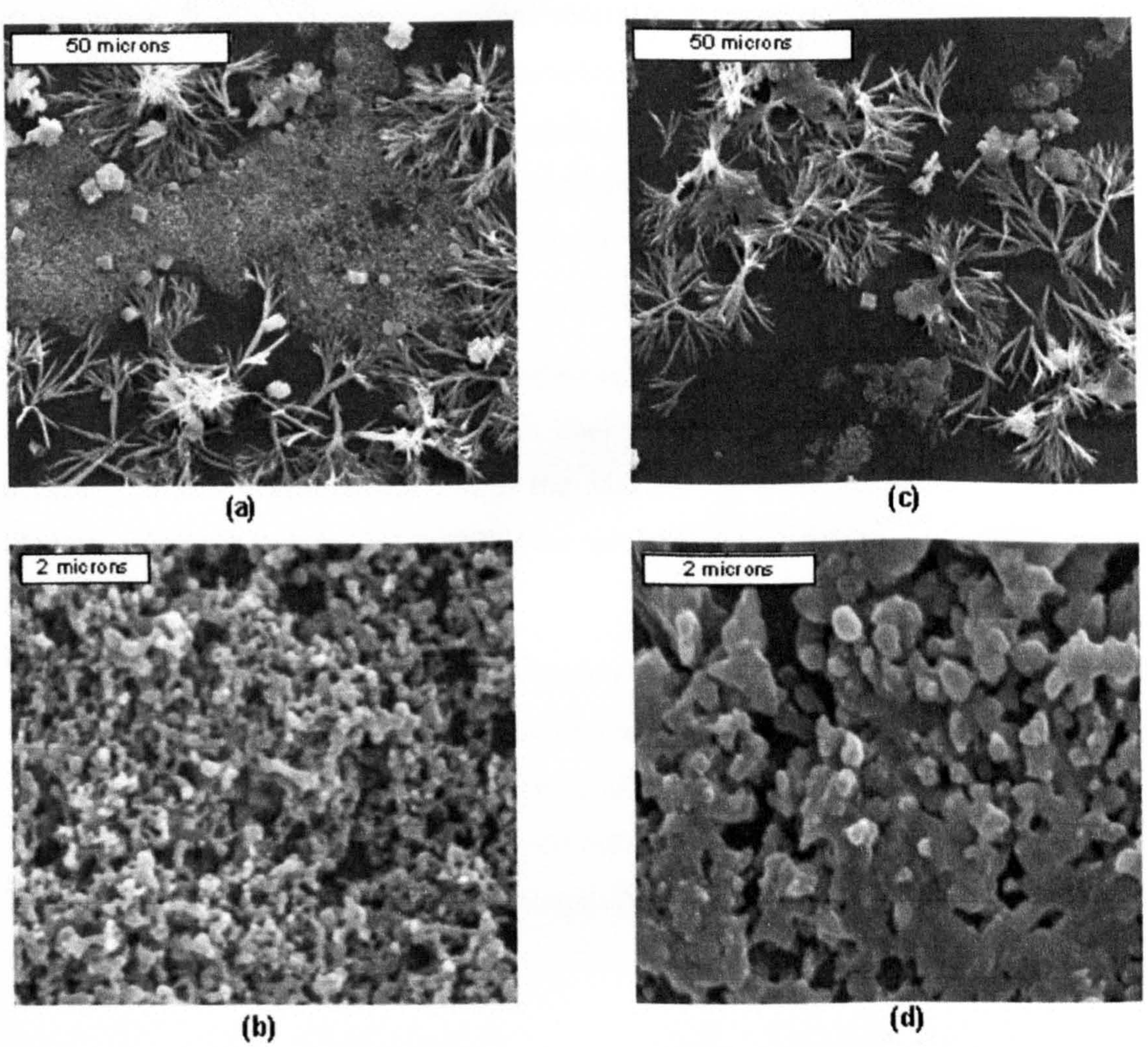


**Figure 7.9 Micrographs of batch and SDR products from $S_o$=180**

From figure 7.9 both the batch and SDR produce 3 forms of crystal. There are long needle-like structures, very small, agglomerated spherical crystals and some rhombic-cubic forms.

Needles tend to be formed by rapid mass transfer, low supersaturation environments, which is the case here, mixing of both the batch and SDR coupled with the low nucleation rates lead to these needle-like crystals to form. Needles might find application but are difficult to classify due to structure (e.g. in laser diffraction analysis

their shape factor is very much unlike spheres or cubes), the material is sensitive to breakage in both SDR and batch.

The very small crystals, possibly vaterite (seen in figure 7.9 b and d), might have been formed at the interface between reactants as the initial mixing occurred. The rhombs are also seen in the gas-liquid work and were assumed to be calcite.

There is a difficulty with morphological control in both cases. There is the possibility of there being 3 polymorphs in that samples. Needle-like structures of $CaCO_3$ are reported in literature to be that of aragonite. There are cases in the literature (Wray and Daniels, 1957) of at least two polymorphs precipitating simultaneously, depending on the conditions. This would appear to be the case here, however no X-ray diffraction was carried out on any samples, so this remains inconclusive.

For the SDR and batch at this supersaturation, the product is irregular and difficult to quantify relative amounts of crystal for each morphology. It is difficult to get any accuracy in size classification due to the Mastersizer assuming spherical types and changing shape factor can only modify the results by changing the shape factor to that of one other shape.

In general, the CSD data gleaned for these experiments shows bimodal distribution indicative of the small spherical material and of the larger needles and rhombs. Taking the average size by whatever method would allow for a good estimation of nucleation rate, since nucleation rate requires a well-defined median size even to make a crude estimate. More regular material (i.e. shape and/or size) would facilitate a nucleation rate estimate.

### 7.5.2 SEM analysis of the batch and SDR crystals formed at an initial supersaturation ratio of 720

In figure 7.10 below are a set of micrographs showing the product of both batch and SDR operations at a supersaturation ratio of 720

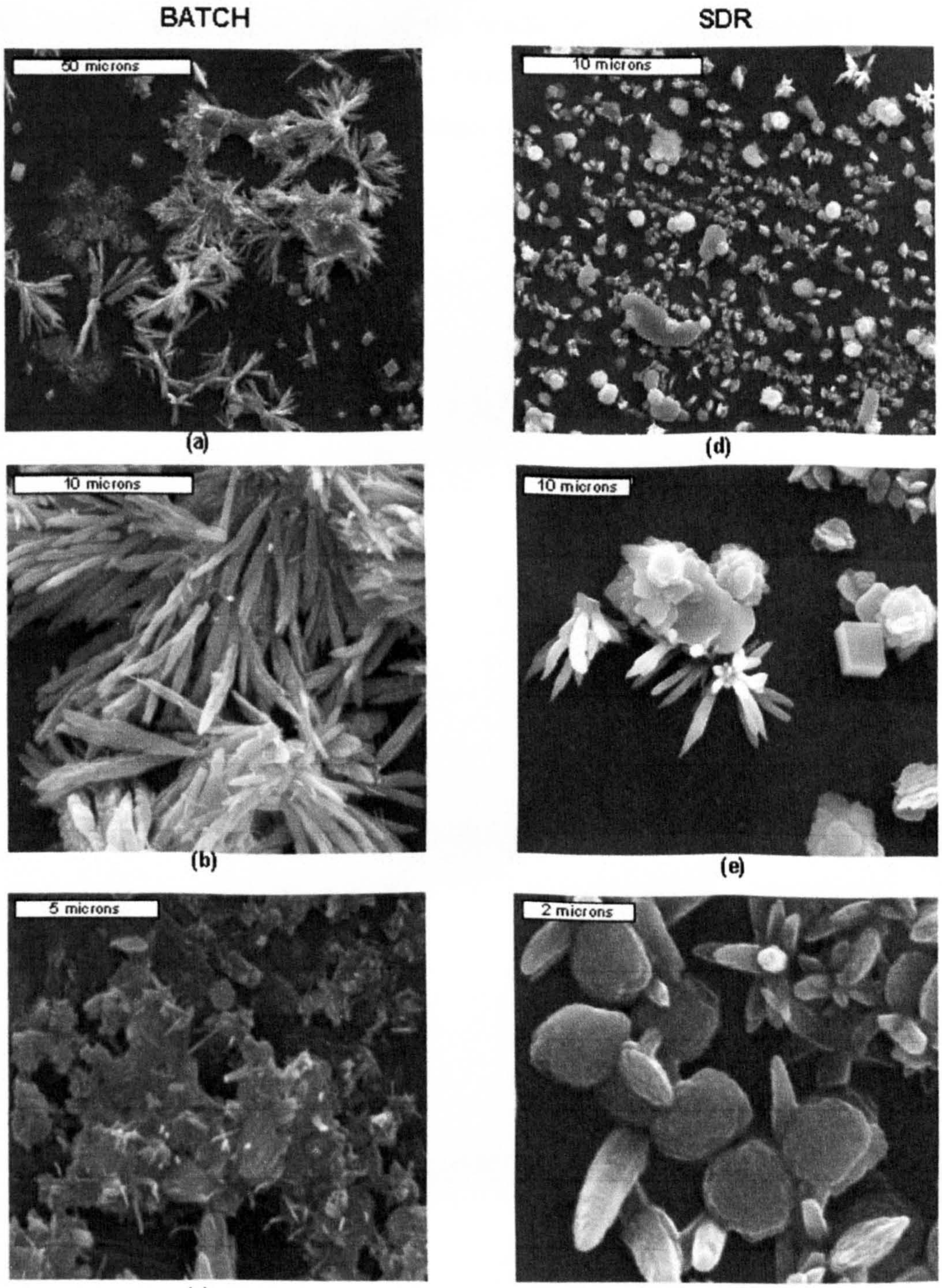


**Figure 7.10 Micrographs of batch and SDR products from So=720**

From figure 7.10 there is seen to be a difference between the batch and SDR products. The batch (fig 7.10 a, b and c) has agglomerates of very small crystals and larger needles seen at the lower supersaturation ratio of 180, however the needles formed on the SDR have not grown into long needles (with high aspect ratios) but rather have produced a shorter, spiky crystal along with platelets of around 2μm in size. These spiky crystals would have produced the needle-like structures had further growth occurred. This implies that the supersaturation was depleted quicker in the SDR than in the batch. The SDR also has some larger irregular shaped crystal in the product as well as a small proportion of rhombs.

### 7.5.3 SEM analysis of the batch and SDR crystals formed at an initial supersaturation ratio of 1800

In figure 7.11 below are a set of micrographs showing the product of both batch and SDR operations at a supersaturation ratio of 1800.

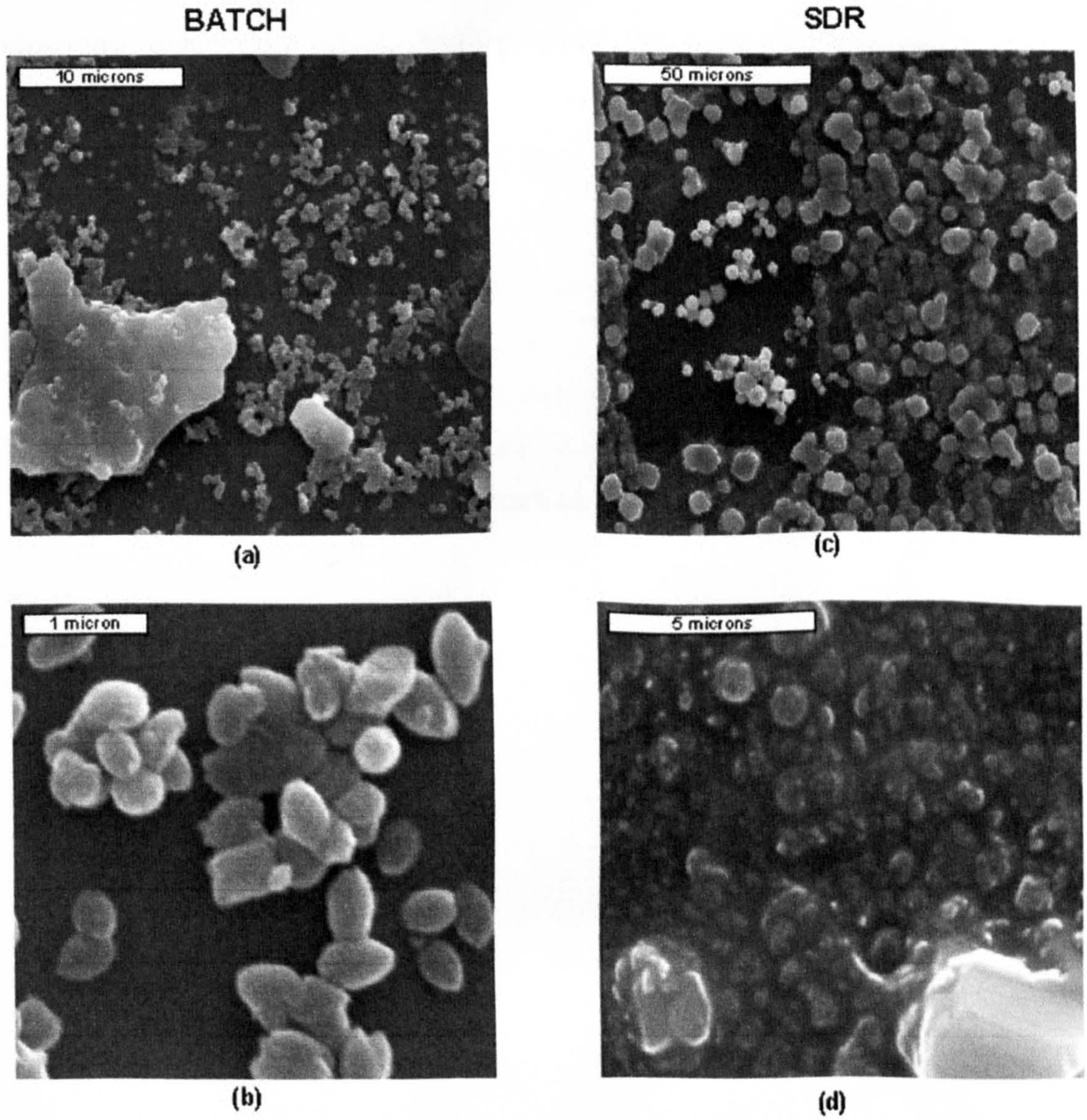


**Figure 7.11 Micrographs of batch and SDR products from So=1800**

For the supersaturation ratio of 1800, the batch had produced small (0.3 to 0.5 microns) rugby ball shaped crystals that have appeared to have agglomerated and growth between the individual crystals has occurred (see figure 7.11 a).

The SDR has produced rough spheres and cubes, appearing slightly amorphous in the picture suggesting dissolution and growth after the slide was taken or that the product

is the amorphous form of $CaCO_3$. There could be some nano-sized particles in there but it is difficult to tell from the slide.

In the experiments at this supersaturation, the product was initially very viscous, then as time progressed, it became free flowing again perhaps indicating a change of phase or a 'relaxing' of the slurry. This initial precipitate could be of the amorphous calcium carbonate form. (Koga, *et al*, 1998) prepared this from the $CaCl_2$-$Na_2CO_3$-NaOH aqueous route in the range $11.2 \leq pH \leq 13.0$ with primary particles of the size 0.05μm.

### 7.5.4 Effect of L-glutamic acid on the morphology of $CaCO_3$ precipitated in the present study

SEM comparisons were made between experiments with and without the presence of L-glutamic acid at an initial supersaturation ratio of 720. Its effect upon $CaCO_3$ morphology is compared in both batch and SDR under the same process conditions. The SDR had a flowrate of 4ml/s for each reactant and rotated at 2000rpm. The batch reaction was stirred at 210rpm with sodium carbonate pumped into the batch at 12ml/s.

### 7.5.4.1 SEM analysis of batch experiments performed in the presence of L-glutamic acid at an initial supersaturation ratio of 720

Comparison of the batch reactions performed with or without L-glutamic acid present are seen in figure 7.12 below.

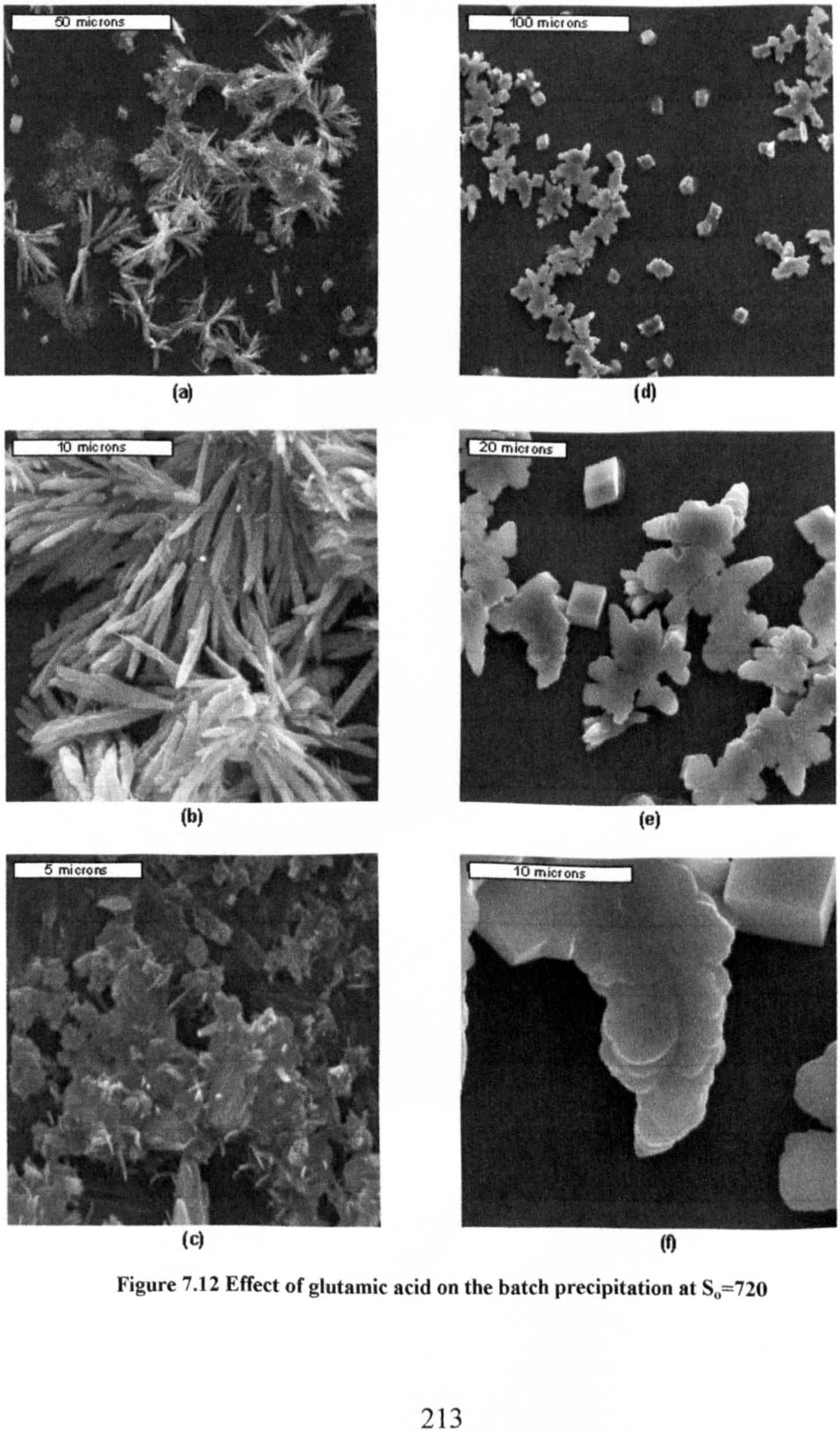


**Figure 7.12 Effect of glutamic acid on the batch precipitation at $S_o$=720**

In the batch reaction without glutamic acid, the crystals form needle-like structures (figure 7.12 (a) and (b) as well as some agglomerated platelet material in figure 7.12 (c). The batch reaction that takes place in the presence of glutamic acid shows different shapes (figure 7.12 (d), (e) and (f)). There are no needles and the crystal form is predominated by irregular fern-like crystals and some rhombs. From the slides, there is seen to be an effect on shape by the presence of glutamic acid. Since there has been no X-ray diffraction analysis of the slides, then it was impossible to tell which polymorphs are present.

### 7.5.4.2 SEM analysis of SDR experiments performed in the presence of L-glutamic acid at an initial supersaturation ratio of 720

Comparison of the SDR reactions performed with or without L-glutamic acid present are seen in figure 7.13.

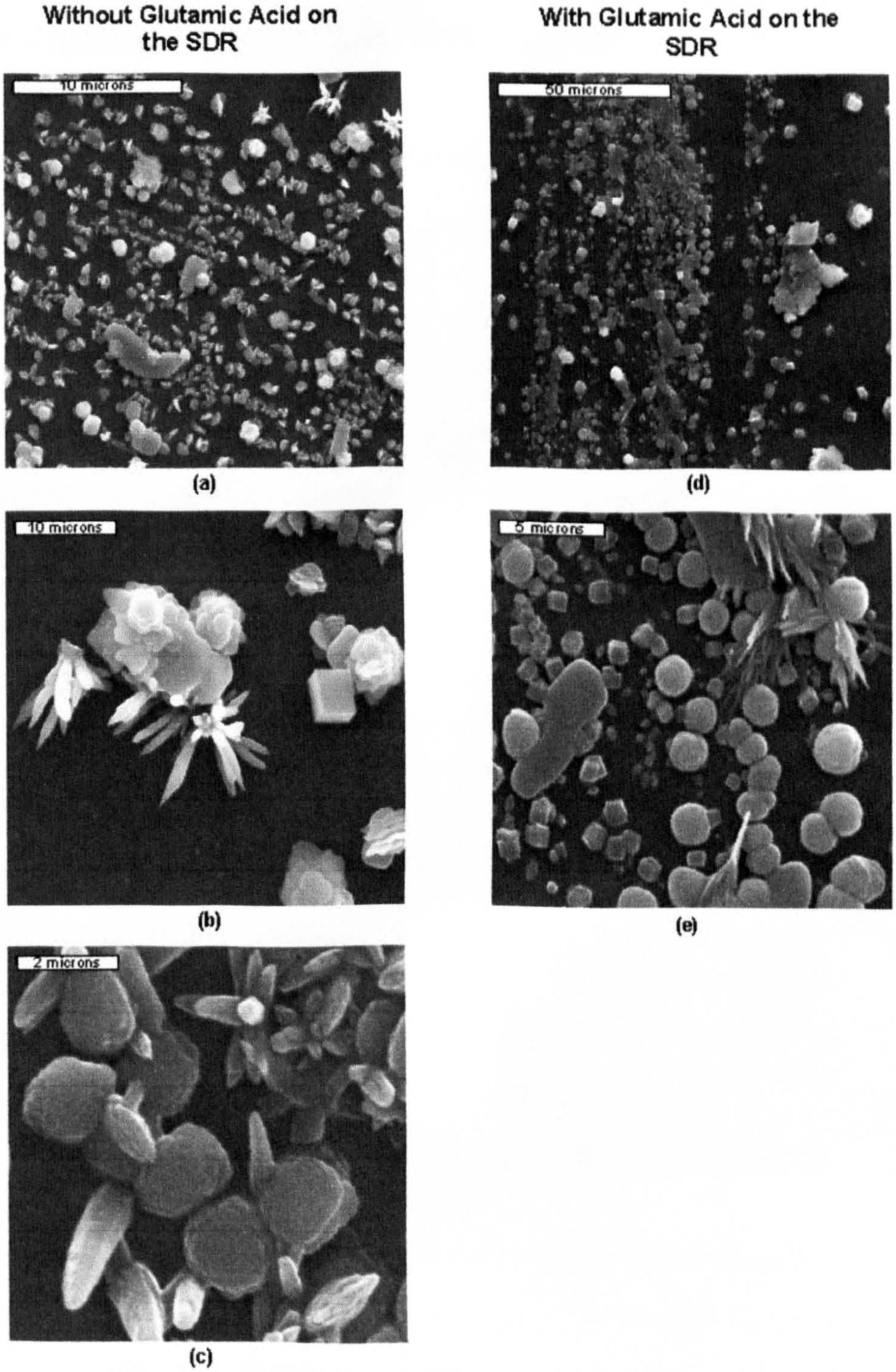


**Figure 7.13 Effect of glutamic acid on the SDR precipitation at $S_o$=720**

In the SDR reaction without glutamic acid, the crystals are predominantly platelet and short spiky in shape (figure 7.13 (a), (b) and (c)). In the presence of glutamic acid, the SDR produces spheres, approximately 2μm in diameter, in a significant proportion with some rhombs and some amorphous material. Some of the spheres seen in figure 7.13 (e) have formed twins.

#### 7.5.4.3 Analysis of batch and SDR experiments performed in the presence of L-glutamic acid

In figure 7.14 the effect of glutamic acid in the batch and SDR reactions is compared.

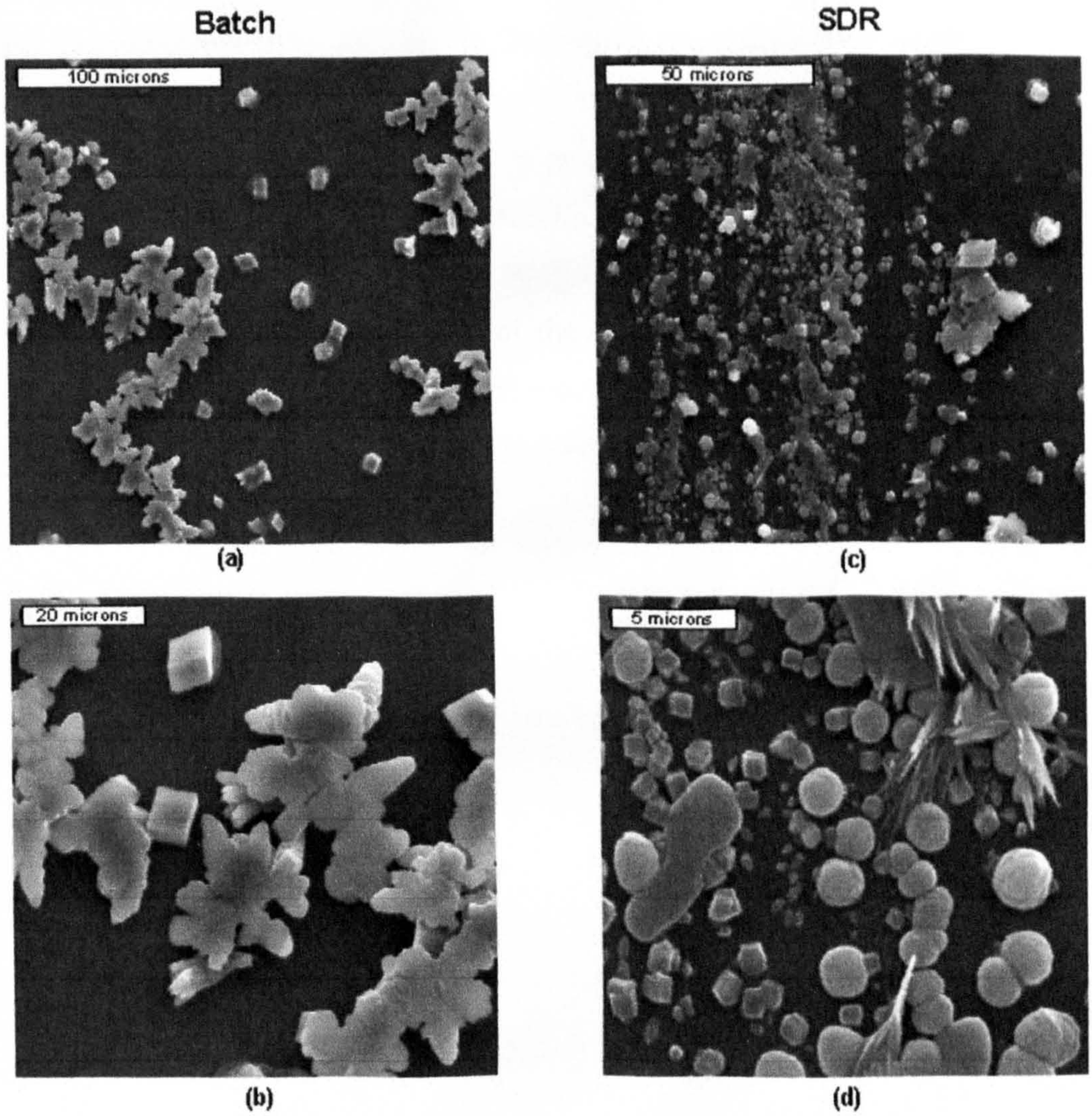


**Figure 7.14 Comparison between batch and SDR products in the presence of glutamc acid at $S_o$=720**

Spherulites are evident in the SDR whereas the batch produces more amorphous forms of crystal. In both cases, rhombs are produced. The relative proportions of each form are undeterminable.

### 7.5.5 Comparisons with other workers

Without the presence of additives in the precipitation process, (Wray and Daniels, 1957) demonstrated that aragonite was exclusively formed over 70°C but also aragonite tended to form at higher pH. The final pH of the $S_o$=180 reactions was in the region of about pH 10.0-10.4. If pH has an effect, then in the batch and (less so) in the SDR, regions of the reaction when higher pH is present (where reactants are poorly distributed), then the needle-like structures of aragonite might be seen. Calcium chloride and the sodium carbonate where both alkali in solution.

The SDR produced a large numbers of spheres in the presence of glutamic acid at an initial supersaturation ratio of 720. In the present study there was not enough time to refine the process enough to produce only vaterite (or just one shape). (Manoli & Dalas, 2001) saw 100% vaterite when in presence of glutamic acid and used seeded experiments. This process was a precisely controlled by a constant composition method using pH-controlled burettes. With a longer experimental study it would be possible to change the reactant, control the relative flowrates to the SDR and also precisely define the pH of the combined reactants. The pH could be kept in a certain region by the addition of non-reacting ion species such as KOH or NaOH.

### 7.5.6 Results: Comparison of SDR and batch final CSD profiles

At each initial supersaturation, the final CSD profile from a SDR and a batch experiment are plotted to see what variations in product size distribution exist between the two types of reactor.

#### 7.5.6.1 SDR vs Batch So=180

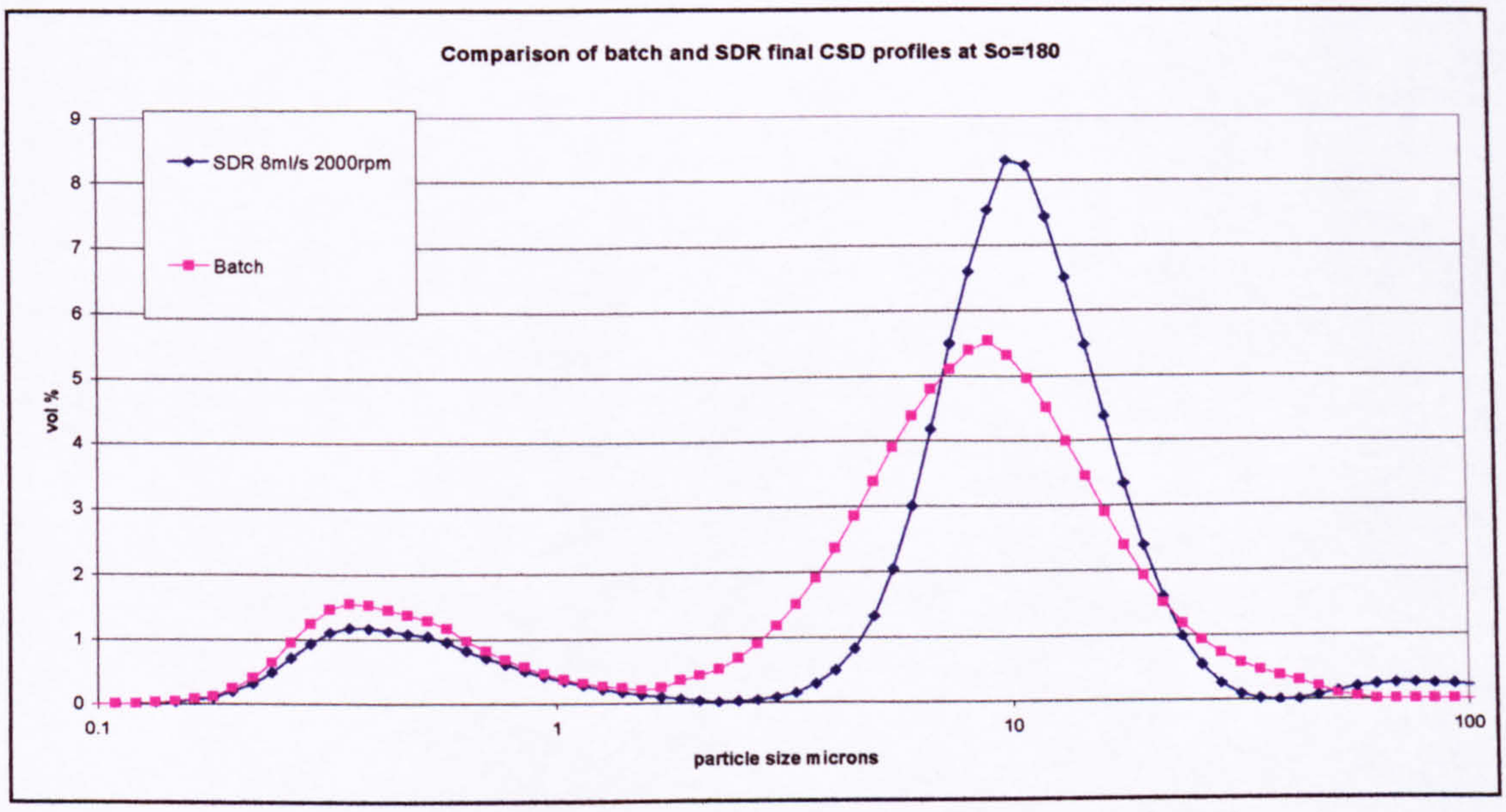


**Figure 7.15 Comparison of batch and SDR final CSD profiles at So=180**

From the SEM study, it was seen that at So=180, the products in the batch and SDR were the same. Both produced small spheres and larger needles. The peak below 1μm in the CSD profile would suggest these spheres whereas the peak at 10μm would suggest the needles. The SDR's CSD suggests it produces needles with a narrower distribution albeit with slightly larger size. This could be attributed to the disc's higher rate of mixing coupled with the low supersaturation leading to higher growth rates.

## 7.5.6.2 SDR vs Batch So=720

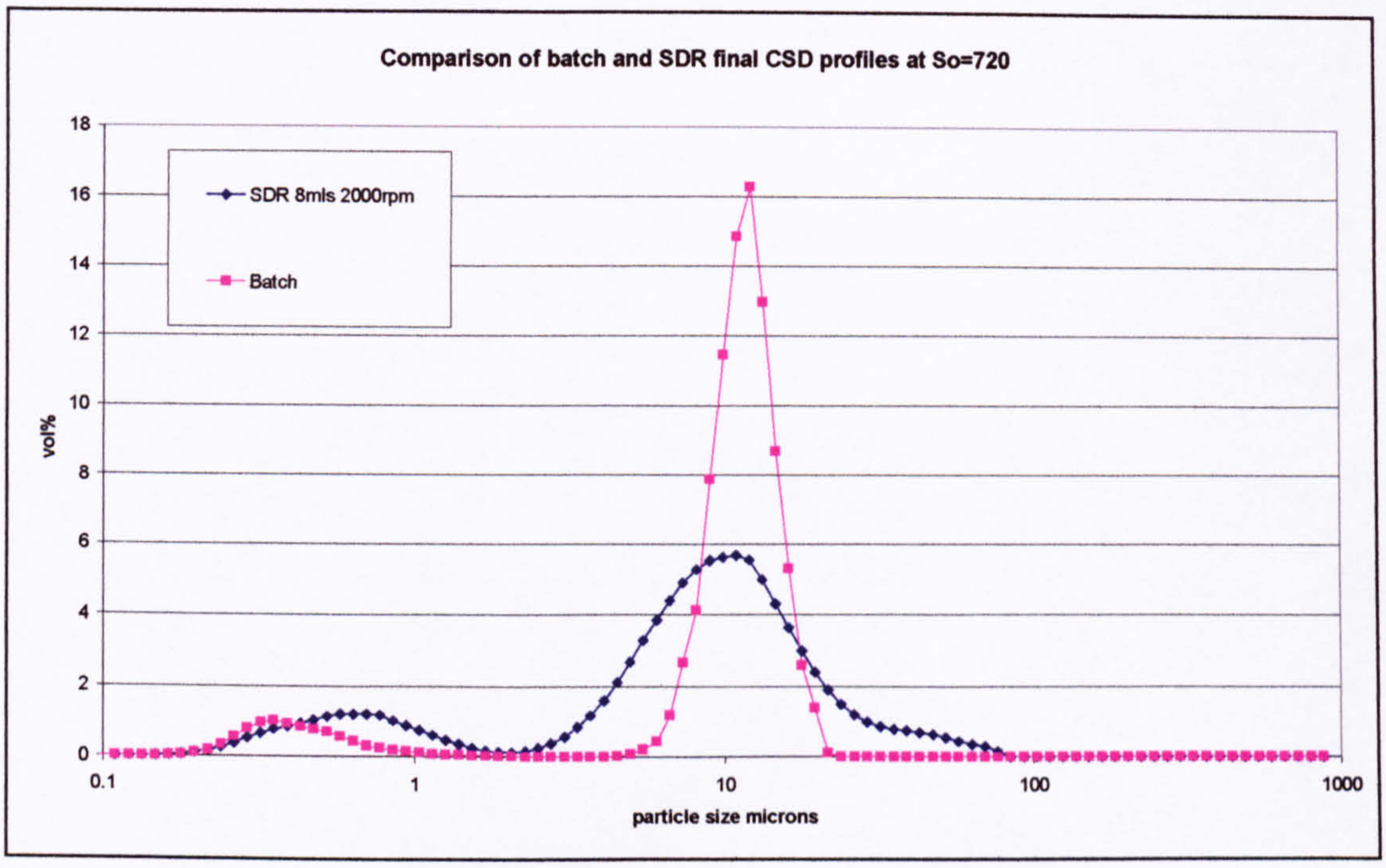


**Figure 7.16 Comparison of batch and SDR final CSD profiles at So=720**

From the SEM study of the experiments performed at So=720, it was seen that there is a difference in morphology between the two reactor types. The batch produced crystals similar to the reaction performed at So=180, producing needles and small spheres whereas the SDR produced shorter, spiky crystals along with platelets of around 2-10μm in size.

### 7.5.6.3 SDR vs Batch So=1800

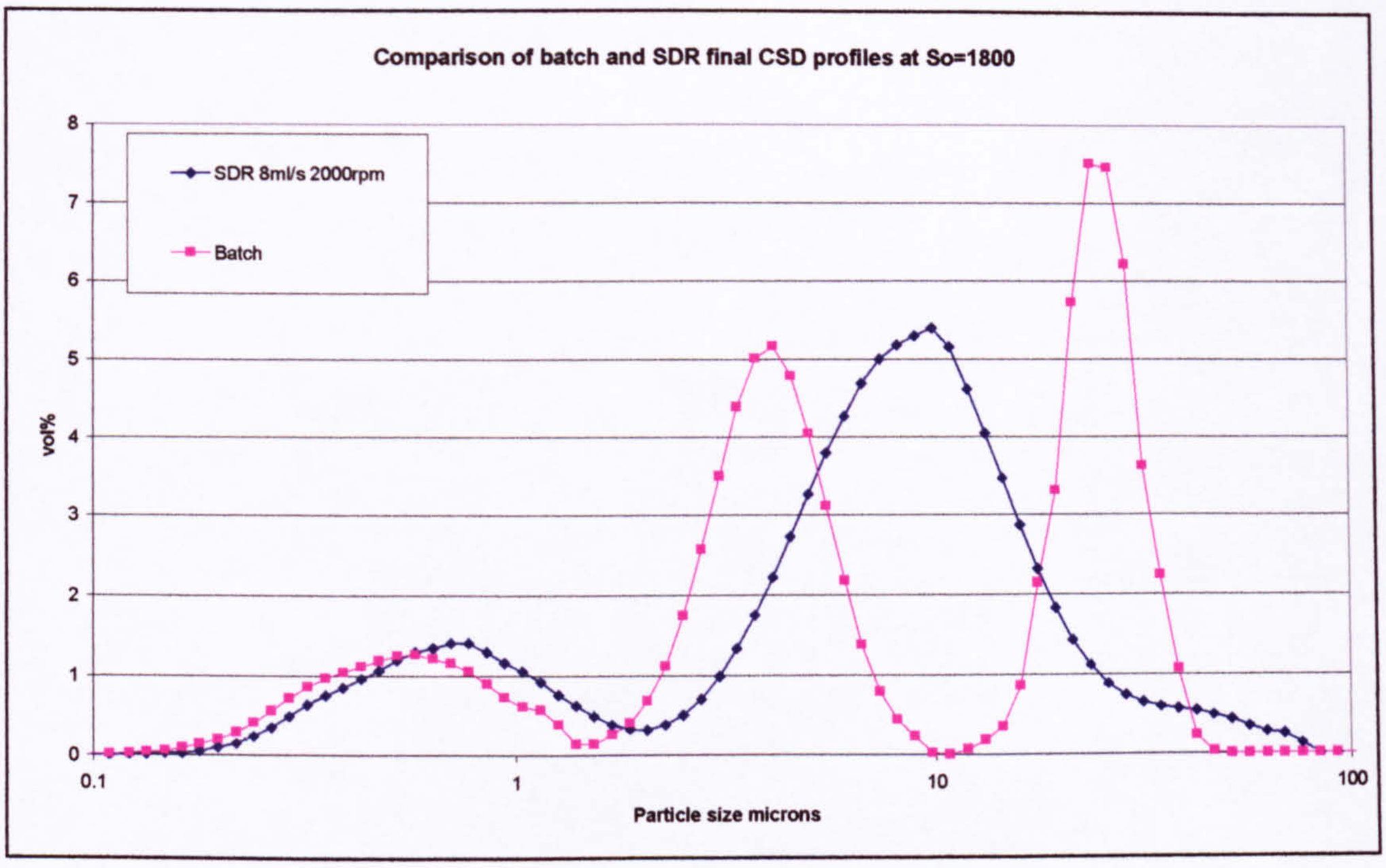


**Figure 7.17 Comparison of batch and SDR final CSD profiles at So=1800**

The SEM study of the experiments performed at So=1800 showed the batch had produced small (0.3 to 0.5μm) rugby ball shaped crystals that have appeared to have agglomerated and growth between the individual crystals has occurred, this is suggested by the peak at.10μm.

The SDR produced rough spheres and cubes approximately 5-10μm in diameter. There were sub-micron particles seen in the SEM slide of the SDR experiment indicated by the lower end peak in the CSD.

## *7.6 Discussion of liquid-liquid work*

The restriction on experimental time for this study was severely prohibitive. Many experimental options were omitted. The second process route planned using calcium nitrate and sodium carbonate is well documented in the literature, exploring that route first would have been advantageous. The original initial experimental plan had included this route. The $CaCl_2$ route was examined first because of the ability to produce a lot of $CaCl_2$ solution at high concentration so that high supersaturations could be interrogated over a range of conditions. Once disruption to laboratory time became overwhelming, the calcium nitrate reagent part of the study was omitted.

In examining the role of supersaturation, the system employed does not allow for the fluids to come together, producing high supersaturating conditions for precipitation without it forming a vicious gel. Hence the level of supersaturation employed was significantly reduced to allow a free flowing slurry suspension to convey in the experimental set-ups. It is highly likely that this would happen regardless of the reagents under these conditions. A reason for this would be very small vaterite crystals or amorphous calcium carbonate (ACC) with high surface energy binding themselves and water together, forming the highly vicious gel. This gel relaxes over a period of minutes and the product begins to flow suggesting there is a transformation of the product.

For each of the three reactant concentrations employed, there is nothing to suggest uniform product is being produced by either reactor method. Complete morphological control has not been achieved by reactor/reaction route alone.

Glutamic acid has been seen to have an effect on morphology especially in the batch case and produces a proportion of spheres in the SDR case. Since there was no study on the effect of concentration of glutamic acid on the morphology, then at present, there is no way of determining its efficacy in morphological control of precipitating in this manner. Some further experimentation would resolve this issue. Further examining the role of other organic additives and inorganic co-ions in the reaction might one day lead to the development of a SDR based process for the liquid-liquid based route to calcium carbonate for a product that has well controlled size and shape.

The CSD data showed products distribution that was unstable over time. These two methods of precipitation compound the problem inherent in $CaCO_3$ crystallisation, high supersaturation and low residence times produce thermodynamically unstable crystals. Arresting agglomeration, growth and aging by chemical agents might be applicable in this case. A stable product would allow the data to be taken further along the analysis route. Other parameters could come into play for carrying out trend analysis (e.g. to study the effect of fluid residence time or shear rate on the crystal size). In the case of $BaSO_4$ studies, agar solution was added after the experiment to arrest agglomeration; perhaps agar or some other chemical agent could be used in this case.

X-ray diffraction was considered for this study to differentiate between polymorphs obtained. In fact, slides went over to a student in the Chemistry department for analysis. After several months of questioning and pestering, the machine was forever broken (apparently) and delay after delay beset the analysis until any hope of getting it done was lost! This would have added something to the data, at least only to confirm the presence of $CaCO_3$ regardless of crystal form. The slides are out there, somewhere!

Due to an oversight too late to rectify, the experiments performed with glutamic acid at the low supersaturation ratio of 180 were not examined using the SEM. This would have indicated what happens to morphology under different concentrations.

## 7.7 Conclusions to the liquid-liquid study

The liquid-liquid reaction for the precipitation of $CaCO_3$ has been performed on the SDR and in the batch from the process route of calcium chloride and sodium carbonate. Analysis of crystal size distribution showed products that were unstable with the distribution changing over several minutes. This was attributed to firstly agglomeration of the reactor product and then the onset of aging of the crystals as the smaller unstable vaterite dissolved and grew on larger calcite crystals.

SEM analysis of the product samples revealed that different crystal shapes and sizes were formed at different supersaturation ratios. At low supersaturation, needles were formed alongside small agglomerated spherulites. At high supersaturation, larger spherulites were the predominant form.

With experiments performed in the presence of glutamic acid at moderate supersaturation, the glutamic acid altered the form of the crystals. The batch reaction formed fern-like shapes as opposed to the needles and small spheres. The SDR formed spherulites and rhombs as opposed to spiky and platelet forms.

The initial objective of the study was to try and achieve what had been accomplished with the $BaSO_4$ precipitation on the spinning cone.

Hypothesis: *Given that the particle size and quality of $BaSO_4$ precipitated on a spinning cone can be controlled by manipulation of process conditions (reactant concentration, rotational speed and reactant flowrate), can the same manipulation be applied to $CaCO_3$ precipitation to the same effect?*

This has not been achieved; the product has been seen to be unstable upon CSD analysis and has produced several crystal forms over the experimental range within the batch and SDR devices.

Given that the experimental time was plagued by lack of equipment availability and then by severe interruption by building work, then there was simply not enough time to carry out experimental investigations to understand the complexities of the precipitation. The Mastersizer was fundamental to the understanding of the products, the gap between loan periods meant techniques could not be honed, experiments could not be performed and understanding could not progress. When it was available, there was such a mad rush to use it (by several workers) that there was no time to reflect and interrogate results and change tack according to the data coming in. It was only after the experimental time was over could the data be interpreted adequately.

Most techniques of $CaCO_3$ precipitation reported in the literature use controlled experiments with low supersaturation and operate over a period more akin to hours than tenths of a second. High supersaturation levels in the present study experiments lead to and incredibly viscous product, which would not stir or flow away from the disc periphery, this suggests that there is a physical barrier to this method for $CaCO_3$. Any further work requires the understanding of the mechanisms involved and using the right level of supersaturation.

This brief study asked a lot of questions that were difficult to answer due to the ambiguities and omissions in the data set obtained. More analysis was required, especially in the SEM study of more slides and in the use of X-ray diffraction to determine relativistic quantities of each polymorph.

Any future study of calcium carbonate precipitation by liquid-liquid reaction should consider the following:

- Further studies should ensue ways of controlling pH at set levels by buffering with none reactants are employed. A pH over 8.6 prevents dissolution, higher pHs might favour a particular polymorph.
- Make available as many analysis techniques as possible in order to get the most understanding of the product. X-ray diffraction and SEM techniques are a must when defining which polymorphs are present in the product.

- Aim to have a precipitation method by which a stable product is attained before testing process parameters. Arresting these secondary processes immediately after the precipitation has finished should be a goal of such a study.
- Further investigate the role of additives, organic or inorganic in influencing crystal size, shape and stability.
- Study the effect of excess ion concentration using a molar excess of one of the reactants to examine this influence on shape and size.
- In studying the effect of feed point on CSD, $BaSO_4$ should be employed, as it seems to give a single stable product distribution for a given supersaturation which would elude to the level of mixing in different feed configurations.
- Make use of higher rotational speed devices. The spinning cone used in the $BaSO_4$ work operated in the range 2000 to 10000rpm. These conditions would create very high rates of mixing (at all length scales).
- Study the effect of flowrate and mixing using stoichiometric amounts but with unequal concentrations mixing (i.e. dilute reagent A mixed with concentrated reagent B) in the reactor, this reduces hydrodynamic load on SDR, implies better mixing could be achieved as diffusional path lengths are reduced e.g. feed lower flowrate in middle and higher one through ring feeder or vice versa.
- Do not attempt to conduct a PhD experimental study during major laboratory refurbishments and make sure exclusive rights to particle size analysis equipment over a set period are obtained! Set out with the ways and means to carry out qualitative and quantitative analysis by a variety of techniques. Perhaps then that a fully comprehensive and scientifically valid study may be achieved.

# 8 Conclusions, directions for future work and development potential for SDR precipitation technology

In concluding the present study, direction is given as to what areas future examination of the SDR as a potential technology for calcium carbonate production might follow. A theoretical full-scale production design scenario is presented in order to represent a part of a possible real industrial-sized process for the gas-liquid precipitation of calcium carbonate.

## *8.1 Conclusion to the present study with direction for future work*

### 8.1.1 Overall conclusion to the experimental study

During the present study it took quite some time for the necessary equipment to be properly available. SDR laboratory time was the least critical issue. Although the rig was shared among other workers, there would have been ample time to program a satisfactory number of experiments. The main issue was the loan periods of the Mastersizer, the short duration of the loan, six to 8 weeks, and sharing it's use (and SDR) with other workers meant that experimentation and analysis time where seriously curtailed. Since the research group were just opening up to crystallisation studies at the time, access to such analysis was limited. Any further study should rely on better access to size distribution analysis with the availability of having such analysis present over long periods (say 6 months).

### 8.1.2 Concluding remarks to the gas-liquid study

With regard to the gas-liquid study, a further restriction on the experimentation was the requirement to make up and filter fresh calcium hydroxide solutions as feed to the experiments. The size of the filters became the literal bottleneck to the whole experimental exercise.

It was shown from this study that in the case of the batch, increasing the gas flow and stirrer speeds up to a critical level resulted in an increase of the carbonation rate. Above this threshold no further rate increase was achievable. The 15cm diameter SDR in comparison to the 1-litre batch was seen to have more than double the mass transfer

rate than the batch. In increasing the gas to liquid flow ratio in the SDR, higher absorption rates could be achieved. Further optimisation would be required to push the operating parameters of the SDR.

The crystals formed in the SDR were shown to be smaller than that of the batch. In comparing the range of product sizes produced by the SDR, it was seen that higher changes in pH led to smaller crystals being produced. This higher concentration change meant higher supersaturation conditions were being evolved which led to higher nucleation rates, lower growth rates and ultimately, smaller crystals.

The presence of spheres in some of the SDR experiments suggested vaterite formation. Although high supersaturation is believed to have a role in this, a full understanding of it is not presented here as a full SEM analysis or XRD analysis was carried out on all of the experiments.

Any further study of mass transfer and crystal growth may look to proceed along the following approaches.

- Simplify the understanding of the mass transfer rate by using a non-precipitating system. Absorption of $CO_2$ into solutions of NaOH or KOH could be simply analysed by pH measurement and titration. This removes the complication of a solid phase and allows for higher solution concentrations to be used. This may then be compared with calcium hydroxide carbonation in the same reactor configuration. Making sodium or potassium carbonate solutions may allow for this to be reacted with calcium hydroxide slurries on another SDR whereby supersaturation is better controlled from the liquid-liquid route. Fundamental mass transfer work should be further extended to examine the role of increased gas pressure on mass transfer performance. An appropriate rig would require adequate design for such a study. Further, examining the mass transfer performance of dilute $CO_2$ streams would indicate the SDR's potential to act as an absorber/reactor for clean up of flue gas streams to mitigate emissions. A final part in investigating mass transfer performance would be to investigate increasing the disc diameter to accommodate higher throughput. The effect of developing a co/counter current gas stream to the liquid film may also be investigated.

- In measuring change in concentration, pH measurements were taken at the exit of the SDR. The shell wall of the SDR provided a large area for mass transfer to potentially occur in the draining film down the walls leading to the possibility of making the mass transfer results from the disc to be inaccurate. A sampling technique to collect material from the disc periphery would indicate any discrepancies between the disc, shell and exit.
- Agglomeration and polymorphism were seen to be an issue in the present study. In investigating these phenomena further, repetition and extensive analysis of experiments in the present study using CSD, SEM and XRD analyses should throw further light as to the nature of these. The use of surface modifiers such as starch and glutamic acid may allow for better control of crystal size and morphology.

### 8.1.3 Concluding remarks to the gas-liquid-slurry study

This study, although rather short in terms of the number of experiments performed yielded some interesting information. Increasing the concentration of calcium hydroxide to the batch carbonation resulted in increasing the average particle size. Intuitively, calcium carbonate crystals in a supersaturated solution will continue to grow as either primary crystals or to agglomerate and grow. Therefore increasing the suspension density increases the amount of supersaturating material and therefore the potential for crystal growth. In using the SDR as the absorber, it was seen that the disc produced approximately the same size crystals as the 2-litre batch (for the same suspension density) by whichever mode of operation it used (recirculation or individual passes. However the carbonation time was reduced by approximately 11% by using the SDR. The data was not wholly conclusive as so few experiments were performed. This area should be examined further as to it's potential with many more experiments covering different rotational speeds, flowrates and slurry concentrations and the use of calcium oxide as a reactant as well as calcium hydroxide. In controlling particle size the effect of surface modifiers should be examined.

In comparing the particle size with that produced in a rotating packed bed, the RPB produced incredibly small particles in the mean size range 30 to 80 nanometres whereas the SDR yielded particles with a mean size of 5.45μm. How these were made so small in a RPB should be investigated further. Comparisons should be drawn

between SDR and RPB technologies in view of developing an intensified carbonation process.

### 8.1.4 Concluding remarks to the liquid-liquid study

In developing high levels of supersaturation from rapidly mixing two liquid reactants together there was no evidence to suggest that by increasing supersaturation, smaller crystals could be achieved. The polymorphic nature of calcium carbonate makes the crystallisation a complex mechanism. At the lower supersaturation ratio of 180, in both SDR and batch reactions, large needles and agglomerated spherulites were seen. At higher supersaturation ratios of 1800, larger spherulites were the dominant form from both reactors. Size distribution analysis over a period of time suggested the product to be unstable suggesting secondary processes at work such as agglomeration and aging. These processes might be arrested by the addition of inhibitors or surfactants fed near the disc periphery as a separate stream. The high supersaturation, rapid mixing on the SDR as a continuous reactor method requires further investigation as to whether it is suitable for the calcium carbonate process.

The addition of glutamic acid in the reaction mixture at the lower supersaturations, it was seen that the glutamic acid could affect morphology. A large proportion of the product was formed as spheres suggesting vaterite formation. This required confirmation by XRD. Further experimentation is required to find the best ratio of glutamic acid to reactant mixture along with finding the optimum reactant concentrations in order to maximise vaterite formation and therefore control of morphology.

All reactions in the present study were carried out at room temperature. There is prior evidence that at a temperature of around 70°C, the precipitation produces 100% aragonite. The SDR with it's good control of temperature should be investigated of carrying out precipitations at elevated temperatures to ascertain whether or not morphology may be controlled by a combination of recipe, heating and rapid mixing.

Many other organic and inorganic species as well as different reacting species have demonstrated habit modification in the precipitation of calcium carbonate. The combinations of precipitation conditions are almost boundless. Experiments looking at controlled pH, seeding the reaction with crystals and altering the reaction stoichiometry were not carried out. The SDR might provide a suitable environment

where electronic or magnetic field might be applied to yield novel effects on crystal lattice orientation. A separate study might be used to best suit the SDR with the correct recipe for tailor made crystal size and shape. These studies should be backed up by the extensive use of CSD, SEM and XRD analysis.

### 8.1.5 Investigating intensified methods for crystallisation

Further investigations might be able to employ the use of computational fluid dynamics and population balance modelling in order to predict and understand the mixing and crystallisation methods employed in this study.

The SDR and RPB have both demonstrated the potential to be processors for crystallisation processes. Other crystallisation methods (cooling, evaporative etc) are under investigation on the SDR, its rapid heat and mass transfer being able to control supersaturation ratios effectively is the key in its success. Microreactors have also been seen in precipitation roles. Other wet crystallisation technologies are emerging such as Couette-Taylor reactors and bubble-tube reactors (Vacassy et al, 2000) which are demonstrating their potential in such processes. Ultimately, in the modern era of product engineering they must come up to the scrutiny of being able to control crystal size and shape and produce the large volumes required by modern industry.

## *8.2 Future development of SDR technology as process for calcium carbonate production: Theoretical scale up of the SDR carbonation process*

The issue of scaling up any reactor design to a full production process is always complex. Heat and mass transfer are not always kept constant as the process transfers to larger and larger reactor. Scaling an SDR process might be a simpler issue.

In the present study a 15cm diameter disc was employed which had (say) a nominal liquid flowrate of 10ml/s for contacting with $CO_2$. A rule of thumb for scaling the reactor is scaling flowrate with the square of the diameter for a set rotational speed – i.e. if the diameter of the disc is doubled, the area (and flowrate) is quadrupled. By scaling the flow with the diameter, approximately the same average film thickness, mean velocity and residence time can be achieved. So a 30cm diameter disc would have a nominal flow of 40ml/s, a 75cm diameter disc would have a flow of 200ml/s.

In the gas-liquid slurry experiments, it took 9 passes over the SDR at 17ml/s and 1000rpm to process calcium hydroxide slurry of a density of 15g/l. If it is assumed that the overall mass transfer rate is proportional with interfacial area, then having a 45cm diameter disc (3 times the diameter, 9 times the interfacial area), then complete conversion may be achieved in 1 pass over the disc at a flow of 17ml/s.

To scale the flow to a bigger disc – a 90cm diameter disc with 15g/l slurry flowing at 68ml/s could be processed in 1 pass. This would be the equivalent slurry flowrate of 1958 $m^3$ p.a. from one disc (8000hrs operating time). This would be the equivalent of producing 40 tonnes p.a. of dry chalk product. This figure is based on doubling the diameter and thus quadrupling the flow.

74% of all PCC goes into the manufacture of paper. With that, many PCC plants are situated next to paper mills. Recovery of carbon dioxide from the paper drying process allows for recycling of waste and reduction in greenhouse emissions. (Roskill, 2000) estimated that PCC production would be in the region of 3.9Mtpa in 2004 and there would be approximately 150 PCC plants worldwide. Therefore each plant would have a capacity on average of 26000t.p.y. So to use an SDR process, an average PCC plant would require 650 discs. Discs mounted on a horizontal shaft could employ both sides of the disc to process fluid; therefore 325 discs would be required – each side of the disc would have its own liquid feed pipe and the $CO_2$ would be pumped into the shell. This seems a lot but assuming these can be made into stacked modules, a 90cm diameter disc 2mm thick and spaced 20mm apart, then on 1 metre of shaft approximately 41 discs could be mounted. If this constituted 1 reactor array, then 8 arrays would be required to make up the absorption/reaction process to make the capacity 26000t.pa. The shell would be about 1.0m diameter and the bearings, mounts and motor might make its length about 1.6m.

8 of these stacks operating in parallel would be required to process 15g/l slurry concentration. If the slurry concentration was 8 times higher (120g/l) the arrays may be deployed in series to achieve a continuous cascade and process the same amount of calcium carbonate.

The floor area for the entire absorption/reaction process for a 26000t.pa. process would be no greater than a large domestic living room and be contained within one storey. Compared to a typical PCC plant which might utilise stirred tanks, bubble columns or

spray towers, this represents a serious reduction in the size of plant and the possibility of dramatic cost savings of civil and structural work.

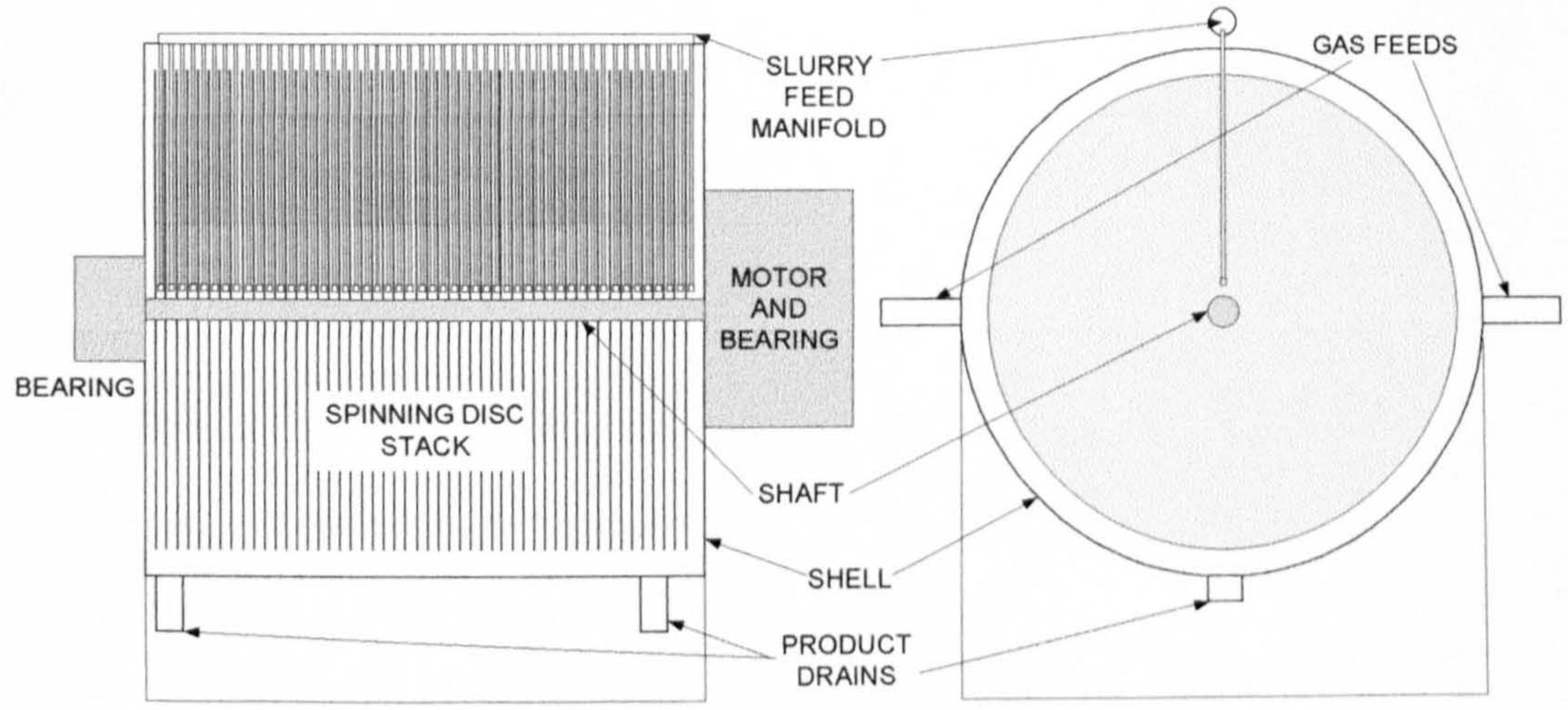


**Figure 8.8.1 Conceptual spinning disc stack array for gas-liquid contacting**

This conceptual design is built on a number of assumptions and can only be backed up by further research and development of scaling up from single 15cm to 90cm diameter and larger discs and the ability to correctly manifold a number of liquid feed to the discs in the array. Furthermore, this process many only achieve success once the ability to control calcium carbonate particle size and shape is attained. The devil is in the detail of finding the right conditions and additives for this to occur. These issues are for another study.

On a wider outlook, considering a 26000t.pa. PCC plant would consume 11340 tonnes of $CO_2$ p.a. this represents a considerable amount of sequestration of carbon emissions. This is however negated by the fact that limestone is calcined in the first place to produce CaO and generates a large amount of $CO_2$. Other carbon sequestration process such as the absorption of $CO_2$ in amine solutions could benefit from intensification technologies such as the thin film absorption using a SDR or RPB. These processes may provide cost-effective end-of-pipe solutions to flue gas cleaning. With demand for calcium carbonate expected to rise and with the continued push toward lowering emissions, the carbonation process might prove a linchpin in providing for both. Distributed intensified precipitated calcium carbonate process plants could contribute significantly to that demand.

# 9 Appendices

## 9.1 Gas-liquid solution data

### 9.1.1 SDR A-set results data

| Experimental conditions | | | | | | pH measurement | | |
|---|---|---|---|---|---|---|---|---|
| Expt ref | $Ca(OH)_2$ Flow ml/s | $CO_2$ Flow ml/min | $N_2$ Flow ml/min | Disc Speed Hz | Disc speed rad/s | Initial pH | Final pH | d[OH-] |
| AA1 | 4 | 240 | 0 | 4.7 | 52.4 | 12.45 | 9.15 | 0.0282 |
| AA2 | 8 | 480 | 0 | 4.7 | 52.4 | 12.4 | 8.5 | 0.0251 |
| AA3 | 12 | 720 | 0 | 4.7 | 52.4 | 12.45 | 8.8 | 0.0282 |
| AA4 | 16 | 960 | 0 | 4.7 | 52.4 | 12.4 | 8.8 | 0.0251 |
| AA5 | 20 | 1200 | 0 | 4.7 | 52.4 | 12.4 | 9 | 0.0251 |
| AB1 | 4 | 240 | 0 | 7.0 | 78.0 | 12.5 | 8.8 | 0.0316 |
| AB2 | 8 | 480 | 0 | 7.0 | 78.0 | 12.4 | 9.2 | 0.0251 |
| AB3 | 12 | 720 | 0 | 7.0 | 78.0 | 12.5 | 9.15 | 0.0316 |
| AB4 | 16 | 960 | 0 | 7.0 | 78.0 | 12.4 | 9 | 0.0251 |
| AB5 | 20 | 1200 | 0 | 7.0 | 78.0 | 12.4 | 9 | 0.0251 |
| AC1 | 4 | 240 | 0 | 9.3 | 103.6 | 12.4 | 11.2 | 0.0235 |
| AC2 | 8 | 480 | 0 | 9.3 | 103.6 | 12.4 | 9.6 | 0.0251 |
| AC3 | 12 | 720 | 0 | 9.3 | 103.6 | 12.4 | 9.25 | 0.0251 |
| AC4 | 16 | 960 | 0 | 9.3 | 103.6 | 12.4 | 9.2 | 0.0251 |
| AC5 | 20 | 1200 | 0 | 9.3 | 103.6 | 12.4 | 9.6 | 0.0251 |
| AD1 | 4 | 240 | 0 | 14 | 156.0 | 12.4 | 12 | 0.0151 |
| AD2 | 8 | 480 | 0 | 14 | 156.0 | | | 0.0000 |
| AD3 | 12 | 720 | 0 | 14 | 156.0 | 12.4 | 11.6 | 0.0211 |
| AD4 | 16 | 960 | 0 | 14 | 156.0 | | | 0.0000 |
| AD5 | 20 | 1200 | 0 | 14 | 156.0 | 12.4 | 11.4 | 0.0226 |
| AE1 | 4 | 240 | 0 | 18.6 | 207.2 | 12.5 | 12.1 | 0.0190 |
| AE2 | 8 | 480 | 0 | 18.6 | 207.2 | | | 0.0000 |
| AE3 | 12 | 720 | 0 | 18.6 | 207.2 | 12.5 | 12 | 0.0216 |
| AE4 | 16 | 960 | 0 | 18.6 | 207.2 | | | 0.0000 |
| AE5 | 20 | 1200 | 0 | 18.6 | 207.2 | 12.5 | 11.8 | 0.0253 |
| AA4(2) | 16 | 960 | 0 | 4.7 | 52.4 | 12.4 | 9.6 | 0.0251 |
| AC1(2) | 4 | 240 | 0 | 9.3 | 103.6 | 12.4 | 11.65 | 0.0207 |

**Table 9.1 A-set data: experimental parameters and pH measurement**

| Expt ref | Residence Time s | d[OH-]/tres | Mean Radial Velocity (inner radius) m/s | Mean Radial Velocity (outer radius) m/s | Power Dissipated W | Specific Dispersed Power (W/kg) | Kolmogoroff Microscale (m) | Fluid vol on surface of disc (m^3) |
|---|---|---|---|---|---|---|---|---|
| AA1 | 0.3213 | 0.0877 | 0.4201 | 0.1704 | 0.0307 | 23.7 | 1.43E-05 | 1.29E-06 |
| AA2 | 0.2024 | 0.1241 | 0.6669 | 0.2704 | 0.0614 | 37.0 | 1.28E-05 | 1.62E-06 |
| AA3 | 0.1544 | 0.1824 | 0.8739 | 0.3544 | 0.0921 | 47.6 | 1.20E-05 | 1.85E-06 |
| AA4 | 0.1275 | 0.1970 | 1.0587 | 0.4293 | 0.1228 | 56.5 | 1.15E-05 | 2.04E-06 |
| AA5 | 0.1099 | 0.2285 | 1.2285 | 0.4981 | 0.1536 | 64.1 | 1.12E-05 | 2.20E-06 |
| AB1 | 0.2463 | 0.1283 | 0.5479 | 0.2222 | 0.0681 | 68.6 | 1.10E-05 | 9.85E-07 |
| AB2 | 0.1552 | 0.1618 | 0.8698 | 0.3527 | 0.1362 | 107.7 | 9.82E-06 | 1.24E-06 |
| AB3 | 0.1184 | 0.2669 | 1.1398 | 0.4621 | 0.2044 | 139.2 | 9.21E-06 | 1.42E-06 |
| AB4 | 0.0978 | 0.2568 | 1.3807 | 0.5599 | 0.2725 | 166.1 | 8.81E-06 | 1.56E-06 |
| AB5 | 0.0842 | 0.2980 | 1.6022 | 0.6497 | 0.3406 | 189.4 | 8.52E-06 | 1.68E-06 |
| AC1 | 0.2038 | 0.1155 | 0.6622 | 0.2685 | 0.1202 | 146.6 | 9.09E-06 | 8.15E-07 |
| AC2 | 0.1284 | 0.1953 | 1.0512 | 0.4262 | 0.2405 | 230.5 | 8.12E-06 | 1.03E-06 |
| AC3 | 0.0980 | 0.2562 | 1.3774 | 0.5585 | 0.3607 | 298.7 | 7.61E-06 | 1.18E-06 |
| AC4 | 0.0809 | 0.3103 | 1.6686 | 0.6766 | 0.4810 | 357.3 | 7.27E-06 | 1.29E-06 |
| AC5 | 0.0697 | 0.3598 | 1.9363 | 0.7851 | 0.6012 | 408.8 | 7.03E-06 | 1.39E-06 |
| AD1 | 0.1552 | 0.0974 | 0.8698 | 0.3527 | 0.2725 | 437.0 | 6.92E-06 | 6.21E-07 |
| AD2 | 0.0978 | 0.0000 | 1.3807 | 0.5599 | 0.5450 | 688.7 | 6.17E-06 | 7.82E-07 |
| AD3 | 0.0746 | 0.2833 | 1.8092 | 0.7336 | 0.8175 | 894.8 | 5.78E-06 | 8.95E-07 |
| AD4 | 0.0616 | 0.0000 | 2.1917 | 0.8887 | 1.0900 | 1073.6 | 5.52E-06 | 9.85E-07 |
| AD5 | 0.0531 | 0.4260 | 2.5433 | 1.0313 | 1.3625 | 1232.7 | 5.34E-06 | 1.06E-06 |
| AE1 | 0.1284 | 0.1482 | 1.0512 | 0.4262 | 0.4810 | 932.9 | 5.72E-06 | 5.14E-07 |
| AE2 | 0.0809 | 0.0000 | 1.6686 | 0.6766 | 0.9620 | 1472.2 | 5.11E-06 | 6.47E-07 |
| AE3 | 0.0617 | 0.3503 | 2.1865 | 0.8866 | 1.4430 | 1915.6 | 4.78E-06 | 7.41E-07 |
| AE4 | 0.0510 | 0.0000 | 2.6488 | 1.0740 | 1.9239 | 2302.2 | 4.57E-06 | 8.15E-07 |
| AE5 | 0.0439 | 0.5764 | 3.0736 | 1.2463 | 2.4049 | 2648.4 | 4.41E-06 | 8.78E-07 |
| AA4(2) | 0.1275 | 0.1967 | 1.0587 | 0.4293 | 0.1228 | 56.5 | 1.15E-05 | 2.04E-06 |
| AC1(2) | 0.2038 | 0.1013 | 0.6622 | 0.2685 | 0.1202 | 146.6 | 9.09E-06 | 8.15E-07 |

**Table 9.2 A-set Data: Nusselt model**

| Run ref | Record No | D [3,2] | D [4,3] | D[v,0.1] | D[v,0.5] | D[v,0.9] | Std Dev (v) | Uniformity |
|---|---|---|---|---|---|---|---|---|
| AA1 | 18 | 4.501 | 6.246 | 3.209 | 4.716 | 9.026 | 7.432 | 0.556 |
| AA2 | 16 | 4.812 | 6.639 | 3.066 | 5.717 | 11.844 | 3.832 | 0.498 |
| AA3 | 14 | 3.221 | 9.325 | 1.719 | 3.734 | 13.006 | 23.452 | 1.853 |
| AA4 | 12 | 7.58 | 39.39 | 3.866 | 7.754 | 135.927 | 56.949 | 4.422 |
| AA5 | 9 | 5.834 | 7.035 | 3.798 | 6.175 | 11.754 | 3.386 | 0.408 |
| AB1 | 20 | 4.126 | 6.402 | 2.228 | 4.567 | 10.537 | 6.606 | 0.696 |
| AB2 | 22 | 2.556 | 6.488 | 1.39 | 2.966 | 7.044 | 21.73 | 1.55 |
| AB3 | 24 | 5.752 | 7.445 | 3.673 | 6.464 | 12.927 | 3.958 | 0.46 |
| AB4 | 27 | 5.224 | 9.196 | 3.511 | 5.654 | 13.794 | 12.571 | 0.923 |
| AB5 | 28 | 6.599 | 8.287 | 3.983 | 7.146 | 14.021 | 4.48 | 0.447 |
| AC1 | 29 | 6.168 | 7.322 | 3.922 | 6.62 | 11.917 | 3.196 | 0.378 |
| AC2 | 30 | 9.126 | 12.456 | 4.912 | 10.798 | 22.434 | 7.072 | 0.497 |
| AC3 | 31 | 12.965 | 18.34 | 6.966 | 15.996 | 33.419 | 10.447 | 0.508 |
| AC4 | 32 | 9.676 | 13.389 | 5.282 | 11.676 | 24.143 | 7.537 | 0.496 |
| AC5 | 33 | 7.525 | 9.599 | 4.239 | 8.473 | 16.533 | 4.942 | 0.445 |
| AD1 | 39 | 9.195 | 12.287 | 5.104 | 10.838 | 21.575 | 6.676 | 0.469 |
| AD2 | | | | | | | | |
| AD3 | 37 | 16.18 | 22.1 | 9.002 | 19.718 | 39.029 | 11.806 | 0.47 |
| AD4 | | | | | | | | |
| AD5 | 40 | 11.862 | 16.733 | 6.473 | 14.27 | 30.756 | 9.897 | 0.525 |
| AE1 | 35 | 6.807 | 8.615 | 4.029 | 7.445 | 14.699 | 4.647 | 0.454 |
| AE2 | | | | | | | | |
| AE3 | 36 | 13.709 | 19.594 | 7.386 | 16.951 | 35.856 | 11.476 | 0.519 |
| AE4 | | | | | | | | |
| AE5 | 34 | 9.275 | 12.439 | 5.08 | 11.024 | 22.066 | 6.642 | 0.469 |
| AA4(2) | 330 | 7.692 | 9.716 | 4.392 | 8.657 | 16.432 | 4.848 | 0.426 |
| AC1(2) | 326 | 5.359 | 6.049 | 3.766 | 5.597 | 9.28 | 2.267 | 0.321 |

**Table 9.3 A-set Mastersizer data**

## 9.1.2 2-litre solution batch CSD summary data

| Experiment | D(v,0.1) | D(v,0.5) | D(v,0.8) | D(v,0.9) | D(3,2) | D(4,3) |
|---|---|---|---|---|---|---|
| BATCH A1 | 3.2 | 6.37 | 10.68 | 17.97 | 5.72 | 77.97 |
| BATCH A2 | 3.1 | 5.7 | 8.75 | 10.96 | 5.04 | 6.77 |
| BATCH A3 | 4.21 | 9.73 | 16.43 | 21.26 | 7.99 | 11.48 |
| BATCH A3 | 3.7 | 6.92 | 10.05 | 12.22 | 6.17 | 7.91 |
| BATCH A3 | 5.85 | 9.63 | 12.48 | 14.23 | 8.74 | 9.86 |
| BATCH A3 | 5.99 | 9.89 | 12.96 | 14.84 | 9.0 | 10.19 |
| BATCH A3 | 6.14 | 10.34 | 13.81 | 15.96 | 9.36 | 10.73 |

**Table 9.4 2-litre solution batch CSD summary data**

## 9.1.3 Appendix Gas-liquid solution graphs

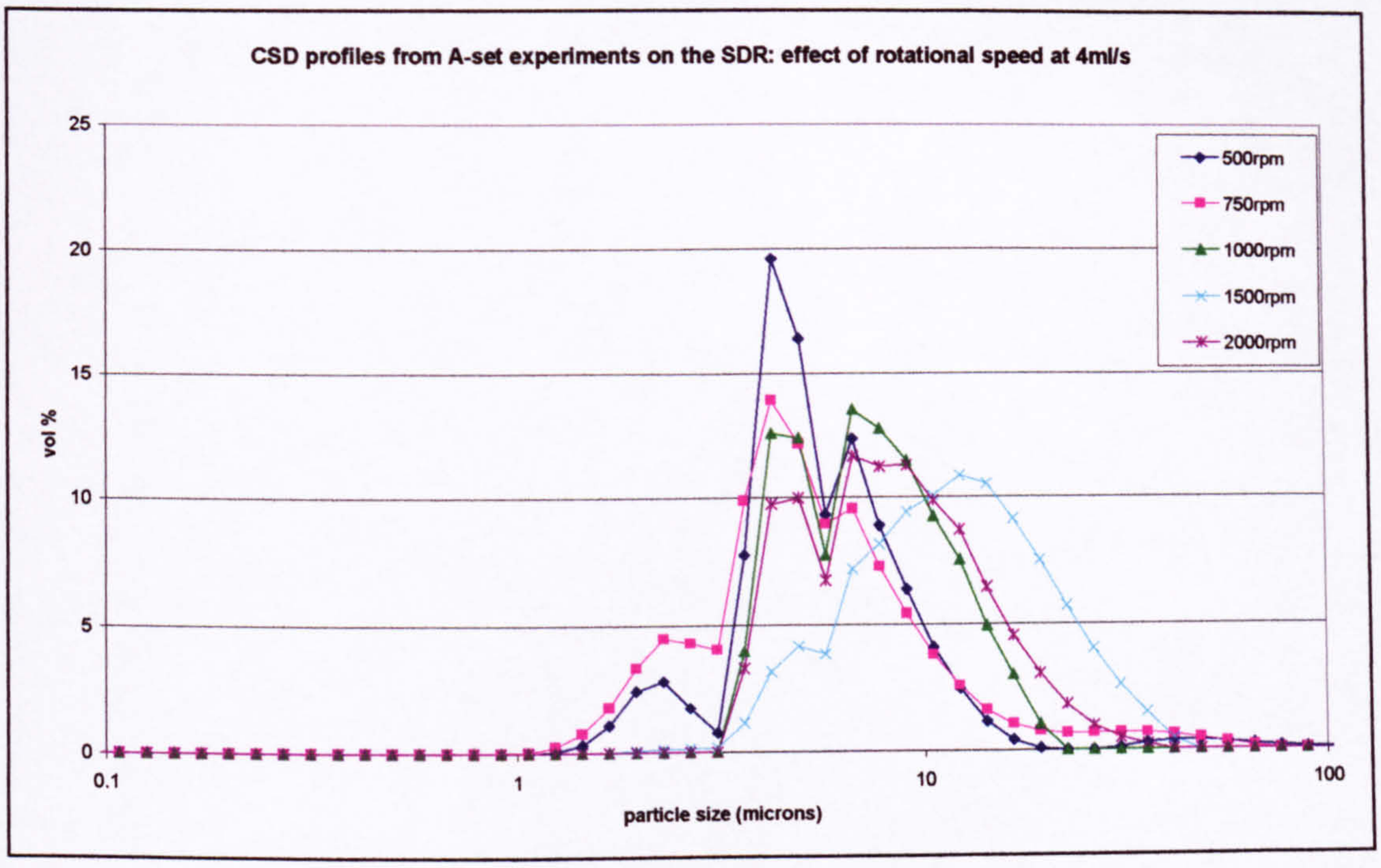


**Figure 9.9.1 The effect of rotational speed on the CSD profile at 4ml/s**

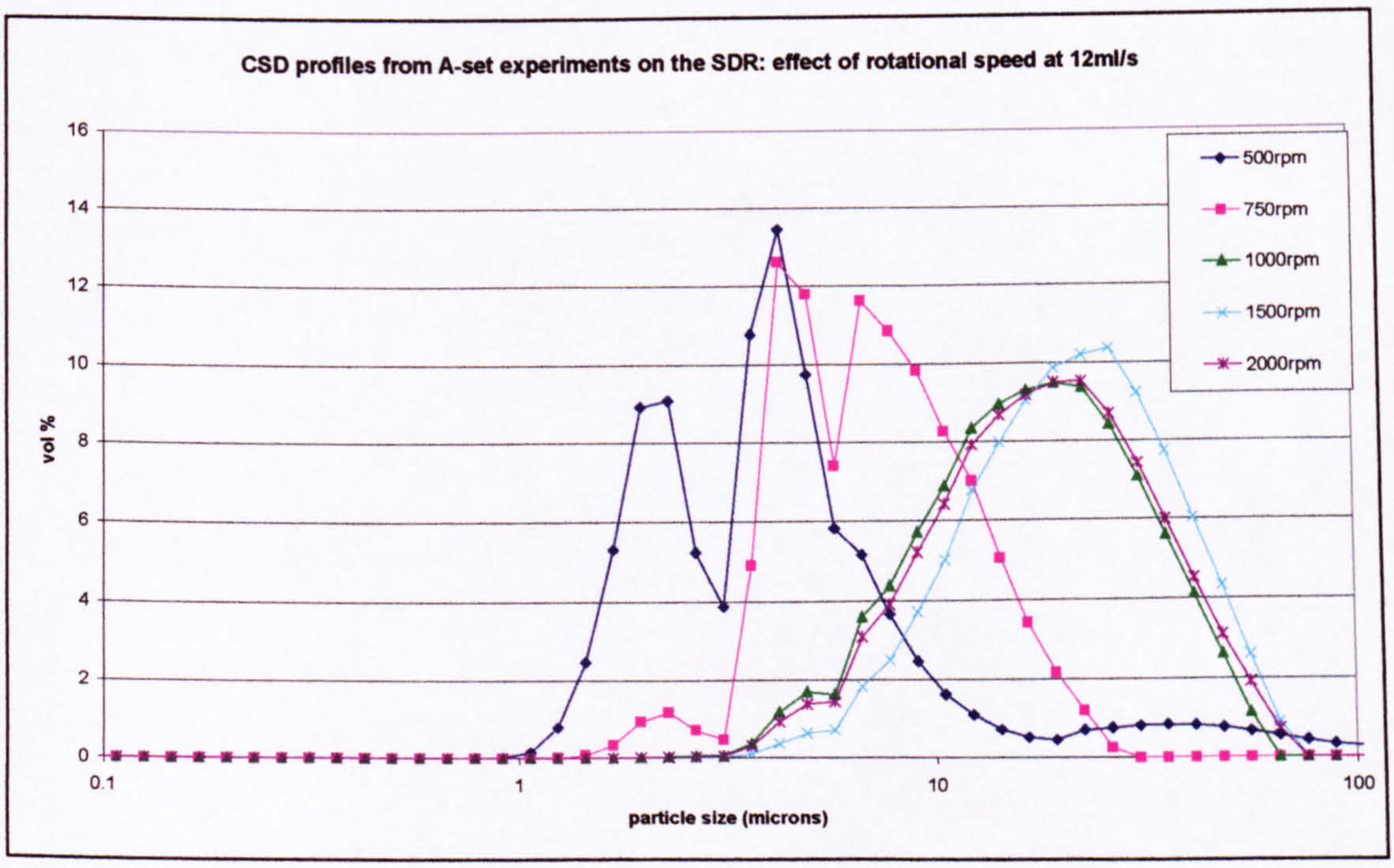


**Figure 9.2 The effect of rotational speed on the CSD profile at 12ml/s**

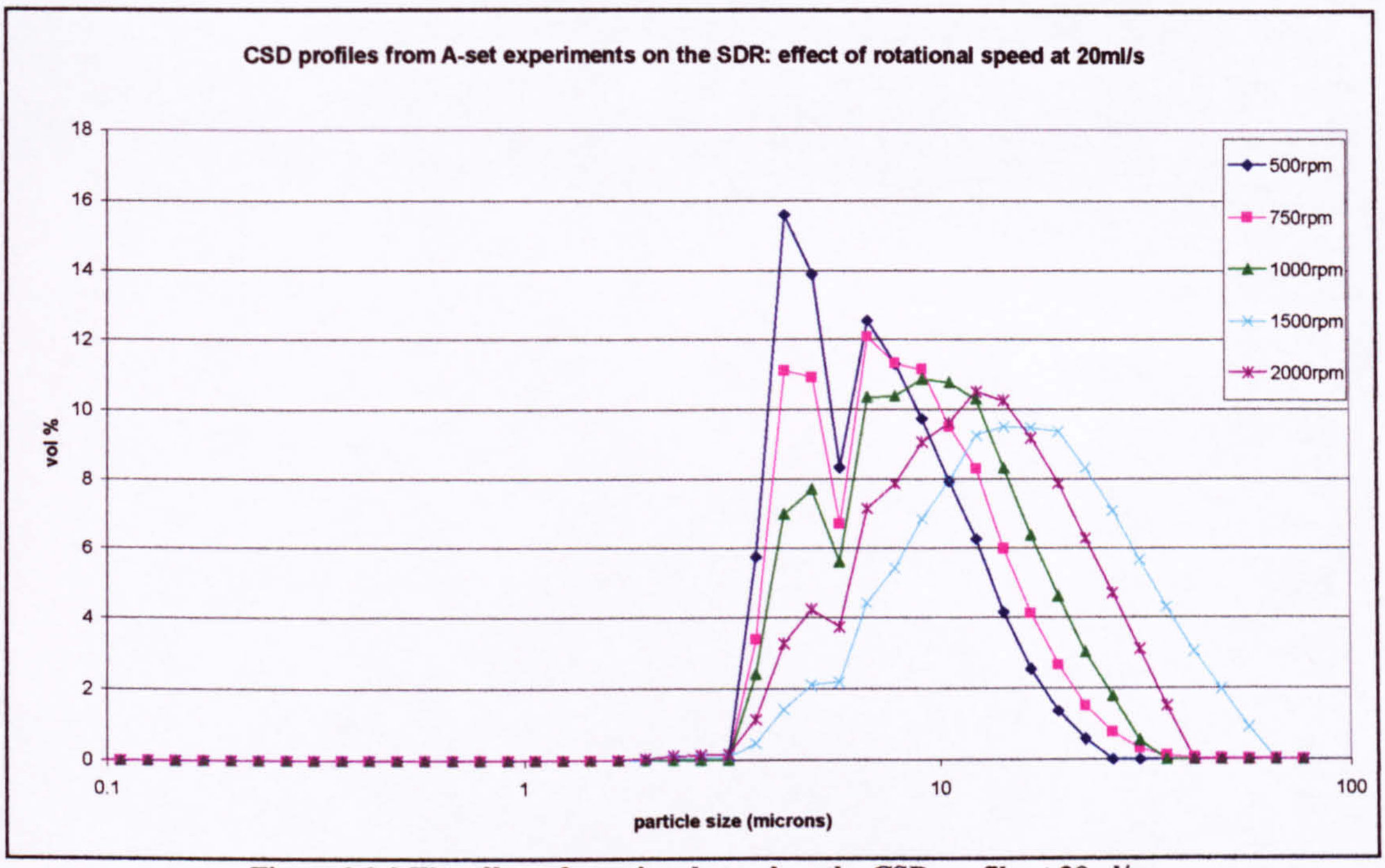


**Figure 9.9.3 The effect of rotational speed on the CSD profile at 20ml/s**

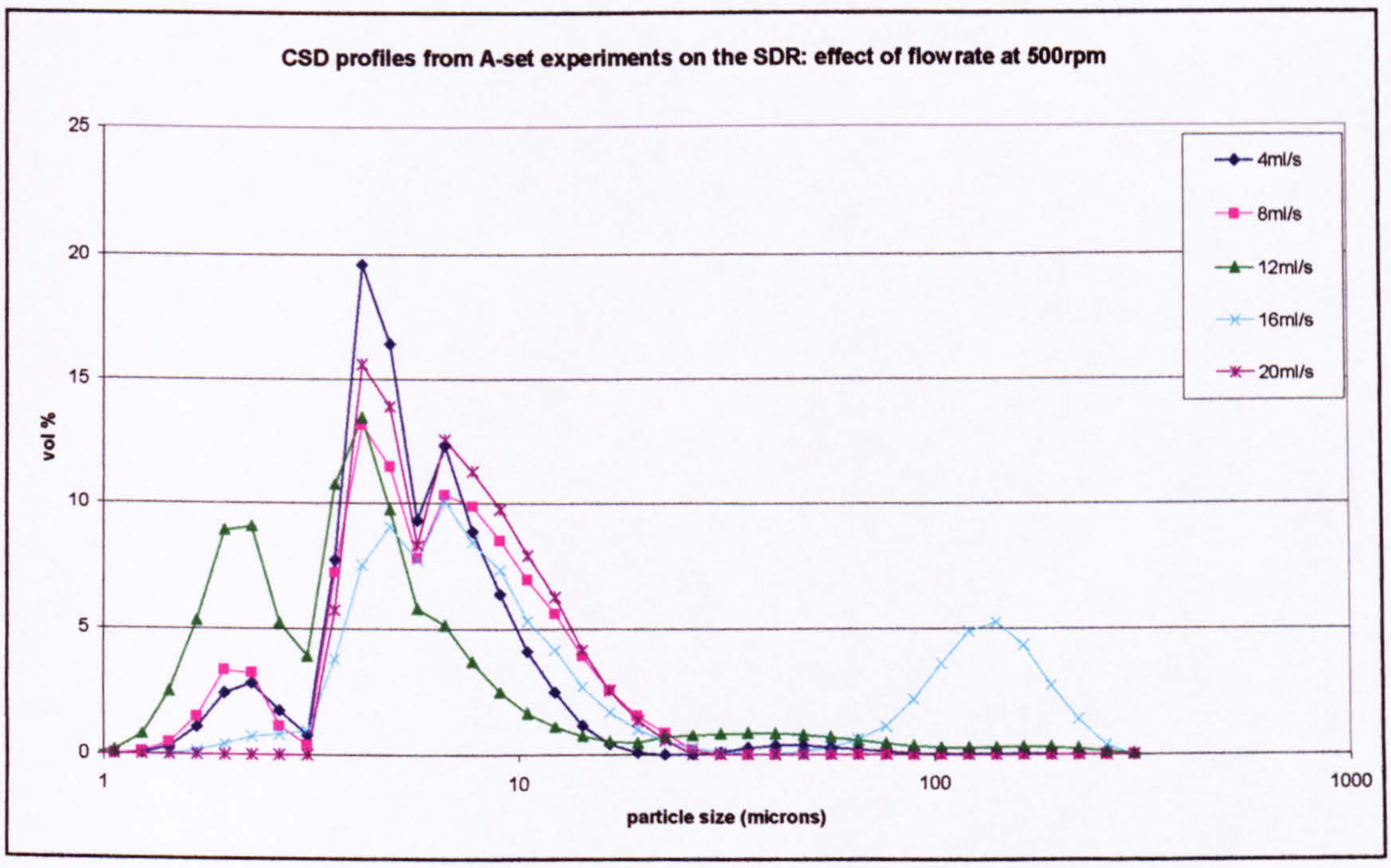


**Figure 9.9.4 The effect of flowrate on the CSD profile at 500rpm**

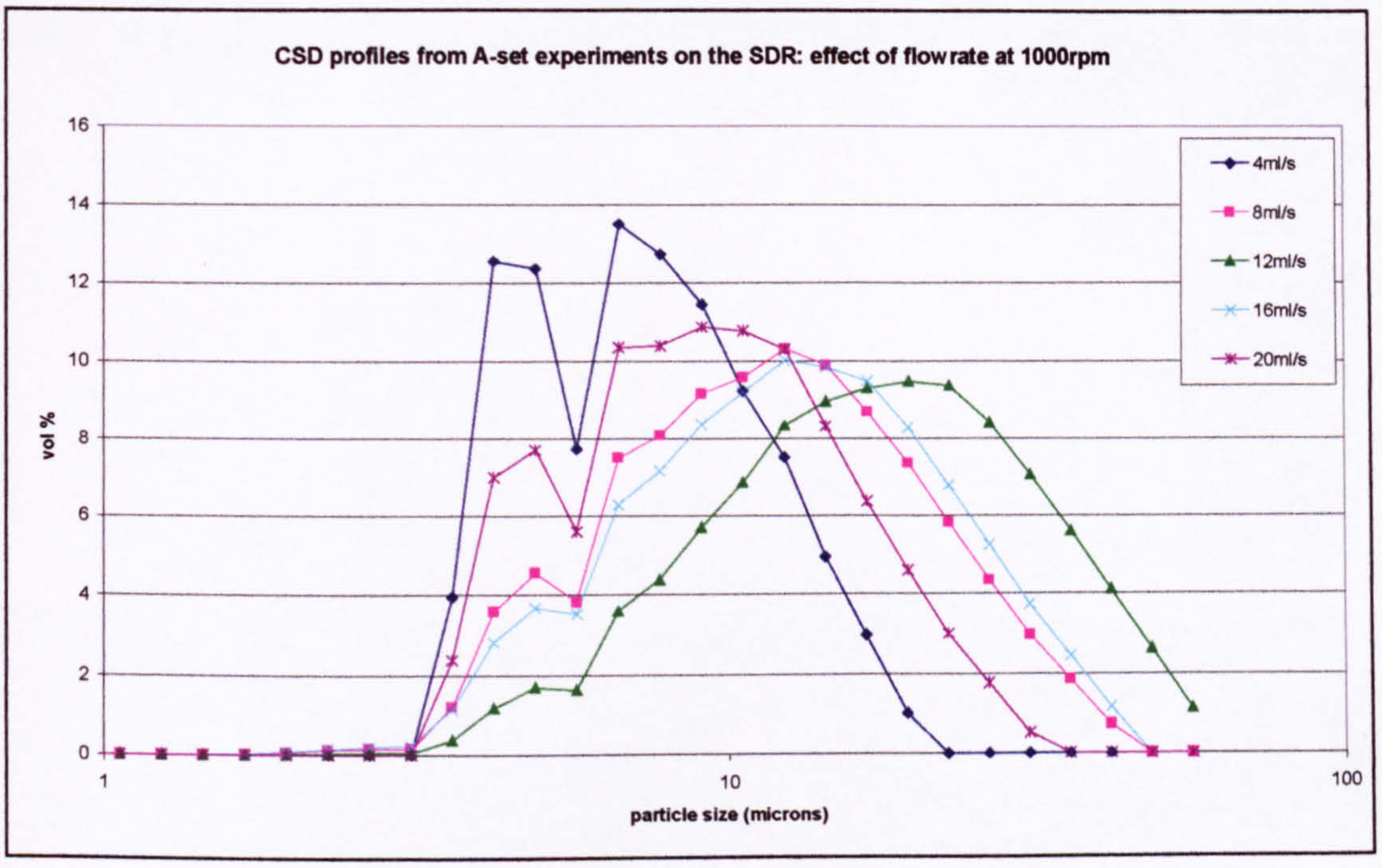


**Figure 9.9.5 The effect of flowrate on the CSD profile at 1000rpm**

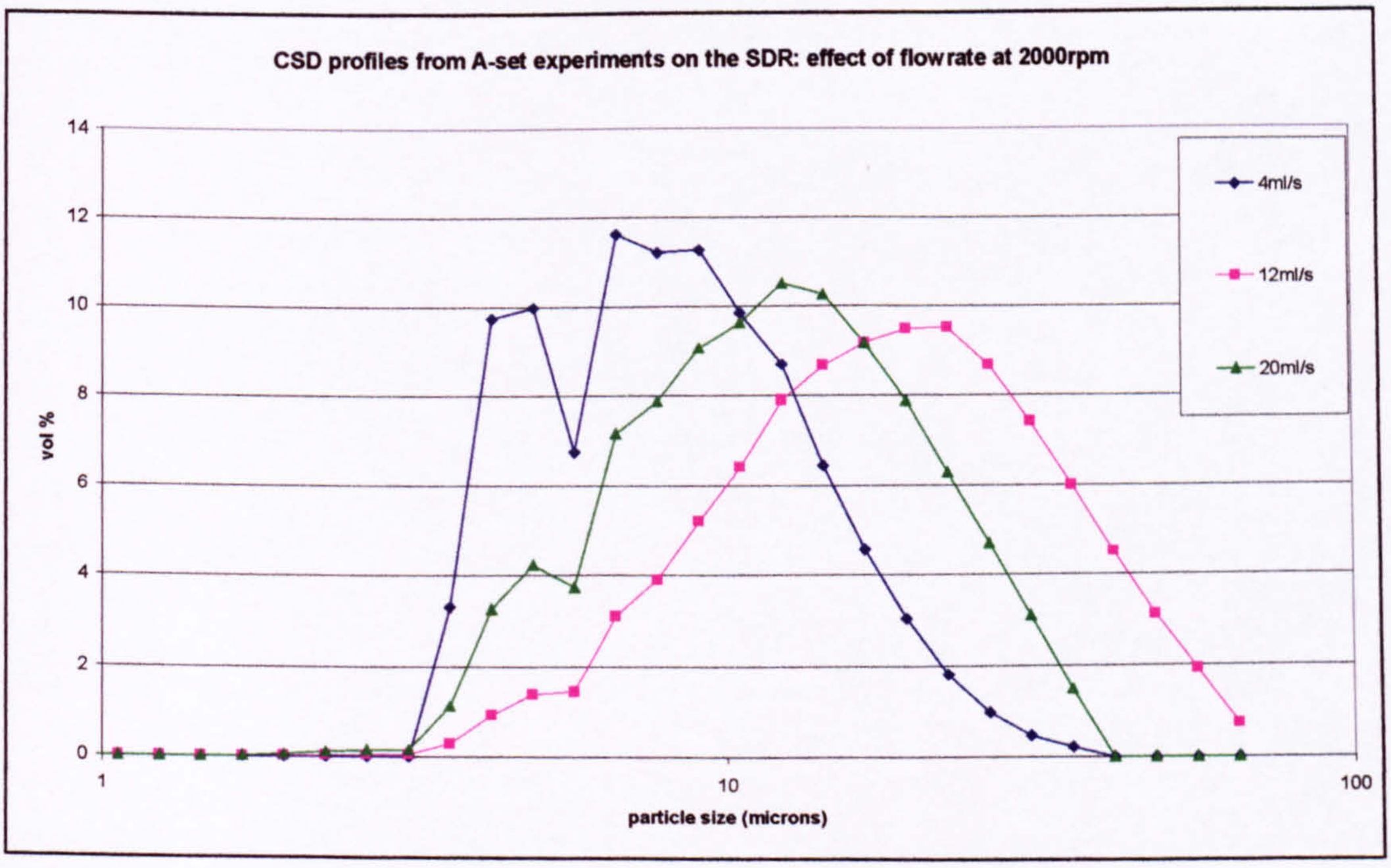


**Figure 9.9.6 The effect of flowrate on the CSD profile at 2000rpm**

### 9.1.4 Approximation of film thickness and flow velocity down the shell walls

Coulson and Richardson (vol.1 5th Ed. p82-83) give expressions for a liquid flowing with a free surface exposed to the atmosphere flowing down and inclined plane.

The mass flow, G, of the liquid down the surface can be calculated as

$$G = \frac{\rho^2.g.\sin\theta.w.\delta^3}{3.\mu} \quad \text{(eq 9.1)}$$

where

$\rho$ is the density of the fluid

$\mu$ is the viscosity of the fluid

w is the is the plane surface width (here assumed to be the circumference of the shell)

$\delta$ is the film thickness

$\theta$ is the angle of inclination

As the walls are vertical, $\sin\theta = 1$, rearranging to find film thickness, $\delta$, the equation becomes

$$\delta = \sqrt[3]{\frac{3.G.\mu}{\rho^2.g.w}} \quad \text{(eq 9.2)}$$

The mean velocity, u, of the falling film down a vertical surface is given by

$$u = \frac{\rho.g.\delta^2}{3.\mu} \quad \text{(eq 9.3)}$$

Therefore, the residence time, $t_{res\ shell}$ of the film draining down the height of the shell, $h_s$,

$$t_{res\_shell} = \frac{h_s}{u} \quad \text{(eq 9.4)}$$

For the 16cm diameter shell surrounding the disc used in the present study with 10cm height, the film thickness, mean velocity and are determined and displayed below for 4,8,12,16 and 20ml/s (assumes density and viscosity of slurry is the same as water)

Disc Data

shell radius 0.08 m

shell height 0.1 m

circumference of shell 0.503 m

density of fluid 1000 kg/m$^3$

viscosity of fluid 0.001 Ns/m$^2$

gravitational constant 9.81 m/s$^2$

| Flowrate (ml/s) | mass flow (kg/s) | film thickness (μm) | mean film velocity (m/s) | draining residence time (s) |
|---|---|---|---|---|
| 4 | 0.004 | 136 | 0.06 | 1.66 |
| 8 | 0.008 | 171 | 0.10 | 1.05 |
| 12 | 0.012 | 196 | 0.13 | 0.80 |
| 16 | 0.016 | 215 | 0.15 | 0.66 |
| 20 | 0.020 | 232 | 0.18 | 0.57 |

**Table 9.5 Film thickness, mean film velocity and residence time of film draining down shell wall for flowrates used in 15cm diameter SDR**

## 9.2 *Liquid-liquid reaction data*

### 9.2.1 supersaturation ratio in the liquid-liquid experiments

| | | M.W. |
|---|---|---|
| Calcium Chloride | $CaCl_2$ | 111 |
| Sodium Carbonate | $Na_2CO_3$ | 106 |
| Calcium Carbonate | $CaCO_3$ | 100.9 |
| Calcium Nitrate | $Ca(NO_3)_2.4H_2O$ | 236.15 |

$CaCO_3$ solubility: 0.0014 g/100g $H_2O$

0.014 g/litre

Note: When mixing the two solutions together in equimolar volumes, the concentration of the resulting supersaturated solution is halved because the volume doubles

| Molarity | Grams/litre solution | | | | Supersaturation |
|---|---|---|---|---|---|
| | $CaCl_2$ | $Na_2CO_3$ | $Ca(NO_3)_2$ | $CaCO_3$ slurry conc | |
| 0.01 | 1.11 | 1.06 | 2.36 | 0.5045 | 36.0 |
| 0.02 | 2.22 | 2.12 | 4.72 | 1.009 | 72.1 |
| 0.05 | 5.55 | 5.3 | 11.81 | 2.5225 | 180.1 |
| 0.1 | 11.1 | 10.6 | 23.61 | 5.045 | 360.3 |
| 0.2 | 22.2 | 21.2 | 47.23 | 10.09 | 720.7 |
| 0.5 | 55.5 | 53 | 118.08 | 25.225 | 1801.7 |
| 1.0 | 111 | 106 | 236.15 | 50.45 | 3603.5 |

**Table 9.6 Supersaturation ratio for different molar concentrations of reactants mixed in stiochiometric ratios and equal concentration**

## 9.2.2 Summary tables of final CSD parameters from SDR and batch experiments

| Experiment ID | Flowrate ml/s | rotational speed rpm | D(v,0.1) | D(v,0.5) | D(v,0.8) | D(v,0.9) | D(3,2) | D(4,3) |
|---|---|---|---|---|---|---|---|---|
| 180FMRH | 16 | 2000 | 0.49 | 8.07 | 12.68 | 15.94 | 1.92 | 8.83 |
| 180FHRM | 24 | 1000 | 1.07 | 9.83 | 19.16 | 51.89 | 2.89 | 17.51 |
| 180FHRL | 24 | 500 | 0.52 | 7.44 | 11.44 | 14.23 | 2.05 | 7.79 |
| 180FLRM | 8 | 1000 | 0.56 | 8.85 | 13.61 | 16.8 | 2.31 | 9.26 |
| 180FLRL | 8 | 500 | 0.66 | 11.22 | 19.26 | 24.89 | 2.59 | 12.81 |
| 180FMRM | 16 | 1000 | 0.54 | 9.37 | 14.42 | 17.91 | 2.31 | 9.89 |
| 180FMRL | 16 | 500 | 0.57 | 9.53 | 13.99 | 17.06 | 2.47 | 9.83 |
| 180FHRH | 24 | 2000 | 0.51 | 8.49 | 12.9 | 16.35 | 2 | 12.19 |
| 180FLRH | 8 | 2000 | 0.54 | 9.19 | 13.67 | 17.14 | 2.15 | 12.24 |
| | | | | | | | | |
| | Flowrate ml/s | rotational speed rpm | D(v,0.1) | D(v,0.5) | D(v,0.8) | D(v,0.9) | D(3,2) | D(4,3) |
| 180BATCH-FM | 8 | 210 | 0.44 | 6.89 | 12.23 | 16.46 | 1.68 | 8.15 |
| 180BATCH-FH | 12 | 210 | 0.52 | 7.39 | 11.44 | 81.33 | 2.16 | 25.89 |

**Table 9.7 CSD data for liquid-liquid reactions carried out at a supersaturation ratio of 180**

| ID | Flowrate ml/s | rotational speed rpm | D(v,0.1) | D(v,0.5) | D(v,0.8) | D(v,0.9) | D(3,2) | D(4,3) |
|---|---|---|---|---|---|---|---|---|
| 720FMRH | 16 | 2000 | 0.84 | 12.27 | 17.94 | 22.24 | 2.46 | 15.6 |
| 720FHRM | 24 | 1000 | 0.67 | 7.03 | 19.01 | 37.5 | 2.04 | 13.11 |
| 720FHRL | 24 | 500 | 0.65 | 8.62 | 14.61 | 18.44 | 2.16 | 9.31 |
| 720FLRH | 8 | 2000 | 0.83 | 8.57 | 21.83 | 31.06 | 2.59 | 12.96 |
| 720FMRM | 16 | 1000 | 1.82 | 198.03 | 286.41 | 328.18 | 3.94 | 164.56 |
| 720FLRL | 8 | 500 | 0.71 | 9.22 | 13.09 | 15.62 | 2.5 | 10.36 |
| 720FMRL | 16 | 500 | 0.62 | 6.03 | 10.92 | 14.66 | 1.97 | 7.1 |
| 720FHRH | 24 | 2000 | 0.88 | 8.29 | 12.52 | 15.33 | 2.48 | 8.73 |
| 720FLRH | 8 | 2000 | 0.66 | 8.33 | 14.56 | 20.59 | 2.32 | 10.55 |
| | | | | | | | | |
| | Flowrate ml/s | rotational speed rpm | D(v,0.1) | D(v,0.5) | D(v,0.8) | D(v,0.9) | D(3,2) | D(4,3) |
| 720BATCH-FM | 8 | 210 | 5.4 | 10.63 | 12.92 | 14.37 | 2.91 | 10.13 |
| 720BATCH-FH | 12 | 210 | 0.64 | 7.46 | 15.05 | 21.48 | 2.19 | 14.35 |

**Table 9.8 CSD data for liquid-liquid reactions carried out at a supersaturation ratio of 720**

| ID | Flowrate ml/s | rotational speed rpm | D(v,0.1) | D(v,0.5) | D(v,0.8) | D(v,0.9) | D(3,2) | D(4,3) |
|---|---|---|---|---|---|---|---|---|
| 1800FLRL | 8 | 500 | 0.74 | 4.3 | 7.72 | 12.59 | 1.94 | 6.03 |
| 1800FHRL | 24 | 500 | 0.86 | 8.47 | 12.77 | 15.6 | 2.63 | 8.7 |
| 1800FHRH | 24 | 2000 | 0.74 | 7.52 | 12.58 | 16.21 | 2.41 | 8.57 |
| 1800FLRH | 8 | 2000 | 0.65 | 7.12 | 12.79 | 17.87 | 2.16 | 9.15 |
| | | | | | | | | |
| 1800BATCH-FH | 12 | 210 | 0.56 | 4.83 | 23.88 | 27.37 | 1.9 | 11.67 |

**Table 9.9 CSD data for liquid-liquid reactions carried out at a supersaturation ratio of 1800**

## 9.2.3 CSD profiles of individual experiments in the liquid-liquid reactions

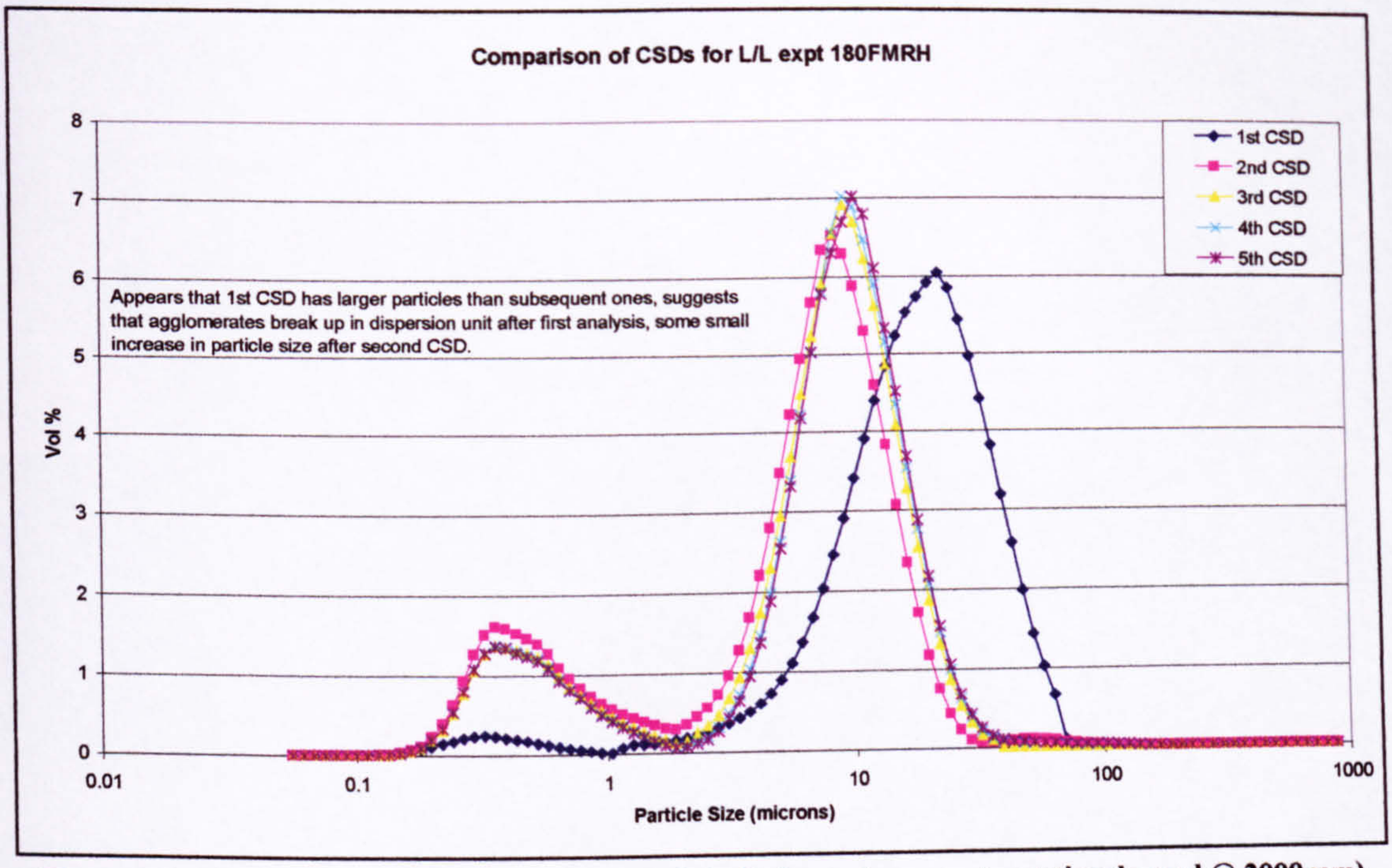


**Figure 9.9.7 CSD profiles: 180FMRH (SDR: flow @ 8ml/s for each reactant, rotational speed @ 2000rpm)**

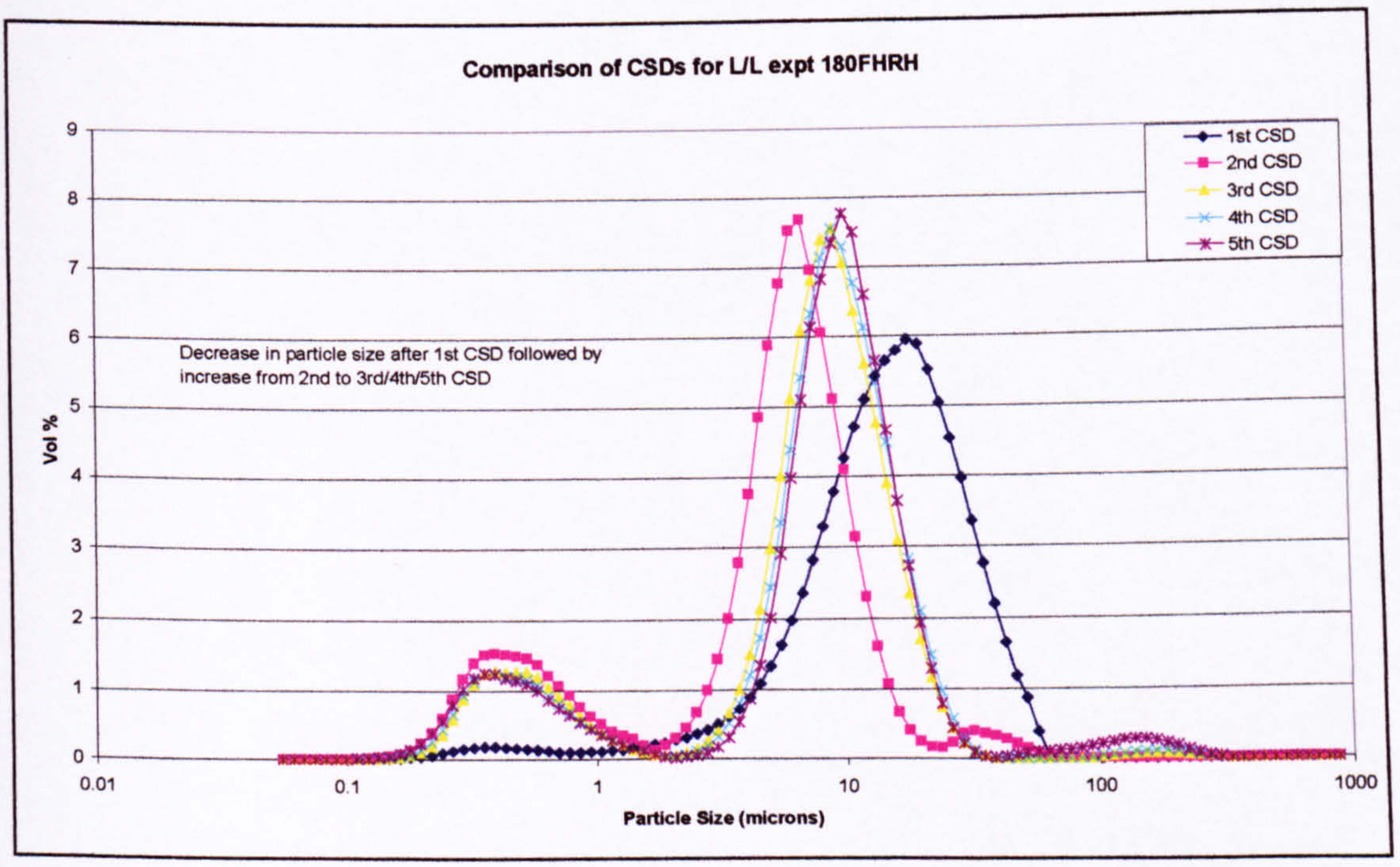


**Figure 9.9.8 CSD profiles: 180FHRH (SDR: flow @ 12ml/s for each reactant, rotational speed @ 2000rpm)**

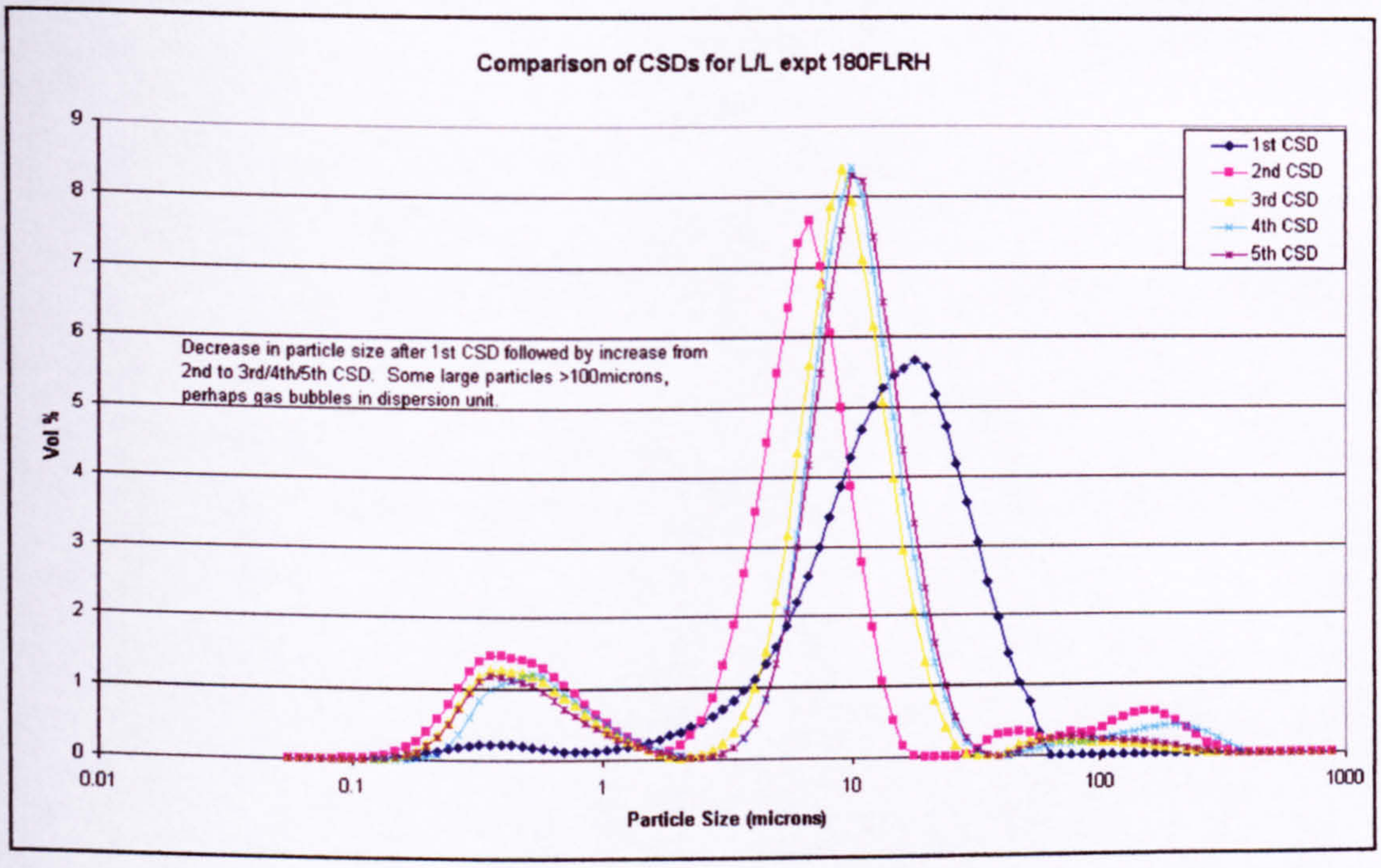


**Figure 9.9.9 CSD profiles: 180FLRH (SDR: flow @ 4ml/s for each reactant, rotational speed @ 2000rpm)**

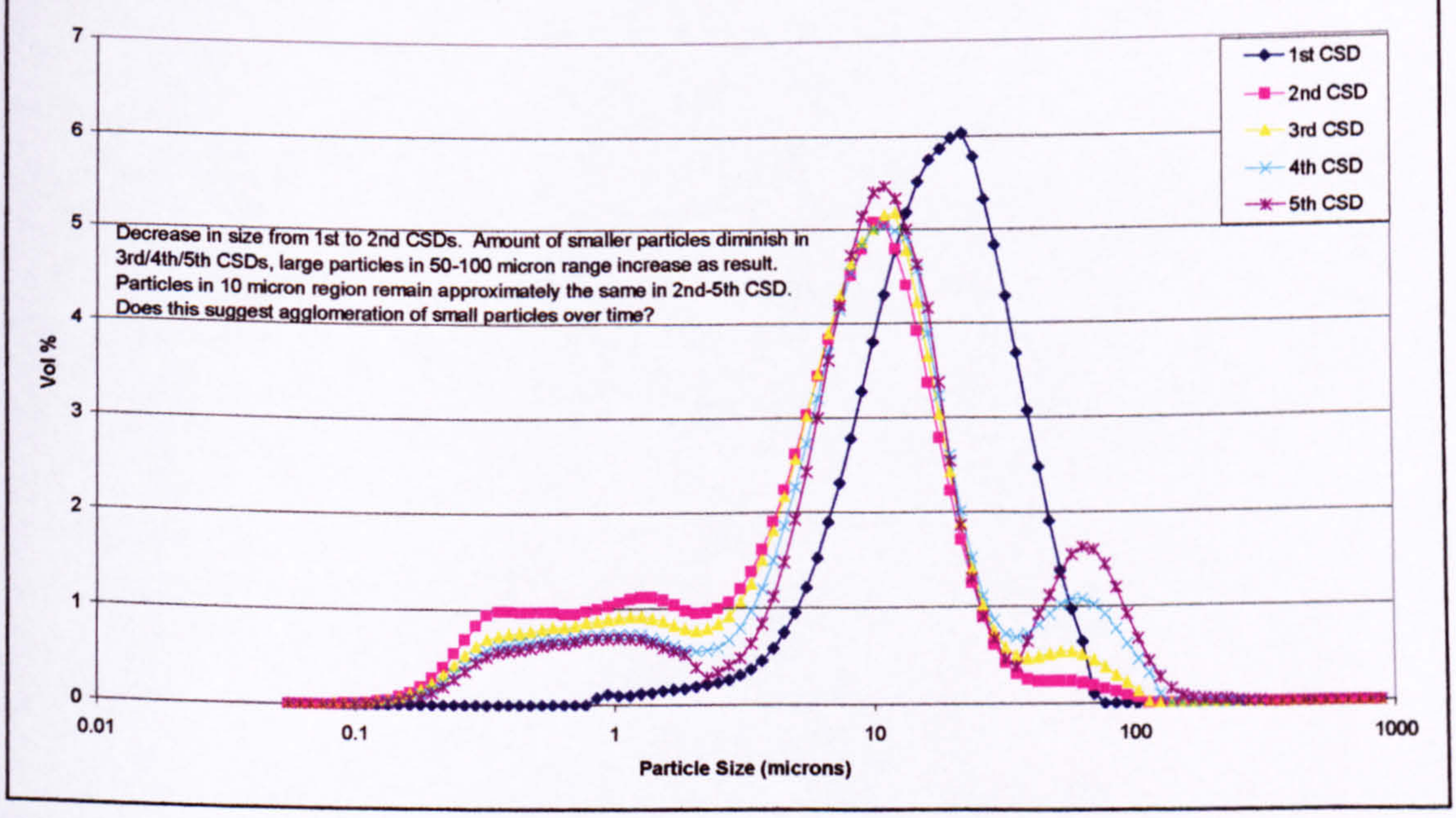


**Figure 9.9.10 CSD profiles: 180FHRM (SDR: flow @ 12ml/s for each reactant, rotational speed @ 1000rpm)**

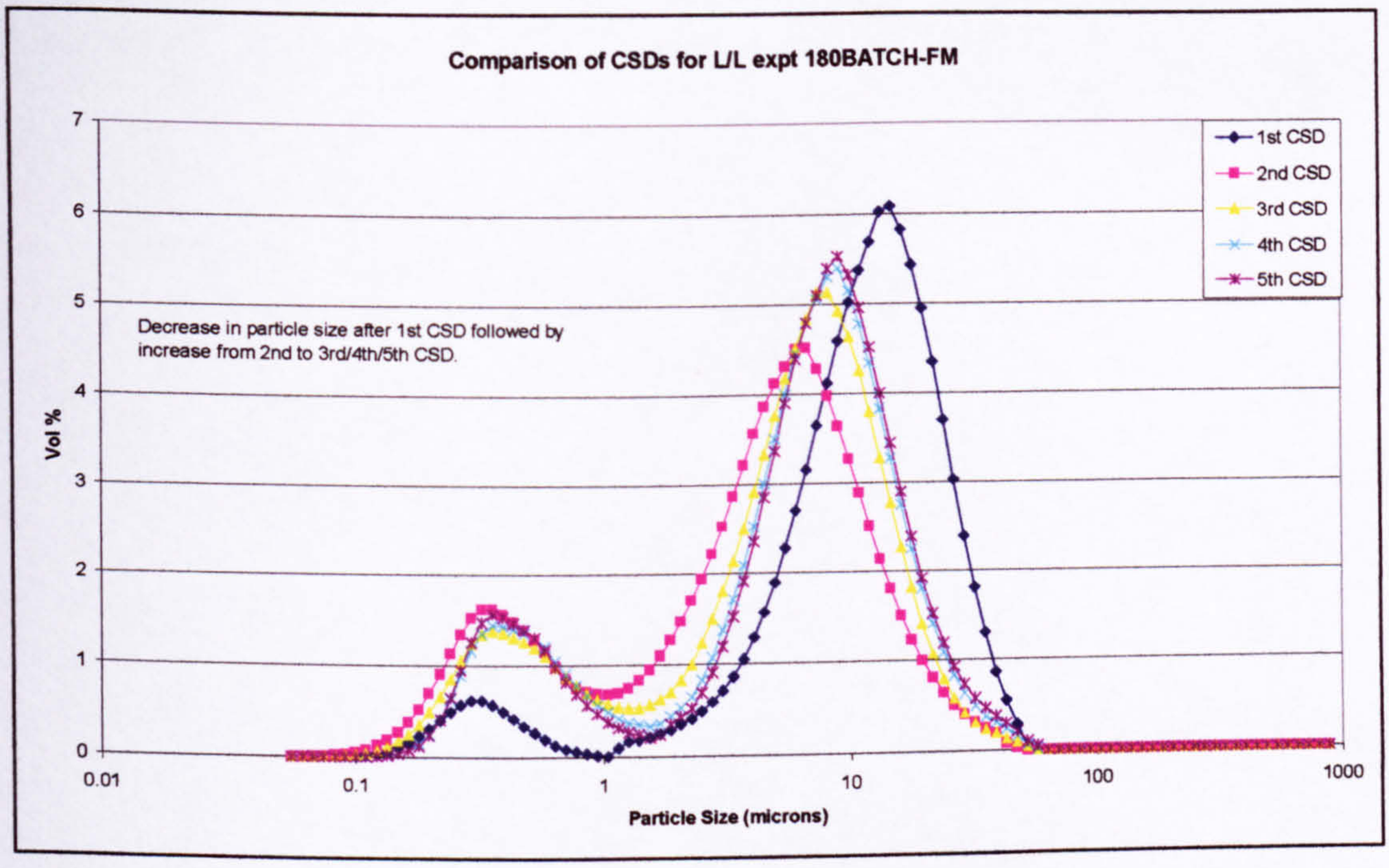


**Figure 9.9.11 CSD profiles: 180BATCH-FM (stirred batch containing 500ml $CaCl_2$ with $Na_2CO_3$ added at 8ml/s, stirrer speed 210rpm)**

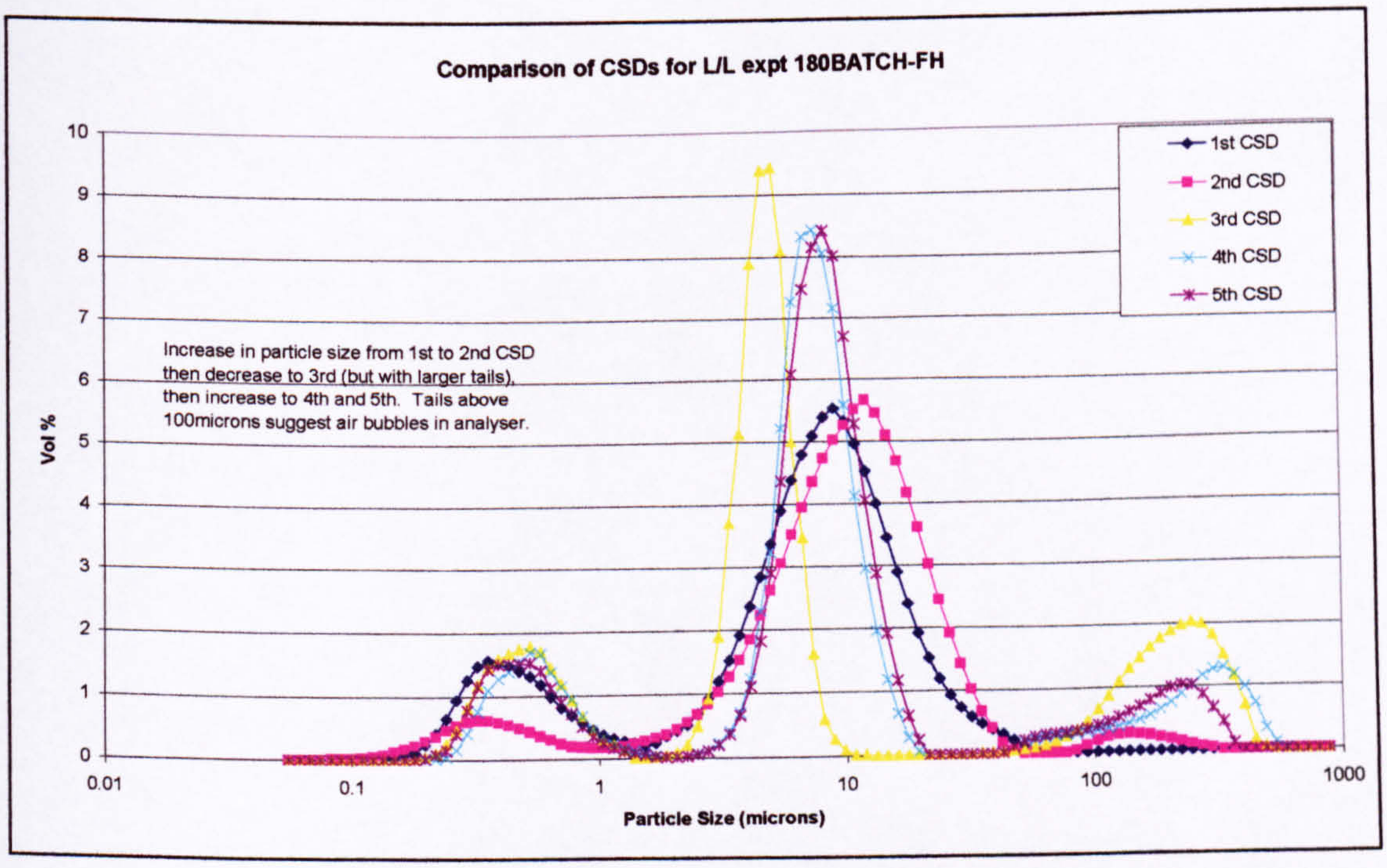


**Figure 9.9.12 CSD profiles: 180BATCH-FH (stirred batch containing 500ml CaCl2 with $Na_2CO_3$ added at 12ml/s, stirrer speed 210rpm)**

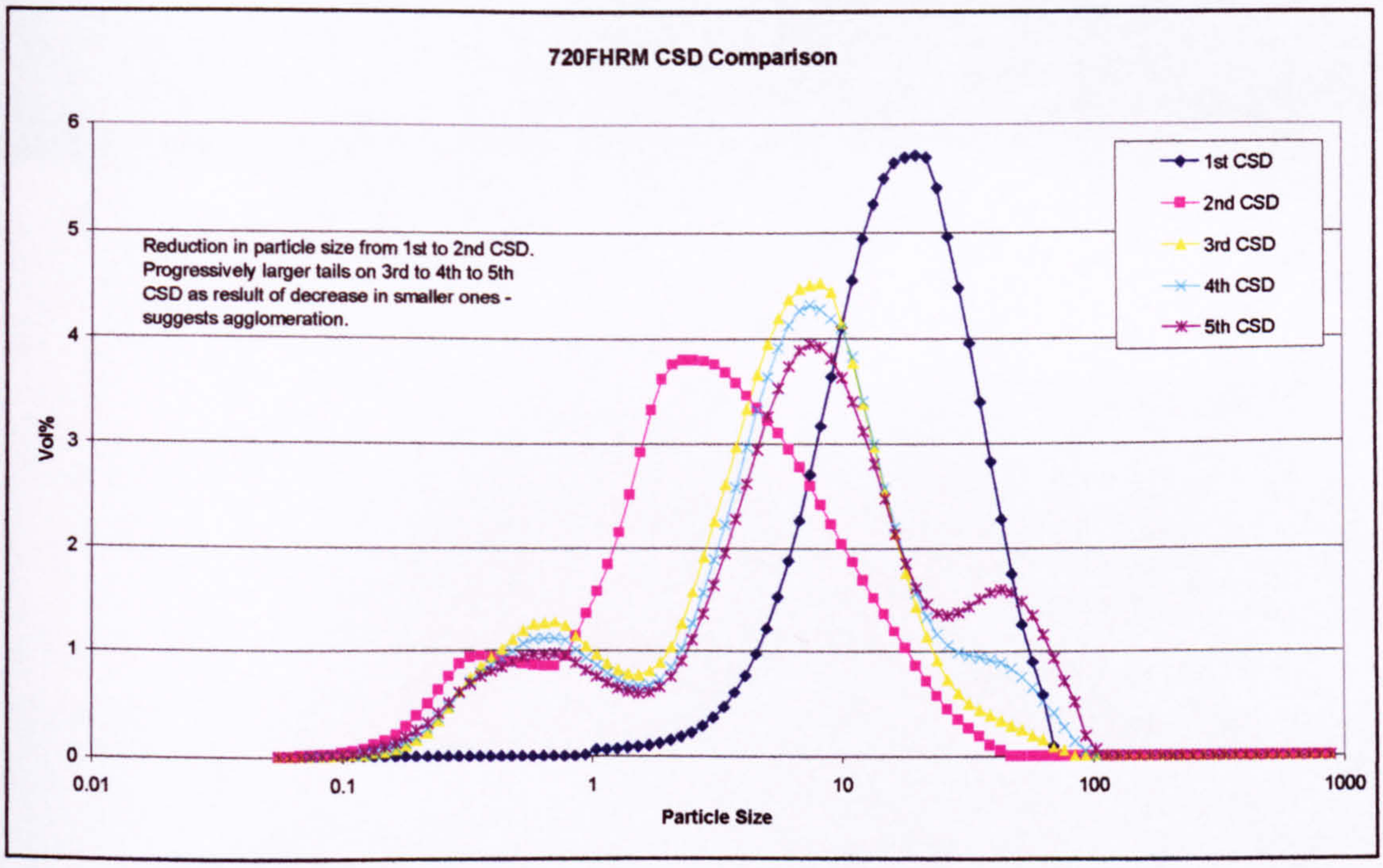


**Figure 9.9.13 CSD profiles: 720FHRM (SDR: flow @ 12ml/s for each reactant, rotational speed @ 1000rpm)**

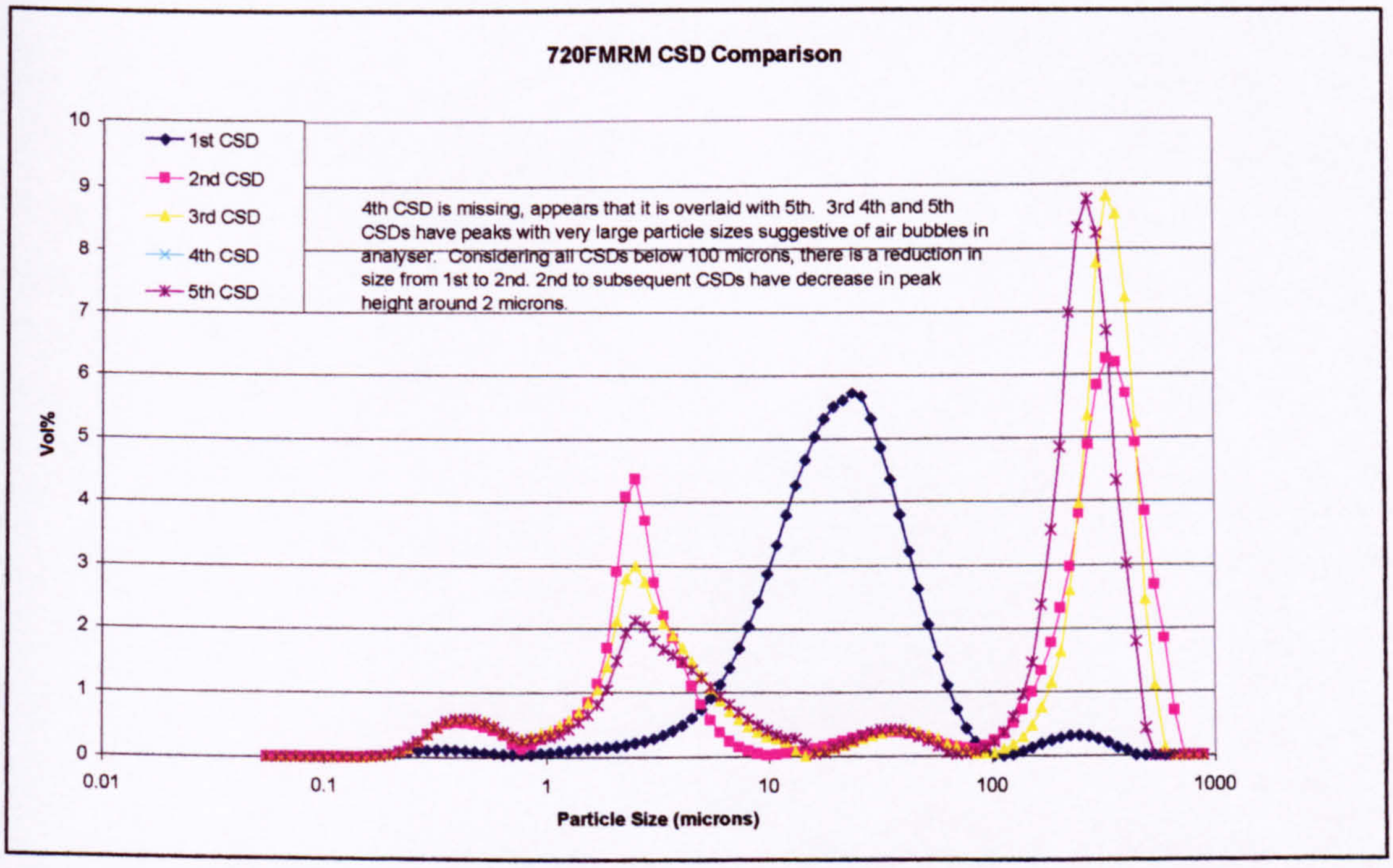


**Figure 9.9.14 CSD profiles: 720FMRM (SDR: flow @ 8ml/s for each reactant, rotational speed @ 1000rpm)**

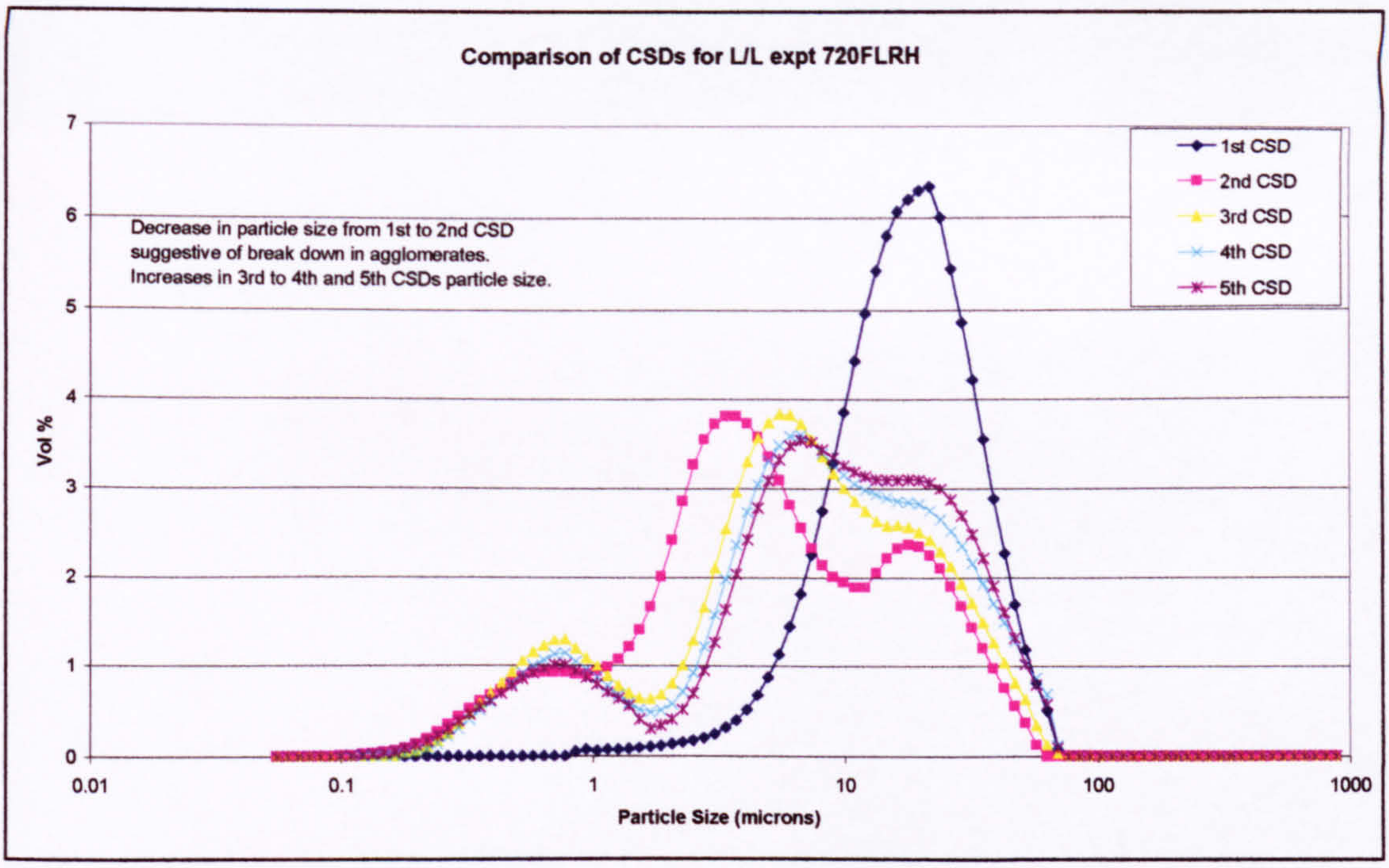


**Figure 9.9.15 CSD profiles: 720FLRH (SDR: flow @ 4ml/s for each reactant, rotational speed @ 2000rpm)**

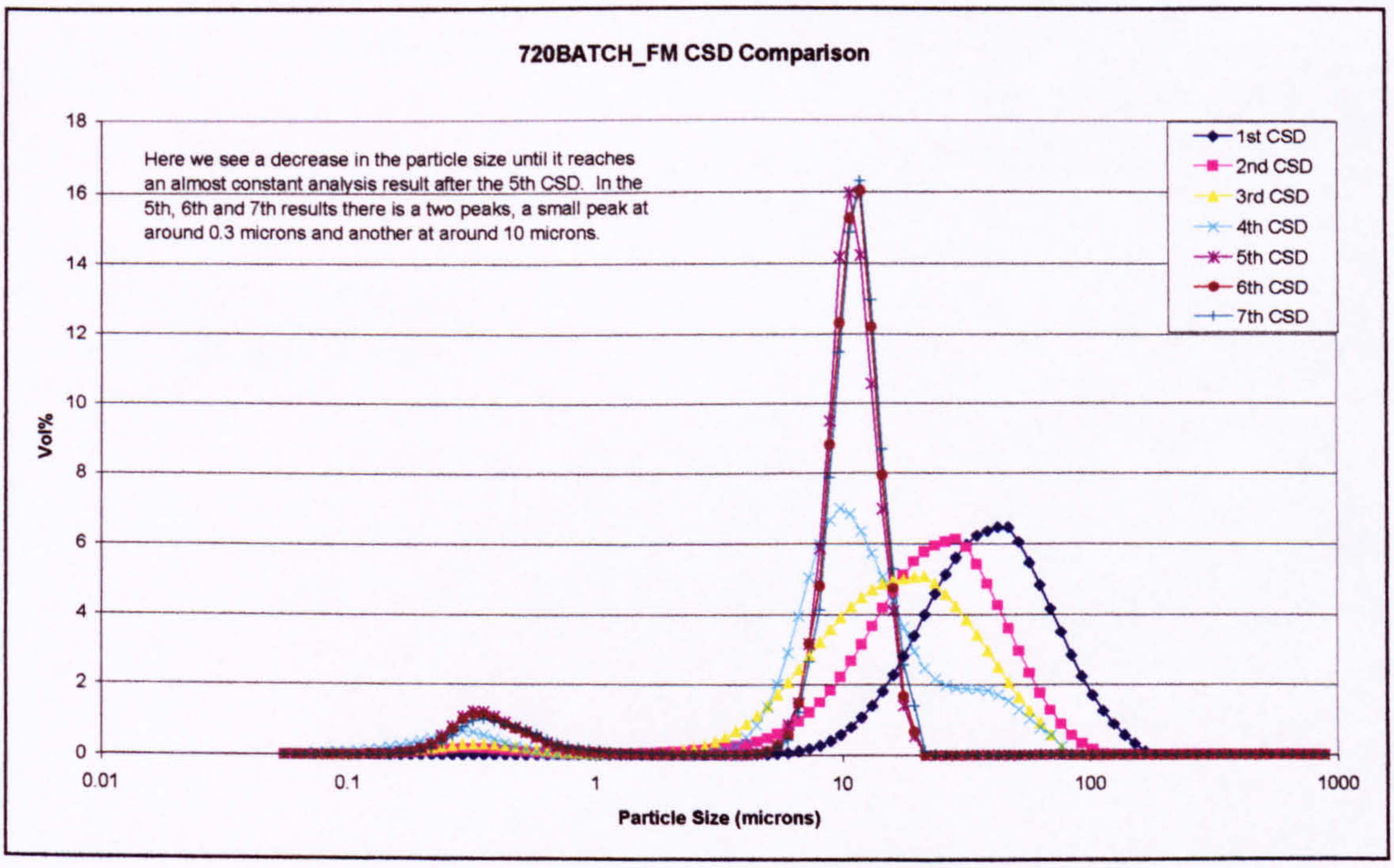


**Figure 9.9.16 CSD profiles:720BATCH_FM (stirred batch containing 500ml $CaCl_2$ with $Na_2CO_3$ added at 8ml/s, stirrer speed 210rpm)**

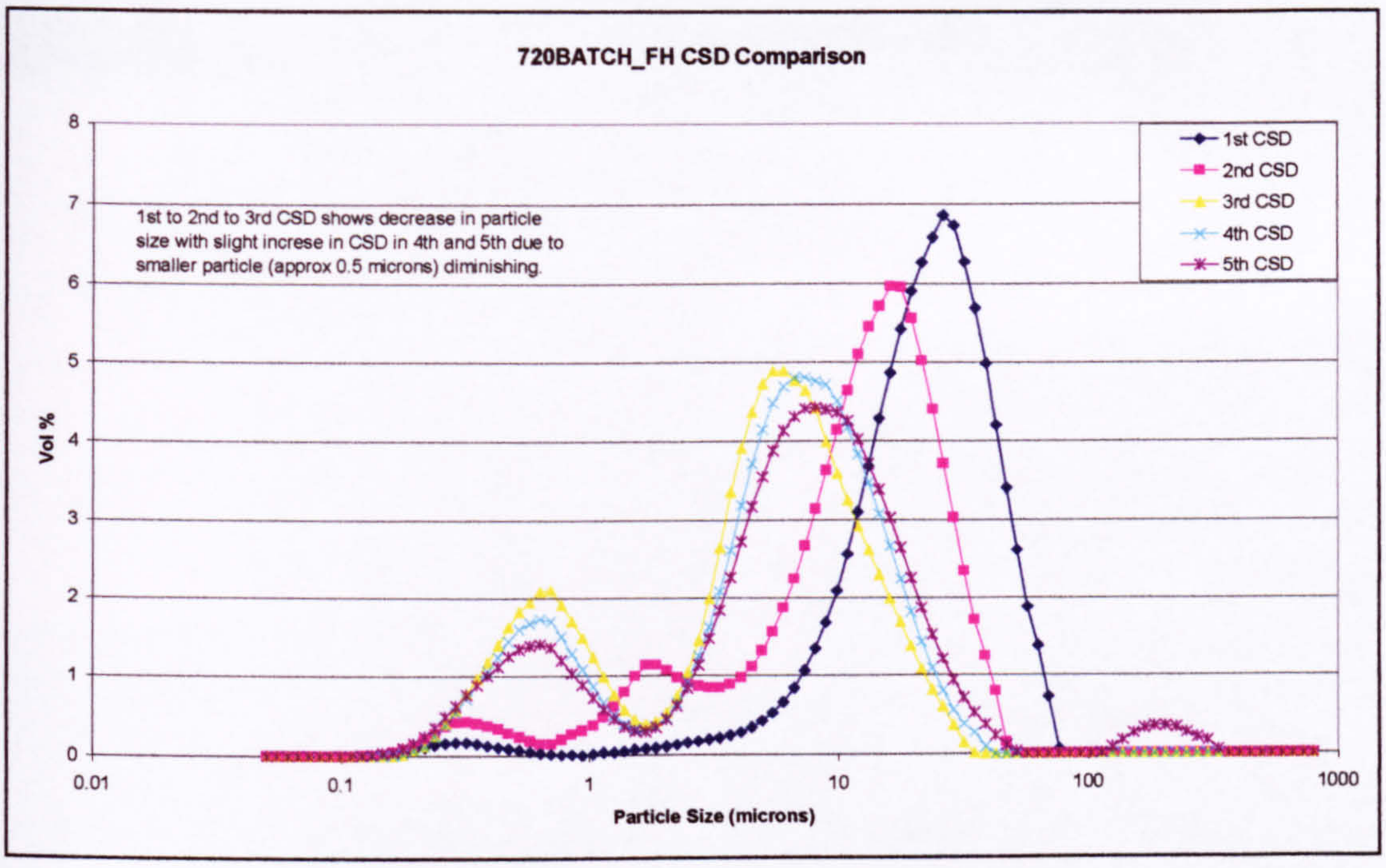


**Figure 9.9.17 CSD profiles: 720BATCH_FH (stirred batch containing 500ml $CaCl_2$ with $Na_2CO_3$ added at 12ml/s, stirrer speed 210rpm)**

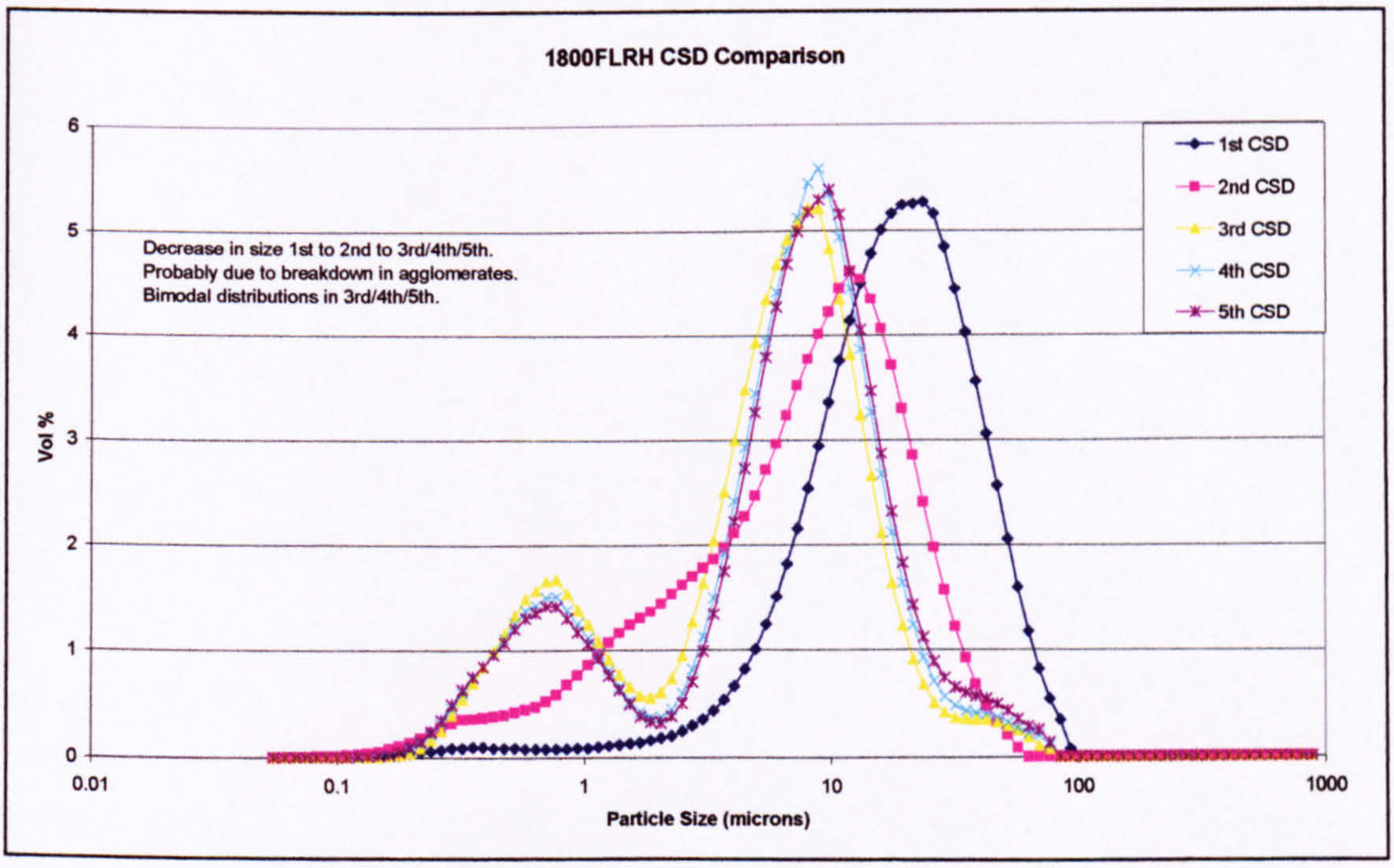


**Figure 9.9.18 CSD profiles: 1800FLRH (SDR: flow @ 4ml/s for each reactant, rotational speed @ 2000rpm)**

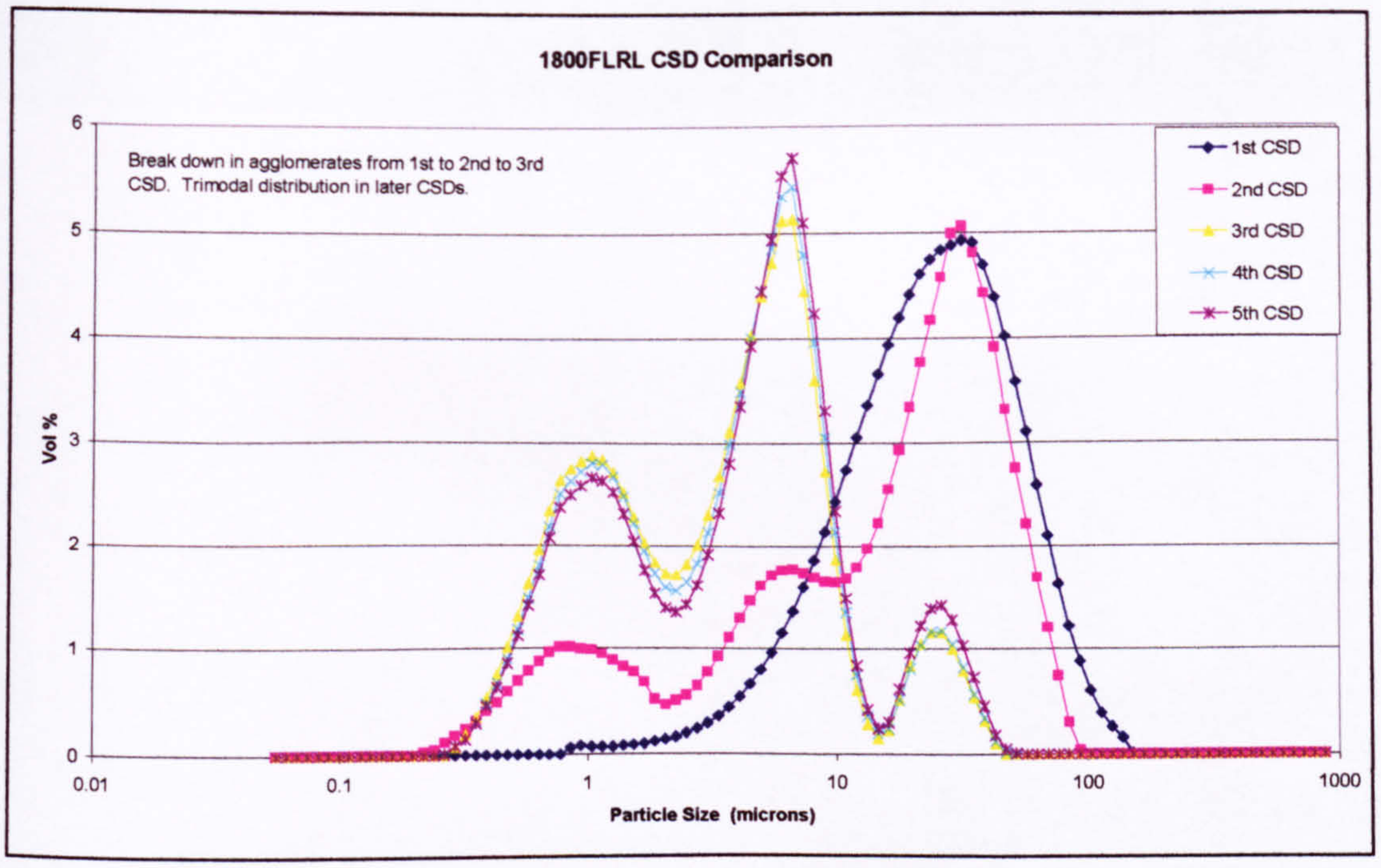


**Figure 9.9.19 CSD profiles: 1800FLRL (SDR: flow @ 4ml/s for each reactant, rotational speed @ 500rpm)**

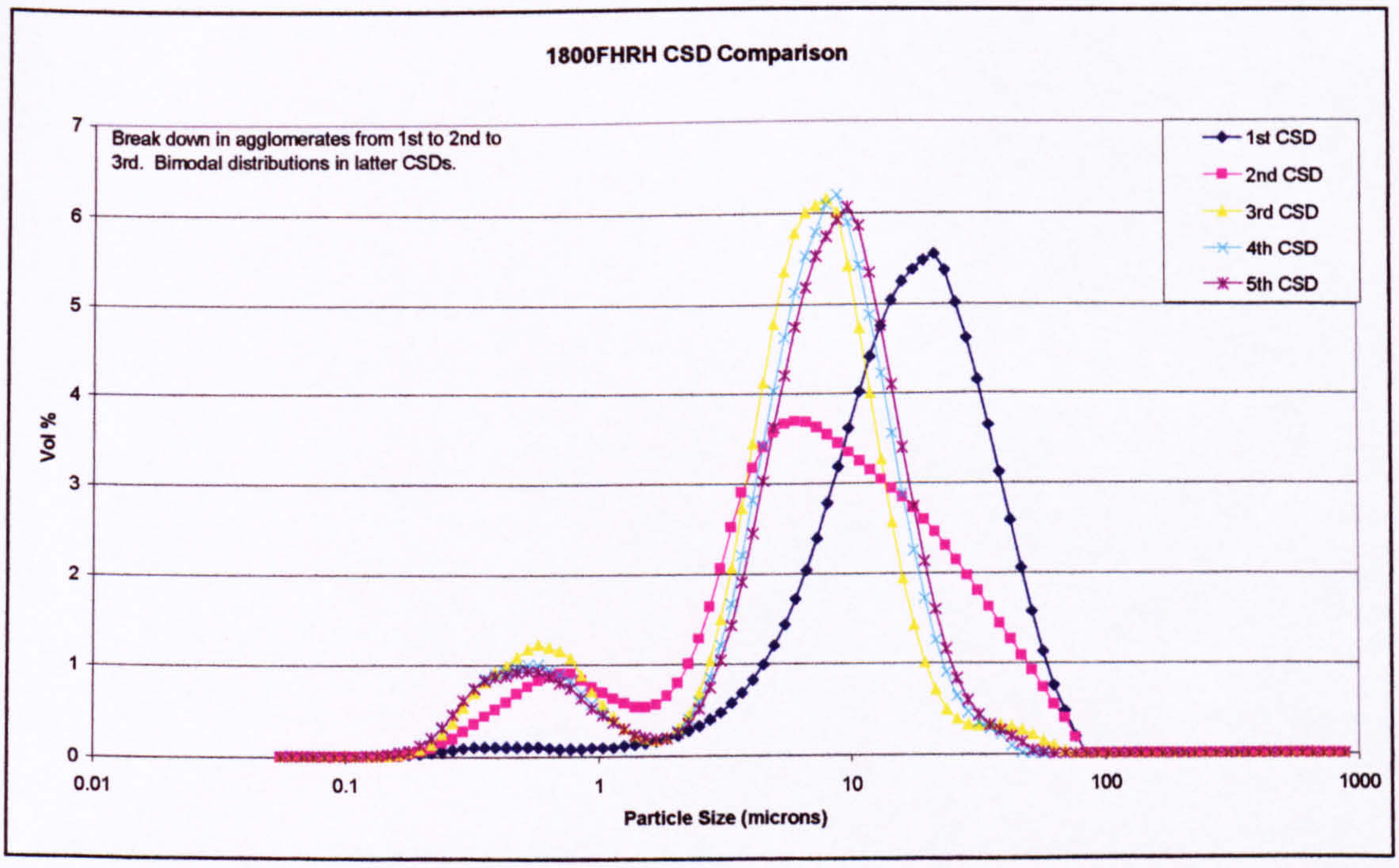


**Figure 9.9.20 CSD profiles: 1800FHRH (SDR: flow @ 12ml/s for each reactant, rotational speed @ 2000rpm)**

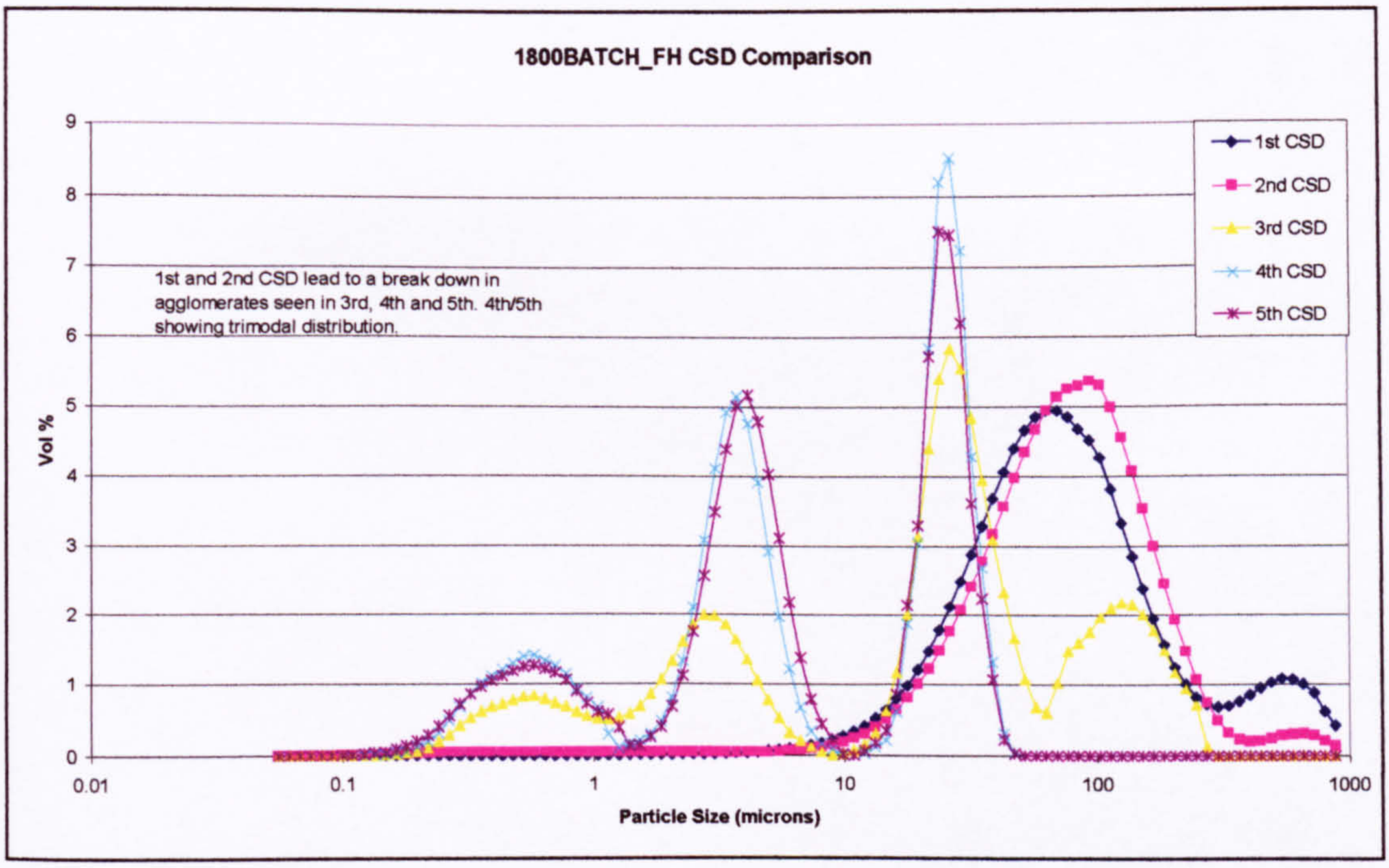


**Figure 9.9.21 CSD profiles: 1800BATCH_FH (stirred batch containing 500ml $CaCl_2$ with $Na_2CO_3$ added at 12ml/s, stirrer speed 210rpm)**

## 9.3 Mass Transfer Contributions

The three elements of gas-liquid mass transfer on the disc are made up of the following contributions.

- Absorption into the thin film generated by centrifugation on the disc.
- Absorption into the droplets that form as the film breaks at the periphery.
- Absorption into the free draining film on the shell walls.

Other elements of possible mass transfer were neglected such as in the floor of the shell, the liquid flowing down the drain tubes, the liquid exiting the feed nozzle and any entrained spray developed as a result of rotation. There is no estimation of the contribution by the gas being sheared by the disc as it rotates generating a velocity relative to the wall or the disc surface. However, this implies that the gas is well mixed and that concentration is uniform.

For each element, the overall mass transfer rate and number of moles absorbed was estimated.

$$N = K_l.A(c_1-c_0)\ (mol/s) \qquad (9.5)$$

$$\therefore \text{Total moles absorbed} = N^* \text{residence time of contributing element} \qquad (9.6)$$

In estimating these, the simple case of the $CO_2$ absorption in water was evaluated without the effect of chemical reaction. The estimate considered cumulative contributions. In other words, it was assumed that there was zero $CO_2$ concentration in the water as it entered onto the disc and left the periphery with a calculated concentration. This concentration was then used for the initial concentration in the droplets. After calculating the number of moles transferred to the drops, this $CO_2$ concentration (disc plus drops) gave the initial concentration of $CO_2$ in water at the top of the shell wall.

The concentration of $CO_2$ in the liquid phase is assumed to be uniform. The gas side and liquid side film resistances are considered. From equation 9.5 above, the carbon dioxide absoption rate (mol/s) transferred to the liquid phase will be

$$N = K_L A\left(\frac{p_{CO_2}}{H_{CO_2,w}} - [CO_2]\right) \qquad (9.7)$$

where A is the gas-liquid contact area for each contributing element, $p_{CO2}$ is the carbon dioxide partial pressure (in this case assumed to be 1 atm), $H_{CO2,w}$ is the Henry's Law coefficient for the absorption of $CO_2$ in water (atm/mol.m$^3$), [$CO_2$] is the concentration of carbon dioxide in the bulk of the liquid and $K_L$ is the overall mass transfer coefficient in the liquid phase.

$$\frac{1}{K_L} = \frac{1}{k_L} + \frac{1}{H^*_{CO_2,w} k_G} \qquad (9.8)$$

$k_L$ and $k_G$ are the mass transfer coefficients in the liquid and gas phase respectively and $H^*_{CO_2,w}$ is the dimensionless Henry's constant for the system, given by

$$H^*_{CO_2,w} = H_{CO_2,w} \frac{c_T}{P} \qquad (9.9)$$

where P is the total gas phase pressure and $c_T$ is the total concentration of the liquid phase. For gases that are only sparingly soluble in water, like $CO_2$, the Henry's constant has very high values (in the current study $H^*_{CO_2,w} \cong 1.42 \times 10^3$ at 1 atm and 20°C). This makes the gas-side resistance term negligible compared to the liquid-side term. By simplification:

$$K_L \approx k_L$$

Which can be used in equation 9.7 in determining the overall rate of mass transfer in the contributing element

### 9.3.1 Spinning disc contribution

In estimating the disc's contribution, Venkataraman's model is used to develop the mass transfer estimate. This is described in detail in the Literature section. (Wood and Watts, 1973) had used the model and compared it with experiments they had performed on absorbing pure $CO_2$ into water on a spinning disc and found the model to be in broad general agreement with their results although the experimental results did not follow the $Q^{1/3}$ relationship of the model. Here, the assumptions of the Nusselt model are required to hold for flow as well as the assumptions for penetration theory that the penetration depth was small. This model does not take into account the effect of pressure, vortices or gas turbulence above the disc.

### 9.3.2 Droplet contribution

In estimating the droplets' contribution, the assumption was made that the drops broke free from the periphery of the disc at the component velocities of the angular disc velocity plus the radial velocity of the film at the periphery calculated from the Nusselt model. The residence time of the droplet is the radial distance between disc periphery and shell wall divided by the radial velocity. The distance between disc periphery and the shell wall was measured at 5mm. The further assumption was made that each drop is formed of uniform size. As each one was a uniform size, for a given flowrate onto the disc, the number of droplets in existence at any given time was estimated.

(Bayvel and Orzechowski 1993) present an equation for the approximate determination of droplet diameter developed at the edge of a spinning disc atomiser on the condition that the centrifugal force is higher than the surface tension force.

$$d_{drop} = \frac{C}{\omega}\left(\frac{\sigma}{\rho_L r}\right)^{1/2} \qquad (9.10)$$

Where C is a coefficient (2.36 for water) (eq 9.10)

$\omega$ is the rotational speed of the disc

$\sigma$ is the surface tension of the liquid (=7.29E-02 J/m$^2$ for water)

$\rho_L$ is the density of the liquid

r is the radius of the disc

The number and size of the droplets were dependent of disc rotational speed and flowrate. From the determination for average droplet diameter, assuming spherical droplets in flight, its volume was determined. From this volume, the total number of drops generated at the edge of the disc was determined for a given flowrate onto the disc.

An estimate for the mass transfer coefficient was made using correlation from Perry's Chemical Engineers' Handbook p5-69 for a single water drop in air.

$$k_{l,drop} = 2\left(\frac{D}{\pi t}\right)^{1/2} \qquad (9.11)$$

where D is the diffusion coefficient of water and t is the residence time of the drop as it travels from periphery to wall. t is used as an approximation of the surface element exposure time in the penetration model. The total surface area of the droplets in existence at any given time was used in determining the mass transfer rate. This was determined from the number of drops generated per second and the flight residence time from periphery to wall.

### 9.3.3 Shell wall contribution

In estimating the shell contribution it was assumed that a uniform film formed which fully wetted the wall. The film thickness, average film velocity and residence time of this film were calculated and are shown in Appendix 9.1.4 These parameters where governed by the flowrate of the liquid and were seen to be of low Reynolds Number (8 < Re < 40). No account was made of the ripples in the film or of the effect of shear by the gas revolving as a result of the disc spinning. An estimate for the mass transfer coefficient was made using a correlation from Perry's Chemical Engineers' Handbook p5-61 for a wetted wall column.

$$k_{l,film} = 3.41\frac{D}{\delta} \qquad (9.12)$$

Where δ is the film thickness. In reality, the stainless steel shell wall was seen to not properly wet with water under the low flow conditions in the present study and formed rivulets instead. This would have effectively reduced the mass transfer due to lower surface area, lower residence times and thicker films. The wetted area of the shell (height multiplied by circumference) was used as the mass transfer area.

### 9.3.4 Overall surface area

The surface area of the liquid film on the disc and running down the wall does not change as it is assumed to approximate the area of the disc and the area of the shell wall respectively, however the number of drops and their total available surface area is determined by rotational speed and flowrate.

| Experiment | Disc ($m^2$) | Drop ($m^2$) | Wall ($m^2$) | total surface A ($m^2$) | Relative contributions | | |
|---|---|---|---|---|---|---|---|
| | | | | | %disc | % drop | % wall |
| 500rpm 4ml/s | 0.0176 | 0.00048 | 0.0503 | 0.0683 | 25.73 | 0.71 | 73.56 |
| 500rpm 20ml/s | 0.0176 | 0.00083 | 0.0503 | 0.0687 | 25.60 | 1.20 | 73.19 |
| 2000rpm 4ml/s | 0.0176 | 0.00077 | 0.0503 | 0.0686 | 25.63 | 1.12 | 73.26 |
| 2000rpm 20ml/s | 0.0176 | 0.00131 | 0.0503 | 0.0692 | 25.42 | 1.90 | 72.68 |

**Table 9.10 Relative surface areas at given disc conditions**

Table 9.10 shows that the area of mass transfer for the droplets only account a small contribution of the total surface area for the given conditions.

### 9.3.5 Residence time

| | Disc residence time (s) | Drop residence time (s) | Wall residence time (s) | Total residence time (s) | Relative contributions | | |
|---|---|---|---|---|---|---|---|
| | | | | | % disc | %drop | %wall |
| 500rpm 4ml/s | 0.3213 | 0.0294 | 1.66 | 2.0110 | 15.97 | 1.46 | 82.57 |
| 500rpm 20ml/s | 0.1099 | 0.0100 | 0.5685 | 0.6884 | 15.96 | 1.46 | 82.58 |
| 2000rpm 4ml/s | 0.1284 | 0.0117 | 1.6604 | 1.8005 | 7.13 | 0.65 | 92.22 |
| 2000rpm 20ml/s | 0.0439 | 0.0040 | 0.5685 | 0.6164 | 7.12 | 0.65 | 92.23 |

**Table 9.11 Residence time on disc, as drops and as falling film**

Table 9.11 shows the residence time on the walls to have a significant contribution whereas the droplets have only a small contribution.

### 9.3.6 Mass transfer model results

The total number of moles transferred in each of the elements was calculated and the relative percentage of each determined. This was calculated at the boundary conditions of flowrate and rotational speed in the present study (4-20ml/s, 500-2000rpm)

| | Disc (moles absorbed) | Drop (moles absorbed) | Wall (moles absorbed) | Sum (moles absorbed) | %disc | %drop | %wall |
|---|---|---|---|---|---|---|---|
| 500rpm 4ml/s | 2.27E-05 | 2.08E-09 | 1.48E-06 | 2.42E-05 | 93.88 | 0.01 | 6.11 |
| 500rpm 20ml/s | 1.33E-05 | 2.08E-09 | 2.96E-07 | 1.36E-05 | 97.80 | 0.02 | 2.18 |
| 2000rpm 4ml/s | 1.43E-05 | 2.08E-09 | 1.48E-06 | 1.58E-05 | 90.63 | 0.01 | 9.36 |
| 2000rpm 20ml/s | 8.36E-06 | 2.08E-09 | 2.96E-07 | 8.66E-06 | 96.56 | 0.02 | 3.42 |

**Table 9.12 Numerical data from the mass transfer model**

Overall, as rotational speed increases, the total mass transferred decreases. As flowrate increases at constant rotational speed, again the total mass transferred decreases. Both of these are due to the decreased residence time in the system and the in the case of flowrate, the increase in film thickness on the disc surface and the wall.

The table shows that the droplets only have a small contribution of the overall mass transfer in the system but the contribution increases with increasing rotational speed. Mass transfer into the droplets is limited by low surface area and residence time contributions. The contribution of the wall is higher at lower flow rates than at higher flowrates. As the rotational speed increases, there is a higher contribution from the disc for a given flowrate.

In conclusion, the wall was shown to have a significant proportion (9.36%) of the available mass transfer under low flow, high rotational speed conditions used in the present study. This model only served as a crude indicator to the overall mass transfer in the reactor configuration used. More sophisticated models are being developed by other workers and will take into account reaction rates and many other parameters not described here. In validating the theoretical modelling, experimental sampling techniques should reflect taking instantaneous 'snap-shots' and samples throughout the reactor in order to better reflect the actual mass transfer within the system at given points as was the case with Burns and Jachuck (2005).

# 10 References


Agnihotri, R.,. Mahuli S.K., et al. (1999). "Influence of surface modifiers on the structure of calcium carbonate." Industrial and Engineering Chemistry Research **38**: 2283-2291.

Al-Rashed, M.H. and. Jones, A.G., (1999). "CFD modelling of gas-liquid reactive precipitation." Chemical Engineering Science **54**: 4779-4784.

Aoune, A. and Ramshaw, C., (1998). "Process intensification: heat and mass transfer characterisitics of liquid films on rotating discs." International Journal of Heat and Mass Transfer **42**: 2543-2556.

Balasundaram, V.,. Porter, J. E., et al. (1990). Process Intensification: A Rotary Seawater Deaerator. Separation of Gases: 5th BOC Priestley Conference.

Bayvel, L. and Orzechowski, Z. (1993). "Liquid Atomization.", Taylor and Francis, ISBN 0-89116-959-8

Boodhoo, K. V. K. and Jachuck, R. J., (2000). "Process intensification: spinning disk reactor for styrene polymerisation." Applied Thermal Engineering **20**(12): 1127-1146.

Brauer, H. (1958). Chem. Ing. Tech **30**(75).

Brauner, N. and Maron, D.M., (1983). Chemical Engineering Science **38**(5): 775-788.

Brecevic, L. and Nielsen, A.E., (1989). Journal of Crystal Growth **98**: 504.

Bunker, B.C., Rieke, P.C., et al. (1994). Science **264**: 48.

Burns, J.R. and R.J. Jachuck (2001). "Condensation studies using cross-corrugated polymer film compact heat exchanger." Applied Thermal Engineering **21**: 495-510.

Burns, J.R. and Jachuck, R.J., (2005). "Monitoring of $CaCO_3$ production on a spinning disc reactor using local conductivity measurements." A.I.Ch.E Journal **51**(5): 1497-1507.

Burns, J.R. and Ramshaw, C., (1999). "Development of a microreactor for chemical production." Trans. IChemE **77**(Part A): 206-211.

Burns, J.R. and Ramshaw, C., (2001). "The intensification of rapid reactions in multiphase systems using slug flow in capillaries." Lab on a Chip **1**: 10-15.

Cafiero, L., Jachuck, R.J., et al. (1999). 13th International Symposium on Industrial Crystallisation, IChemE.

Chakraborty, V.K., Agarwal, S., et al. (1994). "Steady-state transitions and polymorph transformations in continuous precipitation of calcium carbonate." Industrial and Engineering Chemistry Research **33**: 2187-2197.

Chen, J.-F., Wang, Y-H. et al. (2000). "Synthesis of nanoparticles with novel technology: high-gravity reactive precipitation." Industrial and Engineering Chemistry Research **39**(4): 948-954.

Colfen, H. and. Antonetti, M (1998). "Crystal design of calcium carbonate microparticles using doublehydrophilic block copolymers." Langmuir **14**: 582-589.

Danckwerts, P.V. (1970). Gas-Liquid Reactions, McGraw-Hill.

Doraiswarmy, L.K. and Sharma M.M., (1984). Heterogeneous Reactions: Analysis, Examples and Reactor Design Volume 2: Fluid-Fluid-Solid Reactions, John Wiley and Sons.

Elfil, H. and Roques, H. (2001). "Role of hydrate phases of calcium carbonate on the scaling phenomenon." Desalination **137**: 177-186.

Fitchett, D.E. and Tarbell, J.M. (1990). "Effect of mixing on the precipitation of barium sulphate in an MSMPR reactor." AIChE J. **36**: 511.

Garside, J. and Davey, R. (1980). Chemical Engineering Science **4**: 694.

Gomez-Morales, J., Torrent-Burgues, J. et al. (1996). "Precipitation of calcium carbonate from solutions with varying Ca2+/carbonate ratios." Journal of Crystal Growth **166**: 1020-1026.

Green, A. (1998). "Process intensification: the key to survival in global markets?" Chemistry and Industry: 168-172.

Harnby, N., et al. (1992). Mixing in the Process Industries, Butterworth-Heinemann Ltd.

Harris, D.C. (1999). Quantitative chemical analysis, W.H. Freeman.

Hendershot, D.C. (2000). "Process Minimization: Making Plants Safer." Chemical Engineering Progress **88**: 35-40.

Heyer, C. and Mersmann, A. (1999). The influence of operating conditions on the precipitation of nanoparticles. Industrial Crystallisation, IChemE.

Hostomsky, J. and Jones, A.G. (1991). "Calcium carbonate crystallisation, agglomeration and form during continuous precipitation from solution." J. Phys. D: Appl. Phys. **24**(1991): 165-170.

Hostomsky, J. and Jones, A.G. (1995). "A penetration model of the gas-liquid reactive precipitation of calcium carbonate crystals." Trans IChemE **73**(Part A April 1995).

Incropera, F.P. and De Witt, D.P. (1990). Introduction to heat transfer, John Wiley & Sons, Inc.

Ishley, J.N. and Osterhuber, E.J. (1998). "Precipitated calcium carbonate for paper coating." Coating Materials: Pigments, Binders and Additives; TAPPI

Jachuck, R.J., Hetherington, P., et al. (2001). Process intensification: continuous production of barium sulphate using a spinning cone reactor. Better Processes for Better Products: 4th International Conference on Process Intensification for the Chemical Industry, Brugge, BHR Group.

Jachuck, R.J., Lee, J., et al. (1997). "Process intensification for energy saving." Applied Thermal Engineering **17**(8-10): 861-867.

Jachuck, R.J. and Ramshaw, C. (1994). "Process Intensification: Heat transfer characteristics of tailored rotating surfaces." Heat Recovery Systems and CHP **14**(No. 5): 475-491.

Jachuck, R.J., Ramshaw, C., et al. (1997). "Process intensification: The opportunity presented by spinning disc reactor technology." Institution of Chemical Engineers Symposium Series: 417-424.

Jassim, M. S. (2002). Process intensification: absorption and desorption of carbon dioxide from monoethanolamine solutions. School of Chemical Engineering and Advanced Materials. Newcastle Upon Tyne, University of Newcastle Upon Tyne.

Jones, A.G., Hostomsky, J., et al. (1992). "On the effect of liquid mixing rate on primary crystal size during the gas-liquid precipitation of calcium carbonate." Chemical Engineering Science **47**(No. 13/14): 3817-3824.

Jung, W.M., Kang, S.H., et al. (2000). "Particle morphology of calcium carbonate precipitated by gas liquid reaction in a Couette-Taylor reactor." Chemical Engineering Science **55**: 733-747.

Juvekar, V.A. and Sharma, M.M., (1973). "Absorption of $CO_2$ in a suspension of lime." Chemical Engineering Science **28**: 823-837.

Kastanek, F., Jahradnik, J., et al. (1993). Chemical Reactors for Gas Liquid Systems.

Katsifaras, A. and Spanos, N., (1999). "Effect of inorganic phosphate ions on the spontaneous precipitation of vaterite and on the transformation of vaterite to calcite." Journal of Crystal Growth **204**: 183-190.

Kelleher, T. and Fair, J.R. (1996). "Distillation studies in a high gravity contactor." Industrial and Engineering Chemistry Research **35**: 4646-4655.

Keller, G.E. and. Bryan, P.F (2000). "Process Engineering: Moving in New Directions." Chemical Engineering Progress **88**: 41-50.

Khan (1986). PhD thesis, Universtiy of Newcastle upon Tyne.

Kirk, R.E., Othmer, D.F, et al., Eds. (1992). Kirk-Othmer encyclopedia of chemical technology.

Kitano, Y. and. Hood, D.W., (1965). Geochim Cosmochim. Acta **29**: 29.

Klabunde, K. J. (2001). Nanoscale Materials in Chemistry, John Wiley and Sons.

Koga, N., Nakagoe, Y., et al. (1998). "Crystallisation of amorphous calcium carbonate." Thermochimica Acta **318**: 239-244.

Kotaki, Y. and Tsuge, H., (1990). "Reactive crystallization of calcium carbonate by gas-liquid and liquid-liquid reactions." The Canadian Journal of Chemical Engineering **68**: 435-442.

Levenspiel, O. (1972). Chemical Reaction Engineering, John Wiley and Sons.

Lim, S.T. (1980). Hydrodynamics and mass transfer processes associated with the absorption of oxygen in liquid films flowing across a rotating disc, PhD thesis, Universtiy of Newcastle upon Tyne, UK.

Manoli, F. and Dalas, E. (2001). "Calcium carbonate crystallization in the presence of glutamic acid." Journal of Crystal Growth **222**: 293-297.

Marcant, B. and David, R. (1991). AIChE J. **37**: 1698-1710.

Meldrum, F. C. and. Hyde, S.T. (2001). "Morphological influence of magnesium and organic additives on the precipitation of calcite." Journal of Crystal Growth **231**: 544-558.

Merris, C. S. (1997). "Preparing high opacity precipitated calcium carbonate using the causticizing reaction." AIChE J. 1997 Annual Meeting Session 246(Paper 246d).

Mersmann, A. (1995). Crystallization technology handbook., Marcel Dekker Inc.

Mersmann, A. (1999). "Crystallisation and Precipitation." Chemical Engineering and Processing **38**(345-353).

Mohanty, R., Bhandarkar, S., et al. (1988). "Characterisation the product crystals from a mixing tee process." AIChE J. **34**: 2063-2068.

Moore, S. R. (1986). Mass Transfer to Thin Liquid Films on Rotating Surfaces, With and Without Chemical Reaction, PhD Thesis, University of Newcastle upon Tyne.

Morse, J. W. and F. T. Mackenzie (1990). Geochemistry of Sedimentary Carbonates, Elsevier.

Mullin, J. W. (1972). Crystallisation, Butterworth & Co.

Myerson, A. S. (1993). Handbook of industrial crystallization., Butterworth-Heinemann.

Nancollas, G. H. and Reddy, M. M. (1971). "The Crystallization of Calcium Carbonate: II. Calcite Growth Mechanism." Journal of Colloid and Interface Science **37**(4): 824-830.

Nielsen, A. E. (1961). "Homogeneous nucleation in barium sulphate precipitation." Acta Chemica Scandinavica **15**: 441-442.

Nielsen, A. E. (1964). Kinetics of Precipitation, Pergamon, Oxford.

Nielsen, A. E. (1980). Croat. Chem. Acta **53**: 255.

Ogino, T., T. Suzuki, et al. (1987). Geochim Cosmochim. Acta **51**: 2757.

Oldshue, J. Y. (1983). Fluid Mixing Technology, McGraw-Hill.

Ostwald, W. (1897). Z physik. Chem. (Leipzig) **22**(289).

Oxley, P., Brechtelsbauer, C., et al. (2000). "Evaluation of spinning disk reactor technology for the manufacture of pharmaceuticals." Industrial and Engineering Chemistry Research **39**(7): 2175-2182.

Pach, L., Duncan, S., et al. (1996). "Morphological control of precipitated calcium carbonates and phosphates by colloidal additives." Journal of Material Sciences **31**: 6565-6569.

Peel, J., Howarth, C.R., et al. (1998). "Process intensification: Higee seawater deaeration." Chemical Engineering Research & Design, Transactions of the Institute of Chemical Engineers, Part A **76**(A5): 585-593.

Perry, R.H. and Green D.W. (1997). Perry's Chemical Engineering Handbook 5th Edition.

Pohorecki, R. and Baldyga, J. (1983). Chemical Engineering Science **38**: 79.

Pohorecki, R. and Baldyga, J. (1985). 6th European Conf. on Mixing, Paper 12.

Pohorecki, R. and Baldyga, J. (1988). Chemical Engineering Science **43**: 1949.

Rahman, M. M. (1998). "Transport to a chemically active thin liquid film over a spinning disk." Journal of Energy Resources Technology, Transactions of the ASME **120**(4): 293-298.

Rahman, M. M. and Faghri, A. (1993). "Gas absorption and solid dissolution in a thin liquid film on an rotating disk." Inst J. Heat and Mass Transfer **36**(1): 189-199.

Ramshaw, C. (1983). "Hi-gee distillation - an example of process intensification." The Chemical Engineer: 13-14.

Ramshaw, C. (1985). "Process intensification: a game for n players." The Chemical Engineer(July/August): 30-33.

Reddy, M.M. and Nancollas, G.H. (1971). "The Crystallization of Calcium Carbonate: I. Isotopic Exchange and Kinetics." Journal of Colloid and Interface Science **36**(No2): 166-172.

Rigopoulos, S. and Jones, A.G. (2001). "Dynamic modelling of a bubble column for particle formation via a gas-liquid reaction." Chemical Engineering Science **56**: 6177-6184.

Roskill (2000). "The economics of precipitated calcium carbonate." Roskill ISBN 0 86214 827 8.

Saxl, O. (2000). Opportunities for industry in the application of nanotechnology, www.nano.org.uk.

Sherwood, T.K. and. Pigford, R.L (1952). Absorption and Extraction, McGraw-Hill.

Sohnel, O. (1981). Cryst. Res. Technology **16**: 651.

Sohnel, O. and Garside, J. (1992). Precipitation: Basic Principles and Industrial Applications, Butterworth-Heinemann Ltd.

Sohnel, O. and Mullin, J.W. (1982). Journal of Crystal Growth **60**.

Stankiewicz, A. I. and Moulijn, J. A. (2000). "Process Intensification: Transforming Chemical Engineering." Chemical Engineering Progress **88**: 22-34.

Swinney, L.D., Stevens , J.D., et al. (1982). "Calcium Carbonate Crystallisation Kinetics." I&EC Fundamentals **21**: 31.

Tai, C.Y. and. Chen, P-C (1995). "Nucleation, Agglomeration and Crystal Morphology of Calcium Carbonate." AIChE J. **41**(1): 68-77.

Tavare, N.S. and Garside, J. (1985). "Mixing, reaction and precipitation: limits of micromixing in an MSMPR crystalliser." Chemical Engineering Science **40**(No. 8): 1485-1493.

Thomas, A.J., Seton, L., et al. (2002). "Using a liquid membrane system for the encapsulation of organic and inorganic substrates within inorganic microcapsules." Chem. Commun: 1072-1073.

Tracy, S.L., Francois, C.J.P., et al. (1998a). "The growth of calcite spheres from solution I. Experimental deign techniques." Journal of Crystal Growth **193**: 374-381.

Tracy, S.L., Williams, D.A. et al. (1998b). "The growth of calcite spherulites from solution II Kinetics of formation." Journal of Crystal Growth **193**: 382-388.

Trent, D. and Tirtowidjojo D. (2001). Commercial operation of a rotating packed bed (RPB) and other applications of RPB technology. 4th International Conference on Process Intensification for the Chemical Industry, Brugge, BHR Group.

Trippa, G., Hetherington, P., et al. (2002). Process intensification: precipitation of calcium carbonate from the carbonation reaction of lime water using a spinning disc reactor. 15th International Symposium on Industrial Crystallisation, IChemE, Sorrento, Italy.

Vacassy, R., Lemaitre, J. et al (2000). "Calcium carbonate precipitation using new segmented flow tubular reactor." AIChE Journal **46**: 1241-1252

Vankataraman, R.S. (1966). PhD Thesis, University of Leeds.

Vucak, M., Peric, J. et al. (1997). "Precipitation of calcium carbonate in a calcium nitrate and monoethanolamine solution." Powder Technology **91**: 69-74.

Wachi, S. and Jones, A.G. (1991). "Effect of gas-liquid mass transfer on crystal size distribution during the batch precipitation of calcium carbonate." Chemical Engineering Science 46(No. 12): 3289-3293.

Wachi, S. and Jones, A.G. (1992). "Dynamic modelling of particle size distribution and degree of agglomeration during precipiation." Chemical Engineering Science **47**(No 12): 3145-3148.

Watts, B.E. (1971). PhD Thesis, University of Wales.

Wei, S-H., Mahuli, S.K., et al. (1997). "High surface area calcium carbonate: pore structural properties and sulphonation characterisitics." Industrial and Engineering Chemistry Research **38**: 2283-2291.

Wood, R. M. and Watts, B. E. (1973). "The flow, heat and mass transfer characteristics of liquid films on rotating discs." Trans Instn Chem Engrs **315-322**.

Woods, W. (1995). The hydrodynamics of thin liquid films flowing over a rotating disc, PhD thesis, University of Newcastle upon Tyne.

Wray, J.L. and. Daniels, F (1957). "Precipitation of calcite and aragonite." Journal of the American Chemical Society **79**: 2031-2034.

Yagi, H., Iwazawa, A. et al. (1984). "Crystallisation of calcium carbonate accompanying chemical absorption." Industrial and Engineering Chemistry Fundamentals **23**: 153-158.

Yanniotis, S. and Kolokotsa, D. (1996). "Experimental study of water vapour condensation on a rotating disc." International Communications in Heat and Mass Transfer **23**(5): 721-729.

Yanniotis, S. and Kolokotsa, D. (1996). "Boiling on the surface of a rotating disc." Journal of Food Engineering **30**: 313-325.

Zhang, Y. and Dawe, R.A. (2000). "Influence of $Mg^{2+}$ on the kinetics of calcite precipitation and calcite crystal morphology." Chemical Geology **163**: 129-138.

## Patents

Bleakley, I. S. and T. R. Jones (1993). Precipitated calcium carbonate. USPTO No 5,232,678.

Bleakley, I. S. and T. R. Jones (1994). Precipitated calcium carbonate. USPTO No 5,342,600.

Bleakley, I. S. and T. R. Jones (1996). Precipitated calcium carbonate. USPTO No 5,558,850.

Bleakley, I. S., P. M. McGenity, et al. (1998). Paper coating pigments and their production and use USPTO No 5,833,747.

Chapnerkar, V. D. and M. N. Badgujar (1994). Process for production of rhombic shaped precipitated calcium carbonate USPTO No 5,332,564.

Kroc, V. J. and F. G. H. (1997). Clustered precipitated calcium carbonate particles. USPTO No 5,695,733.

Liu, S.-T., M. J. Martin, et al. (2006). Precipitated calcium carbonate. USPTO No 6,989,142.

Shibazaki, H., S. Edagawa, et al. (1979). Process for preparing precipitated calcium carbonate. USPTO No 4,133,894.

Vanderheiden, D. B. (1983). Process for the preparation of finely divided precipitated calcium carbonate. USPTO No 4,367,207.

Vanderheiden, D. B. (1987). Spherically shaped precipitated calcium carbonate, its preparation and use USPTO No 4,714,603.

Woode, R. D. A. (1977). Production of calcium carbonate USPTO No 4,018,877.

You, K. J. (1998). Process for producing calcium carbonate particles having a size of 0.1 to 1.0 .mu.m. USPTO No 5,811,070.